Particle Emissions from Domestic Gas Cookers

Wagner, Ayten Yilmaz

Publication date:
2009

Document Version
Publisher's PDF, also known as Version of record

Particle Emissions from Domestic Gas Cookers

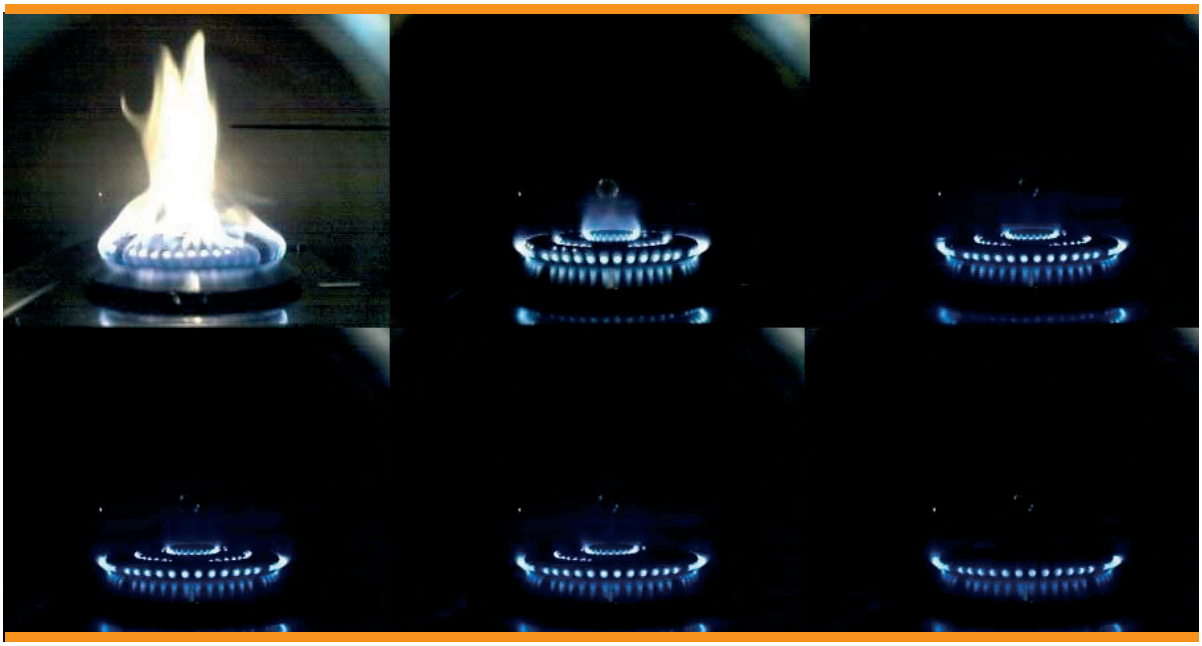

Ayten Yilmaz Wagner

Ph.D. Thesis

2009

DTU Chemical Engineering
Department of Chemical and Biochemical Engineering

PARTICLE EMISSIONS FROM DOMESTIC GAS COOKERS

Ph.D. Thesis

By

AYTEN YILMAZ WAGNER

18th March, 2009

Supervisors

Peter Glarborg, DTU
Hans Livbjerg, DTU
Per Gravers Kristensen, DGC

CHEC Research Centre
Department of Chemical and Biochemical Engineering
Technical University of Denmark

Preface

This dissertation is written in partial fulfillment of the requirements of the Ph.D. degree. The work was carried out at the Department of Chemical and Biochemical Engineering at the Technical University of Denmark under the guidance of Peter Glarborg, Hans Livbjerg and Per Gravers Kristensen. The work was co-financed by DTU, Danish Gas Technology Center (DGC) and Danish Ministry of Science, Technology and Innovation.

First of all, I would like to thank to all my supervisors for their continuous guidance and support, as well as their constructive criticisms and valuable inspirations throughout this study. I sincerely thank to my main supervisor Peter Glarborg, who originally introduced me to combustion phenomena and trickled my interest which leaded to this Ph.D. thesis, and to Hans Livbjerg who introduced me to aerosols and guided me throughout this study, even in his retirement. I also would like to thank to all my colleagues, academic, technical and administrative staff at CHEC and KT Workshop, for their useful discussions and practical help in the course of the three years. I sincerely thank to Carsten Nørby and Kristoffer Andersen for their brilliant ideas and troubleshooting services for the design, construction and operation of the experimental set up(s).

Finally, I'd like to thank to my husband for being so understanding, supportive and patient every single day; to my family for accepting the distances and to my friends, for sharing the rainy, stormy and sunny days.

Summary

In the last several years, a growing body of scientific evidence has indicated that the air within homes and other buildings can be more seriously polluted than the outdoor air in even the largest and most industrialized cities. Smoking, cooking and infiltration of the polluted outdoor air have been the focus of many studies. Domestic gas cookers and stoves were also studied, however not that extensively until recently, from particle emissions point of view. In this Ph.D. study, the objective is to provide new results on the particle emissions from domestic gas cookers; i.e: particle number concentrations, particle sizes and the nature of particles.

Experiments were performed using a domestic gas cooker both open to the surrounding atmosphere in a laboratory and in a compartment free from external particle sources. Tested fuels were methane, natural gas and odorant free natural gas. The affect of primary aeration and the sulfur content of the fuel on the particle emissions were also investigated. A question was raised on the likelihood of H_2SO_4–H_2O binary homogeneous nucleation to take place in the emissions from domestic gas cookers. Last but not least, inhalation exposures to the emitted particles were simulated

The experiments showed that primary air has a strong effect on the particle emissions from domestic gas cookers. The diameters of the particles emitted from the studied gases is found to be around 10 nm for diffusion flame and 2-5 nm for partial premixed flames. The particle number concentrations varied between 1E3 – 1E6 particles/cm^3 depending on the fuel, flow rate and the primary air addition. Emission rate of particles with diameters less than 20 nm is calculated to be 3- 4 μg/hr on average. The particles were identified by TEM studies as carbonaceous particles containing oxygen, sulfur and copper. While the source of carbon, oxygen and sulfur under the examined conditions of this study can only be explained by the combustion, the source of copper could be explained by either its presence in the natural gas or in the materials that were used in this study, i.e: the burner and the sampling probe.

A combined evaluation of the experimental findings with the modeling efforts constituted the required evidences to conclude that the presence of sulfur favors the particle formation process in the domestic gas cookers, despite the very small amounts of sulfur present in natural gas via the odorant. Since particle emissions from methane and natural gas experiments were very close to each other, it is evident that those particles can not be due to

sulfur only. Based on their carbonaceous nature and their diameters in the range of a few nanometers, it is believed that these particles are soot precursor particles just as those particles identified and communicated recently by d'Anna et al (2008).

Based on the inhalation exposure simulations using IAQX (Simulation Tool Kit for Indoor Air Quality and Inhalation Exposure, it is concluded that air exchange ratios of 2.2 would provide a significant reduction in the inhalation exposures. The importance of these emissions from health impact point of view, however, depends on whether it is the mass or numbers of particles inhaled which creates the adverse health effects.

Resume (Summary in Danish)

I de seneste år videnskabeligere beviser indikeret at indendørs luft i private hjem og andre bygninger kan være mere alvorligt forurenede end luften i selv de største og mest industrialiserede byer. Rygning, mad lavning og filtrering af den forurenede udendørs luft har været i fokus i mange studier. Private hjems komfurer og ovne har også været forsket, dog ikke så detaljeret fra partikel emissioner synspunkt indtil nu. Målet med dette Ph.D studie er objektivt at bidrage med nye resultater for partikel emissioner for privathjems miljø, for eksempel nummer koncentration af partikler, partiklers størrelser og identitet.

Eksperimenter blev udført ved brug af et gas komfur både i almindelige daglige omgivelser i et laboratorium og i et indbygget reaktor fri for eksterne partikler kilder. Testet brændstof var metan, naturgas og naturgas uden tilsætning komponenter. Effekten af den primære luft tilføjelse og svovl indholdet af brændstoffet blev også undersøgt. Der opstod et spørgsmål om ligheden af H_2O – H_2SO_4 binære homogene nukleation ville finde sted i emissionen af gas komfuret. Sidst men ikke mindst, blev de frigjorte partikler simuleret i inhalerings eksponering program IAQX.

Eksperimenter viste at primær luft har en stærk effekt på partikler emissioner fra gas komfuret. Diameterne af frigjorte partikler udviklede sig til cirka 10 nm for diffusion flamme of 2 til 5 nm for delvist blandet flamme. Nummer koncentration af partikler varierede mellem 1E3 – 1E6 partikler/m^3 afhængig af brændstof, flow og primær luft-tilførsel. Emissioner af partikler mindre end 20 nm blev kalkuleret til 3 – 4 µg/timer i gennemsnit. Partiklerne blev identificeret af TEM studier som karbon partikler indeholdende oxygen, svovl og kobber. Selvom karbon, oxygen og svovl kan være kun fra forbrænding i undersøgte konditioner af denne studie, kobber kan være enten fra natur gas eller materialerne som var brugt i denne studie, for eksempel gas komfur eller sampler.

En kombineret evaluering af resultater fra eksperimenter og beregninger viser at svovl i brændstof forårsager partikel formation i gas komfuret, til trods for den meget lille mængde af svovl i naturgas via tilsætnings komponenter. Da partikler emissioner fra metan og naturgas eksperimenter var meget lig hinanden, er beviset at disse partikler ikke kun skyldes svovl. Baseret på deres karbon karakter og deres diameter i størrelser af et par nm, partiklerne er troede at være forløber af sodpartikler, ligesom d'Anna et al (2008) har identificeret og overført i den seneste tid.

Baseret på simulationer af inhalerings eksponering, er det konkluderet at udskiftning af luft i forholdet 2.2. vil medføre en markant reduktion i inhalerings eksponering. Vigtigheden af disse emissioner af helbredsmæssige hensyn afhænger af om det er mængden eller antal af partikler inhaleret som giver dårligt heldbred.

TABLE OF CONTENTS

LIST OF TABLES

PART A: INTRODUCTION

Chapter 1: Aerosols/Particles

Particles, or particulate matter, in general, may be solid or liquid, with diameters between ~ 0.002 and ~100μm. The lower end of the size range is not sharply defined because there is no accepted criterion at which a cluster of molecules becomes a particle. The upper end corresponds to the size of fine drizzle or very fine sand; these particles are so large that they quickly fall out and hence do not remain suspended for significant periods of time.

Aerosols are defined as relatively stable suspensions of solid or liquid particles in a gas. Thus aerosols differ from particles in that an aerosol includes both the particles and the gas in which they are suspended. However, while this is the rigorous definition of aerosols, the term is often used in atmospheric chemistry literature to denote just the particles [Finlayson and Pitts (2000)]. Aerosols are formed by the conversion of gases to particles or by the disintegration of liquids or solids. They may also result from the resuspension of powdered material or the break up of agglomerates. Compared to trace gases, aerosols are relatively complex to characterize because of their multi-component chemical composition, and because of the large range in particle size, ranging from nanometers to several micrometers [Friedlander (2000), Dingenen et al (2004)].

Some aerosols contain microscopic solids or liquid droplets that are so small that they can penetrate deep into the lungs and cause serious health problems. Deposition probability of inhaled particles in the respiratory tract according to particle size is presented in Figure 1.

Numerous scientific studies have linked particle pollution exposure to a variety of problems, including; increased respiratory symptoms, such as irritation of the airways, coughing, or difficulty breathing; decreased lung function; and aggravated asthma; development of chronic bronchitis; irregular heartbeat; nonfatal heart attacks; premature death in people with heart or lung disease. The World Health Organization (WHO), estimated that particulate matter is considered to be responsible for 100 000 deaths and 750 000 life years lost annually in a selection of European cities (WHO 2004). The more recent estimates of the air pollution impact made within the European Commission 'Clean air for Europe' (CAFE) program found that about 350 000 people in the EU died prematurely in 2000 due to the outdoor air pollution caused by fine particulate matter ($PM_{2.5}$) alone. This corresponds to an average loss of life expectancy of about 9 months for every European Union (EU) citizen.

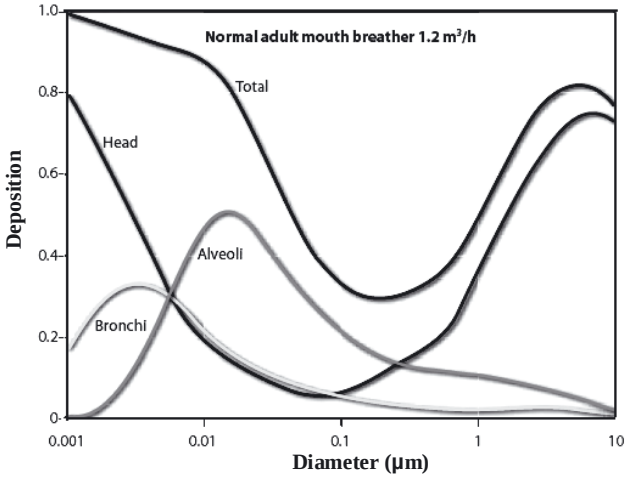

Figure 1: Deposition probability of inhaled particles in the respiratory tract according to particle size [WHO (2004)].

People with heart or lung diseases, children and older adults are the most likely to be affected by particle pollution exposure. However, healthy people may also experience temporary symptoms from exposure to elevated levels of particle pollution [www.epa.gov].

Studies on indoor air (e.g., Particle Total Exposure Assessment Methodology -PTEAM- study of United States' Environmental Pollution Agency (US EPA) and US EPA's Building Assessment and Survey Evaluation (BASE) study [www.epa.gov] have shown that particulate matter is a significant indoor pollutant. Indoor exposures to particulate matter can be significant, and there is inadequate information as to whether indoor particles originate outdoors or whether there is a substantial component from indoor sources that would add to the health impacts from particle exposure. One of the particular concerns is the particulate matter from indoor combustion appliances [US EPA Program Needs for Indoor Environments Research (2005)].

1.1. Expression and Classification of Particles

Particles are usually referred to as having a radius or a diameter, implying they are spherical. However, many particles have quite irregular shapes for which geometrical radii and diameters are not meaningful. Some means of expressing the size of such particles is essential since many important properties of the particle such as volume, mass, and settling velocity depend on the size.

One of the most commonly used means of expressing the size is the aerodynamic diameter [Finlayson and Pitts (2000)]. The aerodynamic diameter is the size of a unit-density (1 g/cm^3) sphere with the same aerodynamic characteristics. It is convenient to classify particles by their aerodynamic properties since it governs the transport and removal of particles from the air together with the deposition in the respiratory system. The aerodynamic diameter is also associated with the chemical composition and sources of particles [Flagan and Seinfeld (1988)]. Because of the effect of the particle density on the aerodynamic diameter, a spherical particle of high density will have a larger aerodynamic diameter than its geometric diameter. However, for most substances, ρ_p<10 so that the difference is less than a factor of ~3 [Finlayson and Pitts (2000)]. The three most commonly used aerodynamic diameters are Stokes diameter, Classical aerodynamic diameter and aerodynamic impaction diameter. [Flagan and Seinfeld (1988)]. The reader should visit the referred text books for further explanations.

Airborne particulate matter is composed of two principal groups based on mass and composition: coarse particles mostly larger than 2.5 μm in aerodynamic diameter, and fine particles mostly smaller than 2.5 μm in aerodynamic diameter ($PM_{2.5}$). The smaller particles contain the secondarily formed aerosols (gas-to-particle conversion), combustion particles and recondensed organic and metal vapours. The particles formed directly from the gas are usually smaller than 1μm in diameter. Soot consists of very fine particles agglomerating into larger ones after the flame. [WHO (2000), Flagan and Seinfeld (1988), Baumbach (1996)]

The fine particle mode can be further broken into particles with diameters between 0,08 and 1-2 μm, known as the accumulation range, and those with diameters between 0,01 and 0,08 μm, known as the transient or Aitken nuclei range. As the technology for measuring small particles has improved, ultrafine particles (sometimes referred as nano-particles), have also been increasingly studied. While there is no fixed definition of these particles, they are usually taken to mean those with diameters less than 0,01 μm [Baumbach (1996)].

A single aerosol particle may be composed of many chemical compounds and the entire aerosol may consist of mixed particles of differing composition. If particles all have the same chemical composition, the aerosol is said to be internally mixed. If the chemical components are segregated so that the particles are chemically different depending on their sources, the aerosol is said to be externally mixed. The two limiting cases can be distinguished by determining the chemical compositions of the individual particles [Friedlander (2000)].

Because the size of atmospheric particles play such an important role in both their chemistry and physics in the atmosphere as well as their effects, it is important to know the distribution of sizes. Real particle size distributions are the outcome of many competing processes – compensation, sedimentation, evaporation, agglomeration, impaction, gas to particle conversion. We can therefore expect the distribution to be very variable.

Particle size data can be displayed either graphically or through a table format. The distribution can be expressed by two methods: cumulative distribution or differential distribution. Differential distribution is the percentage of particles from the total that are within a specified sized range; for example, 30% within 1-10μm range, 50% within 10-20μm range, and 20% within 20-30μm range. Frequency can be plotted (on the Y-axis) by number count, surface area, or mass. Cumulative distribution is the sum of the differential distributions. The cumulative distribution is obtained by accumulation of differential distribution. For the previously given example, 30% of the particles are smaller than 10μm; 80% of the particles are smaller than 20μm and 100% of the particles are smaller than 30μm. The distribution is then plotted as the fraction of particles greater than or less than the corresponding diameter on the X-axis.

An obvious way to express the distribution of particle sizes found in the atmosphere would be to plot, in the form of a histogram, the number (ΔN) of particles found in certain arbitrarily chosen intervals of diameter (ΔD). However, since there tend to be a much greater number of small particles relative to large particles in the atmosphere, a linear plot of ΔN against ΔD would give what would be a narrow spike at the origin whose details could not be distinguished. Plotting the same data but with the horizontal axis on logarithmic scale, allows one to show a much larger particle size range than that which can be shown using a linear scale for the diameter.

For many manmade sources, the observed particulate matter distribution approximates a lognormal distribution. Thus atmospheric aerosol size distributions are usually presented graphically in terms of the logarithmic number distributions $n_n(\log D_p)$, the logarithmic surface area distributions $n_s(\log D_p)$, logarithmic volume distributions $n_v(\log D_p)$ or the logarithmic mass distributions $n_m(\log D_p)$. In situations for which a single log-normal distribution cannot represent the real data, several log-normal distributions may be combined. Whitby et al (1980) have indicated that the many atmospheric aerosol size distributions that they have measured under a variety of conditions and at many locations can be fit reasonably well assuming three additive log-normal distributions corresponding to Aitken nuclei

range, the accumulation range, and the coarse particle range, respectively. Each of these log-normal distributions has its own characteristic value of standard deviation, σ_g , as well as average diameters.

The number distribution is dominated by the smallest mode, and the volume or the mass distribution is dominated by the largest mode of particles. For instance a 10µm particle has 10^6 times the surface area of a 0,01µm particle, and 10^9 times the volume. Thus the area and the volume or mass dependencies can give very different significance to different diameters. There are often only two modes in the mass distribution of the atmospheric aerosols. Figure 2 presents the mass distribution of particles in ambient air [WHO (2000)]. The nucleation mode is still present in these distributions however the peak is not significant.

Number distributions while showing clearly changes in the particle number for smaller sizes, do not show the substantial changes in volume concentration associated with small changes in the number concentration for particles of D_p>1 µm. For example, National Ambient Air Quality Standards of the United States' Environmental Protection Agency [US EPA National Air Quality Guidelines (1996)]

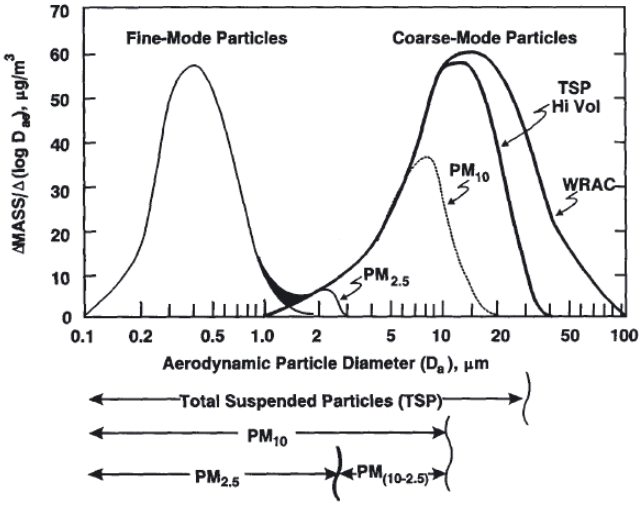

Figure 2: Schematic representation of the size distribution of particulate matter in ambient air [US EPA Air quality criteria for particulate matter (1996), World Health Organisation' Air quality guidelines for Europe (2000)]. TSP hi-vol, the high volume air sampler is U.S. EPA's Federal Reference Method for sampling total suspended particulates (TSP) in ambient air. WRAC, Wide Range Aerosol Classifier, is a size selective sampler for large particles.

for particles are expressed in terms of mass of PM_{10} and $PM_{2,5}$ per unit volume of air. It is thus important to know the mass distribution of atmospheric particulate matter. Similarly, surface and volume distributions are important when considering reactions of gases at the surface of particles or reactions occurring within the particle themselves. If one is interested in seeing the relationship of the various size ranges of the distribution to properties such as the surface area or volume, a better plot is one in which $dS/dlogD_p$ or $dV/dlogD_p$ is plotted on a linear ordinate versus $logD_p$ on the abscissa. From this type of plot, it is much easier to discern modes in the distribution and to see the relative number, surface area, or mass in the different size ranges of the distribution. [Baumbach (1996), Seinfeld (1986)].

1.2. Sources of Particles

$PM_{2.5}$ is composed of particles that are directly emitted and particles that are products of chemical reactions of gases in the atmosphere. Particles emitted directly from a source are referred as *primary particles*. Examples of primary particles (both $PM_{2.5}$ and larger, or "coarse," particles) include those from combustion sources such as residential wood combustion; agricultural open burning, coal and oil fired power plants and industries, as well as dust particles from roads, fields and construction sites. Particles formed via complicated reactions in the atmosphere of chemicals such as sulfur dioxides and nitrogen oxides that are emitted from power plants, industries and automobiles are referred as *secondary particles*. The majority of the secondary particles in many areas of US are from gases from fuel combustion in automobiles, trucks, and power plants such as sulfur dioxide (SO2) and nitrogen oxides (NOx) released by anthropogenic and natural sources [www.epa.gov].

Atmospheric particles in the accumulation range with diameters from ~0.08 to ~1.2 μm typically arise from condensation of low-volatility vapours (e.g following combustion) and from coagulation of smaller particles in the nuclei range either with themselves or, more likely with the larger particles in the accumulation range. The coagulation rates for particles in the nuclei range with the larger particles in the accumulation range are usually much larger than for self-coagulation of the small particles; this occurs because of the high mobility of the smaller particles combined with the larger target area of the bigger particles.

The Aitken nuclei, with $0,01<D<0,08\mu m$, arise from ambient-temperature gas to particle conversion as well as combustion processes in which hot, supersaturated vapours are formed and subsequently undergo condensation. These particles act as nuclei for the condensation of low-vapour-pressure

gaseous species, causing them to grow toward the accumulation range; alternatively, these nuclei may grow larger by coagulation.

High-temperature combustion sources produce particles in the Aitken nuclei and the accumulation mode. For example, the mass median diameters of particles emitted from a variety of combustion sources, including incinerators, coal-and oil fired boilers, automobiles and trucks, typically fall in the range of 0,05 – 0,35 μm [Hildemann et al (1991)]. The relative numbers of particles produced in the Aitken Nuclei range compared to the accumulation range depend on the nature of the combustion process as well as the conditions of dilution. Because the particles generated in high-temperature combustion processes contain hydroscopic compounds, water vapour can be taken up or evapourate, depending on the atmospheric conditions. The condensed-phase water provides a medium for atmospheric reactions that generate low-volatility species ; the best known example is the oxidation of SO_2 to sulphate.

As discussed by Hughes and co-workers, although nucleation mode particles do not contribute a large amount (only ~1 μg/ m^3) to the particulate mass, about 10^{11} of these ultrafine particles will be deposited in one day in the respiratory tract of a typical person breathing this air. Hence if toxicological effects are determined primarily by the number of particles, rather than their mass, these ultrafine particles could ultimately prove to be quite important.

In developing countries with high mortality rates overall, indoor air pollution ranks fourth in terms of the risk factors that contribute to disease and death; due to inefficient and poorly ventilated stoves burning biomass fuels such as wood, crop waste and dung, or coal [WHO (2002)]. In the last several years, a growing body of scientific evidence has indicated that the air within homes and other buildings can be more seriously polluted than the outdoor air in even the largest and most industrialized cities. Other research indicates that people spend approximately 90 percent of their time indoors. Thus, for many people, the risks to health may be greater due to exposure to air pollution indoors than outdoors [www.epa.gov].

Inadequate ventilation can increase indoor pollutant levels by not bringing in enough outdoor air to dilute emissions from indoor sources and by not carrying indoor air pollutants out of the home. Outdoor air enters and leaves a house by: infiltration, natural ventilation, and mechanical ventilation. In a process known as infiltration, outdoor air flows into the house through openings, joints, and cracks in walls, floors, and ceilings, and around windows and doors. In natural ventilation, air moves

through opened windows and doors. Air movement associated with infiltration and natural ventilation is caused by air temperature differences between indoors and outdoors and by wind. Finally, there are a number of mechanical ventilation devices, from outdoor-vented fans that intermittently remove air from a single room, i.e bathrooms and kitchen; to air handling systems that use fans and duct work to continuously remove indoor air and distribute filtered and conditioned outdoor air to strategic points throughout the house. The rate at which outdoor air replaces indoor air is described as the air exchange rate. When there is little infiltration, natural ventilation, or mechanical ventilation, the air exchange rate is low and pollutant levels can increase [US EPA The Inside Story (2008)].

1.3. Current Legislations

When particles are measured as mass, the greatest contribution comes from the largest particles, but the greatest number of particles by far is the submicron ones. The relevance of particle mass, surface area or number concentration as risk indicators for health effects in non-industrial buildings has been assessed by a European interdisciplinary group of researchers called EUROPART [EUROPART (2003)] by reviewing papers identified in Medline, Toxline and OSH. Excluding the studies dealing with dermal effects or cancer or specifically addressing environmental tobacco smoke, house dust mite, cockroach or animal allergens, micro organisms and pesticides, a total of 70 papers were reviewed and 8 were identified for the final review: Five experimental studies involving mainly healthy subjects, two cross sectional office studies and one longitudinal study among elderly on cardiovascular diseases. The EUROPART group concluded that there is inadequate scientific evidence that airborne, indoor particulate mass or number concentrations can be used as generally acceptable risk indicators of health effects in non-industrial buildings and there is inadequate scientific evidence for establishing limit values or guidelines for particulate mass or number concentrations.

The WHO air quality guidelines (AQGs) are intended for worldwide use but have been developed to support actions to achieve air quality that protects public health in different contexts. Air quality standards, on the other hand, are set by each country to protect the public health of their citizens. National standards vary according to the approach adopted for balancing health risks, technological feasibility, economic considerations and various other political and social factors, which in turn depends on, among other things, the level of development and national capability in air quality management.

First produced in 1987, revised in 1997 and updated in 2005, *Air quality Guidelines for Europe* are based on expert evaluation of current scientific evidence, given the wealth of new studies on the health effects of air pollution that have been published in the scientific literature, including important new research from low-and middle-income countries where air pollution levels are at their highest. Several key findings that have emerged in recent years merit special mention; especially the evidence for particulate matter (PM) indicates that there are risks to health at concentrations currently found in many cities in developed countries. Moreover, as research has not identified thresholds below which adverse effects do not occur, it must be stressed that the guideline values provided by WHO cannot fully protect human health. In fact, the low end of the range of concentrations at which adverse health effects has been demonstrated is not greatly above the background concentration, which for particles smaller than 2.5 μm ($PM_{2.5}$) has been estimated to be 3 – 5 $\mu g/m^3$ in both the United States and western Europe. The updated guideline values for particulate matter are given by WHO as:

$PM_{2.5}$: 10 $\mu g/m^3$ annual mean ; 25 $\mu g/m^3$ 24-hour mean
PM_{10}: 20 $\mu g/m^3$ annual mean ; 50 $\mu g/m^3$ 24-hour mean

At present, most routine air quality monitoring systems generate data based on the measurement of PM_{10} as opposed to other particulate matter sizes. Consequently, the majority of epidemiological studies use PM_{10} as the exposure indicator. PM_{10} represents the particle mass that enters the respiratory tract and, moreover, it includes both the coarse (particle size between 2.5 and 10 μm) and fine particles (measuring less than 2.5 μm, $PM_{2.5}$) that are considered to contribute to the health effects observed in urban environments. The former is primarily produced by mechanical processes such as construction activities, road dust re-suspension and wind, whereas the latter originates primarily from combustion sources. In most urban environments, both coarse and fine mode particles are present, but the proportion of particles in these two size ranges is likely to vary substantially between cities around the world, depending on local geography, meteorology and specific PM sources. In some areas, the combustion of wood and other biomass fuels can be an important source of particulate air pollution, the resulting combustion particles being largely in the fine ($PM_{2.5}$) mode. Although few epidemiological studies have compared the relative toxicity of the products of fossil fuel and biomass combustion, similar effect estimates are found for a wide range of cities in both developed and developing countries. It is, therefore, reasonable to assume that the health effects of $PM_{2.5}$ from both of these sources are broadly the same. By the same token, the WHO AQG for PM can also be applied to the indoor environment, specifically in the developing world, where large populations are exposed to high levels of combustion particles derived from indoor stoves and fires [WHO (2005)].

Ultrafine particles (UF), i.e. particles smaller than 0.1μm in diameter, have recently attracted significant scientific and medical attention. These are usually measured as a number concentration. While there is considerable toxicological evidence of potential detrimental effects of UF particles on human health, the existing body of epidemiological evidence is insufficient to reach a conclusion on the exposure–response relationship of UF particles. Therefore no recommendations can be provided as to guideline concentrations of UF particles.

In the United States (US), the air quality standards for particulate matter were first established in 1971 and were not significantly revised until 1987, when Environmental Protection Agency (EPA) changed the indicator of the standards to regulate inhalable particles smaller than, or equal to, 10 micrometers in diameter. Ten years later, after a lengthy review, EPA revised the PM standards, setting separate standards for fine particles ($PM_{2.5}$) based on their link to serious health problems ranging from increased symptoms, hospital admissions and emergency room visits for people with heart and lung disease, to premature death in people with heart or lung disease. Recently –in 2006, EPA revised the air quality standards for particle pollution, as presented in Table 1. The 2006 standards tighten the 24-hour fine particle standard from 65 micrograms per cubic meter ($\mu g/m^3$) to 35$\mu g/m^3$, and retain the annual fine particle standard at 15 $\mu g/m^3$. The Agency decided to retain the existing 24-hour PM_{10} standard of 150 $\mu g/m^3$. The Agency revoked the annual PM_{10} standard, because available evidence does not suggest a link between long-term exposure to PM_{10} and health problems. The Clean Air Act requires EPA to review the latest scientific information and standards every five years. Before new standards are established, policy decisions undergo rigorous review by the scientific community, industry, public interest groups, the general public and the Clean Air Scientific Advisory Committee (CASAC).

Table 1: National Ambient Air Quality Standards of US EPA for Particle Pollution

Pollutant	Primary Stds.	Averaging Times
Particulate Matter (PM_{10})	Revoked [1]	Annual [1] (Arith. Mean)
	150 $\mu g/m^3$	24-hour [2]
Particulate Matter ($PM_{2.5}$)	15.0 $\mu g/m^3$	Annual [3] (Arith. Mean)
	35 $\mu g/m^3$	24-hour [4]

Units of measure for the standards are micrograms per cubic meter of air ($\mu g/m^3$). Footnotes:
(1) - Due to a lack of evidence linking health problems to long-term exposure to coarse particle pollution, the agency revoked the annual PM_{10} standard in 2006 (effective December 17, 2006).
(2) - Not to be exceeded more than once per year on average over 3 years.
(3) - To attain this standard, the 3-year average of the weighted annual mean $PM_{2.5}$ concentrations from single or multiple community-oriented monitors must not exceed 15.0 $\mu g/m^3$.
(4) - To attain this standard, the 3-year average of the 98th percentile of 24-hour concentrations at each population-oriented monitor within an area must not exceed 35 $\mu g/m^3$ (effective December 17, 2006).

1.4. Measurement of Particulate Matter

Appropriate measurement of airborne particulate matter presents problems, since it is not known for sure which of its various components are responsible for its observed harmful effects. Most measurements in the past have been of mass, either indirectly as Black Smoke or directly as the weight of particles below a certain size. Lately, there has been interest in counting the number of particles below a certain diameter. There is increasing interest in the so-called ultrafine particles, for which the common metric is the particle number concentration.

Ambient particulate matter contains inorganic elements and ions, including trace metals, as well as graphitic (elemental) carbon and a wide variety of organic compounds and water. A wide variety of methods are available to measure their concentration. Some common methods used to measure selected inorganic elements and ions in atmospheric particles are presented in Table 2. A number of inter-comparison studies are available in literature, reporting relatively good agreement between different methods of elemental analysis for atmospheric particles, with many of the observed discrepancies being due to differences in sampling rather than analysis. When it comes to carbon, despite it has been addressed in a number of ways by many workers over a period of years, there is still no accepted accurate and reliable standard method of sampling and analysis for the separate determination of organic and elemental carbon in atmospheric particles. Thermal methods, digestion, extraction and optical techniques are the major methods that have been used to separate the organic and elemental carbon. [Finlayson and Pitts (2000), Cadle et al (1983)]

Table 2: Common methods to measure selected inorganic elements & ions in atmospheric particles

	XRF	PIXE	Col	AA	NA	ASV	MS	ES	ESCA	ICP[1]	IC[1]	SIE[1]	IR[1]
Aluminum	+	+		+	+					+			
Copper	+	+		+	+	+	+	+		+			
Iron	+	+	+	+	+	+	+	+		+			
Lead	+	+	+	+		+	+	+	+	+			
Nickel	+	+		+	+		+	+		+			
Nitrogen									+				
Sulfur	+	+			+		+		+	+			
Zinc	+	+		+	+	+	+	+		+			
NH_4^+			+						+		+	+	+
SO_4^-			+						+		+		+
NO_3^-			+						+		+	+	+

1.)XRF: X-ray Fluorescence analysis; 2.)PIXE: Particle-induced X-ray Emission; 3.)Col: Colorimetry; 4.) AA: Atomic Absorption Spectrometry; 5.)NA: Neutron Activation Analysis; 6.)ASV: Anodic Stripping Voltammetry; 7.)MS:Mass Spectrometry; 8.)ES: Emission Spectrometry; 9.)ESCA: Electron Spectroscopy for Chemical Analyses (X-ray photoelectron spectroscopy); 10.)ICP: Inductively coupled plasma spectroscopy; 11.)IC: Ion Chromatography; 12.) SIE: Selective Ion Electrodes; 13.) IS: Infrared Spectroscopy

Particle concentrations can be measured as mass (weight) of particles within a certain size range; as the number of particles; as the mass of one or several chemicals; or as a specific surface area, all in a given volume of air. There are two basic approaches to the measurement of aerosol particles. The traditional approach is to sample the particles onto a collection surface and then analyze the collected particles in the laboratory. The principal drawback of the sample collection techniques is the long time delay between sampling and the subsequent analysis. Since collected samples represent specific time intervals, the lack of time resolution in concentration and size distribution are additional drawbacks. Chemical reactions of the collected particles may bias the sample, especially when unstable aerosols are studied. The other approach is to sample the aerosol directly into a real-time, dynamic measuring instrument [Baron and Heitbrink (1993)]. A serious gap in aerosol instrumentation is the lack of instruments for online measurement of aerosol chemical constituents without removing them from the gas. Very large amounts of information would be generated by an instrument capable of continuously sizing and chemically analyzing each particle individually, thereby permitting the determination of the size-composition probability density function. From this function, in principle, many of the chemical and physical properties of aerosols can be obtained by integration. Progress has been made in the development of such a system based on mass spectroscopy.

Mass concentrations are often determined by filtering the gas at a known flow rate and weighing the filter before and after filtration under conditions of controlled humidity. Samples are also collected by filtration for chemical analysis. The principal mechanisms of particle deposition for both fibrous and membrane filters are the diffusion and impaction of particles of finite diameter. Settling and electrostatic effects may contribute to removal. Filter efficiencies are often reported for 0.3 μm particles, because these fall in the size range corresponding to the minimum in the efficiency curve [Friedlander (2000)].

High efficiency filtration is the most common method of collecting particulate matter for the determination of chemical composition. Chemical analysis of filter sample provides information on the composition of the aerosol averaged over all particle sizes and over time interval of sampling. In practice, the average composition of the particles in a discrete size interval is determined by collecting an aerosol sample over a period of several hours using a cascade impactor and analyzing the material on each stage chemically. The cascade impactor is the instrument most frequently used for the classification of aerosol particles according to size for subsequent chemical analysis. The individual levels do not have perfectly separating lines, but each level can be assigned a grain diameter for which the separation probability amounts to 50%. [Friedlander (2000)].

Average concentrations for a given size range may give a misleading impression of particulate effects, however. In the case of lung deposition, for example, the local dosage to tissue may depend on the composition of individual particles. The nucleating properties of a particle for the condensation of water and other vapours also depend on the chemical nature of the individual particles. For detailed information on the size and morphological characteristics of particulate matter, there is no substitute for microscopy, provided that sampling and observation do not modify the particle physically and/or chemically. However for routine monitoring and for studies of aerosol dynamics, it is usually more convenient to use calibrated continuous automatic counters.

The recent research and development in the field has improved the capabilities of the existing methods while developing new methods, especially in regards to detection of the submicron particles. In the past, optical instruments were known to be good for particles of sizes between 0,1 and 10 μm, and devices based on diffusion and electrical mobility for submicron particles, especially those smaller than 0,1 μm that cannot be measured easily by either inertia or the optical –type instruments [Friedlander (2000)]. Today, however, optical methods are capable of detecting nanoparticles and soot. The state-of-the-art of in-situ laser based combustion diagnostics, including particle characterization can be found in the book by Kohse-Höinghaus and J. B. Jeffries (2002) [D'Anna (2008), Lucht (2003)]. In the recent years, combined spectral optical techniques [D'Anna et al (2007), Commodo et al (2007)], time resolved fluorescence polarization anisotropy [Bruno et al (2005), Bruno et al (2006), de Lisio et al (2006), Bruno et al (2008)] photoionisation mass spectrometry [Thierley et al (2007), Happold et al (2007)], infrared analysis [Rusciano et al (2006)] and surface-enhanced Raman scattering [Rusciano et al (2008)] have found applications in the characterization of combustion generated nanoparticles and soot. A review of the different techniques is available from D'Anna (2008). Microscopy methods such as atomic forced microscopy (AFM) and transmission electron microscopy (TEM) combined with X-ray energy dispersive spectroscopy (EDS) have as well found applications in morphology and composition studies of submicron particles [Barone et al (2003), D'Alessio et al (2005), Murr and Soto (2005), Abid et al (2008), Etissa et al (2008)].

Since the commercialization of the scanning electrical mobility spectrometer of Wang and Flagan (1990) with the name Scanning Mobility Particle Sizer (SMPS) Spectrometer, SMPS has been increasingly used for particle studies to determine the size distribution functions of the particles in combustion and emission studies. Instruments are available which count all particles down to 2.5 nm diameter [www.tsi.com]. In practice, the number count is dominated by particles of less than 0.1 μm diameter, hence reflecting freshly formed or emitted nucleation mode particles together with part of

the accumulation mode [Expert Panel on Air Quality Standards (2001)]. In response to the discussions that the commercial instruments loose their sensitivity for nanoparticles smaller than 5 nm because they employ a condensation particle counter (CPC) detector that is totally insensitive to particles smaller than 3–2.5 nm as well as a flow configuration in the electrostatic classifier that is subject to significant losses of particles and resolution due to Brownian motion for particles or molecular clusters having only a few nanometers, Sgro et al (2007) showed that DMAs of particular design can be employed for the size range of particles smaller than 3 nm with good agreement with optical measurements. This is an important result since DMAs can be used to evaluate the performance of practical combustion systems (engines and industrial burners) and particle size distributions in the atmosphere, where optical measurements are difficult or impossible.

1.4.1. Scanning Mobility Particle Sizer (SMPS)

The SMPS spectrometer is a system that measures the size distribution of aerosols in the sub-micrometer size range. Particles are classified with an Electrostatic Classifier and their concentration is measured with a Condensation Particle Counter (CPC). The SMPS spectrometer also uses a personal computer and custom software to control individual instruments and perform data collection and analysis.

The SMPS spectrometer uses a bipolar charger in the Electrostatic Classifier to charge the particles to a known charge distribution. The particles are then classified according to their ability to traverse an electrical field in the DMA, and counted with the CPC.

Total particle number concentrations of particles in the size range from a few nanometres to 1 μm are measured using a Condensation Particle Counter (CPC) alone. As an aerosol is introduced into the CPC, it is saturated with alcohol vapour as it passes over a heated pool of alcohol. The vapour-saturated aerosol than flows into a cold condenser where it is cooled by thermal diffusion. The vapour condenses on the particles and the particles grow into droplets large enough to be counted optically in the size range from 5 to 15 μm. The systems differ according to (a) condensable vapour, (b) the method of producing super-saturation and (c) the detection scheme. The lower limit of particle size detection, generally between 3 and 10 nm, results from the enhanced vapour pressure above small particles and non-uniformities in concentrations of the condensable vapour [Friedlander (2000)].

The saturation ratio is defined as the ratio of actual vapour partial pressure, P, to the saturation vapour pressure, P_s, at a given temperature. The saturation ratio of the condensing vapour thus determines the smallest particle size detected by the CPC. The relationship between the saturation ratio and the minimal particle size is controlled by the Kelvin Equation (Equation 1):

Equation 1:
$$\frac{P}{P_s} = \exp\left[\frac{4\sigma M}{\rho RTd^*}\right]$$

where

σ: the surface tension

M: molecular weight

ρ: the density of the liquid

d*:the Kelvin diameter

R: universal gas constant

T: absolute temperature

The Kelvin diameter is the droplet diameter that will neither grow nor evapourate at the saturation ratio. For every droplet size, there is a saturation ratio that will exactly maintain the particle size. If the saturation ratio is too small, the particle evapourates, if it is too great, the particle grows.

1.5. Aerosol Transport Properties

In the text books by Seinfeld (1986) , Flagan and Seinfeld (1988) and Friedlander (2000) aerosol transport processes and their properties are explained in detail. Here, the author presents a short summary of the basics of aerosol transport processes.

Fluids resist the motion of particles travelling through them. As long as the particle is not moving in a vacuum, the drag force will always be present. For a sphere moving vertically through a fluid under the influence of gravity, the drag force is in the opposite direction of the velocity of the object, tending to retard the motion of the object. Therefore, an upwardly moving sphere will have a downward drag force and a downwardly moving sphere will have an upward drag force, as shown in Figure 3.

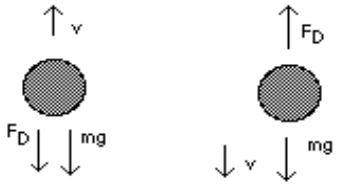

Figure 3: The drag force on a sphere moving vertically through a fluid under the influence of gravity

Particles suspended in a fluid undergo irregular random motion due to bombardment by surrounding fluid molecules. Brownian motion is the name given to such motion. A particle of sufficiently large size would experience only the drag force and its motion would be more or less unaffected by molecular bombardment. As the particle decreases in size, the fluctuations in its motion due to molecular bombardment become increasingly noticeable until at last the particle acts as if its Brownian motion is the chief motion of the particle [Seinfeld (1986)].

The relative importance of Brownian diffusion as compared to gravitational settling can be judged by comparing the distances that a particle travels in both cases. Over a time of 1s, a 1 μm radius particle diffuses a distance of the order of 4μm, while it falls about 200μm under gravity. A 0,1 μm radius particle, on the other hand, diffuses a distance of about 20 μm in 1s compared to a fall distance of 4 μm. For a 0,01 μm radius particle, Brownian diffusion further outweighs gravity; its diffusive displacement in 1 s is almost 1000 times its displacement due to gravity, and several weeks would be required for the small orderly gravity effect to equal that of the random Brownian motion [Seinfeld (1986)].

The movement of particles due to Brownian motion can be described as a diffusion process. The number concentration N of particles undergoing Brownian motion can be assumed to be governed by the diffusion equation (Equation 2):

Equation 2:
$$\frac{\partial N}{\partial t} = D\nabla^2 N$$

where D is the Brownian diffusivity given by the Stokes-Einstein relation (Equation 3).

Equation 3:

$$D = \frac{kTC_c}{3\pi\mu D_p}$$

Diffusion coefficients for particles ranging from 0.001 to 10.0 μm diameter in air at 20°C are presented in Figure 4. The rate at which they diffuse depends on the concentration gradient, dN/dx, the larger the gradient, the faster the rate of diffusion.

Equation 4:

$$J = -D\frac{\partial N}{\partial x}$$

The rate of transport of particles across a surface at a point, expressed as number per unit time per unit area, is called the flux at the point. Common dimensions for the flux are particles/cm2.sec. The presence of an external force field acting on the particles leads to an additional term in the flux (Friedlander, 2000).

Diffusional transport in flowing fluids is called convective diffusion. Particle deposition by this mechanism is of fundamental importance since the collection efficiency by diffusion for particles smaller than abut 0.5 μm increases with decreasing particle size.

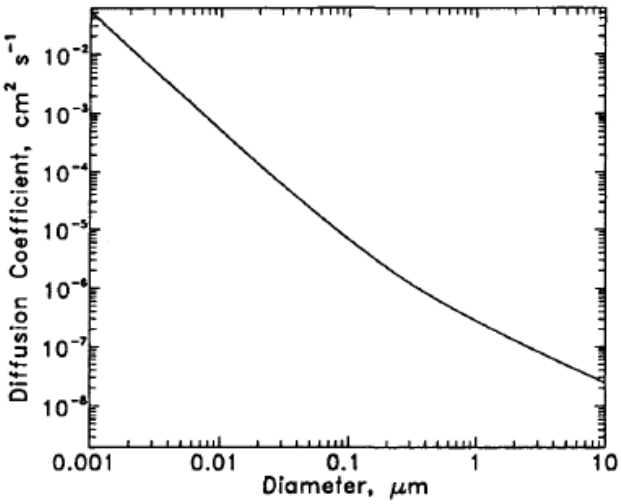

Figure 4: (Calculated) Aerosol diffusion coefficients in air at 20°C as a function of diameter [Seinfeld and Pandis (2006)].

In order to describe the transport processes involving momentum, mass and energy, it is required to reflect how the fluid views the particle. The key dimensionless group which defines the nature of the suspending fluid relative to the particle is the Knudsen number (Equation 5)

Equation 5:

$$Kn = 2\lambda / D_p$$

where λ is the mean free path of the fluid – the average distance travelled between collisions. The mean free path cannot be measured directly; rather its value is inferred from that of a measurable macroscopic property, such as viscosity, thermal conductivity, or molecular diffusivity [Flagan and Seinfeld (1988), Seinfeld (1986)].

If the interest is to characterize the nature of the suspending air relative to the particle, the mean free path that appears in the definition of the Knudsen number is λ_{air}. If the particle radius greatly exceeds λ_{air} (Kn<<1), then the air appears to the particle as a continuum and the particle is said to be in *continuum regime*, and the usual equations of continuum mechanics apply. When the mean free path of air molecules substantially exceeds the particle radius (Kn>>1), the particle exists in a more or less rarified medium, which is called as the *free molecule* or *kinetic regime* and its transport properties are obtained from kinetic theory of gases. The particle size range intermediate between these two extremes is called the *transition range* [Flagan and Seinfeld (1988), Seinfeld (1986)].

The mean free path of air can be calculated from kinetic theory of gases (Equation 6) :

Equation 6:

$$\lambda_{air} = \frac{\mu}{0,499P\sqrt{8M/\pi RT}}$$

where

λ_{air} : mean free path of air (meters),
P: fluid pressure (Pascal),
M: molecular weight of the gas,
μ: gas viscosity.

The mean free path of air molecules at 298 ^{o}K and 1 atm is calculated as 0.0651 μm by the above formula. Thus in air at standard conditions, particles with radii exceeding 0.2 μm or so can be considered, from the point of view of transport properties, to be in the continuum regime. Similarly, the particles with radii about 0.01 μm or smaller can be computed from free molecule kinetic theory. The transition regime would span the range of particle radii approximately from 0.01 to 0.2 μm [Flagan and Seinfeld (1988)].

If the interest is the diffusion of a vapour molecule A toward a particle in the same background gas B, then the value of Knudsen number is defined on the basis of λ_{AB}, the average distance travelled by a molecule of A before it encounters a molecule of B (Equation 7). The particle mean free path λ_p and the particle diffusion Knudsen number are defined by Equation 8 and Equation 9.

Equation 7: $$Kn = \frac{2\lambda_{AB}}{D_p}$$

Equation 8: $$\lambda_p = \frac{2kT}{3\pi\mu\overline{c_p}D_p}$$

Equation 9: $$Kn_p = \frac{4kTC_c}{3\pi\mu\overline{c_p}D_p^2}$$

where k is the Boltzmann's constant, C_c is the Cunningham correction factor and c_p is the mean thermal speed of particle with mass m_p, given by Equation 10.

Equation 10: $$\overline{c_p} = \sqrt{\frac{8kT}{\pi m_p}}$$

1.6. Sampling of Aerosols

The two widely used methods for sampling the high- temperature mixture of gases, particles, and inorganic vapours in which the formation of the particles takes place are extraction and thermophoresis. The extraction method usually employed, i.e., dilution of the sampled gases in an inert, cold gas (typically N_2), is expected to assure the quenching of chemical reactions by a rapid

temperature decrease accompanied by a reduction of the partial pressure of the reactants. This technique, suitable for most applications (e.g., sampling of gases or charring particles in flames), when applied to post-combustion gases, necessarily implies gas-to- particle conversion of the inorganic vapours present. This unavoidable artefact may lead to an unacceptable distortion of the actual particle population and characteristics at the sampling point [Jimenez and Ballester (2005)].

Thermophoretic sampling, as its name implies, adopts thermophoresis for collecting particles in hot gases such as flames. Small particles in a temperature gradient moves from the high temperature region to the low temperature region [Friedlander (2000)]. When a cold plate, normally 3–5mm wide and 0.1–4.0mm thick, is inserted into a hot flame for nominally 0.1 s, particles are deposited on the cold grid due to the thermophoretic effect [Lee et al (2008)]. Thermophoretic velocity, v_T is given by Equation 11.

Equation 11:
$$v_T = Th\frac{\mu}{\rho T}\frac{dT}{dx}$$

where Th is the thermal dimensionless group and dT/dx is the temperature gradient (always<0) in the direction of motion. The dimensionless group Th is essentially constant for those particles for which Kn>>1, indicating that v_T is independent of particle size, directly proportional to the temperature gradient, and only weakly dependent on temperature. The value of Th is predicted theoretically to lie between 0.42 and 1.5, with experimental measurements in the range 0.5 [Flagan and Seinfeld (1988)]. For larger particles, Kn<<1, Th becomes a function of Kn as well as the ratio of the thermal conductivities of gas and particle.

Thermophoretic sampling has been widely used in studies of particle formation in flames and internal combustion engine, with the advantage of an almost constant collection efficiency over a sufficiently broad size range. It is usually based on the rapid immersion of a cold plate (e.g., a TEM grid) into the flame, where particles are collected by thermophoresis. Hence, this might seem a method suitable for the study of fine-particle formation in postcombustion gases. Two difficulties arise, however, when trying to apply this technique to the postcombustion gases in which condensable species appear in significant amounts:

1. the temperature gradient may promote condensation/nucleation of these species, thus altering the sample properties,

2. the low particle concentration imposes relatively long collection times (of the order of seconds), and a cooling system is required to avoid probe damage.

Jimenez and Ballester (2005) identified and compared different artifacts caused by the use of three different probes, respectively based on aerodynamic quenching, N_2 dilution, and thermophoresis, for particle sampling in biomass postcombustion gases from a laboratory reactor at different temperatures (from 1300 to 560◦C). While the classical dilution sampling resulted in the formation (inside the probe) of particles comparable in size and composition to those already existing in the sampled gases, the aerodynamic quenching particle sampling (AQPS) probe always caused the nucleation of vapours into very small (15–20 nm) particles. The difference is attributed to the much higher cooling rate (10^8 K/s) at the entrance of the probe. The preliminary results of their thermophoretic probe also revealed significant deviations between the collected sample and the actual particle population in the sampled gas. In general, their results highlighted the difficulties in obtaining representative samples in this type of systems, as well as the existence of a variety of possible sampling artefacts, whose interpretation is not straightforward.

Using the broad band UV absorption and fluorescence features, Sgro et al (2001) investigated the similarity between the UV-visible spectra observed in situ in rich ethylene air flames and the spectra of extra situ sampled material trapped in water; in order to evaluate the ability of the extra situ technique to isolate the 2±5 nm carbonaceous material, identified by broad band UV absorption and fluorescence features. Their study showed that combustion generated organic carbon particulate can be extracted from flames and isolated from other flame material for further chemical analysis. Following the latter, D'Anna (2008) and Minutola et al (2008) used a water-based sampling technique to collect fine organic aerosol emitted at the exhaust of the home heating burners operated in free atmosphere and in commercial boilers, as well as at the exhaust of cook top burners. Combustion products, sampled by a probe in the exhaust pipe, were cooled in order to condense combustion water and drawn through a reservoir containing deionised water, placed in an ice bath. The sampling of organic carbon produced by the cook-top burner was collected prevalently by bubbling the exhausts in a reservoir containing water, since the combustion water condensed during the sampling time was very low. Water samples, put in a standard 1 cm path-length quartz cell, were than analyzed by light absorption and UV-induced fluorescence measurements.

1.7. References

Abid, A.D., Heinz, N., Tolmachoff, E.D, Phares, D.J., Campbell, C.S., Wang, H. (2008), On evolution of particle size distribution functions of incipient soot in premixed ethylene-oxygen-argon flames, Combustion and Flame, 154 (4) , p. 775-788.

Baron P.A and Heitbrink W.A. (1993), Factors affecting aerosol measurement and quality, In: Aerosol Measurement edited by Baron P.A and Willeke K, Van Nostrand Reinhold, New York, p130-200.

Barone, A.C.; D'Alessio, A.; D'Anna, A. (2003), Morphological characterization of the early process of soot formation by atomic force microscopy, Combustion and Flame, 132 (1) , p. 181-187.

Baumbach G. (1996), Air Quality Control, Springer-Verlag, Berlin, ISBN 3-540-57992-3, p.23-39.

Bruno, A., De Lisio, C., Minutolo, P.(2005), Time resolved fluorescence polarization anisotropy of carbonaceous particles produced in combustion systems, Optics Express, 13 (14) , p. 5393-5408.

Bruno, A; de Lisio, C ; Minutolo, P; D'Alessio, A, (2006), Characterization of ultrafast fluorescence from nanometric carbon particles, Journal of Optics A: Pure and Applied Optics, (7), p. S578-S584.

Bruno, A., Ossler, F., De Lisio, C., Minutolo, P., Spinelli, N., D'Alessio, A. (2008), Detection of fluorescent nanoparticles in flame with femtosecond laser-induced fluorescence anisotropy, Optics Express,16 (8) , p. 5623-5632.

Cadle, S.H., P.J.Groblicki, and P.A. Mulawa (1983), Problems in the Sampling and Analysis of Carbon Particulate, Atmospheric Environment, 17: 593-600.

Commodo, M.; Violi, S.; D'Anna, A.; D'Alessio, A.; Allouis, C.; Beretta, F.; Minutolo, P. (2007), Soot and nanoparticle formation in laminar and turbulent flames, Combustion Science and Technology, 179 (1) , p. 387-400.

D'Alessio, A.; Barone, A.C.; Cau, R.; D'Anna, A.; Minutolo, P., Koylu, U., Shaddix, C., Frenklach, M., Rosner, D.E. (2005), Surface deposition and coagulation efficiency of combustion generated nanoparticles in the size range from 1 to 10 nm, Proceedings of the Combustion Institute, 30 (2) , p. 2595-2603.

D'Anna, A.; Commodo, M.; Violi, S.; Allouis, C., Kent, J. (2007), Nano organic carbon and soot in turbulent non-premixed ethylene flames, Proceedings of the Combustion Institute 31 (1) , p. 621-629.

D'Anna, A. (2008), Combustion – Formed Nanoparticles, Manuscript for the invited topical review at the 32nd International Symposium on Combustion, Montreal, Canada.

De Lisio, C.; Bruno, A.; Alfe, M.; Apicella, B.; Minutolo, P. (2006), Characterization of nanometric carbon materials by time-resolved fluorescence polarization anisotropy, Optics and Lasers in Engineering, 44 (7) , p. 732-46.

Dingenen R.V. et al (2004), "A European aerosol phenomenology- 1: physical characteristics of particulate matter at kerbside, urban, rural and background sites in Europe", Atmospheric Environment, 38, 2561–2577 .

Etissa, D.; Mohr, M.; Schreiber, D.; Buffat, P.A. (2008), Investigation of Particles Emitted From Modern 2-Stroke Scooters, Atmospheric Environment, 42 (1) , p. 183-195.

EUROPART (2003), Indoor Air, 13: 38-48

Expert Panel on Air Quality Standards Airborne Particles (2001), What is the appropriate measurement on which to base a standard? A Discussion Document - ISBN 0117535990, http://www.defra.gov.uk/environment/airquality/aqs/air_measure/ index. htm.

Finlayson B. J, Pitts J.N (2000) , Chemistry of the Upper and Lower Atmosphere, Academic Press, New York, ISBN 012257060X, p. 351 -362.

Flagan R. and Seinfeld J. (1988), Fundamentals of Air Pollution Engineering, Prentice Hall, ISBN 0-13-332537-7, New Jersey, p.290-344.

Friedlander S.K. (2000), Smoke, Dust, and Haze: Fundamental of Aerosol Dynamics, 2nd Edition Oxford University Press, New York, ISBN 0-19-512999-7, p. 1, 5, 23, 171.

Happold, J., Grotheer, H., Aigner, M.(2007), Distinction of gaseous soot precursor molecules and soot precursor particle s through photoionization mass spectrometry, Rapid Communications in Mass Spectrometry, 21 (7) , p. 1247.

Hildemann L.M., Markowski G.R., and Cass G.R (1991) Chemical composition of emissions from urban sources of fine organic aerosol, Environmental Science and Technology: 25: 744–759.

Knutson, E.O., and Whitby, K. T. (1975). Aerosol Classification by Electrical Mobility: Apparatus, Theory, and Applications, Journal of Aerosol Science, 6, 431–451.

Lee J., Altman I.,Choi M. (2008), Design of thermophoretic probe for precise particle sampling, Aerosol Science, 39, 418 – 431.

Lucht R.P (2003), Book Reviews - Applied Combustion Diagnostics (Kohse-Höinghaus and Jeffries, Taylor and Francis, London (2002)), Combustion and Flame, 133, 507–508.

Minutolo P., D'Anna A., Commodo M., Pagliara R., Toniato G., Accordini C. (2008), Emission of Fine Particles from Natural Gas Domestic Burners, Environmental Engineering Science, in press.

Murr, L.E. Soto K.F. (2005), A TEM study of soot, carbon nanotubes, and related fullerene nanopolyhedra in common fuel-gas combustion sources, Materials Characterization, 55: 50–65.

Rusciano, G., Cerrone, G., Sasso, A., Bruno, A., Minutolo, P. (2006), Infrared analysis of nano organic particles produced in laminar flames, Applied Physics B, 82 (1) , p. 155-160.

Rusciano, G., De Luca, A.C., D'Alessio, A., Minutolo, P., Pesce, G., Sasso, A.. (2008), Surface-enhanced Raman scattering study of nano-sized organic carbon particles produced in combustion processes, Carbon, 46 (2) , p. 335-341.

Seinfeld J.H. (1986), Atmospheric Chemistry and Physics of air Pollution, John Wiley & Sons, pages 23-24, 275-289, 307-340.

Seinfeld, J. H. and Pandis, S. N. (2006), Atmospheric Chemistry and Physics - From Air Pollution to Climate Change, 2nd Edition, John Wiley & Sons, ISBN 0470046252, p.417.

Sgro, L.A. (2001), UV-visible spectroscopy of organic carbon particulate sampled from ethylene /air flames, Chemosphere, 42 (5-7) , p. 671-680.

Sgro et al (2007), Characterization of Nanoparticles of Organic Carbon (NOC) Produced in Rich Premixed Flames by Differential Mobility Analysis, Proceedings of the Combustion Institute, 31 (1) , p. 631-638.

Thierley, M.; Grotheer, H.-H.; Aigner, M.; Yang, Z.; Abid, A.; Zhao, B.; Wang, H. (2007), On existence of nanoparticles below the sooting threshold, Proceedings of the Combustion Institute, 31 I , p. 639-647.

TSI (2008), Series 3080 Electrostatic Classifiers Operation and Service Manual, Revision H, p.B-2.

United States Environmental Protection Agency (US EPA), Program Needs for Indoor Environments Research (PNIER) (2005), 402-B-05-001.

US EPA National Air Quality Guidelines (1996), http://www.epa.gov/air/criteria.html

US EPA Air quality criteria for particulate matter (1996), (EPA Report No. EPA/600/P-95/001cF), Washington DC, Vol. III. p.10

US EPA The Inside Story (2008), A Guide to Indoor Air Quality, U.S. EPA/Office of Air and Radiation Office of Radiation and Indoor Air (6609J) cosponsored with the Consumer Product Safety Commission EPA 402-K-93-007EPA;. http://www.epa.gov/iaq/pubs/insidest.html.

Wang, S. C., and R. C. Flagan, (1990), Scanning Electrical Mobility Spectrometer, Aerosol Science and Technology, 13:230-240.

Whitby, K.T., G.M.Sverdrup (1980), California Aerosols: Their Physical and Chemical Characteristics, Advancs in Environmental Science and Technology,8, 477-525.

World Health Organisation (WHO) (2004), Health aspects of air pollution, Results from the WHO project 'Systematic review of healthaspects of air pollution'. WHO Europe, p.10,17.

WHO (2000), Air quality guidelines for Europe, 2nd edition (book version), Copenhagen, WHO Regional Office for Europe, p.1.

WHO (2000), Air quality guidelines for Europe, 2nd edition (CD ROM version), Chapter 7.3, p.2.

WHO (2002), The World Health Report 2002 : Reducing Risks, Promoting Healthy Life., Geneva.

WHO (2005), Air quality guidelines - global update 2005

Internet Sources

www.epa.gov

www.tsi.com

Chapter 2: Combustion of Natural Gas

In 1885, Robert Bunsen managed to create a device that mixed natural gas with air in the right proportions, creating a flame that could be safely used for cooking and heating. The invention of the Bunsen burner opened up new opportunities for the use of natural gas. Today, natural gas is one of the principle sources of energy for many of our day-to-day needs and activities. As many other inventions of the mankind, abundant use of natural gas brought its side effects together with it. Today there are evidences that domestic use of natural gas is one of the factors for the increased respiratory diseases, due to high indoor concentrations of carbon monoxide, nitrogen oxides and particulates, especially in poorly ventilated kitchens.

2.1. Flame types

A flame is a self-sustaining propagation of a localized combustion zone at subsonic velocities. The two classes of flames, premixed and non-premixed (or diffusion), are related to the state of mixedness of the reactants (the fuel and the oxidizer), as suggested by their names. In practical devices, both types of flames may be present in various degrees. Partially-premixed flames are established when less than stoichiometric quantity of oxidizer is molecularly mixed with the fuel stream before entering the reaction zone where additional oxidizer is available for complete combustion [Lewis and von Elbe, (1961)].

The two commonly used terms in discussions of the mixture of the oxidizer and fuel, are fuel to air ratio and equivalence ratio. Although there are several expressions used in the literature for these two, most of the references refer to C/O ratio as the ratio of the available carbon atoms to available oxygen atoms (mole/mole); while the equivalence ratio refers to the ratio of the experimental value of C/O ratio to the stoichiometric value of the C/O ratio.

In addition to the mixedness, another dimension in the classification of the flames is the turbulence. Turbulent flow results when instabilities in a flow are not sufficiently damped by viscous action and the fluid velocity at each point in the flow exhibits random fluctuations. In both laminar and turbulent flows, the same physical processes are active, and many turbulent flame theories are based on an underlying laminar flame structure [Turns (2000)].

In a diffusion flame, the reactants are initially separated, and reaction occurs only at the interface between the fuel and the oxidizer, where mixing and reaction both take place. The term “diffusion” applies strictly to the molecular diffusion of chemical species, i.e, fuel molecules diffuse toward the flame from one direction while the oxidizer molecules diffuse toward the flame from the opposite direction.

In laminar jet diffusion flames, as the fuel flows along the flame axis, it diffuses radially outward, while the oxidizer (air) diffuses radially inward. As a result, the flame velocity is limited by the rate of diffusion. Since chemical reaction is very rapid, the flame boundary is nominally defined to exist where the fuel and oxidizer meet in stoichiometric proportions (Equivalence ratio =1). The length L of the flame is determined by the condition that at the point x=L above the burner rim, sufficient air has arrived at the stream axis to burn the fuel to completion. Above this point, no further combustion takes place, but the process of mixing continues between the combustion products and air. For circular-port jet flames, the flame length does not depend on initial velocity or diameter but rather on the initial volumetric flow rate. Any combination of velocity and diameter resulting in the same flow rate will give the same flame length.

In a premixed flame, the fuel and the oxidizer are mixed at the molecular level prior to the occurrence of any significant chemical reaction. This creates a thin flame front as all of the reactants are readily available. If the mixture is rich, a diffusion flame will generally be found further downstream. The temperature profile through the flame is perhaps its most important characteristic. The flame speed is another important characteristic as it is the property that dictates the flame shape and important flame stability characteristics, such as blow-off and flashback.

It is convenient to divide a flame into two zones: the preheat zone and the reaction zone. In the preheat zone, only a little heat is released; the bulk of the chemical energy is released in the reaction zone. It is useful to divide the reaction zone further into a thin region of very fast chemistry (typically less than a millimeter at atmospheric pressure) followed by a much wider region of slow chemistry (several millimeters at atmospheric pressure). The destruction of the fuel molecules and the creation of many intermediate species occur in the fast chemistry region, dominated by bimolecular reactions. In hydrocarbon flames, within an excess of air, this zone appears blue due to excited CH radicals in the high-temperature zone. With the decrease of air below the stoichiometric proportions, the color turns into blue-green due to excited C2. If the flame is made richer still, soot will form with its consequent black body continuum radiation which human eye sees a bright yellow to dull orange, depending on the flame temperature. Because this zone is thin, temperature gradients and species

concentration gradients are very large. These gradients provide the driving forces that cause the flame to be self-sustaining: the diffusion of heat and radical species from the reaction zone to the preheat zone. In the slow chemistry region, the three- body radical recombination reactions and the final burnout of CO dominate [Turns (2000)]. The typical luminous structure of the fuel-rich premixed hydrocarbon flames exhibits a blue region close to the burner due to the large formation of OH radicals in the flame front, followed by an almost transparent region and downstream by a zone with intense yellow-orange luminosity, which becomes more evident as the C/O ratio of the fuel-air mixture is increased [d'Anna (2008)].

The Bunsen-burner flame is an interesting and a familiar example of premixed laminar flames. A jet of fuel at the base induces a flow of air through the variable area port, and the air and fuel mix as they flow up through the tube. The typical Bunsen-burner flame is a dual flame: a fuel-rich premixed inner flame surrounded by a diffusion flame. The secondary diffusion flame results when the carbon monoxide and hydrogen products from the rich inner flame encounter the ambient air. The shape of the flame is determined by the combined effects of the velocity profile and heat losses to the tube wall. If the flow velocity is below the flame speed, the flame will move upstream until the fuel is consumed or until it encounters a flame holder. If the flow velocity is equal to the flame speed, a stationary flat flame front would be expected normal to the flow direction. If the flow velocity is above the flame speed, the flame front would become conical such that the component of the velocity vector normal to the flame front is equal to the flame speed. As a result, most premixed flames in daily life are roughly conical. The factors influencing the flame speed and thickness of a laminar premixed flame can be listed as, temperature, pressure, equivalence ratio and fuel type. There are extensive numbers of studies available in literature reporting flame speed measurements for various fuels over a range of temperatures and pressures together with correlations. Andrews and Bradley (1972) made an extensive study for the methane-air mixtures. In the last decade, numerical simulations employing both detailed chemical kinetics and mixture transport properties have become standard tools for combustion engineers and scientists. Many simulations are based on the CHEMKIN library of Fortran main programs and subroutines.

2.2. Domestic Gas Burners

At present, the domestic gas burner most widely used is the conventional Bunsen type, i.e.partially aerated. The typical partially aerated burner entrains primary air naturally by a momentum sharing process between the high velocity gas jet and the ambient air [Ko and Lin (2003)]. The fuel gas is premixed with some air before it burns as a laminar jet diffusion flame. Figure 5 shows various

domestic gas cookers. The bright conical flames near the jets of the domestic gas cooker, are the premixed flame front. The remaining blue glow is due to diffusion.

Figure 5: Various domestic gas cookers

The primary air is entrained by a jet of natural gas emerging from a small diameter injector into a mixing tube. The primary air/natural gas mixture flows into the bottom of the burner cap and issues from the burner through the burner ports, a large number of holes around the circumference of the burner cap. This cap sits in an aeration pan, allowing secondary air access to the flames, which are stabilised on the burner ports. A metal framework, called the grate, supports the cooking vessel above the burner [Stubington et al (1994)].

The primary aeration, which is typically 40 – 60 percent of the stoichiometric air requirement, makes the flames short and prevents soot formation, resulting in the familiar blue flame. The maximum amount of air that can be added is limited by safety considerations. If too much air is added, the rich flammability limit may be exceeded. Depending on flow conditions and burner geometry, this flame may propagate upstream, causing flashback. If the flow velocity is too great for flashback to occur, an inner premixed flame will form inside the diffusion flame envelope, as in the Bunsen burner [Turns (2000)].

Flashback and liftoff are two important design criteria for gas burners and they are both related to matching the local laminar flame speed to the local flow velocity [Turns (2000), Lewis and von Elbe (1961)]. Flashback occurs when the flame enters and propagates through the burner tube or port without quenching. Flashback is generally a transient event, occurring as the fuel flow is decreased or turned off. When the local flame speed exceeds the local flow velocity, the flame propagates upstream through the tube or port. When the fuel flow is stopped, flames will flashback through any tubes or

ports that are larger than the quenching distance. Flashback is not only a nuisance, but also a safety hazard. In a gas appliance, propagation of a flame through a port can ignite the relatively large volume of gas in the mixer leading to the port, which might result in an explosion. The controlling parameters for flashback are fuel type, equivalence ratio, flow velocity and burner geometry.

Lift-off is the condition where the flame is not attached to the burner tube or port, but rather, is stabilized at some distance from the port. Flame lifting depends on local flame and flow properties near the burner port. At low flow velocities, the edge of the flame lies quite close to the burner lip and is said to be attached. When the velocity is increased, the edge of the flame is displaced a small distance downstream. With further increases in flow velocity, a critical velocity is reached where the flame edge jumps to a downstream position far from the burner lip. When the flame jumps to this position, it is said to be lifted. Increasing the flow velocity beyond the lift-off value results in increasing the lift-off distance until the flame abruptly blows off the tube altogether, obviously an undesirable condition. In practical burners, flame lifting is generally undesirable for several reasons: 1.) It can contribute to some escape of unburned gas or incomplete combustion. 2.) Ignition becomes difficult to achieve above the lifting limit. 3.) Accurate control of the position of a lifted flame is hard to achieve, so that poor heat-transfer characteristics can result. 4.) Lifted flames can be noisy.

2.3. Natural Gas

The first discoveries of natural gas seeps were made in Iran between 6000 and 2000 BC. Many early writers described the natural petroleum seeps in the Middle East, especially in the Baku region of Azerbaijan. The gas seeps, probably first ignited by lightning, provided the fuel for the “eternal fires” of the fire-worshiping religion of the ancient Persians. About 2500 years ago, the Chinese recognized that natural gas could be put to work: they burned the gas to dry the rock salt [Encyclopaedia Britannica].

Today, natural gas is put to work in many residential, commercial and industrial applications. The most known residential and commercial uses of natural gas are for heating and cooking purposes. Natural gas fired/powered engines, turbines, boilers, furnaces and fuel cells are all used in commercial settings to generate power.

Natural gas is a highly flammable hydrocarbon gas consisting mainly of methane (CH_4). Although methane is always the chief component, it includes other gases such as oxygen, hydrogen, nitrogen, ethane, ethylene, propane, and even some helium.

In natural and synthetic gaseous fuels sulfur occurs in the form of hydrogen sulphide (H_2S). The amount of H_2S in natural gas varies widely from a fraction of 1 ppm in so-called sweet gas to as much as 42% in some gas fields. As H_2S is both a health hazard and causes corrosion in gas pipes, natural gas containing more than about 15 ppm of H_2S is purified before distribution and domestic consumption. This is achieved through alkaline gas washing or aqueous solutions of amines. The bound hydrogen sulphide is then expelled by heating and is processed further in the Claus process. Hereby H_2S is first oxidized to SO_2, which is subsequently used as an oxidizing agent for more H_2S [Baumbach (1996), Strauss (1978)].

Reaction Equation 1 $$2H_2S + 3O_2 \rightarrow 2H_2O + 2SO_2$$

Reaction Equation 2 $$2H_2S + SO_2 \rightarrow 2H_2O + 3S$$

The composition of natural gas changes with time and location. Natural gas from the North Sea contains, among other things, small amounts of hydrogen sulphide. Since the hydrogen sulphide content is especially important for determining whether the pipeline network will be subject to corrosion, the hydrogen sulphide content should be kept as low as possible. When the gas is being processed in fields in the North Sea, the hydrogen sulphide content is reduced in order that the gas deliveries comply with the requirements set out in the Danish Gas Regulation. When the natural gas is delivered for distribution to the customers, a sulfurous smelling substance –an odorant - is added in order to ensure that the otherwise odourless natural gas can be detected by anybody in the near vicinity in the event of a gas leak. The odorant is usually a tetrahydrothiophene (C_4H_8S, also called THT) or a mercaptan (CH_3SH, also called methanethiol) mixture. The amount of the odorant added results in a sulfur content of 4-7 mg/m^3 [http://www.gastra.dk/uk/index.asp].

The specification for the natural gas supplied to the Danish market is laid down by the Danish Safety Technology Authority and can be found in the Section A, Appendix 1A of the Danish Gas Regulation. Natural Gas received, transported and delivered in the Danish Natural Gas System under a Transportation Contract must at all times comply with the Danish Gas Regulation and the specifications in the Danish Network Code. These quality specifications are summarized in Table 3.

Table 3: Natural Gas Quality Specifications in Denmark

	During normal operation		In particularly difficult supply conditions
	Min.	Max.	Max.
Wobbe Index*	51.9 MJ/m^3	55.8 MJ/m^3	56.5 MJ/m^3
Gross Calorific Value	40.2 MJ/m^3	46.0 MJ/m^3	46.8 MJ/m^3
Relative Density:	0.61	0.69	-
CO_2	-	2.7 mol-%.	-
O_2	-	0.1 mol-%	-
H_2S and COS	-	5 mg/m^3	10 mg/m^3 for maximum two hr. 5 mg/m^3 on a 24-hour basis.
Total sulfur content (of unodorised Natural Gas)	-	10 mg/m^3	-
Water dew point	-	-3^{o}C at any pressure <80Bar	-
Hydrate formation	-	-3^{o}C at any pressure <80Bar	-
Hydrocarbon dew point	-	-3^{o}C at any pressure <80Bar	-
Dust and liquids	The natural gas must be technically free of gaseous, solid or liquid substances to the extent that this may involve a risk of blocking and malfunction or corrosion of ordinary gas installations and standard gas equipment. This provision does not apply to such formation of liquid as occasionally occurs in natural gas in the form of very small droplets and that cannot be removed from it.		
Odorisation	The natural gas must be delivered unodorised at the entry point. Odorization of the natural gas shall take place at the transition point.		
Other components and contaminants	The natural gas must not contain other components and/or contaminants to an extent that can mean that it cannot be transported, stored and/or marketed without further adjustment of the quality or treatment of the natural gas.		

* Wobbe Index, given by the ratio of the calorific value to the square root of the specific gravity, offers information about the heating effect a burner is exposed to during combustion of a fuel. The Wobbe Index accounts for composition variations in terms of their effect in the heating value and specific gravity, which affect the flowrate through an orifice. In essence, the Wobbe Index is a measurement of the available potential heat and it can be used in conjunction with the gas flow measurement to produce a measurement of heat flow rate. The greater the wobbe index, the greater the heating effect and thereby the greater the load on the burner. Different gases with the same wobbe index will impose the same load on the burner. The wobbe index is used also as a safety parameter, in the sense that a too high wobbe index can result in the production of carbon-monoxide and thermal overload [Lipták (1994)].

2.4. Natural Gas Combustion

Ideal complete oxidation of hydrocarbon fuels yield only CO_2 and H_2O as combustion products. For a given quantity of fuel a precise amount of oxygen is required for complete combustion according to Reaction Equation 3.

Reaction Equation 3 $$C_xH_y + (x + ¼\ y)O_2 \longrightarrow xCO_2 + ½\ H_2O$$

An air-fuel mixture that is theoretically of the precise ratio to obtain complete combustion, with no excess oxygen, is termed a stoichiometric mixture. If the air-fuel mixture contains less than the stoichiometric amount of air it is said to be rich, whereas with excess air the mixture is termed lean.

Since natural gas is composed of ~90% methane, consequently in combustion models it is represented by methane. For methane combustion, Mendiera et al (2004) developed an augmented reduced mechanism which consists of 18 reactions and 22 chemical species, from the kinetic scheme of Glarborg et al (1998), which was formed by 447 elementary reactions (438 in the original reference) and 65 chemical species. For the main species in methane combustion (CH_4, CO, and CO_2), Mendiera et al (2004) reported a good agreement between their experimental and chemical kinetic modelling results. Their mechanism is presented in Table 4.

Table 4 : Augmented Reduced Mechanism of Mendiera et al (2004) for methane combustion

reaction number	reaction
R(1)	$O + OH \rightleftharpoons O_2 + H$
R(2)	$O + H_2 \rightleftharpoons OH + H$
R(3)	$OH + H_2 \rightleftharpoons H + H_2O$
R(4)	$2H \rightleftharpoons H_2$
R(5)	$O_2 + H \rightleftharpoons HO_2$
R(6)	$O + CO \rightleftharpoons CO_2$
R(7)	$OH + CH_2O \rightleftharpoons H + H_2O + CO$
R(8)	$H + CH_3 \rightleftharpoons CH_4$
R(9)	$O + CH_3 \rightleftharpoons H + CH_2O$
R(10)	$OH + 2CH_3 \rightleftharpoons H + H_2O + C_2H_4$
R(11)	$OH + CH_3 \rightleftharpoons CH_3OH$
R(12)	$2CH_3 \rightleftharpoons C_2H_6$
R(13)	$O + C_2H_4 \rightleftharpoons CH_3CHO$
R(14)	$C_2H_4 \rightleftharpoons H_2 + C_2H_2$
R(15)	$OH + CH_3CHO \rightleftharpoons H_2O + CH_3CO$
R(16)	$OH + CO + CH_3 \rightleftharpoons H_2O + CH_2CO$
R(17)	$CO + 2CH_3 \rightleftharpoons C_2H_5CHO$
R(18)	$H + C_2H_5CHO \rightleftharpoons H_2 + C_2H_5CO$

Although natural gas is represented by methane in many combustion models, Tan et al (1994) emphasized the necessity of taking into account the presence of higher hydrocarbons in natural gas and including the kinetics of those higher hydrocarbons together with methane kinetic schemes in order to improve natural gas combustion modelling. As a result of their experimental and modelling work, Tan et al (1994) concluded that methane reactivity is significantly affected by the presence of ethane and /or propane. In both cases, the production of C_2H_5 radicals is an important step since this species rapidly produces H atoms. Methane consumption then takes place at much lower temperatures than observed for pure methane oxidation in the same experimental conditions. In their further studies, Tan et al (1995) showed the importance of traces of ethane (10% of methane mole fraction) on the oxidation of methane. Their computations indicated that the oxidation of methane is initiated by its reaction with O_2 and by thermal dissociation when no other hydrocarbon is present. However, in the methane/ethane mixtures, they showed that ethane reacts before methane leading to the formation of OH, H and O radicals which initiate methane oxidation.

Although natural gas is known to be the cleanest fossil fuel, the combustion of natural gas releases some harmful emissions, such as carbon monoxide, carbon dioxide, methane, nitrogen oxides, sulfur dioxide, volatile organic compounds and particles. As carbon monoxide, carbon dioxide and methane emissions are dependent on the efficiency of the combustion process; these will not be covered here.

The only source of nitrogen oxides in the combustion of natural gas is the oxidation of atmospheric molecular nitrogen at the high temperatures of the combustion. NOx formed by this route is referred to as thermal NOx. The mechanism of thermal NOx production has been studied extensively. The thermal NOx forming reactions involve oxygen–nitrogen system and are effectively decoupled from the combustion process. High temperature and high oxygen concentration favor NO formation, and preventing one or both of the conditions is the basis of most thermal NOx control technology [Seinfeld (1986)].

The predominant sulfur-containing product formed by the combustion or slow oxidation of sulfur compounds and elementary sulfur is almost invariably sulfur dioxide. The recent flow reactor studies of SO_2 oxidation under post-flame conditions [Glarborg et al (1996), Mueller et al (2000)] indicate fractional conversions of SO_2 to SO_3 in the order of a few percent. Because of the enormous attraction between sulfur trioxide and water, only a very small amount of sulfur trioxide in combustion gas is enough to draw water from the gas and form a fairly concentrated acid [US EPA (1998)]. High temperature chemistry of SO_2 and SO_3 and formation of sulfuric acid aerosols are further discussed in Chapter 3 of this part (Part B) of the thesis.

A complex set of chemical reactions occurring in the gas phase leads to formation of poly aromatic hydrocarbons (PAH), which by combined clustering, dehydrogenation and/or condensation subsequently can result in homogeneous inception of the first primary soot particles. Once formed these soot particles can coagulate and produce fractal structured agglomerates according to the dynamics of aerosols [Rasmussen (2003)]. It has been established through sustained research that acetylene is an important precursor of soot in flames [Mishra et al (2005)]. Soot formation is further discussed in Chapter 3 of this part (Part B) of the thesis.

2.5. References

Andrews E., Bradley D. (1972), The Burning Velocity of Methane-Air Mixtures, Combustion and Flame, 19, p.275-288.

Baumbach G. (1996), Air Quality Control, Springer-Verlag, Berlin, ISBN 3-540-57992-3, p.23-39.

D'Anna, A. (2008), Combustion – Formed Nanoparticles, Manuscript for the invited topical review at the 32nd International Symposium on Combustion, Montreal, Canada.

DGC (2005), Naturgas – Energi og Miljø, http://www.dgc.dk/publikationer/infobestilling. htm.

Encylopedia Britannica, http:// www.britannica.com.

Finlayson B. J, Pitts J.N (2000) , Chemistry of the Upper and Lower Atmosphere, Academic Press, New York, ISBN 012257060X, p. 351 -362.

Glarborg, P. Kubel, D.; Dam-Johansen, K.; Chiang, H. M.; Bozzelli, J. W.(1996), Impact of SO_2 and NO on CO oxidation under post-flame conditions, International Journal of Chemical Kinetics 28, 773-790.

Glarborg, P. et al (2000); Kinetic Modeling of Hydrocarbon/Nitric Oxide Interactions in a Flow Reactor, Energy & Fuels, 14, p. 828-838.

Ko Y.C., Lin T.H. (2003), Emissions and efficiency of a domestic gas stove burning natural gases with various compositions, Energy Conversion and Management, 44, p.3001-3014.

Lewis B., von Elbe G. (1961), Combustion, Flames and Explosions of Gases, 2nd Edition, p.220-224

Lipták B. (1994), Analytical instrumentation, CRC Press, p.69-71.

Mendiera T. et al (2004), An Augmented Reduced Mechanism for Methane Combustion, Energy & Fuels, 18, p.619-627.

Mishra T.K., Datta A., Mukhopadhyay A. (2005), Concentration measurements of selected hydrocarbons in methane/air partially premixed flames using gas chromatography, International Journal of Thermal Sciences, 44, p.1078–1089.

Mueller, M. A.; Yetter, R. A.; Dryer, F. L. (2000) International Journal of Chemical Kinetics, 32, 317-339.

Rasmussen, M. S. (2003), Modelling of Soot Formation in Autothermal Reforming, PhD Thesis, DTU.

Rasmussen M.S., Glarborg P., Østberg M., Johannessen J.T., Livbjerg H., Jensen A.D. and Christensen T.S (2004), Formation of polycyclic aromatic hydrocarbons and soot in fuel-rich oxidation of methane in a laminar flow reactor, Combustion and Flame, 136, p. 91–128.

Seinfeld H. (1986), Atmospheric Chemistry and Physics of air Pollution, John Wiley & Sons, New York, pages 23-24, 275-289, 307-340.

Strauss W. (1978), Air Pollution Control Part III Measuring and Monitoring Air Pollutants, John Wiley, New York, p.466.

Stubington J.F., Beashel G., Murphy T., Junus R., Ashman P.J. and Sergeant G.D.(1994), Emissions and Efficiency from Production Cooktop Burners Firing Natural Gas, Journal of Institute of Energy, 67, p.143-155.

Tan Y., Dagaut P., Cathonnet M., Boettner J.C. (1994), Oxidation and Ignition of Methane-Propane and Methane –Ethane – Propane mixtures: Experiments and Modelling, Combustion Science and Technology 103:133-151.

Tan Y., Dagaut P., Cathonnet M., Boettner J.C. (1995), Pyrolysis, Oxidation and Ignition of C_1 and C_2 hydrocarbons: Experiments and Modelling, Journal de Chimie Physique et de Physico-Chimie Biologique, 92, p.726 – 742.

Turns S. R (2000), An Introduction to Combustion Concepts and Applications, 2nd Edition McGraw Hill, New York, ISBN 0-07-235044-x, p. 253-298, 305-354.

US EPA (1998), Emergency Planning and Community Right-To-Know Act - Section 313, Guidance for Reporting Sulfuric Acid (acid aerosols including mists, vapours, gas, fog, and other airborne forms of any particle size).

Internet Sources

http://www.gastra.dk/uk/index.asp (accessed in 2005)

Chapter 3: Combustion and Aerosols

3.1. Particle emissions from various combustion sources

Combustion emissions account for over half of the fine particle ($PM_{2.5}$) air pollution and most of the primary particulate organic matter. Primary carbonaceous particles are classified into organic and black carbon. The airborne particles less than 2.5 μm ($PM_{2.5}$), often called fine or respirable particles, may be referred to in older literature as soot since most fine particles from combustion have a high content of black elemental carbon [Lewtas (2007)]. Black carbon (BC) refers to the 'black', light-absorbing aerosol that composes mainly from elemental carbon and is commonly known as soot. It can also be referred as 'elemental' (EC), depending on whether the context is chemical or optical. Organic carbon (OC) comprises numerous organic compounds. The particulate organic matter (POM) or organic extractable matter associated with $PM_{2.5}$ includes thousands of chemical ranging from alkanes and aromatic compounds to polar substituted aromatics and carboxylic acids [Lewtas (2007)].

As the motor vehicle emissions have been identified as one of the major source of particles in most urban cities, there are many recent studies available in this field. From these studies, it is obvious that the different fuel types of the on-road vehicles and their driving conditions have a direct effect on the characterization of vehicle exhaust gaseous and particle emission factors [Chan et al (2007), Liu (2007), Lim et al (2007)] According to Hildemann et al (1993), diesel particulate matter is almost pure carbon and exists as submicrometre-sized aggregates of ultrafine carbon spheroids with aerodynamic diameters of around 0.1 μm and petrol fuelled cars with catalytic converters emit much lower particle masses than those without, while diesel trucks emit about 100 times the particle mass, per kilometre driven, of a passenger car with a catalytic converter. According to Sakurai et al (2003), emissions from a modern, heavy-duty diesel engine operated at light and medium loads generate fractal-like agglomerates of solid carbon nano-particles, typically coated with organics and having mobility diameters in the ultrafine range (< 0.15 μm). Hildemann et al. (1993) showed that industrial-scale boilers, fireplaces, cars with and without catalytic converters, diesel trucks and meat cooking operations all emit particles primarily in the range 0.1–0.2 μm.

In addition to the primary particulate matter emissions, combustion emissions account for formation of secondary particulate matter via a series of chemical and physical reactions involving different precursor gases, such as sulfur and nitrogen oxides, and ammonia reacting to form sulphate, nitrate and ammonium particulate matter. Condensable vapours such as sulfuric acid form aerosols in the

atmosphere by the competing mechanisms of condensation on existing aerosol and the nucleation of new aerosol. The role of H_2SO_4–H_2O binary homogeneous nucleation (BHN) in the formation of nanoparticles (NP) has been addressed by several researchers for many different areas, ranging from aircraft emissions to diesel particulate emissions, as well as in the atmosphere.[Brown et al (1997), Clement and Ford (1999), Srivastava et al (2004), Hua and Fangqun (2006)].

During combustion of sulfur-containing fuels, sulfuric acid aerosols are produced via the oxidation of the sulfur contained in the fuel. Sulfuric acid aerosols are also formed in the stacks of the combustion facilities burning sulfur-containing fuels. Because of the enormous attraction between sulfur trioxide and water, only a very small amount of sulfur trioxide in combustion gas is required to draw water from the gas and form a fairly concentrated acid [US EPA (1998)]. The emissions of SO_3 from coal and fuel oil fired combustion devices depend on coal sulfur content, combustion conditions, flue gas characteristics, and air pollution control devices being used. It is well known that the catalyst used in the selective catalytic reduction (SCR) technology for nitrogen oxides control, oxidizes a small fraction of SO_2 in the flue gas to SO_3. The extent of this oxidation depends on the catalyst formulation and SCR operating conditions [Srivastava et al (2004), Yilmaz et al (2006), Irvin and Monroe (2006)]. Table 5 and Table 6 present the expected sulfur trioxide levels in flue gas resulting from the combustion of fuel oil and coal fired units respectively.

Table 5 :SO_3 Concentration in Flue Gas (ppm) from fuel –oil fired units [Reproduced from US EPA (1998)]

Sulfur in fuel (%)	0.5	1.0	2.0	3.0	4.0	5.0
Excess air (%)	SO_3 Concentration in Flue Gas (ppm)					
5	2	3	3	4	5	6
11	6	7	8	10	12	14
17	10	13	15	19	22	25
25	12	15	18	22	26	30

Table 6 : SO_3 Concentration in Flue Gas (ppm) from coal fired units, operated with 25% excess air [Reproduced from US EPA (1998)]

Sulfur in coal (%)	0.5	1.0	2.0	3.0	4.0	5.0
SO_3 Concentration in Flue Gas (ppm)	3-7	7-14	14-28	20-40	27-54	33-66

More than three billion people worldwide continue to depend on solid fuels, including biomass fuels (wood, dung, agricultural residues) and coal, for their energy needs. Cooking and heating with solid fuels on open fires or traditional stoves results in high levels of indoor air pollution [WHO]. Burning solid fuels produces extremely high levels of indoor air pollution: typical 24-hour levels of PM_{10} in biomass-using homes in Africa, Asia or Latin America range from 300 to 3000 micrograms per cubic metre ($\mu g/m^3$). Peaks during cooking may be as high as 10 000 $\mu g/m^3$. As cooking takes place every day of the year, most people using solid fuels are exposed to levels of small particles many times higher than accepted annual limits for outdoor air pollution. The more time people spend in these highly polluted environments, the more dramatic the consequences for health [WHO (2006)].

A burning cigarette is a classic example of an incomplete combustion system and the adverse health effects of its combustion products are well known. Secondhand smoke is a mixture of the smoke given off by the burning end of a cigarette, pipe, or cigar, and the smoke exhaled by smokers. Secondhand smoke is also called environmental tobacco smoke (ETS) and exposure to secondhand smoke is sometimes called involuntary or passive smoking. Secondhand smoke contains more than 4000 substances, several of which are known to cause cancer in humans or animals [http://www.epa.gov/smokefree/ healtheffects. html]. Article 8 of the WHO Framework Convention on Tobacco Control, recognizes that exposure to tobacco smoke causes death, disease and disability, and asks countries to adopt and implement legislation that provides protection from second-hand smoke. In regards to particle emissions, Klepeis et al (2003) provided an equivalent total particle emission rate of 0.2-0.7 mg/min for cigars and 0.7-0.9 mg/min for cigarettes, with average mass median diameter of 0.2 μm.

3.1.1. Soot

Soot generated in combustion processes is not a uniquely defined substance. It normally looks black, but it is different from graphite. The main constituents are carbon atoms. It contains up to 10 mole percent hydrogen and even more if it is young, as well as traces of other elements [Wagner (1978)]. Most commonly, soot particles are agglomerates of small, roughly spherical particles such as those shown in Figure 6.

Although the chemistry and physics of soot formation is exceedingly complex, the view has emerged that soot formation in diffusion flames proceeds in a four-step sequence:

- Formation of precursor species

- Nucleation / Particle inception

- Surface growth and particle agglomeration

- Particle oxidation

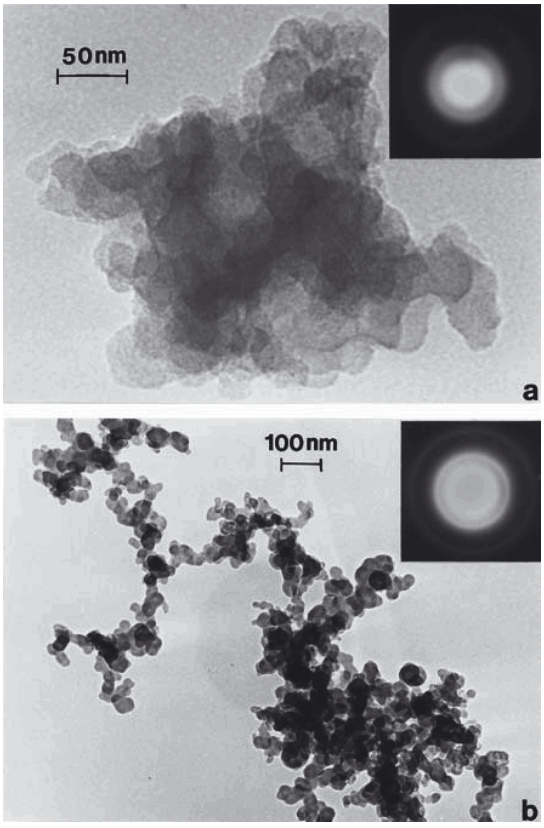

Figure 6: Typical TEM image examples of characteristic hydrocarbon combustion soot aggregates collected from diesel engine exhaust. (a) Carbonaceous spherule aggregate. (b) Complex, fractal-like carbonaceous branched spherule aggregate. SAED pattern inserts in (a) and (b) show diffuse diffraction rings indicative of a mostly amorphous carbon structure [Murr et al (2004)].

3.1.1.1. Formation of precursor species

There are two schools of thought on how soot originates in a fuel-rich flame: The ionic theory and the theory based on the reactions of free radicals. Although the detailed chemical mechanisms involved and the identity of the specific precursors are still subject of research, the formation of ring structures and their growth via reactions with acetylene have been identified as important processes [Turns (2000)].

The ionic theory postulates that small ions, such as $C_3H_3^+$, act as nuclei, so that species such as C_2H_2 and C_4H_2 add on to them, and occasionally liberate H_2 in a repetitive growth process. Once these ions become large (2000 a.m.u.) they supposedly dissociate and produce an uncharged, but large, hydrocarbon "molecule," which can grow, coalesce or coagulate to give soot particles. Simultaneously this dissociation produces a very small ion, which repeats the process of adding on C_2, C_3, and C_4 species, etc. In Figure 7, soot formation according to the ionic theory is illustrated schematically.

The other school of thought believes that fairly similar processes occur, but the species involved are not ions, but uncharged radicals and molecules [Hall-Roberts et al (2000)]. The formation of soot precursor species, polycylic aromatic hydrocarbons (PAH) are thought to be important intermediates between the original fuel molecule and what can be considered a primary soot particle. Chemical kinetics play an important role in this first step.

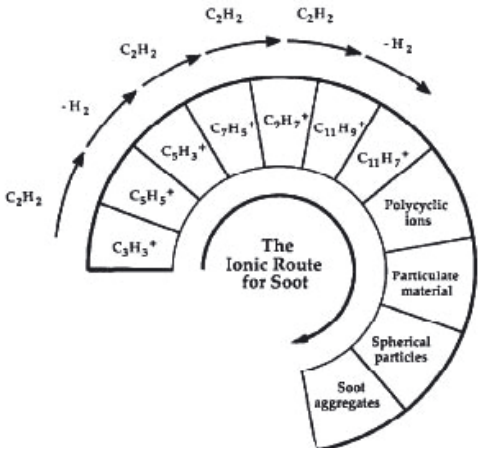

Figure 7: A schematic illustration of soot formation according to the ionic theory [Egsgaard, (1996)]

Ionic theory is primarily advocated by Calcote and his co-workers (1998). Calcote argues against the nature of chemical reactions being responsible for the formation of soot and claims that neutral species simply cannot explain the fast growth rates, whereas ions can. However advances in detailed chemical kinetic modelling of free radical reactions have demonstrated that radical reactions are sufficiently fast to account for the experimentally observed rates of soot formation [Lindsted (1994), Rasmussen (2003)]. Furthermore, Hall Roberts et al (2000) performed experiments based on the theory that if soot originates from ions such as $C_3H_3^+$, the addition of a relatively large quantity of easily ionized cesium should reduce the soot formation since cesium removes $C_3H_3^+$ ions from the flame. Hall Roberts et al (2000) reported that cesium itself had no effect on the sooting level, indicating that there is no evidence for ions acting as nuclei for soot. Calcote's (2001) comment in response was basically that the single experiment of Hall Robert et al (2000) was performed under conditions in which no effect would be expected. According to Calcote (2001), the consensus remains an unchallenged argument in support of the ionic mechanism of soot formation despite many others supporting the free radicals theory.

The molecular precursors of soot particles are thought to be heavy PAHs of molecular weight 500–1000 amu. The growth process from small molecules such as benzene or phenyl to larger and larger PAH appears to involve both the addition of C_2, C_3 or other small units, among which acetylene has received much attention, to PAH radicals, and reactions among the growing aromatic species, such as PAH–PAH radical recombination and addition reactions. In the case of aliphatic fuels such as acetylene, ethylene or methane, the first aromatic ring must be formed from fuel decomposition products by a sequence of elementary reactions [Wang and Frenklach (1997)].

As the formation of the first aromatic component is commonly regarded to be a primary bottleneck in soot formation, there had been numerous efforts in research on the reaction pathways. Despite many uncertainties concerning detailed reaction mechanisms, it is now possible to predict benzene production in hydrocarbon flames with a reasonable degree of accuracy [Wang and Frenklach (1997), Richter and Howard (2000)]. The benzene formation pathway proposed by Miller and Melius (1992) is strongly supported by many others. Miller and Melius (1992) argue that the "first ring" is most likely formed by reaction of two propargyl radicals via Reaction Equation 4 and Reaction Equation 5.

Reaction Equation 4 $$C_3H_3 + C_3H_3 \longleftrightarrow C_6H_5 + H$$

Reaction Equation 5 $$C_3H_3 + C_3H_3 \longleftrightarrow C_6H_6$$

According to some others, in flames of non-aromatic fuels, the formation of the first aromatic ring starts with the joining of vinyl and acetylene. At high temperatures, this ring is formed by a combination of acetylene with the n-C_4H_3 radical produced by detachment of H from vinyl acetylene H. At low temperatures, the interaction of acetylene with vinyl yields n-C_4H_5, which leads to benzene formation [Mansurov (2005)]. This mechanism is presented in Figure 8.

Wang and Frenklach (1997) demonstrated that reactions of n-C_4H_x + C_2H_2 leading to the formation of one-ring aromatics are as important as the propargyl recombination, particularly at low temperatures. The reader is referred to Richter and Howard (2000) for a detailed review of potential reaction pathways.

Rasmussen et al (2004) investigated the conversion of methane to higher hydrocarbons, polycyclic aromatic hydrocarbons (PAHs), and soot under fuel-rich conditions in a laminar flow reactor in the temperature range 1073 ^{o}K and 1823 ^{o}K. In sooting systems, their calculations indicated that the cyclopentadienyl radical has a significant influence on growth of PAH, particularly in the formation of naphthalene and phenanthrene. They reported that both naphthalene and phenanthrene appear to be important intermediates in PAH growth, and they have a significant influence on the formation of pyrene, which subsequently results in formation of soot in the applied model. They reported a decrease in the concentrations of both acetylene and soot with increasing addition of water vapour. The enhanced oxidation of acetylene is attributed to higher levels of hydroxyl radicals, formed from the reaction between the water vapour and hydrogen atoms. Rasmussen et al's (2003) outline for soot formation during methane combustion is presented in Figure 9, while Figure 10 illustrates the examples of proposed mechanisms for formation and growth of PAH species.

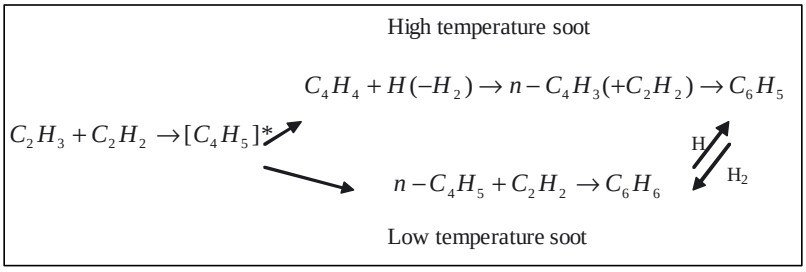

Figure 8: A potential pathway for the formation of first aromatic ring [Mansurov (2005)].

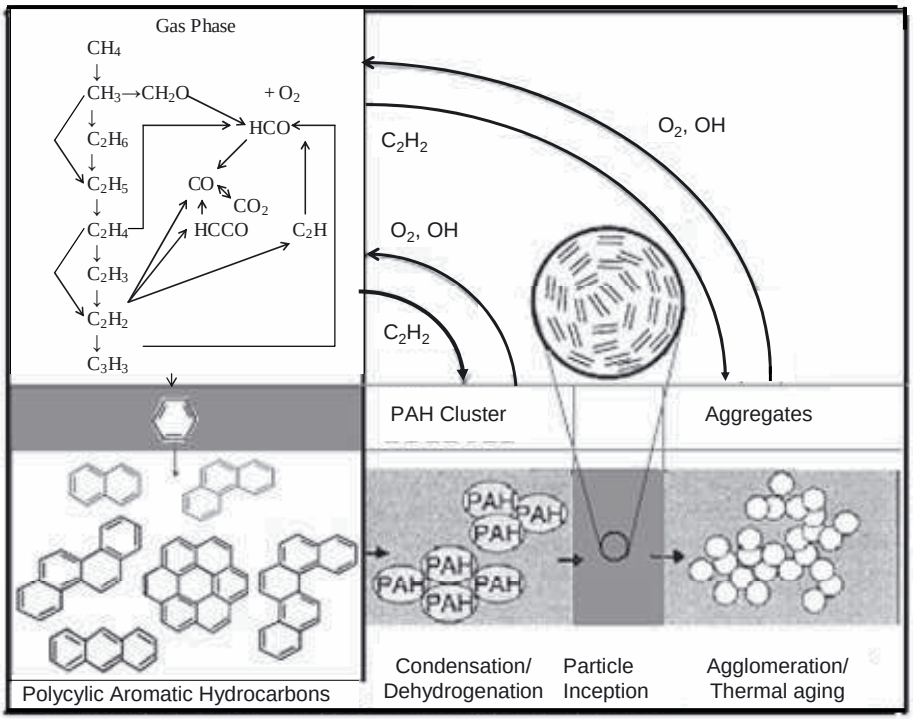

Figure 9: A schematic presentation of the processes involved in the formation of soot during combustion of methane. Darker backgrounds outline assumed bottlenecks in the soot formation process [Reproduced from Rasmussen et al (2003)]

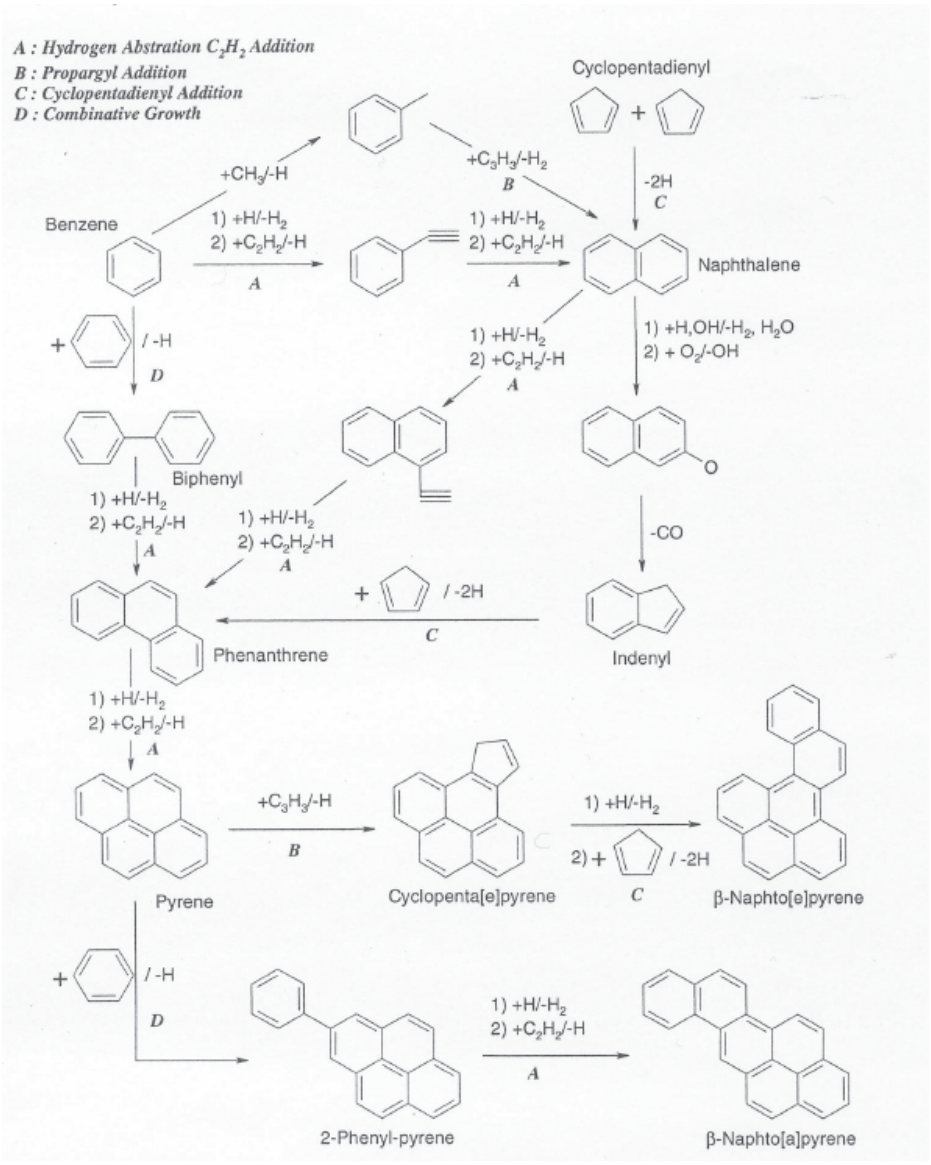

Figure 10: Illustration of mechanisms for formation and growth of PAH species [Rasmussen (2003)].

3.1.1.2. Nucleation / Particle Inception

The particle inception step involves the formation of small particles of a critical size from growth by both chemical means and coagulation. It is in this step that large molecules are transformed to, or become identified as particles. PAHs of large sizes are formed primarily by chemical reactions of radicals of small size PAHs with acetylene, PAHs, and PAH radicals. In this process mass is converted from molecular to particulate systems. Having a definite size, different kinds of PAHs continue to grow; particle formation (nucleation) occurs. Heavy PAH molecules form nascent soot particles with a molecular mass of approximately 2000 amu (3.32E-24 kg) and an effective diameter of about 1.5 nm [Mansurov (2005), Richter and Howard (2000)]. Other experimental work available on laminar premixed ethylene flames [Minutolo et al (1998), Bruno et al (2005), d'Allessio et al (2005), Minutolo et al (2008), d'Anna (2008)] also confirm the presence of nanoparticles with a typical size of about 2–3 nm, which are considered as precursors of the soot particles with typical sizes of 20– 30 nm and no major differences is expected in these features for the process of soot formation in flames of other fuels.

Chemical details of the formation of nascent soot particles are relatively poorly understood, mostly because of experimental difficulties. Efficient identification of species produced at different stages of the growth process is limited to molecular masses less than about 300 amu (4.982E-25 kg) using gas chromatography while the observation and counting of soot particles by high resolution electron microscopy has been limited to particle diameters of larger than about 1.5 nm [Richter and Howard (2000)].

Using laser light scattering and UV absorption spectras, d'Anna (2008) measured the spectra along the flame axis of a C/O=0.77 ethylene/air flame. Subtracting the contribution of gaseous products and soot absorption from the measured spectra, there was still extra absorption in the UV which is attributed by d'Anna (2008) to other UV-absorbing, visible-transparent molecules/particles. In order to qualify the chemical nature of the formed particles, d'Anna (2008) measured the laser induced fluorescence (LIF) spectra at the same locations of the absorption measurements, which gave typical of fluorescence from aromatic compounds and soot. Taking advantage of this distinct spectral behavior between soot and visible transparent species, d'Anna (2008) followed their evolution along the flame axis and calculated the volume fractions of the two classes of species, mean diameters and number concentrations. In the downstream of the main reaction zone of the flame, he observed that the volume fraction of visible-transparent species increases and a large number concentration of particles of the order of 1E13 cm^{-3} with sizes below 3nm is present. Beyond the maximum value, he

observed that the volume fraction of visible transparent species decreases in correspondence with the formation of visible-absorbing, soot particles, which have a much lower number concentration of the order of 1E11 cm^{-3} but larger sizes ranging from 5 to 25 nm.

D'Anna (2008) also performed AFM measurements, as this method gives the three dimensional structure of particles deposited on a substrate. According to his work, all single particles measured by AFM in non-sooting and sooting flames have shown a non-spherical shape on the mica substrate. The shape in the x-y plane was almost always circular, and the aspect ratio (maximum height/base diameter) was always less than unity. The author agrees with d'Anna (2008) in that this result might suggest that the measured particles have elongated structures or they are probably spherical and they spread out on the mica substrate upon impact or over time. The aspect ratio measured for all particles sampled in the sooting flame (C/O=0.77) vs. their spherical equivalent diameter is presented in Figure 11. Early in the flame, where optical measurements find only 2-3 nm particles, the AFM measurements show particles with very low aspect ratios (about 0.05). Higher in the flame, a wider bimodal distribution of sizes is measured and the aspect ratio of particles larger than about 10 nm increases toward the spherical limit (aspect ratio=1) with increasing particle sizes. The result that the smaller particles spread out more than larger particles indicates that they have a different structure; they may be more liquid and/or more polar.

In their experimental and modelling study of particulate formation in premixed flames burning methane, d'Anna et al (2008) distinguished between two fundamental types of particles by size: molecular particles with mass between 500 amu (=8.3E-25 kg) and 100,000 amu (=1.7 E-22kg); particles with size from 1 to 7 nm; and soot particles with masses higher than 100,000 amu (=1.7 E-22kg); particles with sizes larger than 7 nm. In Figure 12, the concentration of particles measured by D'Anna et al (2008) along the axis of two laminar premixed methane/oxygen flames produced with C/O = 0.44 and C/O = 0.50, are presented. The figure indicates that the concentration of molecular particles is higher than the concentration of soot particles. Last but not least, higher particle concentrations (both soot and the precursors) are observed in the richer flame. For instance, at 20 mm above the burner, the concentration of the precursor particles and soot particles were ~4E-9 g/cm^3 and ~5E-9 g/cm^3 respectively for the flame produced with C/O = 0.50, where as in the other flame only precursor particles were present with a concentration of 5E-10 g/cm^3.

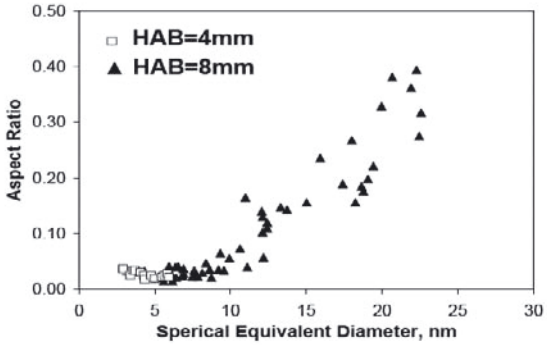

Figure 11: Aspect ratio of the particles measured by d'Anna (2008) using AFM at 4mm (□) and 8mm (▲)above the burner outlet in the C/O=0.77 ethylene/air flame.

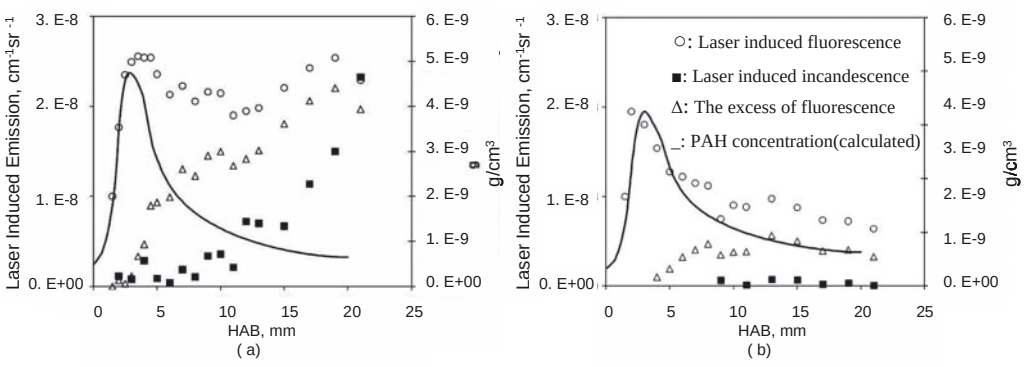

Figure 12: The laser induced fluorescence and incandescence signals measured by D'Anna et al (2008) along the axis of two laminar premixed methane/oxygen flames with (a)C/O = 0.50 and (b) C/O = 0.44 at different heights above the burner (HAB). Circular symbols (o), denote the Laser induced fluorescence. The fluorescence signal is due to both gas-phase aromatic compounds and molecular particles. Filled, square symbols (■) denote the laser induced incandescence. The incandescence signal can be attributed to soot particles. The solid line denotes the PAHs concentration profile calculated by their model. The signal due to molecular particles is obtained by subtracting the calculated PAHs (solid line) concentrations from the measured fluorescence (o). Triangular symbols (Δ) denote this excess of fluorescence which can be attributed to molecular particles.

3.1.1.3. Surface growth and particle agglomeration

After being formed through the inception process, the small primary soot particles continue to be exposed to the bath of species from the pyrolizing fuel as they travel through the flame thus they experience surface growth and agglomeration [Turns (2000)].

Surface growth of particles proceeds in conjunction with coagulation. Coagulation is a physical process while the surface growth is a chemical process in nature. The particle mass is increased via the addition of gas phase species such as acetylene and PAH, including PAH radicals. These reactions are believed to involve radical sites on the soot particles in the case of stable reactants such as acetylene and stable PAH but not necessarily so in the case of PAH radicals. This process does not affect the number of soot particles. The relative contributions of acetylene and PAH is the subject of current discussions in the combustion community [Richter and Howard (2000)].

When particles are small and surface growth is active, collisions between particles generally lead to the formation of a larger spheroid via the process of coalescence. Sticking collisions between particles during the mass growth process significantly increases particles size and decreases particle number without changing the total mass of soot present [Richter and Howard (2000)]. The rates of coagulation in the free molecule regime and the continuum regime are fairly well understood. More difficulties arise in the transition regime. In the absence of surface growth, an aerosol will tend to produce a so-called self preserving size distribution under the impact of coagulation [Kennedy (1997)].

At higher residence times under pyrolytic conditions in the postflame zone, the polyaromatic material comprising the yet formed particles undergoes functional group elimination, cyclization, ring condensation and ring fusion attended by dehydrogenation and growth and alignment of polyaromatic layers. This process converts the initially amorphous soot material to a progressively more graphitic carbon material, with some decrease in particle mass but no change in particle number. Recently, additional interest in this process has been motivated by the observation of soot containing curved or fullerenic layers [Richter and Howard (2000)].

Most of the soot in a flame is produced by surface growth on a particle. The surface growth rate depends on the local temperature, the gas composition, and the available aerosol surface area [Kennedy (1990)]. Some researchers proposed that the rate of growth is described by the aerosol surface area and the concentration of growth species. However in their experiments Wieschnowsky et

al (1988) observed different growth rates for the aerosols with the same appearent surface areas. They attributed the differences to the role of active sites on the surface of particles in determining the growth rates [Kennedy (1997)].

The actual emission of soot from a combustion device can be much less than the amount generated within fuel-rich zones. The difference arises because of the oxidation of soot particles in oxygen-rich regions beyond the soot-formation zone [Lewis and von Elbe (1961)].

3.1.1.4. Particle oxidation

Oxidation of PAH and soot particles is a process competing with the formation of these species. It decreases the mass of PAH and soot material through the formation of CO and CO_2. Depending upon flame type, oxidation may occur simultaneously with formation as in premixed aromatics flames and well-mixed combustors, or it may occur subsequent to formation as in diffusion flames or staged combustors [Wang and Frenklach (1997)]. At some point in their history, the soot particles must pass through an oxidizing region of the flame. For a jet flame, this region is invariably the flame tip, since the soot is always formed interior to the reaction zone lower in the flame, and the flow streamlines, which the particles largely follow, do not cross the reaction zone until near the flame tip. If all of the soot particles are oxidized, the flame is termed non-sooting, while, conversely, incomplete oxidation yields a sooting flame [Turns (2000)]. The main oxidation reactants are OH, O and O_2, the largest contributor in general being OH under fuel-rich conditions and O_2 under fuel-lean conditions.

Oxidation of aromatics removes carbon mass from further growth. However, even more important is the removal of mass at the earlier stages, those preceding the aromatics formation. As reported by Egsgaard (1996), numerical simulations identify oxidation of C_2H_3 as the key point of branching between carbon growth and carbon oxidation. The effect of oxidation at this small molecule level is twofold:

1.) It diverts carbon mass from further growth.

2.) Added in relatively small quantities in high temperature pyrolytic environments, molecular oxygen actually promotes formation of soot by building up the radical pool, and specifically H atoms.

3.1.1.5. Factors affecting soot formation

In technical combustion processes, soot usually forms at temperatures from 1000 to 2500^{o}C. The total amount of soot formed is always very small compared to the amount of carbon present in the fuel consumed. The time available for soot formation is of the order of mili-seconds [Wagner (1978)].

Soot formation is favoured when the molar ratio of carbon to oxygen (m/2y) approaches 1.0, as suggested by the stoichiometry of Reaction Equation 6.

Reaction Equation 6 $$C_m H_n + yO_2 \rightarrow 2yCO_2 + \frac{n}{2} H_2 + (m-2y)C_s$$

Experimentally determined limits of soot formation in premixed flames, however, do not occur at C/O = 1 but at C/O ratios that are less than 1 and depend on the type of fuel. The lower C/O ratio suggests that soot formation is controlled by the kinetics and occurs in flames under oxidation conditions. In post-flame gases with C/O ratios somewhat lower than the soot formation threshold there are the same unburned hydrocarbons present as in mixtures with ratios C/O > $(C/O)_{cr}$. Therefore, the main processes of soot formation in the flames occur in the main reaction zone, in which there is competition between the oxidation and formation of sufficient concentrations of higher hydrocarbons [Mansurov (2005)].

In diffusion flames, the combustion process is mixing controlled. Under such circumstances, where the term “diffusion” applies strictly to the molecular diffusion of chemical species, the C/O ratio cannot stay below its critical limit everywhere. Thus the formation and emission of soot from diffusion flames depend, among other things, on the flow situation [Wagner (1978)].

Shaddix et al (1994) performed quantitative measurements of the local soot volume fraction in a co-flowing, flickering CH_4/air diffusion flame burning at atmospheric pressure. Their measurements showed that soot production is four times greater for a forcing condition in which flame tip clipping occurs, compared with a steady flame burning with the same mean fuel flow velocity. They reported that their results suggest that the flickering flame exhibits similar number densities but larger particle sizes than the corresponding steady flame. According to their work, the particle number densities remain near 2-3 E9 particles/cm ^{3} through both the steady and flickering flames, whereas the effective

particle diameters increased from a maximum of ~60 nm in the steady flame to ~90 nm in the flickering flame. However, it was suggested by Shaddix et al (1994) that the extent of particle size increase shown should not be over interpreted .

The propensity to form soot (as measured by the critical C/O ratio at which soot formation begins) is a complex function of flame type, temperature, and the nature of fuel [Flagan and Seinfeld (1988)]. Temperature is the parameter which most strongly effects the formation of soot. Regardless of the fuel type and pressure, the dependency of the temperature results in a bell-shaped profile of the soot volume fraction, which typically has a maximum between 1700K up to 1900K. The formation of soot at the low temperature side of the bell-shaped temperature dependency is controlled by the kinetics of soot formation, while the fall off in soot volume fraction at higher temperatures is controlled by thermodynamics [Wagner (1981), Rasmussen (2003)]. The effect of pressure on soot formation in diffusion flames is generally such that low pressure reduces carbon formation while high pressure promotes it [Lewis and von Elbe (1961), Haynes and Wagner(1981)].

In premixed flames, sooting appears to be determined by a competition between the rate of pyrolysis and growth of soot precursors and the rate of oxidative attack on these precursors. As the temperature increases, the oxidation rate increases faster than the pyrolysis rate, and soot formation decreases. In diffusion flames, oxygen is not present in the pyrolysis zone, so the increase in pyrolysis rate with temperature leads to an increasing tendency to soot. Small amounts of oxygen in the pyrolysis zone appear to catalyze the pyrolysis reaction and increase sooting [Flagan and Seinfeld (1988)]. High soot volume fractions well-downstream in the flames can lead to significant loss of energy by radiation. As a result, the temperatures near the tip of a laminar diffusion flame may be many hundreds of degrees below the adiabatic flame temperature [Kennedy et al (1990)].

Examining the detailed chemical processes of soot formation and oxidation, one notes how very complex the overall system is. The extent to which a given fuel system will produce soot depends strongly on the type of combustion system (flame structure) controlling the process and the temperature of that system. Since the amount of soot formed from a particular fuel has a complex dependence on the overall combustion process, there is no one characteristic parameter that can define the amount formed per unit weight of fuel consumed [Kennedy et al (1990)]. Soot formation is favored by lack of oxygen in the flame base, e.g., by inadequate mixing of fuel and air and by high temperatures in this phase. It depends not only on combustion conditions but also on the fuel used. If there is a lack of air, fuels with a high C/H ratio are rather more prone to soot formation than fuels with a low C/H ratio. Thus, when burning natural gas which consists largely of methane (CH_4), only

alight soot formation will occur even with a lack of air compared to an acetylene flame (C_2H_2) which produces large flakes of soot when there is a lack of air [Baumbach (1996)]. The emission of soot from a combustor or from a flame is determined by the competition between soot formation and oxidation. [Turns (2000)]. Depending on the conditions in the flame (temperature, mixture and excess of air) the resulting soot burns out more or less completely. The eventual emission of soot from the flame occurs when the flame temperature is reduced sufficiently by radiation so that the burnout reactions are inhibited [Kennedy et al (1990)].

One can see by the color of the flame whether soot is being formed in the flame. The burning soot particles have a radiation behaviour resembling a black body. Depending on the temperature the sooting flame has a dark yellow to a light yellow hue. Flames without soot formation and oxidation release a pure gas radiation, e.g with a transparent blue hue. On the other hand, there are oil flames, so-called blue burning flames, which do not emit any soot even with a lack of air but merely CO and hydrocarbons [Baumbach (1996)].

One of the earliest detailed diagnostic efforts on sooting diffusion flames was that of Wagner and his co-workers [Wagner (1978); Haynes and Wagner (1981)]. Their results show quite clearly that soot particles are generated near the reaction zone (early in the flame) and are convected further towards the center of the fuel stream as they travel up the flame. The earliest particles are of the order of 1 nm in diameter and they form in large numbers. The particle number densities and generation rates decline with distance from the flame zone. The soot formation rate appears to have its peak values about 2-3mm on the fuel side of the reaction zone. The particle number density decreases by coagulation and gradually levels off. This process leads to an increase in particle size and a simultaneous increase in soot volume fraction as the particles absorb hydrocarbon species [Wagner (1978) ; Kennedy et al (1990), Glassman (1988)].

3.1.1.6. Soot Formation and Oxidation Models

Frenklach (2002) made an excellent review of the soot formation models. According to Frenklach, soot formation models can be classified as empirical and physical, based on their nature.

Empirical models offer mathematical simplicity but suffer from unreliable predictability. Recent models in this class have usually been constructed assuming arbitrary nucleation, asymptotic regime of coagulation, and empirical growth and oxidation. Most of the empirical modelling of soot

formation and emissions that can be found in literature is related to gas turbine and diesel engines. Having some success with predicting qualitative trends, such models often miss quantitatively and require reparametrization for different combustion environments. Models that rely on empirical inputs for soot nucleation, growth and oxidation rates are limited inherently to specific conditions and they cannot be applied to conditions far from those under which the rates were measured. Hence, they cannot be extended easily to different fuels or different pressures. A complete description of the kinetics of PAH and soot growth is required for generality [Kennedy (1997)]. Kennedy (1997) reviewed the soot formation models classifying them in three classes: empirical, semi-empirical and detailed. Empirical models use correlations of experimental data to predict trends in soot loadings. Semi–empirical models solve rate equations that are calibrated against experimental data. Detailed models seek to predict the concentrations of all the important species in a flame, from fuel to polyaromatic hydrocarbons to soot. Kennedy's review made it clear that in most cases authors had considered unique experimental conditions that differed from others in the literature which makes it very difficult to evaluate the inherent superiority of any particular approach. Kennedy also concluded that the success demonstrated by all these three classes of models are obtained by adjustments to fit measurements and existing knowledge of some of the fundamental underlying is still open to question.

As Frenklach (2002) concluded, physical models, once established, can be applied with larger confidence over a wide range of conditions. The main problem with physical models is the large size of the computational requirements for implementation with fluid-dynamics codes. This can be overcome by applying various mathematical methods. As Frencklach (2002) reported in his review, most simulations are carried out up to a specified aromatic size, one to four rings, while some treat the aromatic growth up to infinity. Several groups have extended the detailed description to soot particle dynamics. In these latter efforts, the transition from gas phase to soot particles is described assuming the nucleation to take place at the collision of pyrene and larger aromatics or at the collision of benzene molecules. The surface growth is treated either empirically or based on chemical analogy to aromatics chemistry. The coagulation of soot particles is modelled by using either a discrete-sectional method or the method of moments. The method of moments was recently extended to include agglomeration of soot particles into fractual aggregates. The reader is referred to Frenklach's (2002) review for further details.

A detailed kinetic model of soot formation from the perspective of flame modelling can be viewed as comprised of two principal components: gas-phase chemistry, which determines the flame structure, and soot particle dynamics, which describes the evolution of the particle ensemble. The correctness of

the particle dynamics submodel relies, first of all, on the accuracy of species profiles supplied by the gas-phase submodel, those that define the soot particle nucleation and growth rates. Therefore if one is interested in a predictive description of soot evolution, the authenticity of the model for the flame structure must be confirmed [Frenklach (2002)].

In general, an accurate account of both formation and oxidation is needed for the successful modelling of the soot yield or the critical C/O ratio of a premixed flame, or the smoke point of a diffusion flame. In diffusion flames, the onset of soot emissions from a flame is gauged in terms of the sooting height, the flame height at which soot is emitted. This is replaced by a critical threshold equivalence ratio for the premixed flames [Kennedy (1997)].

Semi-empirical correlations of soot oxidation from Nagle and Strickland-Constable (1962) and Lee et al (1962) are still widely used in phenomenological and numerical models of combustion systems. However the reader should be cautious to use these, since the composition of soot is not the same as the pyrographite that Nagle and Strickland-Constable used for their model.

Smooke et al (1999) developed a detailed soot growth model in which the equations for particle production have been coupled to the flow and gaseous species conservation equations has been developed for an axisymmetric, laminar, coflow diffusion flame. The two-dimensional system couples detailed transport and finite rate chemistry in the gas phase with the aerosol equations in the sectional representation. The formulation includes detailed treatment of the transport, inception, surface growth, oxidation, and coalescence of soot particulates. The comparison of their results from the model to experimental data for a confined methane–air flame, showed that the flame heights were somewhat overpredicted and local temperatures and volume fractions were underpredicted. The inability to reproduce accurately bulk flame parameters directly inhibited the ability to predict soot volume fractions. The authors designated these differences to be likely results of uncertainties in the experimental inlet conditions. Predictions of the distributions of particle sizes indicated the existence of (relatively) low-molecular-weight species along the centerline of the burner and trace amounts of the particles that escape from the flame, unoxidized. Oxidation of particulates was dominated by reactions with hydroxyl radicals which attain levels approximately 10 times higher than calculated equilibrium levels. Gas cooling effects due to radiative loss were shown to have a very significant effect on predicted soot concentrations. In a more recent paper, Smooke et al (2005) refined both the prior computations (to include selfabsorption and refined griding) and the experimental measurements of the soot distributions, to extend the simulations to other flames, and to interrogate the

computational solutions. They reported that their simulations agree well with their experimental results.

A more recent model, which includes reaction pathways leading to the formation of nanosized particles and their coagulation and growth to larger soot particles, is available from D'Anna and Kent (2007). They tested their model against literature data in nonpremixed laminar flames of methane, ethylene, and butane. Their tests for methane were compared to the species concentrations and temperature measurements of Smooke et al (1999); and particulate measurements of Smooke et al (1999) and Commodo et al (2006). In their study, they distinguish two fundamental types of particles by size. Particles with sizes up to about 10 nm are termed molecular particle precursors and they are detectable by UV light absorption and laser-induced fluorescence (LIF). Particles larger than 10 nm are termed soot, and these particles are typically detected by visible light absorption and by laser-induced incandescence (LII) techniques. The sum the two types of particles is termed total particulates. In general, they reported reasonably good predictions of gas and particle-phase concentrations and particle sizes without any change to the kinetic scheme for the different fuels. For methane tests, temperature and methane concentration measurements are well predicted. The concentrations of acetylene and benzene on the flame axis are underpredicted, whereas the predictions are better off axis (where soot is formed). The total particulates predictions show good agreement at 30 mm height, but at lower heights the predictions are low. Particulate growth processes are reported to show the correct trends but higher than measured at all locations by a factor of about 2. For details on the other two fuels, the reader is kindly asked to visit the original article [D'Anna and Kent (2007)]. The most important prediction of their model is that in the methane flame small precursor particles dominate the particulate loading, whereas soot is the major component in ethylene and butene flames, in accordance with the experimental data. The driving factors in their model responsible for the quite different soot predictions in the ethylene and butene flames compared with the methane flame are reported as the higher concentrations of benzene and acetylene which are produced in higher concentrations from the ethylene and butane flames. As they reported, the higher benzene concentration enhances particle inception, leading to higher precursor particle formation; and the concurrent presence of high acetylene concentration adds C_2H_2 to the precursor particles, thus forming more soot. In the methane flame, the lack of acetylene reduces the transformation of precursor to soot, resulting in lower total particulates and a much higher proportion of precursor particles.

3.1.2. Sulfuric acid aerosols from combustion sources

The increased awareness on environment and health related issues has created a continuous, even increasing pressure and motivation for the combustion researchers to explore more and more different aspects of combustion processes. Nevertheless all these studies share the common goal of providing cleaner, safer and cheaper processes which give higher yield of energy, in order to meet the energy needs of the modern world. Sulfur has been part and/or focus of similar studies not because of its presence in most of today's available fuels, including biofuels and waste, rather because of all the problems it creates in the combustion processes, namely causing corrosion on the pipelines, boiler walls, superheaters, etc; acid rain and toxic emissions which threaten the health and environment of the world population.

If the sulfur contained in fuel is burned completely, sulfur dioxide is formed. SO_2 is a colorless gas with a pungent odor; it can be detected in the air from approximately 0,6 -1 mg/m^3 by its smell. During incomplete combustion, depending on how high the temperature is, elementary sulfur (S) or hydrogen sulphide (H_2S) can be formed under very reducing conditions from the fuel's sulfur compounds. H_2S formation can be recognized by its characteristic rotten egg smell. The smell detection threshold is very low at approximately 0,002 mg/m^3. During combustion, part of the SO_2 can be oxidized to SO_3. In combination with water vapour sulfuric acid (H_2SO_4) in the form of aerosol is formed from SO_3. The smell threshold value of SO_3 is at approximately 0,6 mg/m^3. According to the law of mass action, considerable SO_2 - SO_3 transformation rates result during the cooling of the gases in a temperature range of 800-400^{o}C with sufficient excess of air. However, the reaction rate constants of the possible reactions are not large enough for the theoretically possible SO_3 content to form during the rapid cooling of the flue gases [Baumbach (1996)].

3.1.2.1. Sulfur in fuels and flames

The presence of sulfur in fossil fuels is both as organic or inorganic compounds. The inorganic sulfur is mostly as pyrite in coal, together with small amounts of sulphates. The organic sulfur exists either in aromatic rings or in aliphatic functional groups, usually categorized as mercaptans (RSH), aliphatic and aryl sulphides (RSR'), disulphides (RSSR') and thiophenes. In oil, polysulphides (RSSR'), hydrogen sulphide (H_2S), carbon disulphide (CS_2) and carbonyl sulphide (COS) may also be present. In natural and synthetic gaseous fuels sulfur occurs mainly in the form of H_2S but CS_2 and COS may also be present [Johnsson et al (2000)].

The total sulfur content in bituminous coals may vary between 0.2 wt% and 10 wt. % [Johnsson et al (2000)]. Gasoline sulfur content is restricted by legislation in Europe and USA. EPA required a 97 % percent reduction in the sulfur content of highway diesel fuel from its current level of 500 ppm (low sulfur diesel, or LSD) to 15 mg/kg (ultra-low sulfurdiesel, or ULSD) [http://www.epa.gov/otaq/highway-diesel/index.htm] whereas gasoline sulfur standard for refinery or importer average is set as 30 mg/kg [http://epa.gov/tier2/frm/fr-t2reg.pdf]. European legislation requires that from 2009, zero sulfur diesel and gasoline fuels -defined as having no more than 10 mg/kg sulfur content—must be available on forecourts in all EU Member States [http://www.irmm.jrc.be/html/press_corner/index.htm]. Biodiesel meets ULSD mandated by EPA.

The amount of H_2S in natural gas varies widely from a fraction of 1 ppm in so-called sweet gas to as much as 42% in some gas fields. As H_2S is both a health hazard and causes corrosion in gas pipes, natural gas containing more than about 15 ppm of H_2S is purified before distribution and domestic consumption. When natural gas is delivered for distribution to the customers, a sulfurous smelling substance –an odorant - is added in order to ensure that the otherwise odourless natural gas can be detected by anybody in the near vicinity in the event of a gas leak. For this purpose, mercaptan mixtures, typically isopropylmercaptan (IPM) or tert-butyl mercaptan (TBM), are used in the USA, the UK and Japan, while in Germany and most of Europe tetrahydrothiophene (THT) is widely used. These odorants typically account for more than 50% of the sulfur compounds in distributed natural gas [Hennings and Reimert (2007)]. The average total sulfur content of natural gas distributed by Energinet in Denmark is reported as 2.4 mg/Nm^3 (< 0.01 ppm) [www.energinet.dk]. The standard on the requirements and test methods for the organic sulfur compounds used as odorants - ISO/NP 13734, is currently under development by International Organization for Standardization (ISO).

In the flames, sulfur has a richness of reactions that are extremely fast. The system can rapidly lock certain species into relationships with one another that then become controlled by an internal partial equilibrium [Schofield (2001)]. Schofield (2001) –based on his work with Muller et al (1979, 1980) reported that the species distributions of H_2S, SH, S_2, S, SO, and SO_2 were totally under the control of the flame radicals H, OH, and O (primarily H and OH in fuel-rich flames), which were in their own partial equilibrium. Also, it appeared, at least in hydrogen flames, that this list of species constituted a reasonable summation of the mass balance for sulfur and as the non-equilibrated H, OH, and O radical pool decayed towards equilibrium, the sulfur chemistry was sufficiently fast to track them change and modify the sulfur species distributions. The set listed in Table 7 is not unique but is self-sufficient in that it relates the entire sulfur species one to another, and then these to the basic flame composition [Schofield (2001)].

Table 7: Main reactions of sulfur chemistry in flames [Schofield (2001)].

$$SH + H_2 \longleftrightarrow H_2S + H$$

$$H + S_2 \longleftrightarrow SH + S$$

$$S + H_2 \longleftrightarrow SH + H$$

$$H + SO_2 \longleftrightarrow SO + OH$$

$$S + OH \longleftrightarrow SO + H$$

$$S_2 + OH \longleftrightarrow S_2O + H$$

$$OH + H_2 \longleftrightarrow H_2O + H$$

Kramlich et al (1981) performed comprehensive sulfur species measurements on combustion gases in a premixed, jet-stirred reactor containing 0.23 mole % total sulfur, in temperature range $1600 \leq T \leq 1800K$. Reactor fuels were C_3H_8, C_2H_2, CH_4, H_2, and a H_2/CO mixture. Sulfur dopants were C_4H_4S, H_2S, and SO_2. For hydrocarbon combustion doped with H_2S and SO_2, the stable sulfurous species measured were SO_2, SO_3, H_2S, COS and CS_2. It was confirmed that SO_2 was always the dominant product. When C_4H_4S was the dopant, it was also measured in the combustion gases. At fuel-lean conditions SO_3 accounted for no more than 2 – 3 % of the total sulfur. At fuel rich conditions, the sum (H_2S + COS + $2CS_2$ + C_4H_4S) accounted for no more than 20% of the total sulfur. Other sulfurous organics, including mercaptans were not detected. For non-hydrocarbon combustion, H_2S was the only non-SO_x species measured. Their data indicated that H_2S is the favoured sampled species when hydrocarbons are lacking and it is replaced by COS and CS_2 as unburned hydrocarbons in the combustion gases increase.

3.1.2.2. High Temperature chemistry of SO_2 and SO_3

The predominant sulfur-containing product formed by the combustion or slow oxidation of sulfur compounds and elementary sulfur is almost invariably sulfur dioxide. Even when oxygen is present in large stoichiometric excess, sulfur trioxide is seldom found in amounts greater than a few percent of the sulfur dioxide [Cullis and Mulcahy (1972)].The latter statement from Cullis and Mulcahy (1972) continues to remain valid , as the more recent flow reactor studies of SO_2 oxidation under post-flame conditions [Glarborg et al (1996), Mueller et al (2000)] indicate fractional conversions of SO_2 to SO_3 only in the order of a few percent. Nevertheless, although the concentrations of sulfur trioxide actually

found in the products of combustion of sulfur-containing fuels are small, their presence has profound effects on combustion technology [Cullis and Mulcahy, (1972)]. The presence of SO_3 has implications for formation of aerosols in biomass-fired systems [Christensen and Livbjerg (1996), Jensen et al (2005)].

Hindiyarti et al (2007) revised Rasmussen's (2007) mechanism for SO_3/SO_2 reactions and they reported a good agreement with a range of experimental data from reactor experiments. According to Hindiyarti et al (2007), the key reactions are those presented in Table 8. Depending on the reaction conditions, steps 1-3 may serve to either consume SO_3 (forward direction) or form SO_3 (reverse direction). Another important reaction for the SO_3/SO_2 ratio is the step 4.

Studies on aircraft aerosol emissions pointed out the necessity to control the sulfur oxidation kinetics during fuel combustion [Schumann et al (2002), Karcher (1997)]. According to Schuman et al (2002), sulfuric acid is formed mainly inside the engine and in the young cooling exhausts jet and is then rapidly depleted from the gas phase within about a second as the plume age increases.

Table 8 : Key reactions in the reaction mechanism of Hindiyarti et al (2007) (Units: cm, mol, s, K)

no.	reaction	*A*	*n*	*E/R*
1	$SO_3 + H \rightleftharpoons SO_2 + OH$	8.4E09	1.22	1670
2	$SO_3 + O \rightleftharpoons SO_2 + O_2$	2.8E04	2.57	14700
3	$SO_3 + OH \rightleftharpoons SO_2 + HO_2$	4.8E04	2.46	13700
4	$SO_2 + O(+M) \rightleftharpoons SO_3(+M)$[a]	3.7E11	0.00	850
	low-pressure limit	2.4E27	−3.60	2610
	Troe parameters 0.442, 316, 7442			
	low-pressure limit (N_2)	2.9E27	−3.58	2620
	Troe parameters (N_2) 0.43, 371, 7442			
5	$SO_2 + OH(+M) \rightleftharpoons HOSO_2(+M)$[b]	5.7E12	−0.27	0
	low-pressure limit	1.7E27	−4.09	0
	Troe parameters 0.10, 1E−30, 1E30			
6	$SO_2 + SO_2 \rightleftharpoons SO_3 + SO$	5.0E07	2.00	37750
7	$HOSO_2 \rightleftharpoons SO_3 + H$	1.4E18	−2.91	27630
8.	$HOSO_2 + H \rightleftharpoons SO_2 + H_2O$	1.0E12	0.00	0
9.	$HOSO_2 + O \rightleftharpoons SO_3 + OH$	5.0E12	0.00	0
10.	$HOSO_2 + OH \rightleftharpoons SO_3 + H_2O$	1.0E12	0.00	0
11.	$HOSO_2 + O_2 \rightleftharpoons HO_2 + SO_3$	7.8E11	0.00	330

[a] Enhanced third-body coefficients: $N_2 = 0$, $SO_2 = 10$, $H_2O = 10$; [b] Enhanced third-body coefficients: $N_2 = 1$, $SO_2 = 5$, $H_2O = 5$.

3.1.2.3. Sulfur trioxide to sulfuric acid

In most circumstances sulfur trioxide in combustion products is converted to sulfuric acid at low temperatures. Its reaction with water in the gas phase is evidently very rapid. Although SO_3 is the primary precursor to H_2SO_4, it is not an accurate description of the chemical compound present in all areas of an exhaust stream [Irvin et al (2006)]. Thermodynamic equilibrium concentrations of the relevant species in a flue gas are shown in Figure 13. At elevated flue gas temperatures (>538^{o}C), the primary sulfur compound present, excluding SO_2, is SO_3. SO_3 is thermodynamically favored at lower temperatures but kinetic limitations and/or high gas cooling rates often prevent an SO_3/SO_2 partial equilibrium from being attained [Johnsson (2000)].

As the flue gas is cooled, the SO_3 present in the flue gas will react with water vapour to form vapour phase sulfuric acid, H_2SO_4, so that all the SO_3 has turned into H_2SO_4 by the time the gas reaches 204^{o}C. Therefore, sulfuric acid dew point depends on the SO_3 conversion rate. If the flue gas is further cooled below the acid dew point, the vapour phase H_2SO_4 can condense with water to form sulfuric acid mist (SAM). Under some conditions, the chemistry and physics associated with the condensation of vapour phase H_2SO_4 can lead to the formation of submicron SAM particles. SAM aerosol particles are a mixture of water and sulfuric acid , and can exist at different levels of water concentrations. Equilibrium concentration of H_2SO_4 in a spherical droplet of H_2SO_4 and H_2O as a function of relative humidity and droplet diameter is presented in Figure 14.

The equilibrium relationship between SO_3, H_2O and H_2SO_4 is given by Gmitro and Vermeulen (1964) by Equation 12.

Equation 12:

$$\ln K_p = -6,71464 \cdot \ln\left(\frac{298}{T}\right) - \frac{81016.1}{T^2} - \frac{9643.04}{T} + 14.74965 - 0.009458 \cdot T + 0.00000219062 \cdot T^2$$

where

$K_p = \dfrac{P_{SO_3} \cdot P_{H_2O}}{P_{H_2SO_4}}$ and T= Temperature (^{o}K)

Using the equilibrium relationship, the fraction of SO_3 converted to H_2SO_4 as a function of temperature and water vapour concentration in the flue gas is presented in Figure 15. The reaction between SO_3 and water vapour is reported to be rapid and can be assumed to proceed to equilibrium in the flue gas. Prediction of the sulfuric acid vapour content is thus equivalent to predicting the amount of SO_3 in the flue gas.

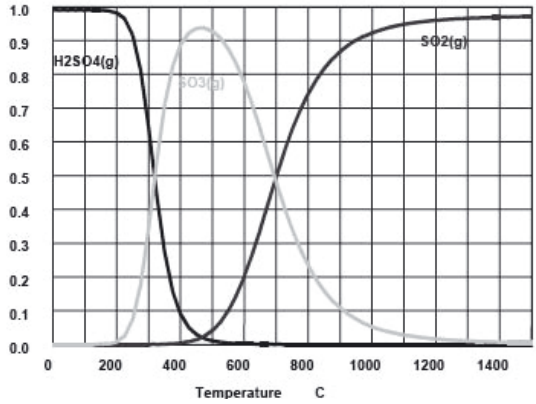

Figure 13: Equilibrium composition of flue gas sulfur species [Gabrielli et al (2000)]

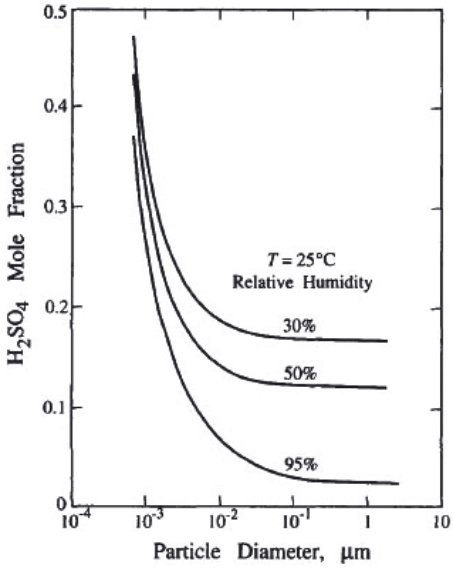

Figure 14: Equilibrium concentration of H_2SO_4 in a spherical droplet of H_2SO_4 and H_2O as a function of relative humidity and droplet diameter [Seinfeld (2006)]

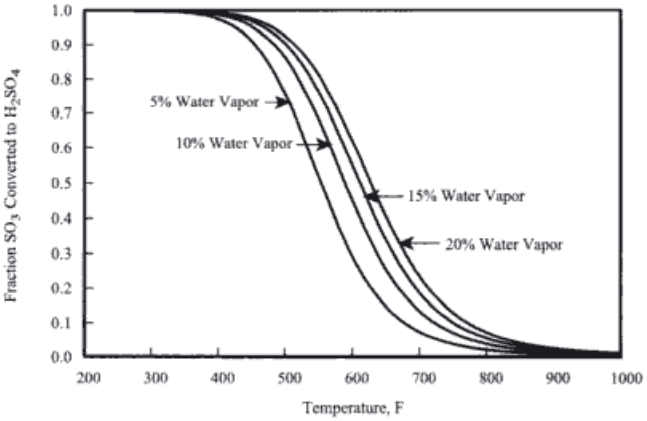

Figure 15: SO_3/ H_2SO_4 equilibrium [Schnelle and Brown (2001)]

The system $H_2O/SO_3/H_2SO_4$ is of immense importance in connection with the combustion of sulfur-containing fuels. It is essential to ensure that the temperature of the combustion gas does not drop below the dew point prior to discharge, since otherwise there is a danger of corrosion by condensing sulfuric acid. Various formulae have been developed for calculating dewpoints theoretically as a function of the total gas pressure as well as the H_2O, SO_3, and H_2SO_4 partial pressures.

In atmosphere, nucleation starts from the formation of sulfuric acid (H_2SO_4), because of its low vapour pressure. Formation of H_2SO_4 involves Reaction Equation 7 to Reaction Equation 9. Reaction Equation 7 is the rate limiting step. Once formed, H_2SO_4 immediately becomes hydrated. The hydrated H_2SO_4 molecules are nuclei, and nucleation takes place by condensation of H_2SO_4 molecules and coagulation. That is, monomer becomes dimer, and dimer becomes trimer, and so on, via Reaction Equation 10 to Reaction Equation 13 .

Reaction Equation 7	$SO_2 + OH \rightarrow HOSO_2$
Reaction Equation 8	$HOSO_2 + O_2 \rightarrow HO_2 + SO_3$
Reaction Equation 9	$SO_3 + H_2O \rightarrow H_2SO_4$
Reaction Equation 10	$H_2SO_4 + H_2SO_4 \rightarrow (H_2SO_4)_2$

Reaction Equation 11 $(H_2SO_4)_2 + H_2SO_4 \rightarrow (H_2SO_4)_3$

Reaction Equation 12 $(H_2SO_4)_3 + H_2SO_4 \rightarrow (H_2SO_4)_4$

Reaction Equation 13 $(H_2SO_4)_4 + H_2SO_4 \rightarrow (H_2SO_4)_5$

The formation of new nuclei from vapour in the atmosphere is expected to be mainly the result of binary homogeneous nucleation of sulfuric acid/water droplets. Because of the strong attraction between sulfuric acid and water molecules, such nucleation is greatly enhanced over the nucleation of the pure species [Clement and Ford (1999)].

Dew Point

Dew point is the temperature to which a given parcel of air should be cooled, at constant pressure and water content, to reach a state at which the saturation vapour pressure is equal to the actual vapour pressure. Any further cooling will result in the formation of liquid (dew) or solid (frost/ice).

In its simplest form, when dealing with clean air, the dewpoint may be directly plotted from the water vapour pressure tables [Weast (1988)]. Dew point of a gas mixture however depends upon not only on the water content but also upon the content of other compounds that condense into liquids at ambient temperature. When other gaseous species are present, such as SO_3 or SO_2, the dewpoint will deviate from the ideal dewpoint line. Dewpoint in the presence of these gases can be calculated by means of the equations of Kiang (1981), Perry and Chilton (1973), and Verhoff and Banchero (1974). The higher the boiling point of the other compound, the more effect it has on the dew point. Because sulfuric acid has a very high boiling point (290°C) it can have a significant effect on the final sample dew point. The reader should refer to Huijbregts and Leferink (2004) for further details.

Saturation vapour pressure

Simonsen (1992) expressed the saturation vapour pressure of sulfuric acid in temperature range 20-160^{o}C with Equation 13. A commonly used data source for chemical engineering students, Perry's [Perry and Green (1997)], used the data from Vermeulen et al (1982); therefore both data is presented in Figure 16, for comparison reasons. The deviation of values calculated by Simonsen's equation from those of Vermeulen, is less than 0.3 % if used in the temperature range 20-160^{o}C. At higher temperatures, the latter increases to 5% for 160^{o}C <T<300^{o}C and to 20% for 300^{o}C <T< 350^{o}C.

Equation 13: $$\ln P_{H_2SO_4}^{sat} = -11607.7(\frac{1}{T} - \frac{1}{T_r}) - 6.01037\ln(\frac{T}{T_r}) + \ln(3.10*10^{-5})$$

where T_r = 373.15 K.

Saturation Ratio

The saturation ratio S_i of a component i in a gas is defined by the ratio between the actual vapour pressure P_i and the vapour pressure over an infinite plane surface of a pure liquid of the component $P_{i\infty}$ at the gas temperature T (Equation 14)

Equation 14: $$S_i = \frac{p_i}{p_{i\infty}(T)}$$

For S_i<1 the gas is unsaturated, for S_i=1 the gas is saturated and for S_i>1 the gas is super saturated with respect to component i. In a gas with only one condensable component S_1=1 gives the dew point. For multi-component condensable gases the saturation ratio for each component can be less than one at the dew point.

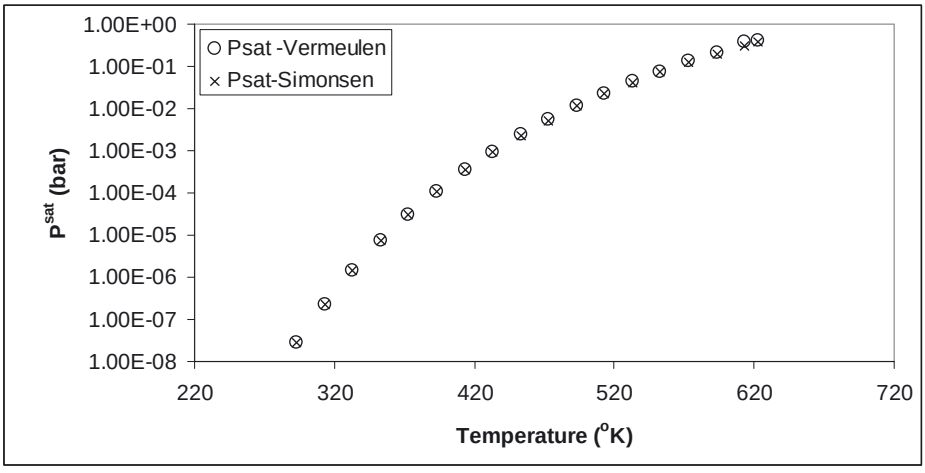

Figure 16: Saturation vapour pressure of sulfuric acid in temperature range 293 – 623 °K

3.1.2.4. Gas to Particle Conversion

Gas to particle conversion may result from homogeneous gas-phase processes, or it may be controlled by processes in the particulate phase. Gas-phase processes, either physical or chemical, can produce a supersaturated state, which then collapses by aerosol formation. Physical processes producing supersaturation include adiabatic expansion or mixing with cooler air or radiative or conductive cooling.

Once a condensable species has been formed in the gas phase, the system is in a nonequilibrium state. It may pass toward equilibrium by the generation of new particles (homogeneous nucleation) or by condensation on existing particles (heterogeneous condensation). Homogeneous or heterogeneous condensation can occur in the same parcel of gas either sequentially or simultaneously. In flow systems, this can lead to sustained oscillations in particle number density. If all collisions among condensable molecules are effective, the process resembles aerosol coagulation. However, in certain important cases, small molecular clusters are unstable; an energy barrier must be surmounted before stable nuclei can form. Heterogeneous condensation may be limited by gas-phase transport processes or by chemical reactions in the aerosol particles.

Ulrich (1971) proposed an approximate criterion (Equation 15) for determining whether nucleation or coagulation is the dominant process for particle formation following the formation of a high density of condensable molecules by a fast chemical reaction or a rapid quench. His criterion is based on the critical particle diameter given by

Equation 15:
$$d_p^* = \frac{\sigma v_m}{kT \ln(p / p_s)}$$

where

p/p_s : the ratio of partial pressure of the condensable vapour to the saturation vapour pressure at the local temperature, T

σ: surface tension

v_m : molecular volume of the material composing the particle

This equation holds best for particles composed of a large number of molecules (>50), but in Ulrich's analysis it is used for an order of magnitude estimate down to molecular dimensions.

When the partial pressure of the condensing vapour is very high compared to the saturation vapour pressure, d_p* approaches molecular dimensions. Equating dp* to d_{pm} which is given by Equation 16, Equation 17 is obtained. Thus, for partial pressures higher than the value corresponding to the latter equation, individual molecules can serve as stable nuclei, and the problem reduces to the case of the coagulation of coalescing sphere. This analysis holds when particle collision leads to coalescence and not to formation of solid primary particles and their aggregates. The assumption of coalescing particles usually holds best during the early stages of particle formation. In the later stages, for the low vapour pressure substances, coalescence slows and solid primary particles form.

Equation 16:
$$d_{pm} = \left(\frac{6v_m}{\pi} \right)^{1/3}$$

Equation 17:
$$\frac{\sigma v_m}{kT \ln(p / p_s)} = \left(\frac{6v_m}{\pi} \right)^{1/3}$$
$$P = P_s \exp\left\{ \left(\frac{\pi}{6} \right)^{1/3} \frac{\sigma v_m^{2/3}}{kT} \right\}$$

3.1.2.5. Homogeneous Nucleation

In the context of air pollution, nucleation is gas-to-particle conversion, in which low volatile gas phase species are converted to aerosol phases. Collisions between the molecules lead to the formation of molecular clusters whose lifetime depends on the strength of the bonds holding the clusters together. When a system becomes supersaturated, these clusters increase in concentration and pass through the critical size, d_p* by attachment of single molecules. The formation of stable nuclei relieves the super-saturation in the gas. Because condensation nuclei are generated by vapour itself, the process is known as homogeneous nucleation or self-nucleation.

The formation of particles from vapour molecules may be visualized to occur as the result of the clustering of vapour molecules to form embryos of the new phase followed by the growth of some of these clusters to form macroscopic quantities of the new phase. In Figure 17, this process is shown.

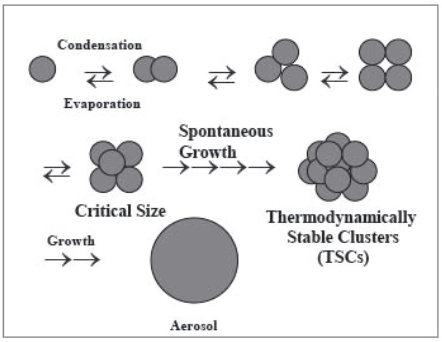

Figure 17: The formation of particles from vapour molecules

Friedlander (2000) gives the correlation for the homogeneous nucleation rate (droplet current) by Equation 18 :

Equation 18 :
$$J = 2\left[\frac{p_1}{\sqrt{2\pi mkT}}\right]\left(n_1 v_m^{2/3}\right)\sqrt{\frac{\sigma v_m^{2/3}}{kT}}\exp\left[-\frac{16\pi\sigma^3 v_m^2}{3(kT)^3(\ln S)^2}\right]$$

where

p_1: monomer partial pressure

m: molecular mass

k: Boltzmann constant

T: temperature

n_1: concentration of monomer

v_m: molecular volume of the liquid

σ: surface tension of the liquid

S: saturation ratio (set equal to p1/ps where ps is the vapour pressure above a plane surface of the liquid)

$\frac{p_1}{\sqrt{2\pi mkT}}$ is the monomer flux (molecules per unit area per unit time)

$n_1 v_m^{2/3}$ is proportional to the monomer surface area per unit volume of gas

$\sqrt{\frac{\sigma v_m^{2/3}}{kT}}$ is dimensionless

Small changes in the saturation ratio, S, result in order of magnitude change in droplet current, because of its dependence on lnS in the exponential term. Although a supersaturated vapour is always unstable, the rate of generation of stable nuclei is negligible for small values of S. When I=1 particle/cm^3.sec, particle formation can be conveniently observed experimentally. The corresponding value of S is called the critical saturation ratio, S_{crit}. The stable nuclei size range from about 2 to 3 nm for all of the substances. The number of molecules in the stable nuclei ranges from 32 to 128. For condensable materials with very low vapour pressures, essentially all collisions are effective and the critical nucleus is a single molecule [Friedlander(2000)].

3.1.2.6. Binary homogeneous nucleation of water-sulfuric acid

Significant particle formation by heteromolecular, homogeneous nucleation between an acid gas and water vapour was first predicted for sulfuric acid and water by Doyle (1961) using the binary nucleation theory developed by Reiss (1950).

As shown by Heist (1974) and Reiss (1950) a plot of ΔG (the Gibbs free energy of formation of a liquid droplet in a binary mixture of vapours) vs n_A and n_W (number of moles of acid and water) in three dimensional space exhibits a saddle point. Once a cluster reaches the saddle point, it is nucleated and will grow to a larger particle. Hence, the radius and composition at this point (denoted by symbols r^*, n_A^*; and n_W^*) are called critical or equilibrium values. Sometimes, they may be referred to as growth parameters. Reiss (1950) derived the theoretical rate of binary nucleation of liquid droplets from a mixture of vapours by assuming that the cluster flux over the saddle follows the direction of steepest descent on the free energy surface in the vicinity of the saddle point. Later investigators showed that the direction of passage deviates from that direction due to the kinetics of cluster growth, and developed concise and general equations for evaluating the total rate of formation of stable clusters. Numerous studies have attempted to improve theoretical predictions by focusing on the nature of the free energy surface [Flagan (2007)].

The homogeneous nucleation rate (particles formed per cm3 per sec) in a binary mixture of vapours with NW >> NA (concentration of water vapour and acid ,molescules/cm3) is expressed byEquation 19 (Kiang and Stauffer (1973), Mirabel and Katz (1974), Hamill and Caddle (1977)):

Equation 19:
$$J = 4\pi r^{*2} \beta_A N_W \exp\left(-\frac{\Delta G^*}{KT}\right)$$

where

K is the Boltzmann constant, and β_A is the impinging rate of gaseous sulfuric acid molecules on a surface of unit area ($cm^{-2}.s^{-1}$):

$$\beta_A = N_A \left(\frac{KT}{2\pi m_A}\right)^{1/2}$$

where m_A is the mass of one molecule of H_2SO_4.

Dimensional analysis:

$$J = 4\pi r^{*2} N_A N_W \left(\frac{KT}{2\pi m_A}\right)^{1/2} \exp\left(-\frac{\frac{4}{3}\pi r^{*2}\sigma}{KT}\right)$$

$$m^{-3}\cdot s^{-1} = m^2 \cdot m^{-3} \cdot m^{-3} \cdot \left(\frac{\frac{kg\cdot m^2}{s^2\cdot K}}{kg}\right)^{1/2} \exp\left(\frac{m^2 \cdot \frac{J}{m^2}}{\frac{J}{K}\cdot K}\right)$$

$$N_A = \frac{P_A}{P_{total}} \cdot \frac{6.02214179\cdot 10^{23}}{0.08205784 \cdot T}$$

where P_A/P_{total} would be the mole faction of acid in the gas phase.

Because of the related health and environmental effects of ultrafine particles, there had been many different applications of the classical binary homogeneous nucleation theory to calculate particle formation from H_2SO_4 – H_2O systems, i.e: in diluting engine exhaust, in the atmosphere. Hua and Fangqun (2006) investigated the role of H_2SO_4–H_2O binary homogeneous nucleation (BHN) in the formation of nanoparticles in the diluting vehicular exhaust, using a kinetic H_2SO_4–H_2O model suitable for studying the nucleation process in rapidly diluting exhaust. For the vehicles running on

the fuel with fuel sulfur content (FSC) of ~330 ppm, they found that BHN may significantly contribute to nanoparticle formation, especially when the ambient temperature is low and the relative humidity is high. Their simulations showed that BHN rate is very sensitive to FSC and sulfur to sulfuric acid conversion efficiency (ε_s). They reported that for ε_s value of 1%, BHN is negligible under typical conditions when FSC is <~100 ppm. However, nanoparticle formation via BHN may still be significant if ε_s > ~4% even after FSC is reduced to below ~50 ppm.

In the recent years, parametrizations became available in order to save computation time in the large-scale models. Bein and Wexler (2007) calculated the nucleation rates for two different interpretations of H_2SO_4 activity and compared their results to the available parameterizations. Their comparison figure shows that the nucleation rates of their work and those of Vehkamaki et al (2002 and 2003) trace each other very well and show the same dependence on temperature and relative humidity; while Vehkamaki's results being orders of magnitude larger than the calculations of their work, as well as the parameterization of Kulmala et al (1998). The critical cluster mole fractions given by the parameterizations of Vehkamaki et al.(2003) are in good agreement with their calculations for the case that activity represents the total concentration above solution rather than the monomer. Despite this, the critical cluster diameters of Vehkamaki et al (2003) are significantly smaller than those calculated in Bein and Wexler's (2007) work, and that may explain why the nucleation rates of Vehkamaki et al (2003) are orders of magnitude larger. Lemmetty et al (2006) used the parameterization of Vehkamäki et al. (2003) and reported that Vehkamaki et al's (2003) parametrisations give sufficient nucleation to explain the formation of the nucleation mode with low-sulfur content fuel in cases where the sulfuric acid conversion is high (over 25%).

In regards to Kulmala's (1998) work, Vehkamaki emphasized that the use of nucleation parametrizations based on atmospheric conditions, and their possible extrapolation to much higher temperatures involved in diesel exhausts makes the validity of those models questionable for their conditions of interest. Regarding their own parametrization, Vehkamaki et al (2003) used experimental data and ab initio results where available to improve the classical model. Strictly speaking, experimental results for surface tension exist only when T<323 K, for density when T<373 K, and for activities T < 350 K. At temperatures above these they have used extrapolations. However, the nucleation rate does not depend significantly on the surface tension and density formulas used. The nucleation rate is an extremely sensitive function of the sulfuric acid concentration. Indeed, a factor of 10 change in the sulfuric acid concentration can lead to a 10 orders of magnitude change in nucleation rate. Vehkamaki et al (2003) noted the validity region and accuracy of their parametrisation as presented in Table 9. As a sensitivity analysis Vehkamaki et al (2003) compared

the nucleation rates obtained using their formulas to rates calculated using the formulas given by Myhre et al. (1998), and they reported that the difference in nucleation rates was at most one order of magnitude, in most cases just 10-20%.

Recently, Jung et al (2008) tested the ability of six different nucleation parameterizations to reproduce the occurrence or lack of a nucleation event. The tested parameterizations are listed below.

(1) the ternary NH_3-H_2SO_4-H_2O nucleation parameterization of Napari et al. (2002),

(2) the binary H_2SO_4-H_2O parameterization of Vehkamaki et al. (2002),

(3) the binary H_2SO_4-H_2O parameterization of the Jaecker-Voirol and Mirabel (1989) theory by Russell et al. (1994),

(4) the semi-empirical first order in sulfuric acid concentration expression proposed by Spracklen et al (2006),

(5) the ion-induced nucleation parameterization of Modgil et al. (2005), and

(6) the barrierless rate expression of Clement and Ford (1999).

The ternary sulfuric acid-ammonia-water theory was the only one that was successful for all tests. Sensitivity tests of the remaining parameterizations suggested that increasing or decreasing the corresponding nucleation rates does not change the overall performance of the parameterizations when both the nucleation and non-nucleation days are included in the tests. They suggested that it is important in similar evaluation studies to consider the performance of the various theories on days when nucleation did not take place.

Table 9: The validity region and accuracy of Vehkamaki et als (2003) parametrisation

$300.15 < T < 400.15$.	
$2 \cdot 10^9/cm^3 \leq N_a \leq 2 \cdot 10^{15}/cm^3$	
$1\% \leq RH \leq 100\%$	
$10^{-1} \leq J\ (/cm^3 s \leq 10^{14}$	$0.02 < J_{theor}/J_{para} < 11$
$0.15 < x^* < 0.54$	$-0.007 < x^*_{theor} - x^*_{para} < 0.006$
$6 < N^*_{tot} < 1330.54$	$-1.4 < N^*_{tot,\ theor} - N^*_{tot,para} < 3.1$
$0.4 < r^* < 1.16$	$-0.11 < r^*_{theor} - r^*_{para}$ (nm) < 0.018

T : Absolute temperature (^oK) /

N_a: Total gas-phase concentration of sulfuric acid ($1/cm^3$)

RH : Relative humidity in percent

J : Nucleation rate ($/cm^3.s$)

x* : Mole fraction of sulfuric acid in the critical cluster

N^*_{tot} : Total number of molecules in the critical cluster

r * : Radius of the critical cluster (nm)

the subscripts theor and para refer to theoretically calculated values and the values calculated using the parametrization.

3.2. Emissions from Gas Cookers

Gas-burning appliances premix some air with the fuel gas before it burns as a laminar jet diffusion flame. In diffusion flames, the combustion process is mixing controlled. Thus the mixture may not be stoichiometric at all points throughout the flame, resulting in CO emissions.

Stubington et al (1994) investigated the emissions (NO, NO_2, CO and hydrocarbons) and efficiencies of production cooktop burners firing natural gas. It was found that the emissions and thermal efficiencies were markedly affected by (1) the thermal input, with or without a load on the burner, and (2) the load height to flame length ratio with a load on the burner. They reported that raising the thermal input or the load height to flame length ratio affects the emission rate of each of the species differently, and it generally reduces the thermal efficiency: Both NOx and NO generally rise with either thermal input or load height to flame length ratio while the emission rate of CO and hydrocarbon fall with increasing thermal input. Ashman et al. (1994) used a single production cooktop burner to determine the effects of loading height and thermal input on its efficiency and gaseous emissions. It was found that the thermal efficiency of the burner decreases with increasing loading height: At a constant (low) loading height the thermal efficiency is higher at lower thermal inputs and NOx increases with increasing loading height, while CO increases with decreasing loading height.

There are studies available in literature reporting the effects of cooktop burner design and operation factors (such as cap material, cap size, port shape, port size, port spacing, central secondary aeration,

flame inserts, load height, load height to flame length ratio, thermal input, etc) on the gaseous emissions (NOx, CO and hydrocarbon emissions) from the natural gas fired cooktop burners, however these studies do not give any correlations for particulate matter or soot emissions [Stubington et al (1994), Junus et al (1994)]. Ko and Lin (2003) studied the influence of five significant parameters, namely gas composition, primary aeration, gas flow rate (heat input), gas supply pressure, and loading height, on the thermal efficiency and CO emissions from domestic gas stoves burning natural gas with various heating values. They reported that using natural gas with high heating value instead of natural gas with low heating value results in a decrease in thermal efficiency (due to higher thermal input) and an increase in CO emission (caused by incomplete combustion). They concluded that using the same gas stove to burn natural gas with various heating values is inappropriate and hazardous due to the possible occurrence of incomplete combustion. Together with the experimentally proved increase in CO emissions, they have pointed to shortcomings such as soot formation, lift-off, flashback and inadequate heat input [Stubington et al (1994)]. Today this is a well known fact to the gas industry, and its control is a matter of using the proper wobbe index as different gases with the same wobbe index will impose the same load on the burner.

Seaton and Dennekamp (2003) carried out outdoor measurements in Aberdeen city as a part of the study of the effects of exposures to particles on the health of individuals with chronic lung disease over the course of 6 months. There they found a striking association between concentrations of nitrogen oxides and the number of particles of <100nm aerodynamic diameter measured simultaneously (Figure 18). These associations were so close that Seaton and Dennekamp (2003) concluded that if NO_2 in these environments is measured as an index of pollution and is shown to be associated with health effects, these effects could equally be due to the numbers of particles since it would be impossible to distinguish their effects in epidemiological studies. Seaton and Dennekamp (2003) also carried out an investigation during which they have measured simultaneously particle number counts (by TSI 3934 scanning mobility particle sizer) and nitrogen oxides (by ML9841A chemo luminescent analyzer). One of these was in an unventilated laboratory during a study of the effects of electric and gas cooking on indoor pollution, the pollution source being a gas cooker. Figure 19 shows the close relationship between the two pollutants when derived from a common source.

Dennekamp et al (2001) also carried out cooking experiments with the gas cooker and the electric cooker, comparing the effects of the two cooking fuels. Figure 20 shows the size range of particles generated while four gas rings were on for 2 hours. 5, 15, and 30 minutes after the rings were turned on, the peak concentration was respectively at 15, 30, and 40 nm diameter. Thus, while the gas rings were burning, the particles grew up to a peak of about 50-70 nm.

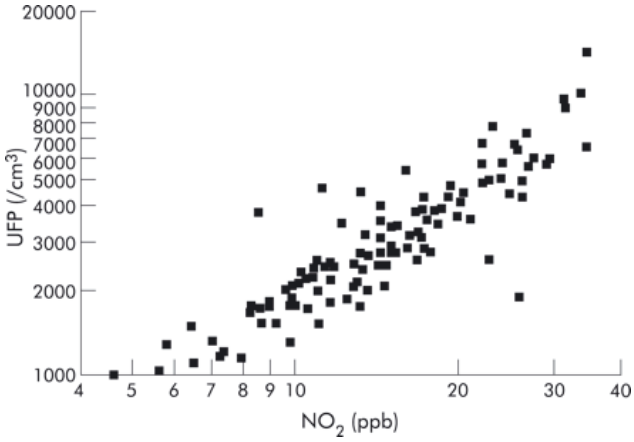

Figure 18: Relationship between mean outdoor air 24 hour counts of particles <100 nm in diameter (UFP) and nitrogen dioxide (NO_2) concentrations in parts per billion. Data represent 6 months of continuous side by side measurement [Seaton and Dennekamp (2003)].

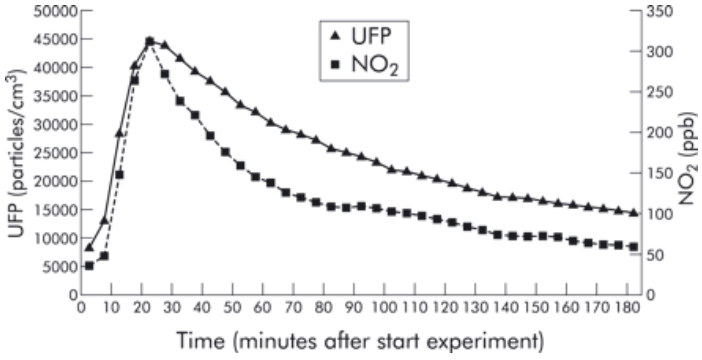

Figure 19 : Indoor ultrafine particle number (UFP) and nitrogen dioxide (NO_2) concentrations in an unventilated laboratory over 3 hours during and after burning of one gas ring for 15 minutes (r = 0.97) [Seaton and Dennekamp (2003)].

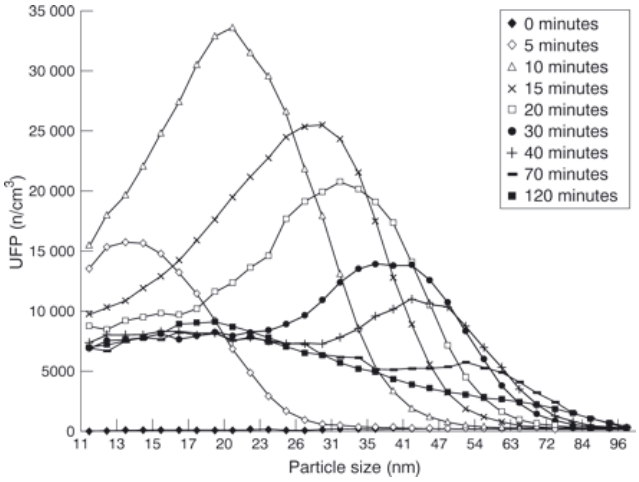

Figure 20: Distribution of particle size at different times while four gas rings were turned on full power for 2 hours [Dennekamp et al (2001)].

Bang et al (2004) communicated recently that like many other phenomena in nature, the presence of carbon nanotubes in blue combustion flames went virtually unrecognized because it was essentially unexpected. Observations of carbon nanotubes and related nano-forms in relatively efficient burning, mostly blue combustion flames such as propane and natural gas suggests that the proliferation of so-called clean- burning gaseous fuel sources, particularly methane-series gases ($C_nH_{2(n+1)}$; n=1,2,3…etc) may, in fact, make a significant contribution of carbon nanocrystal forms to both the indoor and outdoor air environment.

Murr et al (2004) reported aggregated multiwall carbon nanotubes (with diameters ranging from 3 to 30 nm) and related carbon nanocrystal forms ranging in size from 0.4 to 2 μm (average diameter) in the combustion streams for methane/air, natural gas/air, and propane gas/air flames from domestic (kitchen) stoves. These aggregates, shown in Figure 21, are reported to be essentially pure carbon or graphene sometimes exhibiting traces (1–2%) of sulfur. In Figure 22, their samples collected from domestic propane and natural gas (~96% methane) combustion streams (by locating the thermal precipitator roughly 0.3 m vertically and horizontally from the flame or gas stove burner for 0.5 h) are compared with particle aggregates collected from a nearly optimized, pure methane/air flame exhaust (collected by locating the thermal precipitator roughly 1 m from the 7 cm high, essentially blue flame) and the airborne particulate matter (collected on carbon/formvar-coated and/or silicon monoxide/ formvar-coated, 3 mm, 100 mesh nickel transmission electron microscope (TEM) grids placed in a thermal precipitator, described in detail in Bang et al (2003) for periods of 0.5 h, with the thermal

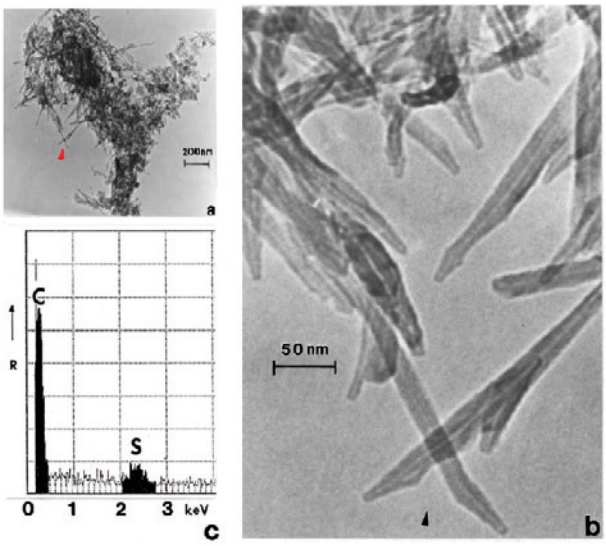

Figure 21: Typical TEM analysis of methane/air nanoparticle aggregate by Murr et al(2004) a.)Bright-field TEM image, b.)Magnified, brightfield TEM image at arrow in (a) showing multi-walled nanotubes, (c) Corresponding EDS spectrum for (a). (Reproduced from Murr et al(2004)).

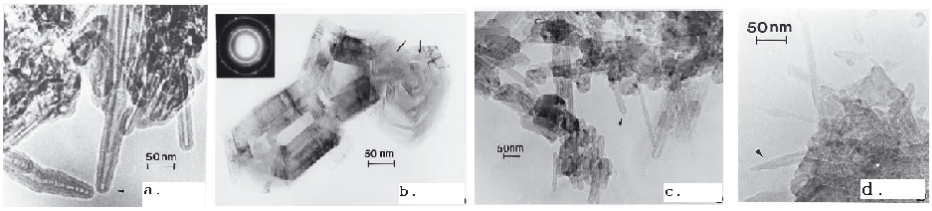

Figure 22: a.) TEM images of large carbon nanoparticle aggregate in methane/air flame exhaust : showing asymmetric cone ends for concentric, multi-walled carbon nanotubes b.) Bright-field TEM image of carbon nanocrystal aggregate from a natural gas/air flame exhaust: containing onion-like features. The SAED pattern insert shows prominent graphite spotty reflection rings c.) Typical TEM image of a carbon nanocrystal aggregate in a propane/air flame exhaust: nanotubes, shells,and spheres consisting of many concentric graphene walls d.) Complex carbon/silica nanocrystal particle aggregate collected in the outdoor air: showing carbon nanotubes and other carbon nanocrystal forms (Reproduced from Murr et al(2004)).

precipitator located approximately 1.5 m from ground level). They reported that all these particulate matter examples exhibit the same variations in carbon nanocrystal structures, while for the airborne particulate matter there has been often an agglomeration or aggregation of other common atmospheric mineral nanocrystals (i.e. silica) with carbon nanotubes and other, related nanocrystal forms. The implications of Bang and Murr's works are that aggregates of carbon nanotubes and other nanocrystals are a common feature of the indoor air in homes utilizing gas cooking stoves, and in the outdoor air as a consequence of a variety of domestic heating sources and other industrial gas combustion sources venting the exhaust to the outdoor air.

Following Murr et al (2004), Murr and Soto (2005) examined the nanoparticle aggregates from conventional common fuel - gas–air combustion flame exhausts, by transmission electron microscopy (TEM) . They collected the particles onto TEM grid substrates by thermophoretic deposition (or thermal precipitation, described in detail in Bang et al., (2003). The thermal precipitator was positioned proximate (~ 0.5 m) to the exhausts or exhaust streams for a laminar methane–air co-flow flame system [Murr et al (2004)], natural gas (~ 96% CH_4)–air and propane (C_3H_8)–air kitchen stove-top burners, home water heater roof-top exhausts, and outdoor locations proximate (~ 50 m–100 m) to industrial/commercial natural gas combustion exhaust systems (e.g. steam tur bine electric power generation units). The most efficient and broadest particulate matter regimes were reported to be obtained from kitchen stove-top burners which, even under normal operation, often produce momentary yellow flame bursts due to short or intermittent air flow interruptions. Collection times normally ranged from 15 min to 30 min. The collection grids were examined in a Hitachi H- 8000 analytical transmission electron microscope. A variety of soot and graphitic particulates as well as complex aggregates of multiwall carbon nanotubes (MWCNT) and other, related fullerene polyhedra were observed in the TEM, and the crystallinities and nanomorphologies of these various carbon nanoforms were observed and compared. Figure 23 and Figure 24 present the TEM image of aggregates collected from natural gas-air stove-top exhaust stream and the roof exhaust for a natural gas–air water heater, in order. They observed that those nanoparticle aggregates consist of occasional aggregates of mostly turbostratic carbon spherules, aggregates of crystalline graphite nanoparticles mixed with other fullerene nanoforms; and aggregates of various sizes of multiwall carbon nanotubes and other multishell, fullerene polyhedra for optimal blue-flame combustion. They reported that nanoparticle aggregation or the occurrence of carbon nanoforms always occurred as aggregates with nominal sizes ranging from about 0.5 Am to 1.5 Am.

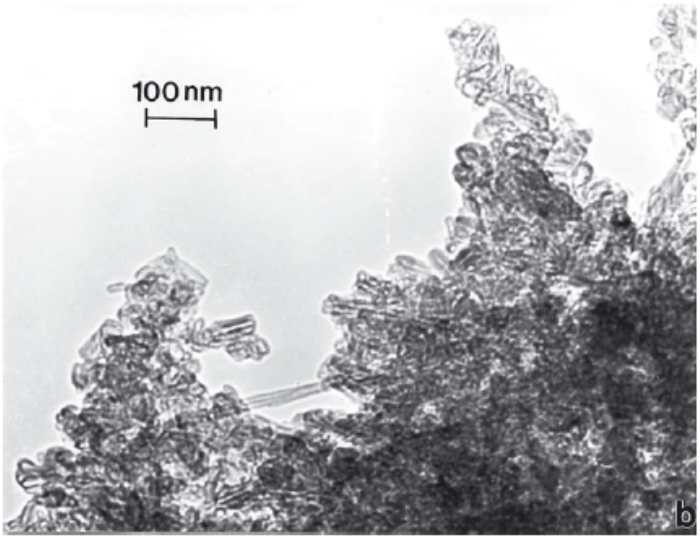

Figure 23: Section of aggregate composed of short carbon nanotubes and other fullerene nanoforms collected in a natural gas–air stove-top exhaust stream [Murr and Soto (2005)]

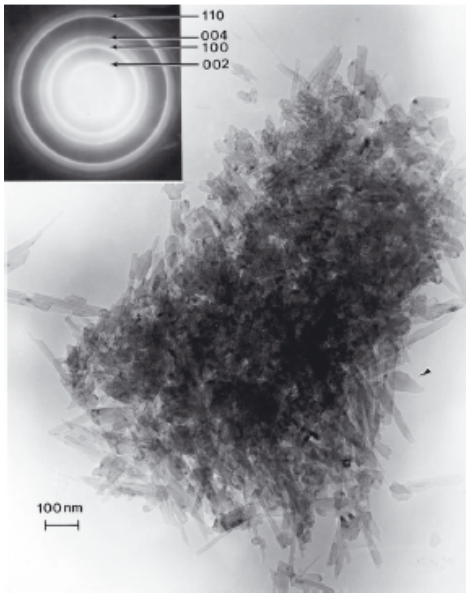

Figure 24 : Representative MWCNT and nanoform aggregate collected at the roof exhaust for a natural gas–air water heater [Murr and Soto (2005)].

The aggregates containing hundreds or thousands of carbon nanotubes and related carbon nanocrystal structures (including multi-layer, concentric, closed cylindrical shells and spheres with C_{60} at the center) are referred by Murr et al (2004) as a remnant form of 'soot' particles. While many soot aggregates exhibit some carbon nanocrystal forms, particularly onion-like or turbostratic structures similar to those shown in Figure 22b, many combustion processes, especially those involving higher temperatures (1000 ^{o}C), produce branched soot aggregates, similar to those shown in Figure 6 (Katrinak et al., 1993).

The most recent findings regarding fine particle emissions from domestic gas burners is communicated by D'Anna et al (2008) and Minutolo et al (2008). D'Anna et al (2008) measured the organic carbon and soot particles in premixed methane flames at atmospheric pressure, produced with equivalence ratios ($(C/O)_{experimental}/(C/O)_{stoichiometric}$) in the range 1.5 to 2.5, by using a calibrated optical procedure based on the use of the light emission induced by an ultraviolet laser source. Their study presents the evidences that methane forms a low amount of particulate, sensibly lower than that produced by other gaseous fuels such as ethylene in similar flame conditions. They reported mainly very small organic carbon particles, with diameters in the range 3–10 nm. The mass concentration of the larger particles is reported to be very low and soot is reported to be formed only in correspondence of very high C/O ratios. In a previous study by Toniato et al (2007), the emitted mass concentration of 1nm – 10nm size range of particles from premixed methane flames produced with air/fuel ratios between the stoichiometric value and 31% excess air, was reported as 0.01ppm, while particles in the 10nm – 100nm range were not formed in their examined conditions.

In their study on emission of fine particles from natural gas domestic burners, Minutolo et al (2008, in press) used advanced in-situ optical diagnostics, based on laser induced emission spectroscopy (LIE), and ex-situ measurements, based on scanning mobility particle sizer (SMPS), and particles collection by water-based sampling technique. Minutolo et al communicated that about 5 mg/Nm^3 organic aerosol is emitted from cook-top burner, together with a relevant amount of water soluble PAHs. The mean size of the particles is communicated to be about 3 nm, while particles larger than 10 nm is communicated to be completely absent, as confirmed by their optical measurements. The typical size distribution function of the particles in their study is presented in Figure 25.

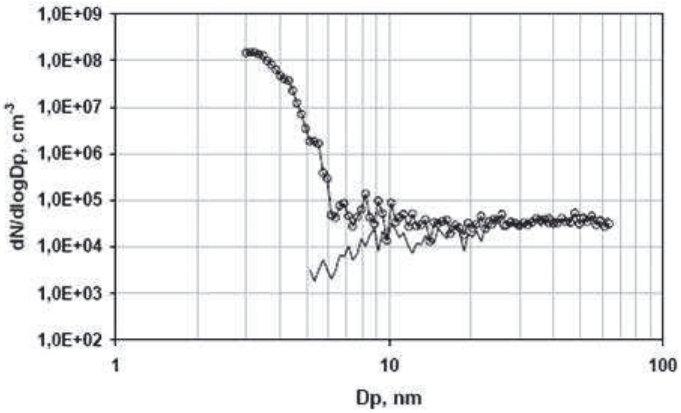

Figure 25: A typical size distribution function of the particles emitted from cook-top burner communicated by Minutolo et al (2008).

3.3. Interpretation Summary

In the last several years, a growing body of scientific evidence has indicated that the air within homes and other buildings can be more seriously polluted than the outdoor air in even the largest and most industrialized cities. Smoking, cooking and infiltration of the polluted outdoor air have been the focus of many studies. Domestic gas cookers and stoves were also studied, however not that extensively until recently, from particle emissions point of view.

Dennekamp et al (2001) measured the concentrations of ultra fine particles (10nm≤ Dp ≤100nm) and oxides of nitrogen generated by cooking with gas and electricity, to comment on possible hazards to health in poorly ventilated kitchens. They used a TSI 3934 scanning mobility particle sizer, collecting samples through a straight copper tubing at face level in front of the cookers, located in an unventilated laboratory of 70 m^3 volume. In the case of using four gas rings on full power for 2 hours, after an initial rapid rise to ~3.8E5 particles/cm^3, the particle concentration declined to around ~1.5E5 particles/cm^3. After turning off the gas rings at the second hour, particle concentration fell to a steady level of ~1.0E4 particles/cm^3 at the end of the third hour. Particles were produced by the gas rings alone and had a peak diameter in the range 15–40 nm, which grew up to a peak of about 50–70 nm while the gas rings were on. NOx concentrations reached a steady level after the rings had been on for 75 minutes, with NO_2 concentrations of 2200 ppb and NO concentrations of 5800 ppb. After turning

of the gas rings at the second hour, NO_2 concentrations fell to 200ppb NO_2 and NO to 600ppb at the end of the third hour.

Seaton and Dennekamp (2003) found a very striking association between concentrations of nitrogen oxides and the number of particles of ≤100 nm aerodynamic diameter both in their outdoor measurements and indoor measurements that, they concluded that if NO_2 in these environments is measured as an index of pollution and is shown to be associated with health effects, these effects could equally be due to the numbers of particles, as it would be impossible to distinguish their effects in epidemiological studies. Moreover, they hypothesised that the lung reacts to particle numbers rather than mass, since its primary defensive role is to counter invasion by microorganisms which may be inhaled in large numbers but never in high mass.

When we measure particles as mass, the greatest contribution comes from the largest particles, but the greatest number of particles by far is the submicron ones. Despite the vast amount of studies investigating different aspects of particles since the early 90s, when it comes to the question whether it is the mass or number concentrations that can be used as generally acceptable risk indicators of health effects of ultrafine particles ($D_p \leq 0.01\mu m$), and the thresholds below which these adverse effects do not occur, the question remains to be open. In most of the recent work involving ultrafine particles, number concentration is the common method of choice for expressing the concentrations.

The most recent findings regarding fine particle emissions from domestic gas burners is communicated by D'Anna et al (2008) and Minutolo et al (2008). In their studies, they distinguish two fundamental types of particles by size. Particles with sizes up to about 10 nm are termed molecular particle precursors and they are detectable by UV light absorption and laser-induced fluorescence (LIF). Particles larger than 10 nm are termed soot, and these particles are typically detected by visible light absorption and by laser-induced incandescence (LII) techniques. The sum the two types of particles is termed total particulates. Minutolo et al (2008, in press) communicated that about 5 mg/Nm^3 organic aerosol is emitted from cook-top burner, together with a relevant amount of water soluble PAHs. The mean size of the particles is communicated to be about 3 nm, while particles larger than 10 nm are communicated to be completely absent, as confirmed by their optical measurements. Other experimental work, available on laminar premixed ethylene flames [Minutolo et al (1998), Bruno et al (2005), d'Allessio et al (2005), Minutolo et al (2008), d'Anna (2008)] also confirm the presence of nanoparticles with a typical size of about 2–3 nm, which are considered as precursors of the soot particles with typical sizes of 20– 30 nm and no major differences is expected in these features for the process of soot formation in flames of other fuels. In the downstream of the

main reaction zone of a premixed ethylene/air flame produced with C/O ratio of 0.77, d'Anna (2008) observed a large number concentration of particles of the order of 1E13 cm^{-3} with sizes below 3nm and beyond this maximum value, he observed a much lower number concentration of soot particles of the order of 1E11 cm^{-3} with sizes ranging from 5 to 25 nm. In premixed methane flames at atmospheric pressure, produced with equivalence ratios $((C/O)_{experimental}/(C/O)_{stoichiometric})$ in the range 1.5 to 2.5, D'Anna et al (2008) reported mainly very small organic carbon particles, with diameters in the range 3–10 nm. The mass concentration of the larger particles is reported to be very low and soot is reported to be formed only in correspondence of very high C/O ratios.

According to the European Aerosol Phenomenology study of Putaud et al (2004), in most atmospheric particles with a diameter ≤150nm, organic matter and black carbon are by far the major components. In regards to domestic gas stoves, there are few studies available. The works of Bang et al (2004) and Murr et al (2004) imply that aggregates of carbon nanotubes (with diameters ranging from 3 to 30 nm) and other nanocrystals (with diameters ranging from 0.4 to 2 μm) are a common feature of the indoor air in homes utilizing gas cooking stoves, and in the outdoor air as a consequence of a variety of domestic heating sources and other industrial gas combustion sources venting the exhaust to the outdoor air. According to Murr et al (2004) these aggregates are essentially pure carbon or graphene sometimes exhibiting traces (1–2%) of sulfur. Further study of these nanoparticle aggregates by transmission electron microscopy (TEM) was carried out by Murr and Soto (2005), utilizing thermal precipitation onto coated TEM grids. TEM examination of this nanoparticulate matter has shown them to consist of essentially amorphous or crystalline structured carbon spherules forming soot aggregates, aggregates of crystalline graphite particles mixed with small multi wall carbon nanotubes and other fullerene multiwall concentric shells forming nanopolyhedra, and aggregates of often equal mixtures of MWCNTs and fullerene polyhedra. According to their observations, nanoparticle aggregation or the occurrence of carbon nanoforms always occurred as aggregates with nominal sizes ranging from about 0.5 μm to 1.5 μm. Despite the numerous available publications from Murr and Bang (2003, 2004), the artifacts of their thermophoretic sampling method and its effect on the morphology of the collected particles is not addressed in any of these publications.

3.4. References

Ashman P J, Junus R., Stubington J.F., Sergeant G. D. (1994), The Effect of Load Height on the Emissions From a Natural-Gas Fired domestic Gas Cooktop Burner, Combustion Science And Technology, Vol. 103, Nr. 1-6, p. 283.

Bang JJ, Trillo EA, Murr LE. (2003), Utilization of selected area electron diffraction (SAED) patterns for characterization of air submicron particulate matter collected by a thermal precipitator, Journal of the Air and Waste Management Association, 53, p.227–36.

Bang J.J., Guerrero P.A., Lopez D.A., Murr L.E., Esquivel E.V. (2004), Carbon Nanotubes and Other Fullerene Nanocarystals in Domestic Propane and Natural Gas Combustion Streams, Journal of Nanoscience and Nanotechnology, 4.7, p. 716- 718.

Baumbach G. (1996), Air Quality Control, Springer-Verlag, Berlin, ISBN 3-540-57992-3, p.23-39.

Brown, R.C., Miake-Lye, R.C., Anderson, M.R., Kolb, C.E. (1997), Aircraft sulfur emissions and the formation of visible contrails, Geophysical Research Letters, 24 (4) , p. 385-8.

Bruno, A., De Lisio, C., Minutolo, P.(2005), Time resolved fluorescence polarization anisotropy of carbonaceous particles produced in combustion systems, Optics Express, 13 (14) , p. 5393-5408.

Calcote H. F., Olson D. B., and Keil D. G. (1988), Are Ions Important in Soot Formation?, Energy & Fuels, 2,p. 494-504.

Calcote H.F. (2001), Comments on “The Origin of Soot in Flames: Is the Nucleus an Ion?” by V. J. Hall–Roberts, A. N. Hayhurst, D. E. Knight, and S. G. Taylor, Combustion And Flame, 126, p.1607–1610.

Chan T. L., Ning Z., Wang J. S., Cheung C. S., , Leung, C. W. and Hung W. T. (2007), Gaseous and Particle Emission Factors from the Selected On-Road Petrol/Gasoline, Diesel, and Liquefied Petroleum Gas Vehicles , Energy & Fuels, 21, 2710-2718.

Choi, M.Y.; Mulholland, G.W.; Hamins, A.; Kashiwagi, T. (1995), Comparisons of the soot volume fraction using gravimetric and light extinction techniques, Combustion and Flame, 102.1, p. 161-169.

Christensen, K.A. and Livbjerg H. (1996), A Field Study of Submicron Particles from the Combustion of Straw, Aerosol Science and Technology, 25, p.185-199.

Clement, C.F. and Ford I.J. (1999), Gas to Particle Conversion in the Atmosphere I: Evidence from empirical atmospheric aerosols, Atmospheric Environment, 33 (3) , p. 475-487.

Clement, C.F. and Ford I.J. (1999), Gas to Particle Conversion in the Atmosphere II: Analytical models of nucleation bursts, Atmospheric Environment, 33 (3) , p.489 - 499.

Commodo M., Violi, S., D'Anna A., Allouis, C.,. Minutolo, P (2006), 29th Meeting of the Italian Section of the Combustion Institute, Pisa.

Cullis and Mulcahy (1972), The kinetics of combustion of gaseous sulfur compounds, Combustion and Flame, 18, 225-292.

D'Alessio, A.; Barone, A.C.; Cau, R.; D'Anna, A.; Minutolo, P., Koylu, U., Shaddix, C., Frenklach, M., Rosner, D.E. (2005), Surface deposition and coagulation efficiency of combustion generated nanoparticles in the size range from 1 to 10 nm, Proceedings of the Combustion Institute, 30 (2) , p. 2595-2603.

D'Anna, A.; Kent, J.H. (2007), A model of particulate and species formation applied to laminar, nonpremixed flames for three aliphatic-hydrocarbon fuels, Combustion and Flame, 152 (4) , p. 573-587.

D'Anna, A. (2008), Combustion – Formed Nanoparticles, Manuscript for the invited topical review at the 32nd International Symposium on Combustion, Montreal, Canada.

D'Anna, A; Sirignano, M; Commodo, M; Pagliara, R; Minutolo, P (2008), An Experimental and Modelling Study of Particulate Formation in Premixed Flames Burning Methane, Combustion Science and Technology, 180 (5) , p. 950.

Dennekamp M, Howarth S, Dick C.A.J, Cherriea J.W, Donaldson K, Seaton A (2001), Ultrafine particles and nitrogen oxides generated by gas and electric cooking, Occupational and Environmental Medicine, 58, p.511-516.

Doyle, G.J. 1961, Self-nucleation in the sulfuric acid-water system, Journal of Chemical Physics, 35 (3), p. 795-799.

Egsgaard H. (1996), Investigation of the Initial Reactions of the Calcote Mechanism for Soot Fo rmation , Journal of the American Society for Mass Spectrometry, 7, p.559.

Flagan R. and Seinfeld J. (1988), Fundamentals of Air Pollution Engineering, Prentice Hall, ISBN 0-13-332537-7, New Jersey, p.290-344.

Flagan, R.C. (2007), A thermodynamically consistent kinetic framework for binary nucleation, The Journal Of Chemical Physics, 127, p. 214503.

Frenklach M. (2002), Reaction Mechanism of Soot Formation in Flames, Physical Chemistry Chemical Physics, 4, p. 2028-2037.

Friedlander S.K. (2000), Smoke, Dust, and Haze: Fundamental of Aerosol Dynamics, 2nd Edition Oxford University Press, ISBN 0195129997 , p: 1, 5, 23, 171.

Gabrielli F., Goodstine S.,Mastronarde T. (2000), Cold-End Corrosion In HRSGs, Alstom Power Inc., Day Hill Road Windsor, CT. (http://www.power.alstom.com/home/about_us/retd/power_plant_ laboratories /recent_papers_and_publications/34767.EN.php?languageId=EN&dir=/home/about_us/retd/power_plant_laboratories/recent_papers_and_publications/)

Glarborg, P. Kubel, D.; Dam-Johansen, K.; Chiang, H. M.; Bozzelli, J. W.(1996), International Journal of Chemical Kinetics, 28, 773-790.

Glarborg, P. and Marshall, P. (2005), Mechanism and modeling of the formation of gaseous alkali sulfates Combustion and Flame, 141, p.22-38.

Glassman I. (1988), Soot Formation in Combustion Process, 22nd Symposium (International)on Combustion / The Combustion Insitute, p. 295-311.

Gmitro and Vermeulen (1964), Vapour-Liquid Equilibria for Aqueous Sulfuric Acid, American Institute of Chemical Engineers , 10, p.740.

Hall-Roberts V. J., Hayhurst A. N., Knight D. E., and Taylor S. G (2000)., "The Origin of Soot in Flames: Is the Nucleus an Ion?", Combustion and Flame, 120:578–584 .

Haynes B.S., Wagner H.Gg. (1981), Soot formation, Progress in Energy and Combustion Science, 7, p.229.

Heist, R.H. (1974), Hydrates in supersaturated binary sulfuric acid-water vapour, Journal of Chemical Physics, 61 (2) , p. 573-81.

Hennings U., Reimert R. (2007), Behaviour of Sulfur-Free Odorants in Natural Gas Fed PEM Fuel Cell Systems, Fuel Cell, 7 (1), p. 63 – 69.

Hildemann, L.M. et al (1993)., Submicrometer aerosol mass distributions of emissions from boilers, fireplaces, automobiles, diesel trucks, and meat cooking operations, Aerosol Science and Technology, 14, p. 138–152.

Hindiyarti L, Glarborg P., Marshall P. (2007), Reactions of SO_3 with the O/H Radical Pool under Combustion Conditions, The Journal of Physical Chemistry A., 111, p.3984-3991.

Hua D. , Fangqun Y. (2006), Role of the binary H2SO4-H2O homogeneous nucleation in the formation of volatile nanoparticles in the vehicular exhaust, Atmospheric Environment, 40 (39) , p. 7579-7588.

Huijbregts, W.M.M.; Leferink, R.G.I. (2004), Latest advances in the understanding of acid dewpoint corrosion: Corrosion and stress corrosion cracking in combustion gas condensates, Anti-Corrosion Methods and Materials, 51 (3), p. 173 – 188.

Irvin N, Monroe S. (2006), A review of Sulfuric Acid Formation and Behaviour in Coal Fired Power Plants, Proceedings of the EPA-DOE-EPRI-A and WMA Power Plant Air Pollutant Control Mega Symposium 2006 , 39.

Jensen, J.R., Nielsen, L.B., Schultz-Moller, C., Wedel, S., and Livbjerg,H. (2000), The Nucleation of Aerosols in Flue Gases with a High Content of Alkali - A Laboratory Study, Aerosol Science and Technology, 33, p.490-509.

Johnsson, J E ; Glarborg, P (2000); Sulfur chemistry in combustion I - Sulfur in fuels and combustion chemistry, NATO ASI Series C Mathematical and Physical Sciences - Advanced Study Institute, 547 , p. 263.

Jung, J. G., Pandis, S. N., Adams, P.J. (2008), Evaluation of nucleation theories in a sulfur-rich environment, Aerosol Science and Technology, 42 (7) , p. 495-504.

Junus R., Stubington J. F., Sergeant G.D. (1994), The Effects of Design Factors on Emissions from Natural Gas Cooktop Burners, International Journal of Environmental Studies, Vol. 45, p.101-121.

Karcher, B. (1997), The role of sulfur emission in volatile particle formation in jet aircraft exhaust plumes, Geophysical Research Letters; 24 (4), p. 389-392.

Katrinak K.A., Rez P., Perkes P.R. & Buseck P.R.(1993), Fractal geometry of carbonaceous aggregates from an urban aerosol, Environmental Science and Technology. 27, p. 539-547.

Katz, J.L. (1974), The generation of aerosols by binary homogeneous nucleation, Water, Air and Soil Pollution 3 (4) , p. 507-13.

Kennedy I. M., Kollmann W., Chen J.Y. (1990), A Model for Soot Formation in a Laminar Diffusion Flame, Combustion and Flame, 81, p.73-85.

Kennedy I. M. (1997), Models of Soot Formation and Oxidation, Progress in Energy and Combustion Science, 23, p.95-132

Kiang, Y.H. (1981), Predicting dew points of acid gases, Chemical Engineering, 9.

Klepeis, N. ,Apte M.G.; Gundel, L.A.; Sextro, R.G.; Nazaroff, W (2003), Determining size-specific emission factors for environmental tobacco smoke particles, Aerosol Science and Technology, 37 (10) , p. 780-790.

Ko Y.C., Lin T.H. (2003), "Emissions and efficiency of a domestic gas stove burning natural gases with various compositions", Energy Conversion and Management 44 , p.3001-3014.

Kramlich, J. C., Malte, P. C., and Grosshandler, W. L. (1981), Reaction of Fuel-Sulfur in Hydrocarbon Combustion, Proceedings of the Combustion Institute, Vol. 18, p. 151.

Lewis B., von Elbe G. (1961), Combustion, Flames and Explosions of Gases, 2nd Edition, p.220-224.

Lee, K. B., Thring, M. W. and Beer, J. M. (1962), On the Rate of Combustion of Soot in a Laminar Soot Flame, Combustion and Flame, 6, 137–145.

Lewtas, J. (2007), Air pollution combustion emissions: Characterization of causative agents and mechanisms associated with cancer, reproductive, and cardiovascular effects , Mutation Research-Reviews in Mutation Research , 636 (1-3) , p. 95-133.

Lim, M.C.H.; Ayoko, G.A.; Morawska, L.; Ristovski, Z.D.; Jayaratne, E.R. (2007), The effects of fuel characteristics and engine operating conditions on the elemental composition of emissions from heavy duty diesel buses, Fuel, 86 (12-13) , p. 1831-1839.

Lindstedt R.P, Bochorn H. (1994), Mechanisms and Models, Soot Formation in Combustion, H., Springer-Verlag, Berlin, p. 417.

Liu, Z.G. (2007), Influence of Engine Operating Conditions on Diesel Particulate Matter Emissions in Relation to Transient and Steady-State Conditions, Environmental Science and Technology, 41 (13), p. 4593-4599.

Mansurov Z.A. (2005), Soot Formation in combustion Processes (Review), Combustion, Explosion and Shock Waves, Vol.41, No.6, p. 727-744.

Miller J. A., Melius C. F., (1992), Kinetic And Thermodynamic Issues In The Formation of Aromatic Compounds In Flames Of Aliphatic Fuels, Combustion and Flame, 91, p. 21-39.

Minutolo, P.; Gambi, G.; D'Alessio, A. (1998,) Properties of carbonaceous nanoparticles in flat premixed C2H4/air flames with C/O ranging from 0.4 to soot appearance limit, Symposium (International) on Combustion.27 (1) , p. 1461-1469.

Minutolo, Patrizia; D'Anna, Andrea; D'Alessio, Antonio (2008), On detection of nanoparticles below the sooting threshold, Combustion and Flame, 152 (1-2) , p. 287-292.

Minutolo P., D'Anna A., Commodo M., Pagliara R., Toniato G., Accordini C. (2008), Emission of Fine Particles from Natural Gas Domestic Burners, Environmental Engineering Science, in press

Mirabel, P. (1974), Binary homogeneous nucleation as a mechanism for the formation of aerosols, Journal of Chemical Physics, 60 (3) , p. 1138-44.

Mueller, M. A.; Yetter, R. A.; Dryer, F. L. (2000), Kinetic modeling of the $CO/H_2O/O_2/NO/SO_2$ system: Implications for high-pressure fall-off in the SO2PLUO(PLUM) EQ SO3(PLUM) reaction, International Journal of Chemical Kinetics 32, 317-339.

Muller, C. H. III, Schofield, K., Steinberg, M., and Broida, H. P. (1979), Proceedings of the Combustion Institute, Vol. 17, p. 867, The Combustion Institute, Pittsburgh, PA.

Muller, C. H. III, Schofield, K., and Steinberg, M.(1980), Am.Chem. Soc. Symp. Proc. 134:103.

Murr L. E., Bang J.J., Esquivel E.V., Guerrero P.A. and Lopez D.A.(2004), 'Carbon nanotubes, nanocrystal forms, and complex nanoparticle aggregates in common fuel-gas combustion sources and the ambient air', Journal of Nanoparticle Research 6: 241–251.

Murr LE, Bang JJ, Lopez DA, Guerrero PA, Esquivel EV, Choudhuri AR, Subramanya M, Morandi M, Holian A. (2004), Carbon nanotubes and nanocrystals in methane combustion and the environmental implications, Journal of Materials Science, 39, p.2199– 204.

Murr, L.E., Soto K.F. (2005), A TEM study of soot, carbon nanotubes, and related fullerene nanopolyhedra in common fuel-gas combustion sources, Materials Characterization, 55, p. 50–65.

Nagle, J., Strickland-Constable, R. F. (1962), Oxidation of carbon between 1000–2000 °C, Proceedings of the 5th Carbon Conference, Vol. 1, p. 154–164.

Perry, R.H. and Chilton, C.H. (1973), Chemical Engineers Handbook, 5th Ed., McGraw-Hill, New York, ISBN 0-07-049478-9.

Perry, R.H.; Green, D.W. (1997), Perry's Chemical Engineers' Handbook, 7th Edition, McGraw-Hill, New York, ISBN 9780070498419.

Rasmussen M. S. (2003), Modelling of Soot Formation in Autothermal Reforming, PhD Thesis, DTU.

Rasmussen, C.L.; Glarborg, P.; Marshall, P.(2007), Proceedings of the Combustion Institute (ISSN: 1540-7489), 31 (1), p. 339-347, Elsevier Science Inc.

Reiss H. J. (1950), The Kinetics Of Phase Transitions In Binary Systems, Journal of Chemical Physics , 18, p.840.

Richter H., Howard J.B. (2000), Formation of polycyclic aromatic hydrocarbons and their growth to soot—a review of chemical reaction pathways, Progress in Energy and Combustion Science, 26, p.565–608.

Robinson, N.F. (1981), A fast numerical procedure for determining the saddle point of a free energy surface, Journal of Aerosol Science,12 (1) , p. 75-78.

Sakurai, H., Tobias, H.J., Park, K., Zarling, D., Docherty, S., Kittelson, D.B., McMurry, P.H., Ziemann, P.J. (2003), On-line measurements of diesel nanoparticle composition and volatility, Atmospheric Environment, 37, 1199–1210.

Schnelle K. B, Brown C. (2001), Air Pollution Control Technology Handbook , CRC Press, ISBN 0849395887, p.273 – 277.

Schofield K. (2001), The Kinetic Nature of Sulfur's Chemistry In Flames, Combustion and Flame, 124, p.137–155.

Schumann, U.; Arnold, F.; Busen, R.; Curtius, J.; Karcher, B.; Kiendler, A.; Petzold, A.; Schlager, H.; Schroder, F.; Wohlfrom, K.-H. (2002), Influence of fuel sulfur on the composition of aircraft exhaust plumes: the experiments SULFUR 1-7, Journal of Geophysical Research; 107 (D15) , p. A2.

Seaton A., Dennekamp M. (2003), Hypothesis: Ill health associated with low concentrations of nitrogen dioxide – an effect of ultrafine particles ?, Thorax, 58, p.1012-1015.

Seinfeld, J. H. and Pandis, S. N. (2006), Atmospheric Chemistry and Physics - From Air Pollution to Climate Change, 2nd Edition, John Wiley & Sons, ISBN 0470046252, p.468.

Shaddix C.R, Harrington J.R, Smyth K. C. (1994), Quantitative Measurements of Enhanced Soot Production in a Flickering Methane/Air Diffusion Flame, Combustion and Flame, 99, 723-732.

Simonsen, 0. (1992). Kinetics of Aerosol Condensation. Ph.D. Thesis, Technical University of Denmark.

Simonsen, 0., Livbjerg H. (1992), The influence of seed nuclei on aerosol condensation, Computers and Chemical Engineering, 16 (1) , p. S379-S386.

Smooke, M.D.; McEnally, C.S.; Pfefferle, L.D.; Hall, R.J.; Colket, M.B.(1999), Computational and experimental study of soot formation in a coflow, laminar diffusion flame, Combustion and Flame, 117 (1-2) , p. 117-139.

Smooke, M.D.; Long, M.B.; Connelly, B.C.; Colket, M.B.; Hall, R.J. (2005), Soot formation in laminar diffusion flames, Combustion and Flame, 143, p.613–628.

Srivastava, R.K.; Miller, C.A.; Erickson, C.; Jambhekar, R. (2004), Emissions of sulfur trioxide from coal-fired power plants, Journal of the Air and Waste Management Association, 54 (6) , p. 750-762.

Stauffer, D. (1974), Nucleation literature review, Journal of Aerosol Science, 5 (2) , p. 157-73.

Stubington J.F., Beashel G., Murphy T., Junus R., Ashman P.J. and Sergeant G.D.(1994), Emissions and Efficiency from Production Cooktop Burners Firing Natural Gas, Journal of Institute of Energy, 67:143-155.

Toniato G., Accordini C., D'Anna A., Commodo M., Minutolo P, Pagliara R. (2007), Proceedings of the 3rd European Combustion Meeting ECM 2007.

Turns S. R (2000), An Introduction to Combustion Concepts and Applications, 2nd Edition McGraw Hill, New York, ISBN 0-07-235044-x, p. 253-298, 305-354.

Ulrich, G.D. (1971), Particle formation in high temperature systems, Combustion Institute (Western States Sect), Fall meeting.

US EPA (1998), Emergency Planning and Community Right-To-Know Act - Section 313, Guidance for Reporting Sulfuric Acid (acid aerosols including mists, vapours, gas, fog, and other airborne forms of any particle size).

Vehkamaki, H. (2003), Modelling Binary Homogeneous Nucleation of Water-Sulfuric Acid Vapours: Parameterisation for High Temperature Emissions, Environmental Science and Technology, 37, 3392-3398.

Verhoff, F.H. and Banchero, J. (1974), Predicting Dew Points of Flue gases, Chemical Enginering Program.

Vermeulen, T., Dong, J., Robinson, S., Nguyen, T.(1982), Vapour-Liquid Equilibrium of the Sulfuric Acid/Water System, American Institute of Chemical Engineers 1982 Spring National Meeting and Chemical Plant Equipment Exposition, Preprints.

Wagner H. GG. (1978), Soot Formation in Combustion, Seventeenth Symposium (International) on Combustion / The Combustion Institute, p. 3-19.

Wang H., Frenklach M. (1997), A Detailed Kinetic Modelling Study of Aromatics Formation in Laminar Premixed Acetylene and Ethylene Flames, Combustion and Flame, 110, p. 173-221.

Weast, R.C. (1988), Handbook of Chemistry and Physics, 69th Ed., CRC Press, Boca Raton, FL, p. B67.

Wieschnowsky et al (1988) , 22nd Symposium (International) on Combustion, p. 343-352

World Health Organization (2006), Fuel for life : household energy and health.

Yilmaz A., Hindiyarti L, Jensen A.D, Glarborg P., Marshall P (2006), Thermal Dissociation of SO_3 at 1000-1400 K, The Journal of Physical Chemistry A, 110, p.6654-6659.

Yue, G.K. (1979), A quick method for estimating the equilibrium size and composition of aqueous sulfuric acid droplets, Journal of Aerosol Science,10 (1) , p. 75-86.

Yue, G. K. (1979), Homogeneous nucleation rates of h//2so//4-h//2o aerosol particles in air", Journal of Aerosol Science, 10 (6) , p. 609-614.

Zachariah M.R., Smith O.I. (1987), Experimental and numerical studies of sulfur chemistry in $H_2/O_2/SO_2$ flames, Combustion and Flame, 69, p.125–139.

Internet Sources

http://www.energinet.dk/da/menu/Systemdrift/Gaskvalitet/Variationer+i+gaskvaliteten/

http://www.epa.gov/smokefree/healtheffects.html

http://www.epa.gov/otaq/highway-diesel/index.htm

http://www.irmm.jrc.be/html/press_corner/index.htm

PART B: EXPERIMENTAL WORK

In this study the objective is to provide new results on the particle emissions from domestic gas cookers; i.e: particle number concentrations, particle sizes and the nature of particles. Three sets of experiments were performed for this purpose. The first set of experiments, referred as ´´Test Experiments´´ were performed using a domestic gas cooker open to the surrounding atmosphere in a laboratory. The second set of experiments, referred as ´´Preliminary experiments´´ were performed in a compartment in order to insure an environment free from external particle sources. The last set of experiments, referred as ´Final Experiments´ were also performed in a compartment. In these experiments however, the affect of primary aeration on particle emissions was investigated using three different fuels: methane, natural gas and odorant free natural gas. Additionally the affect of sulfur content of the fuel on the particle emissions is investigated. The experimental set-up was modified in accordance with the requirements of each set of experiments. Therefore each set of experiments is presented as a separate chapter; Test Experiments, Preliminary Experiments and Final Experiments, where the methods, results and findings of each are presented and discussed separately.

Chapter 1: Test Experiments

Test experiments were carried out using the gas cooker in its normal procedure - natural gas supplied from the city line and air supplied from the surroundings. The purpose of these experiments was to have a very first idea about the particle emissions from the domestic gas stoves. Therefore neither the flow rates nor the gas concentrations were measured. Total particle number concentrations and size distributions were measured before and after turning on the flame, approximately 10 cm above the flame level, in the absence of a pot. The position of the sampler was tried to be kept the same in all experiments, however deviations might have occurred since the probe was not fixed permanently at a certain location.

1.1. Experimental Set-up:

1.1.1. The Gas Cooker

A gas cooker which has been inspected for G20/2H type natural gas has been used in this study. According to Article 2(2) of Council Directive 90/396/EEC of the European Commission, in Denmark 2H refers to natural gas with a gross wobbe index [Wobbe Index = higher heating value/(square root of gas specific gravity)] between 51,9-55,8 MJ/m^3 (at 0^oC) supplied at a nominal supply pressure of 20mbar. Although the technical harmonization in the framework of the Gas Appliances Directive (GAD) of the European Commission covers gas appliances and fittings, there are still differences in the types of gas and corresponding supply pressures in the Member States that have an impact on design. Article 2(2) of the GAD requires the Member States to communicate the types of gas and corresponding supply pressures used on their territory to the other Member States and the Commission. At different countries this range changes slightly, i.e in Austria 47,7-56,5 MJ/m^3, in France 48,2-56,5 MJ/m^3, in Germany 46,08-56,52 MJ/m^3. The full list is available on http://ec.europa.eu/enterprise/gas_appliances/type_gas_en.htm.

The large gas hob of the cooker used in this study had 3.3 kW rated heating capacity, 1200 W reduced flow rate and nozzles with 1.3 mm diameter, while the small gas hob had 1.05 kW rated heating capacity, 380 W reduced flow rate and nozzles with 0.73 mm diameter. The regulation of the primary air was performed in accordance with the recommended nozzle distance by the producer, which is 1.5mm for G20 natural gas.

Figure 26: Gas cooker and the ejector probe

1.1.2. Particle concentrations and Size Data by SMPS

Particle concentrations were measured with a TSI Model 3775 Condensation Particle Counter (CPC). Particles were classified with a Model 3080 Electrostatic Classifier with a Model 3081 LDMA (Long Differential Mobility Analyzer), and/or a Model 3085 NDMA (Nano Differential Mobility Analyzer). The particle size range (generation mode) that can be detected with those are 10 to 1000 nm with 3081 LDMA and 2 to 150 nm with 3085 NDMA. The maximum input concentration is limited to 10^8 particles/cm^3 at 10 nm while the aerosol temperature should be in the range 10 to 40°C (instrument must be within 3°C of aerosol temperature).

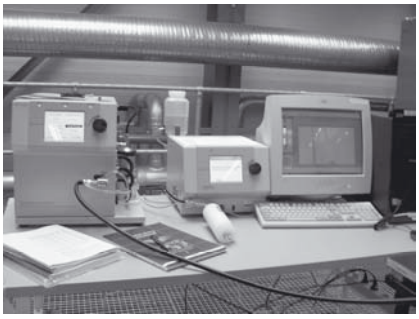

Figure 27: TSI 3080 SMPS

..

1.1.3. Sampling equipment: Gas Ejector Probe

Since the SMPS system imposes certain limits on the aerosol temperature and particle number concentrations, any sample that is sent to the instrument should meet these requirements. As the temperatures above the flame would be much higher and the particle number concentrations are not known, a dilution and cooling system was needed. For this reason, a gas ejector probe developed for particle analysis in a research program instigated to study fine particles [Johannesen et al (2000)] was used. The ejector dilution also lowers the water dew point of the aerosol and this prevents condensation. Although a calibration curve was prepared as presented in Figure 28, as a double check, dilution ratios were calculated from actual measurements of the particle concentrations in the ambient air in the laboratory, by direct sampling to CPC and sampling with the ejector probe.

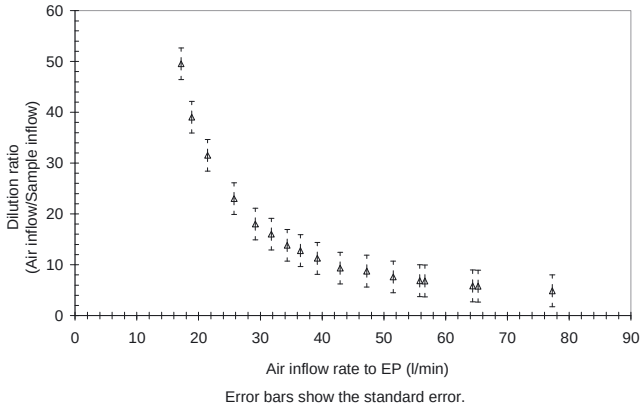

Figure 28: Dilution ratios of the ejector probe when used with a probe, whose length is 35 cm and diameter is 0.08 inch.

1.2. Results

The experiments were carried out using the gas cooker in its normal procedure - natural gas supplied from the city line and air supplied from the surroundings. The cooker was located in our process hall, which has dimensions of 28.8m length, 12.2m width and 10.0m height, built in two floors with no concrete separation between the floors. Particle number concentrations and size distributions were measured before and after turning on the flame, approximately 10 cm above the flame level, in the absence of a pot.

CPC and SMPS measurements showed that particle concentrations increase and size distributions change right after turning on the burner, as presented in Figure 29, Figure 30 and Figure 31. In Figure 32, the logarithmic size distribution function of the particles is presented**.** The measured background concentration of particles varied roughly in a range of 1E3 to 1E4 particles/cm^3 with a bimodal size distribution with median size diameter (half the particles are larger and half are smaller than the median diameter) 28 nm and the mean diameter of the two modes being 25 nm and 129 nm. After igniting the flame, a single mode size distribution was observed with a mean diameter of 10 nm. The elevated particle number concentrations did not go beyond sharp peaks observed once in a while, giving particle concentrations of 1E8 right after ignition, and later on peak concentrations of 1E5 to 1E6 particles/cm^3, which could indicate a release of high amount of fine particles at some instant during gas combustion.

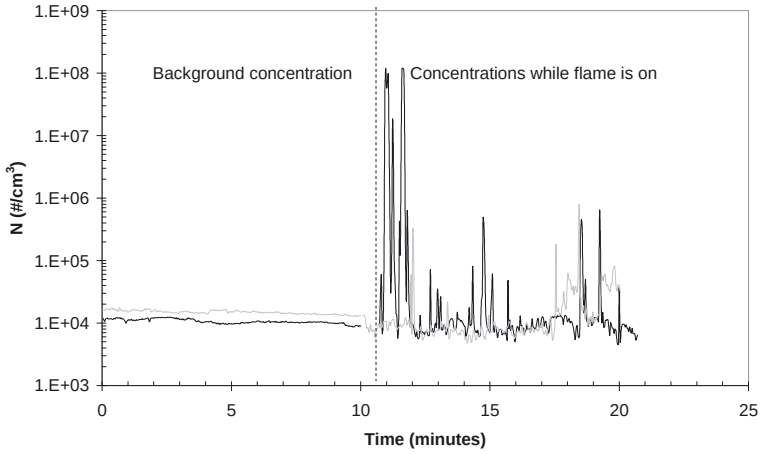

Figure 29: Particle number concentrations measured at 10 cm above the burner level, before and igniting the flame, using CPC 3775.

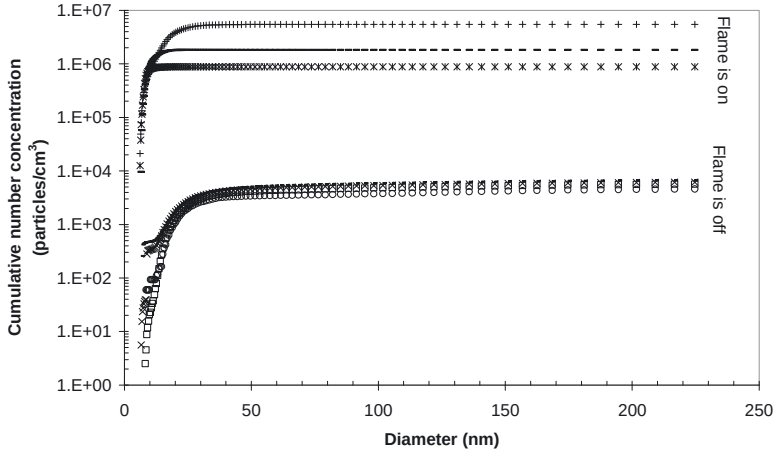

Figure 30: Cumulative number size distribution of particles, measured with 3081 NDMA, using 0.0457 nm impactor, at high flowrate (sheath flow:15 lpm, sample flow 1.5 lpm) giving size range bounds 6.04 – 228.8 nm.

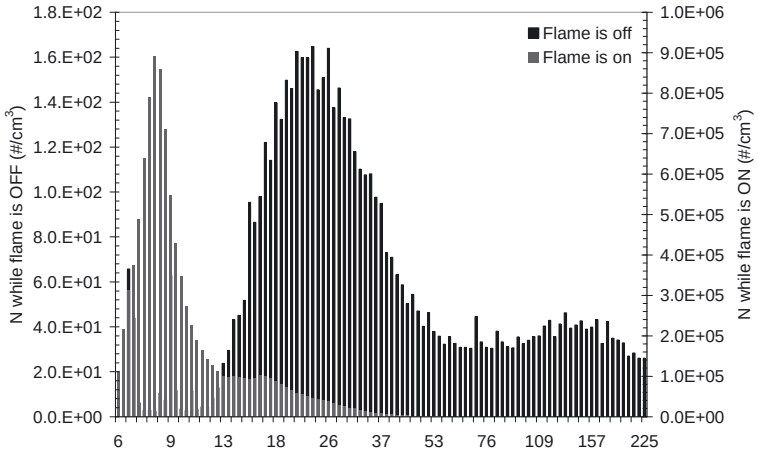

Figure 31: Size distribution data while flame is on and off (Data presented in Figure 30 is averaged)

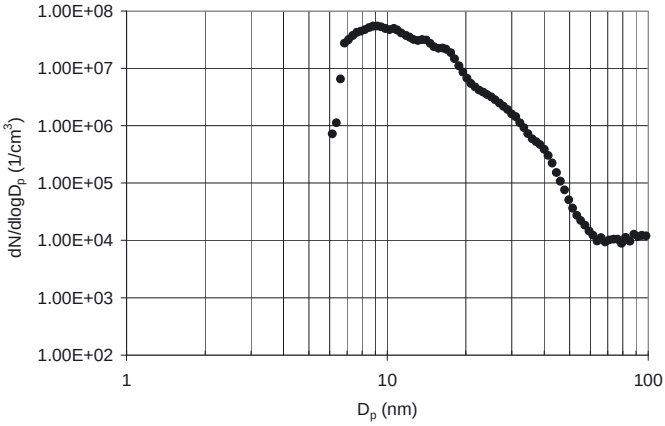

Figure 32: A typical logarithmic size distribution function of the particles emitted from the burner. The SMPS settings allowed the measurement boundary as 6.04 -228.8 nm.

The elevated particle concentrations did not go beyond sharp peaks observed once in a while, which could indicate release of high amount of fine particles at some instant during gas combustion. It was not possible to report a trend for the size and frequency of the peaks, due to their varying appearance in each measurement. Nonetheless, as it could be seen in Figure 33 , the background concentrations were increasing in the course of burner usage.

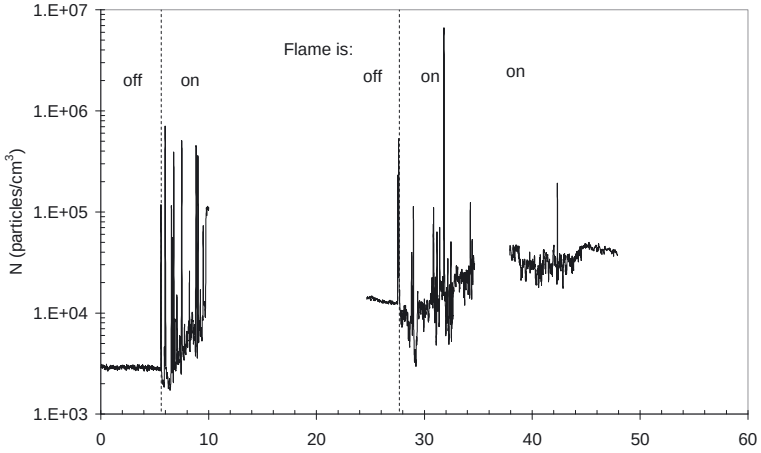

Figure 33 : Increase in the background concentrations as the flame is on.

1.3. Discussions

Comparing these results directly with the results of Dennekamp et al (2001) in terms of number concentrations would not be a proper approach, as there were four gas rings with unknown gas consumption in Dennekamp's study (2001) and only one gas ring in this study. Moreover, Dennekamp's sampling point was at face level (assumable 50 -60 cm above the flame level), and in this study sampling point was at 10 cm above the flame. Considering the different sampling points of the two studies, coagulation and agglomeration of the particles in Dennekamp's study would bring an explanation to the higher particle emissions of this study, despite the less number of gas rings used. The larger diameters of particles observed in Dennekamp's study seem to be supporting the latter statement. Last but not least, counting efficiency of TSI 3080 series SMPS is expected to be somewhat higher than that of TSI 3934 series SMPS, as end of sale date for 3934 series was December 1998, while 3080 series is one of the latest technology available. The components of 3934 series SMPS (3071A Electrostatic Classifier and 3022A CPC) are currently in the trade-in program of TSI in order to replace older instruments that no longer represent the latest technology and have become increasingly expensive to maintain.

The size range of particles which appeared with the combustion is in the range 6 – 40 nm. These findings are in good agreement with the findings of Dennekamp et al (2001), Bang et al (2003, A comparison of the size distribution function of the particles (presented in Figure 32) of this study and

the size distribution data reported by Minutolo et al (2008), (presented in Figure 25) is possible. However, due to the settings of the SMPS system, the size ranges below 6 nm could not be detected in these measurements. Therefore a comparison with the size range reported by D'Anna et al (2008) and Minutolo et al (2008) can not be justified fully. However, the presence of particles smaller than 10 nm in diameter is observed. While Minutolo et al (2008) reported the complete absence of the particles larger than 10 nm, in this work particles upto 40 nm diameter were observed.

However, as there were other activities ongoing in the surroundings, identification of the gas stove as the only source of the observed particles would be an ungrounded decision. It has been observed that the – supposed to be blue flame – was sometimes becoming a colour between yellow to orange. This change in the flame could be due to short or intermittent air flow interruptions. Because of the changing conditions in each experiment, and the abundance of uncertainty factors, it was decided to build a well controlled experimental set up in order to perform the experiments. These experiments are explained in Chapter 2.

1.4 Interpretation summary

The test experiments showed that particle concentrations increase and size distributions change right after turning on the burner. These findings would indicate a release of high amount of fine particles during gas combustion. By igniting the flame, the bimodal size distribution of the background air with the mean diameter (based on number particle size) of the two modes being 25 nm and 129 nm is replaced by a single mode size distribution with a mean diameter of 10 nm. The size range of particles which appeared with the combustion is in the range 6 – 40 nm. These findings are in good agreement with the findings of Dennekamp et al (2001), Bang et al (2003, 2004), Murr et al (2004) and Murr and Soto (2005). Due to the settings of the SMPS system, the size ranges below 6nm could not be detected in these measurements. Therefore a comparison with the size range reported by D'Anna et al (2008) and Minutolo et al (2008) can not be justified fully. However, the presence of particles smaller than 10 nm in diameter is observed.

1.5. References

Bang JJ, Trillo E.A, Murr L.E. (2003), Utilization of selected area electron diffraction (SAED) patterns for characterization of air submicron particulate matter collected by a thermal precipitator, Journal of the Air and Waste Management Association, 53, p.227–36.

Bang J.J., Guerrero P.A., Lopez D.A., Murr L.E., Esquivel E.V. (2004), Carbon Nanotubes and Other Fullerene Nanocarystals in Domestic Propane and Natural Gas Combustion Streams, Journal of Nanoscience and Nanotechnology, 4.7, p. 716- 718.

D'Anna, A. (2008), Combustion – Formed Nanoparticles, Manuscript for the invited topical review at the 32nd International Symposium on Combustion, Montreal, Canada.

D'Anna, A; Sirignano, M; Commodo, M; Pagliara, R; Minutolo, P (2008), An Experimental and Modelling Study of Particulate Formation in Premixed Flames Burning Methane, Combustion Science and Technology, 180 (5) , p. 950.

Dennekamp M, Howarth S, Dick C.A.J, Cherriea J.W, Donaldson K, Seaton A (2001), Ultrafine particles and nitrogen oxides generated by gas and electric cooking, Occupational and Environmental Medicine, 58, p.511-516.

Johannessen, J.T., Pratsinis, S.E., Livbjerg,H. (2000), Chemical Engineering Science, 55(1), 177-191.

Minutolo P., D'Anna A., Commodo M., Pagliara R., Toniato G., Accordini C. (2008), Emission of Fine Particles from Natural Gas Domestic Burners, Environmental Engineering Science, in press

Murr L. E., Bang J.J., Esquivel E.V., Guerrero P.A. and Lopez D.A.(2004), 'Carbon nanotubes, nanocrystal forms, and complex nanoparticle aggregates in common fuel-gas combustion sources and the ambient air', Journal of Nanoparticle Research 6: 241–251.

Murr, L.E., Soto K.F. (2005), A TEM study of soot, carbon nanotubes, and related fullerene nanopolyhedra in common fuel-gas combustion sources, Materials Characterization, 55, p. 50–65.

Internet Sources

http://ec.europa.eu/enterprise/gas_appliances/type_gas_en.htm

Chapter 2: Preliminary Experiments

In order to insure an environment free from external particle sources, the burner was placed in a compartment which is supplied with filtered air from its bottom. The compartment operates as a flow reactor with no mechanical mixing. The details about the reactor are presented in section 2.1.1. In this set of experiments, the effect of flow rates on particle generation from the large burner is studied. The minimum and maximum set point of the large burner corresponds to 0.9 - 4.4 litre/minute gas consumption. Experiments are performed for both 200 and 400 litre/minute secondary air flow-rate, for the minimum and maximum fuel flow-rate. The choice of fuel for these experiments is both natural gas from the city line and methane from a cylinder with 99.97 % purity.

The experimental procedure can be summarized as measurement of total particle concentration, gas concentrations and temperatures along the reactor before, during and after combustion. The gas concentrations of interest are oxygen, carbon monoxide, carbon dioxide, nitric oxide, nitrogen oxides and sulfur dioxide. Between those gases sulfur dioxide concentrations were not measured, since the concentrations would be too small to be detected by any of the gas analyzers available. Samples for gas analyses were collected using a steel probe (~2mm in diameter) through the sampling port S 12 (80 cm above the flame). Gas concentrations are measured by ECO Physics CLD 700 EL Chemiluminescence NO/NO_x Analyzer and Fisher – Rosemount MLT $CO/CO_2/O_2$, which are calibrated before each experiment. Samples for particle concentration and size data measurements were collected from the reactor outlet (S 13) using the ejector gas probe which was previously described in Chapter 1. Fuel flow-rate is calculated from the slope (dV/dt) of the curve which is prepared by plotting the readings of volume of gas spent during combustion at certain time intervals. Gas pressure is kept constant by means of a regulator. Temperatures are measured along the reactor axis, using thermocouples through the sampling points 1 (4 cm above the flame), 7(25 cm above the flame) and 13 (reactor outlet).

2.1. Experimental Set-up

2.1.1. The Reactor

The reactor is composed of two compartments, as presented in Figure 34. The lower compartment where the burner is placed at the bottom with the required gas connections and four ports through which particle free combustion air is supplied to the reactor. The ignition and flow control panel of the burner is kept outside the reactor, leaving the primary air supply nozzle inside the reactor. The reactor bottom allows using different gas rings after the required arrangement of primary air supply nozzle distance. The upper compartment provides extra volume and sampling ports. The first sampling port S1 is located 4cm above the burner level. Following S1, S2-S5 are equidistantly placed, by 4cm. S6 and S7 are located at 25 cm and 30 cm above the burner level respectively. S7 is the last sampling point of the lower compartment of the reactor. S8-S12 are equidistantly placed, by 10cm. S12 is located at 80 cm above the burner level. S13, not indicated in Figure 34, is placed at the reactor outlet line. A silencer is installed at the reactor outlet for preventing noise during experiments.

In order to assure flame stability, flow velocity through the reactor is kept below 10cm/s which is the measured median flow velocity in the kitchens of six occupied homes by Mathews et al (1989). The excess air ratio of the system is kept above 10. Sampling ports are placed along the reactor to allow sampling at different locations above the flame. The glass windows placed at both compartments allows observation and video recording of the flame through the experiments.

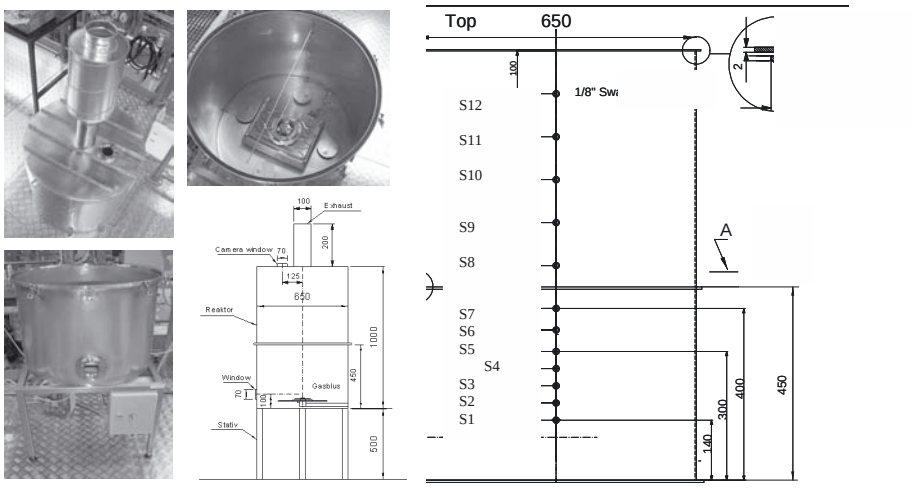

Figure 34: The reactor-technical drawing and the two compartments.

2.1.2. Sample collection for TEM studies – A thermophoretic method

A thermophoretic sampler was designed, based on simple concepts of aerosol dynamics and used to collect samples for TEM studies. The sampler is named KAHLAYPET, combining the initials for Kristoffer Andersen, Hans Livbjerg, Ayten Yilmaz and Peter Glarborg, as an appreciation of their contributions to its design and construction. KAHLAYPET can be described simply as a multi-channel pipe or in other words a sandwich pipe, made of stainless steel with a length of 1m. Cold water- which is kept at a constant temperature of 25°C by means of a water bath is pumped into the innermost channel and pumped out through the middle channel. The sample gas is drawn into the outermost channel by a vacuum pump through the tiny opening located at the end of the sampler. As the gas sample enters the KAHLAYPET, it meets the TEM grid which is safely sitting on a copper surface, kept cold by the water flow behind. The grid is kept in place by a screwed-in part which has an opening slightly smaller than the area of the grid, leaving a part of the grid exposed to the gas flow.

The design equations used for the design of KAHLAYPET covers Brownian diffusion, convective diffusion and thermophoresis of particles from a hot gas to a cold surface. The steepness of the temperature gradient and the concentration gradient determines whether thermophoresis or Brownian diffusion is the dominant mechanism in the deposition of the particles. The competence between convective diffusion and thermophoresis is on the other hand dependent on the thermophoretic velocity and the convection-diffusion velocity.

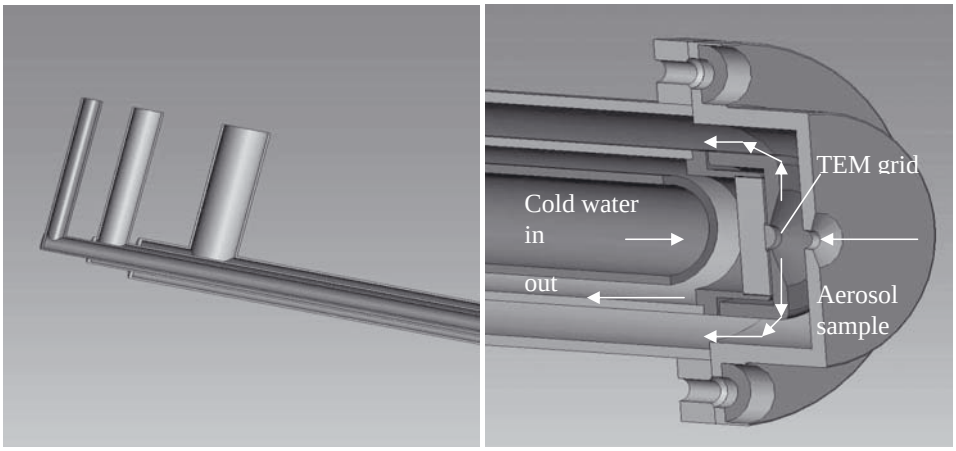

Figure 35: Thermophoretic sampler – KAHLAYPET

Knudsen number for particles of 2 to 100nm diameters in air at a temperature range 200-800^{o}C are presented in Figure 36. As it could be seen, for particles with diameters less than 20 nm, Kn is much larger than 1 (Kn>>1), indicating that v_T is independent of particle size, directly proportional to the temperature gradient, and only weakly dependent on temperature. The dependence of thermophoretic velocity on the temperature gradient is shown in Figure 37. The dependence of convection-diffusion coefficient on the concentration gradient is shown in Figure 38. The temperature and concentration gradients are determined by the choice of geometry, as well as the flow parameters. A comparison of the depositions rate of particles with 2nm and 10 nm diameters with each mechanism (individually) is presented in Figure 39. As seen, thermophoresis and convective diffusion are almost equally contributing to the total deposition rate of 2nm and 10 nm particles, whereas the effect of Brownian diffusion under these circumstances is negligible.

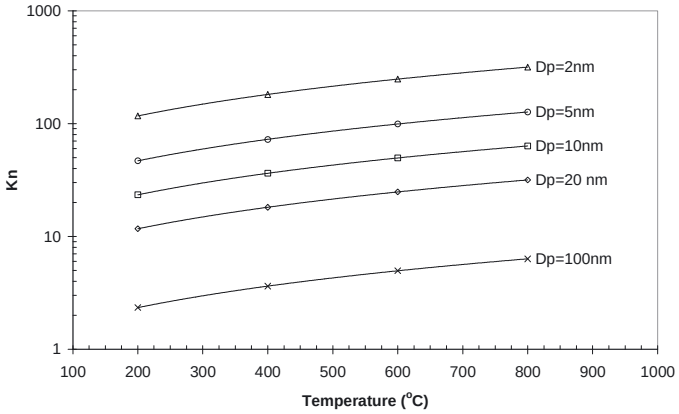

Figure 36: Knudsen number for particles of 2 to 100nm diameters in air at a temperature range 200-800 ^{o}C.

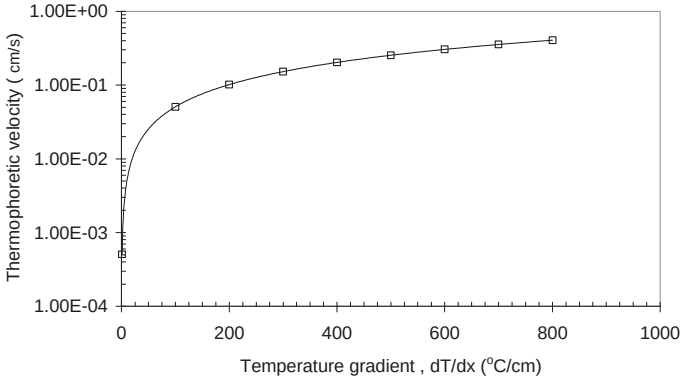

Figure 37: Thermophoretic velocity as a function of the temperature gradient.

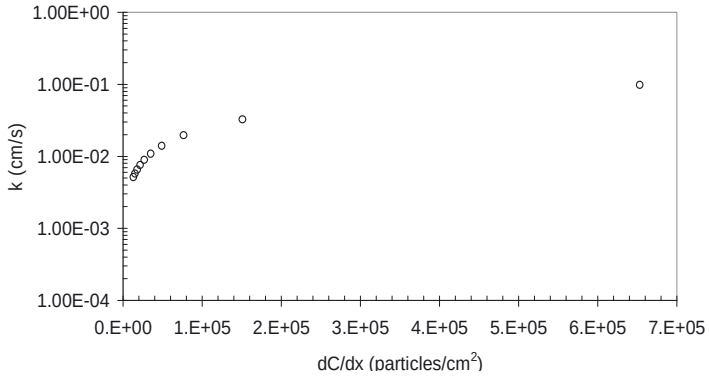

Figure 38: Convection – diffusion coefficient as a function of concentration gradient.

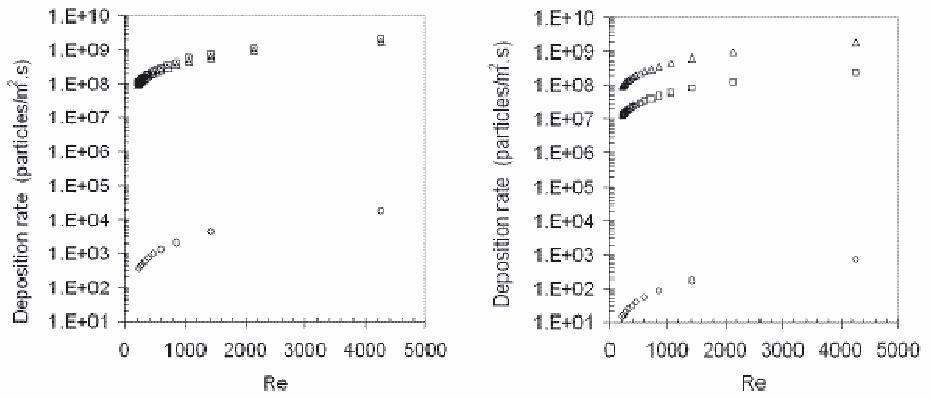

a. Particle diameter = 2nm b. Particle diameter = 10nm

○: Brownian diffusion □: Convective diffusion Δ: Thermophoresis

Figure 39: Deposition rates of 2 nm and 10 nm particles that could be achieved by Brownian diffusion (circular symbols), convective diffusion (square symbols) and thermophoresis (triangular symbols) as a function of Reynolds number. Calculations are performed using a cold surface temperature of 25°C and hot gas temperature of 200°C. Properties of air is used for the calculation of flow parameters.

2.2. Results

2.2.1.Emissions from Natural Gas and Methane Combustion

In order to illustrate a typical experiment, temperature, gas concentrations and particle concentrations measured in the course of an experiment is presented through Figure 40 to Figure 42. The air and gas flow rates in this experiment were 200 liter/minute and 1.44 liter/minute respectively. As soon as the flame is started particle concentrations increase, giving a sharp peak. This initial peak is due to start-up of the flame and it's outside the focus of this study. A similar peak is observed in CO concentrations, which might indicate a relation between CO concentrations and particle concentrations. Once this initial peak disappears, the reactor reaches steady state conditions. Particle, temperature and gas concentration measurements indicate that steady state is reached within ~ 50 minutes after combustion is started.

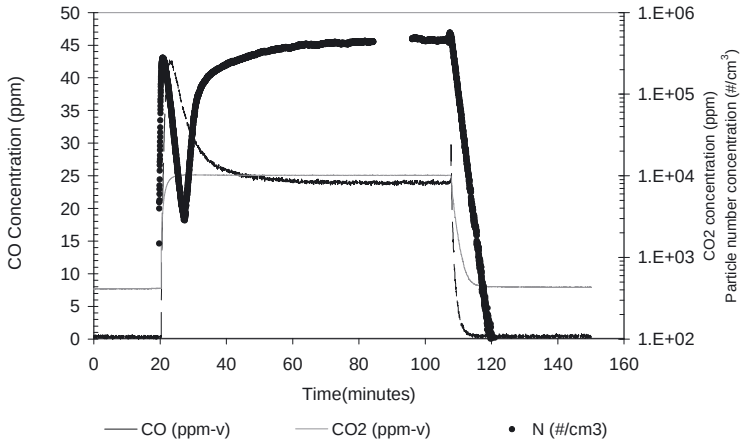

Figure 40 : Particle number concentration measured at reactor outlet (S13) and carbon monoxide and carbon dioxide concentrations measured at sampling port S12, in the course of an experiment carried out with 1.44 slpm natural gas, 200 lpm air flow rate.

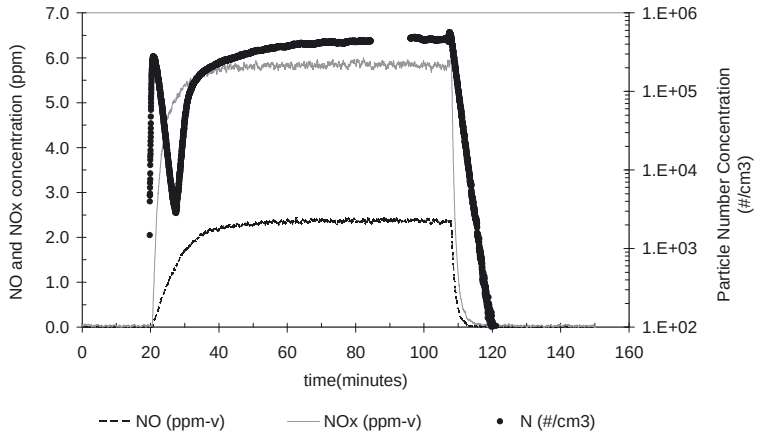

Figure 41: Particle number concentration measured at reactor outlet (S13) and nitric oxide and nitrogen oxides concentrations measured at sampling port S12, in the course of experiment which is presented in Figure 40.

.

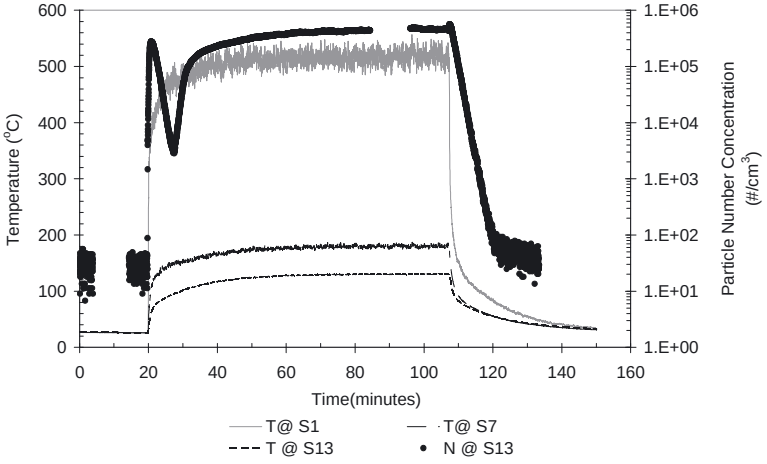

Figure 42: Particle number concentrations and temperatures measured at sampling ports S1, S7 and S13, in the course of experiment which is presented in Figure 40 and Figure 41.

.

In order to identify the difference in particle emissions from natural gas (from the city pipeline) and methane (from cylinder), experiments were carried out at different flow rates of each fuel individually, using the same procedure. The resulting steady state particle concentrations (SSPC) are plotted with respect to fuel flow rate in Figure 43. As it could be seen, quite a wide range of particle number concentrations is observed for a narrow range of methane flow rate, i.e ~4 litre/minute. A similar phenomenon is observed in the gas concentration measurements, as it could be seen in Figure 44 and Figure 45. These could indicate the presence of an uncontrolled factor influencing the measurements.

A comparison of the total particle number concentrations measured by the CPC for the two fuels indicates that, from the combustion of equal flow rates of methane and natural gas, particle concentrations emitted from the natural gas combustion is higher than that of methane. The difference could be both due to difference in the heating values of the two fuels, which would also effect the temperatures inside the reactor, as well as the presence of higher hydrocarbons and odorant in the natural gas.

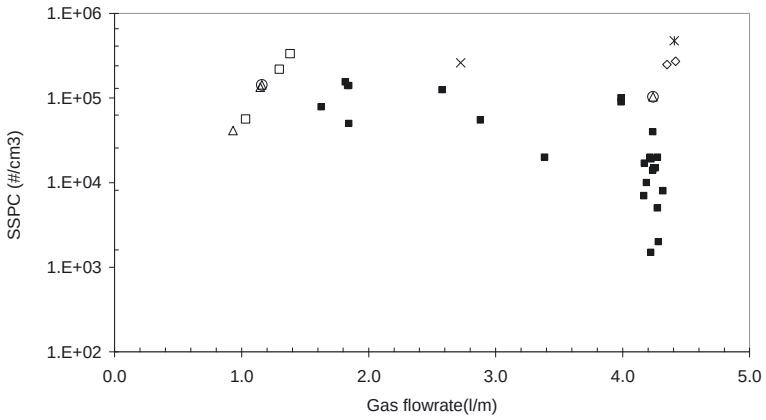

Figure 43: SSPC emitted from natural gas and methane experiments carried out with secondary air flow rate of 400 lpm. Filled square symbols represent methane experiments, and all the other symbols represent natural gas experiments, carried out at different days.

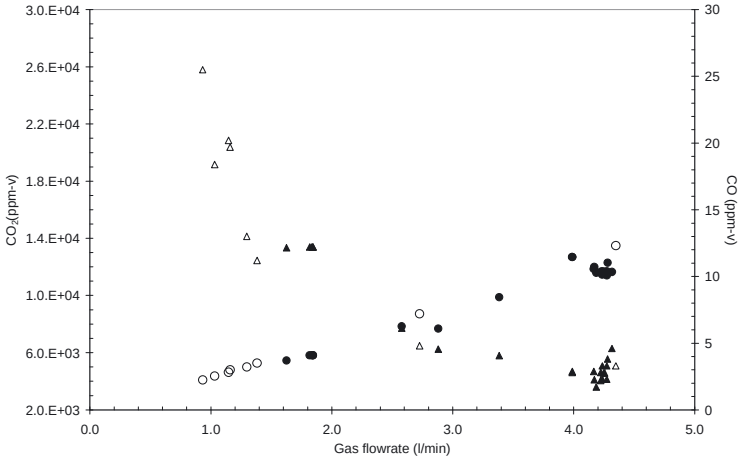

Δ, ▲: CO concentration ○, ●: CO_2 concentration

Figure 44: CO and CO_2 concentrations measured at S12. The triangular symbols represent CO concentrations and the circular symbols represent CO_2 concentrations. Filled symbols represent methane experiments, and the empty symbols represent natural gas experiments.

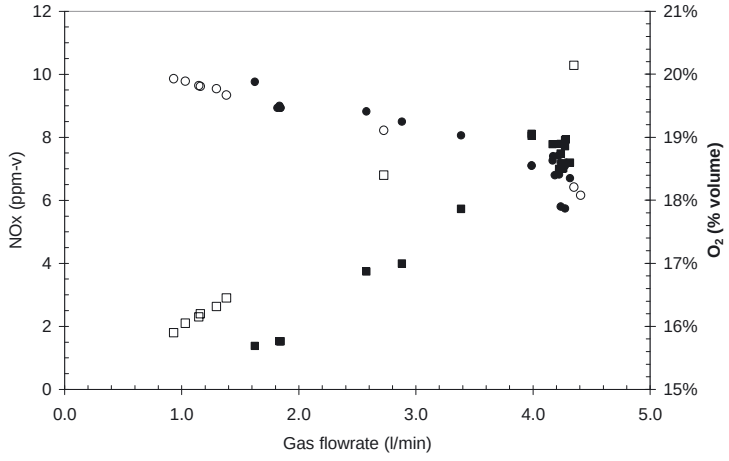

□, ■: NOx concentration ○, ●: O_2 concentration

Figure 45: NOx and O_2 concentrations measured at S12. The square symbols represent NOx and the circular symbols represent O_2 concentrations. Filled symbols represent methane experiments, and the empty symbols represent natural gas experiments.

SMPS measurements were performed before, during and after combustion in the course of natural gas experiments. Examples of these measurements are presented through Figure 46 to Figure 48. Particle free air contained only a few particles, all larger than 80 nm in diameter. During combustion, particles which are smaller than 15 nm in diameter appeared. The large particles (>80nm) which were observed prior to combustion were also observed during combustion. Once the flame was switched off, the small particles (<15nm) disappeared, large particles remained. Scans were also performed in the size range 14.9 nm to 673.2 nm, but this did not indicate the presence of any particles other than the previously observed size ranges. In Figure 49, the size distribution function of the particles emitted during the natural gas combustion is presented for comparison with the latter from the test experiments. Only a few SMPS measurements were performed in the course of methane experiments. As these measurements did not provide any representative size distribution data (only a few peaks of a few particle/m^3) the size data from methane experiments is not presented here.

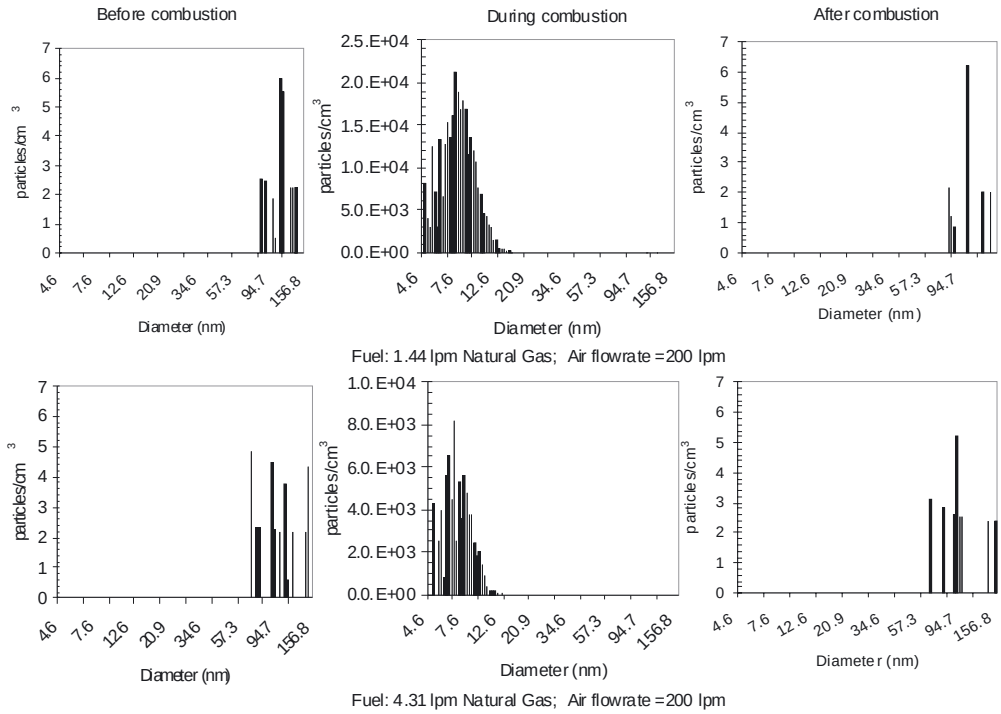

Figure 46: Particle number size distributions before, during and after combustion of natural gas with 200 lpm air supplied to the reactor. Each data point is calculated as the average of 3 consecutive size data measurements carried out in the course of a single experiment.

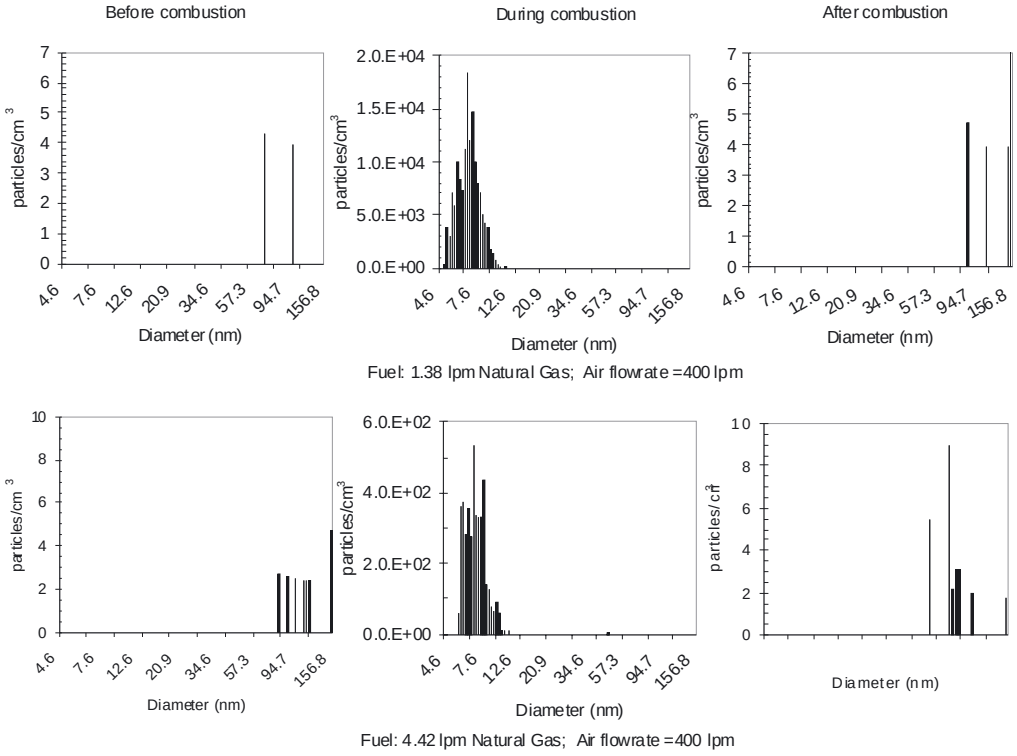

Figure 47: Particle number size distributions before, during and after combustion of natural gas with 400 lpm air supplied to the reactor.

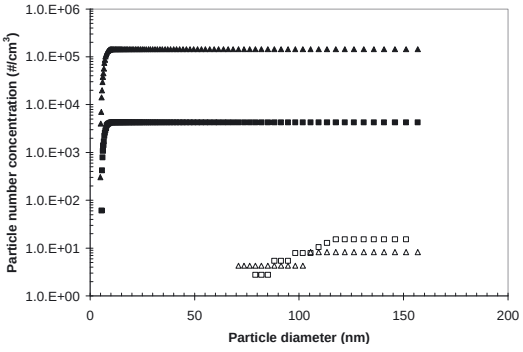

Figure 48 : Cumulative size distribution of particles before and after combustion of natural gas with 400 lpm air supplied to the reactor. The empty symbols denote size data before combustion and filled symbols denote size data during combustion. Triangular symbols denote the experiment where gas flow rate was 1.38 lpm and circular symbols for the experiment where gas flow rate was 4.42 lpm.

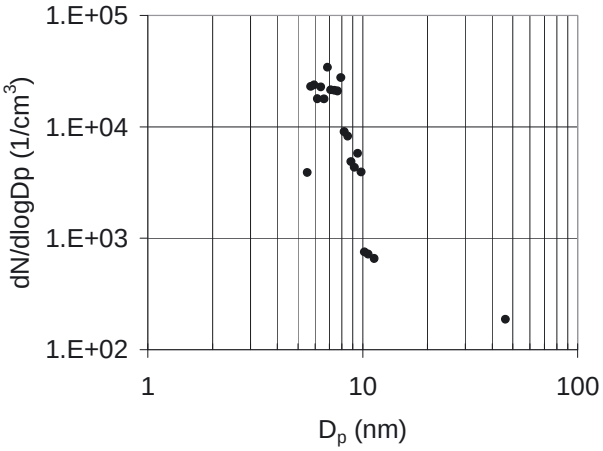

Figure 49: Size distribution data function of the particles emitted from combustion of 4.42 lpm Natural Gas with secondary air flow rate of 400 lpm. The SMPS settings allowed the measurement boundary as 4.53 – 159.6 nm.

2.2.2. Effect of secondary air flow rate on the burner performance

In order to examine whether the secondary air flow would affect the burner performance in terms of completeness of the combustion, experiments were carried out using natural gas from the city pipeline for two different flow rates of the secondary air: 200 and 400 lpm. The resulting steady state particle concentrations (SSPC) are plotted with respect to fuel flow rate in Figure 50 . The comparison of these two sets of data is not straightforward, since the gas quality might be changing from day to day. Therefore, data obtained at each day is represented with a different symbol, assuming that the gas quality is variable from day to day but not within a day. It is also worth to note here that the uncertainty involved in the volumetric air flow rate measurements due to temperature and pressure effects on the monometer readings is calculated as 10%. The differences between steady state particle concentrations observed for different gas flow rates are much larger than 10%, indicating that the differences in the particle concentrations are not only a matter of dilution. However, looking into the carbon dioxide and carbon monoxide concentrations presented in Figure 51, one notices that the difference between the concentrations of those for the two cases is a factor of ~ 2, reflecting the direct effect of the dilution. From here, it can be concluded that the burner performance was not affected by the change in the secondary air flow rate, regarding the completeness of combustion. On the other hand, nitrogen oxides and oxygen concentrations, presented in Figure 52, present a difference which is larger than the effect of dilution. Both NO_x and NO is known to generally rise with either thermal input or load height to flame length ratio of the burner [Stubington et al (1994)]. Based on the fact that

the flame length is determined by the primary air addition, the previously mentioned uncontrolled factor which could be influencing the measurements is believed to be the primary air addition. Despite higher secondary air flow rate provides more nitrogen and oxygen flow into the system, temperatures along the reactor are not as high as in the low air flow rate case, as presented in Figure 53. Thus, despite less nitrogen flow is provided by 200 l/m air flow rate, the higher temperature inside the reactor could explain the oxidation of more nitrogen compared to the 400 lpm air flow rate case.

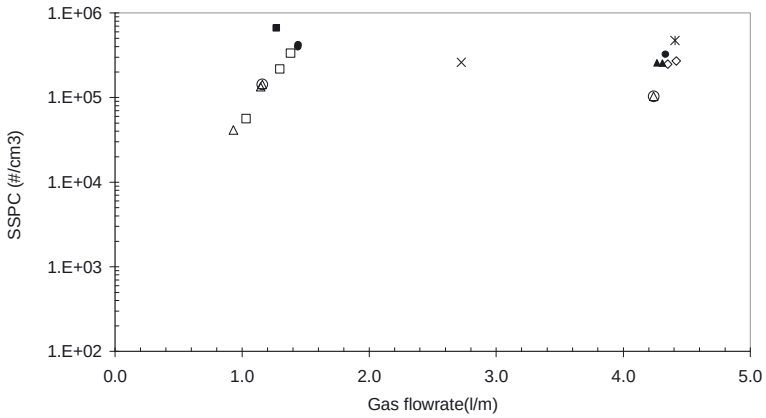

Figure 50: Steady state particle concentration (#/cm^3) vs gas flow rate (liter/minute). The filled symbols denote the experiments carried out at a constant air flow rate of 200 liter/ minute, while the empty symbols denote the experiments carried out at a constant air flow rate of 400 liter/ minute . Data obtained at different days is represented with a different symbol.

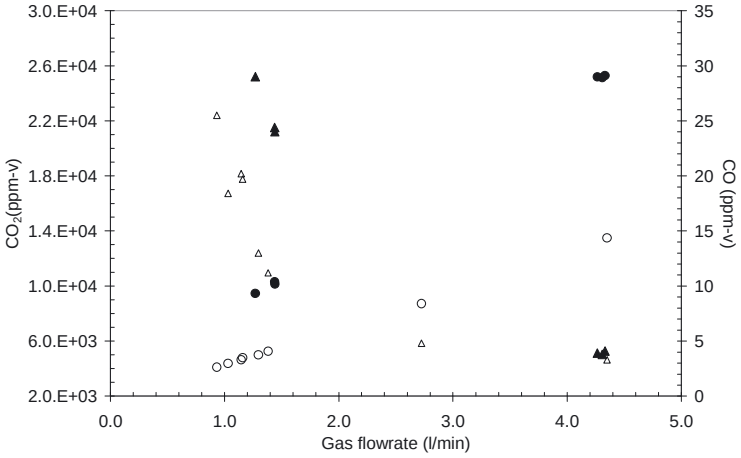

Δ, ▲: CO concentration ○, ●: CO_2 concentration

Figure 51: CO_2 and CO concentrations measured at S12. The triangular symbols represent CO concentrations and the circular symbols represent CO_2 concentrations. The empty and filled forms represent the air flow-rates, 400 and 200 liter/minute respectively.

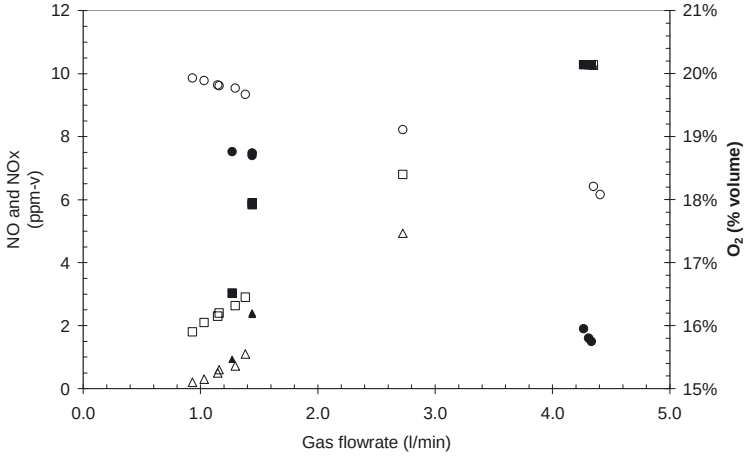

Δ, ▲ : NO concentration □,■: NOx concentration ○, ● : O_2 concentration

Figure 52: NO, NOx and O_2 concentrations measured at S12. The triangular symbols represent NO, square symbols represent NOx and the circular symbols represent O_2 concentrations. The empty and filled forms represent the air flow-rates, 400 and 200 liter/minute respectively.

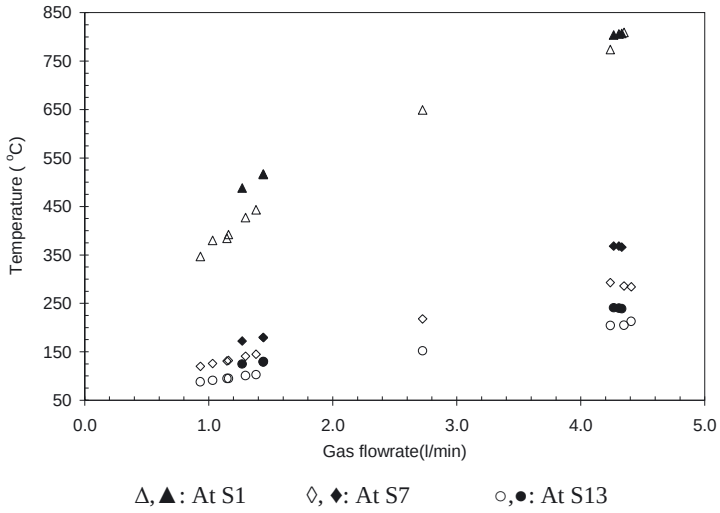

Figure 53: Temperature vs gas flow rate (liter/minute). Triangular symbols denote the measurements at S1, diamond symbols denote the measurements at S7 and circular symbols denote the measurements at S13. The filled symbols denote the experiments carried out at a constant air flow rate of 200 liter/ minute, while the empty symbols denote the experiments carried out at a constant air flow rate of 400 liter/ minute. Data obtained at different days are represented with different symbols.

2.2.3. Particle morphology – TEM and SEM studies

TEM and SEM studies were carried out in order to determine the nature and morphology of the particles. TEM samples were collected on 300 meshed silicon monoxide grids, for 3 hours and 300 meshed lacey carbon films for 24 hours at the reactor outlet. Due to low contrast with the silicon monoxide grids, images obtained from the lacey carbon grids are presented here, Figure 54 to Figure 55. In Figure 56, TEM images of the similar carbon particles of Bang et al (2004)s study and this study are presented. The individual tubular forms reported in Bang et al (2004), Murr et al (2004) and Murr and Soto (2005) were also observed in this study, but not the aggregates. In Figure 57, SEM images obtained from samples collected on a glass fiber filter are presented.

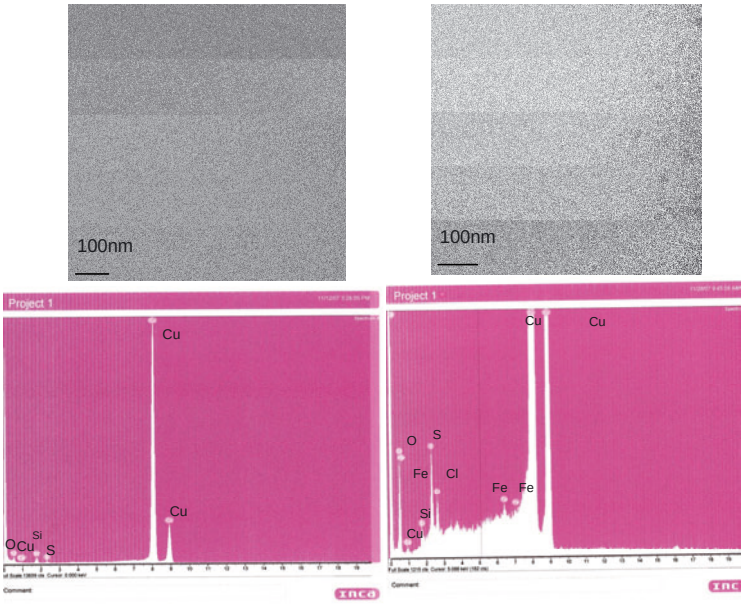

Figure 54: TEM images and the EDX profile of a clean grid at the left hand side, and the grid containing the sample; on the right hand side.

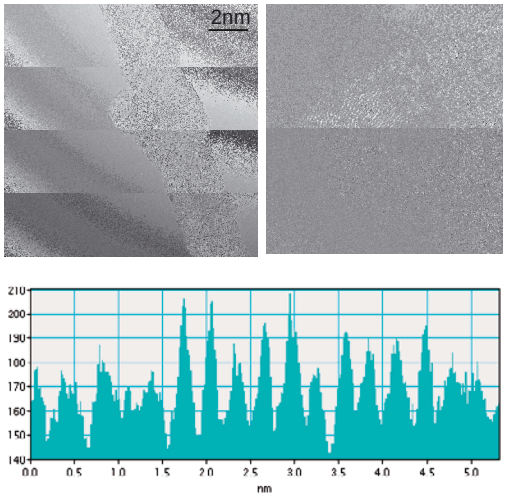

Figure 55: A single particle at the edge of the TEM grid. The same particle is zoomed in to show the onion ring structure. The profile of the structure indicates the interlayer distance to be 0.34 nm.

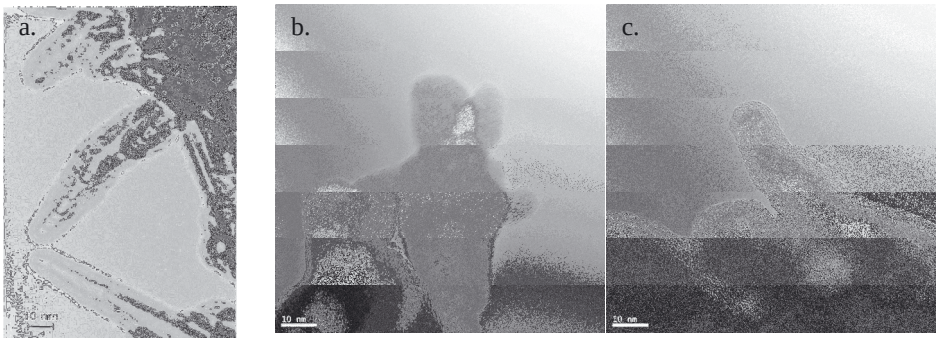

Figure 56: a. Carbon nanocrystals collected in a methane/air flame exhaust by Bang et al (2004) b. and c.) Carbon nonaparticles collected in a natural gas/air flame exhaust in this study.

A comparison of the EDX spectrum obtained from the empty grid and the one containing the sample, indicates the presence of sulfur, copper and iron in the sample. However, as the grid itself contained copper, it could not be identified whether copper signal was from the grid itself or the particles. Onion ring structures, with interlayer distances between 0.31 to 0.39nm were observed; which corresponds to graphite. Most of the particles are 2-3 nm in diameters. Since the grid itself is covered with a carbon film, it was not possible to quantify the amount of carbon in the particles.SEM samples were also collected at the reactor outlet, for three hours. The samples were collected on glass fiber filter, using a pump. There was no visible layer on the filter after sampling, however SEM images showed that there are particles collected; as presented in Figure 57. Most of these particles are 105nm in diameters.

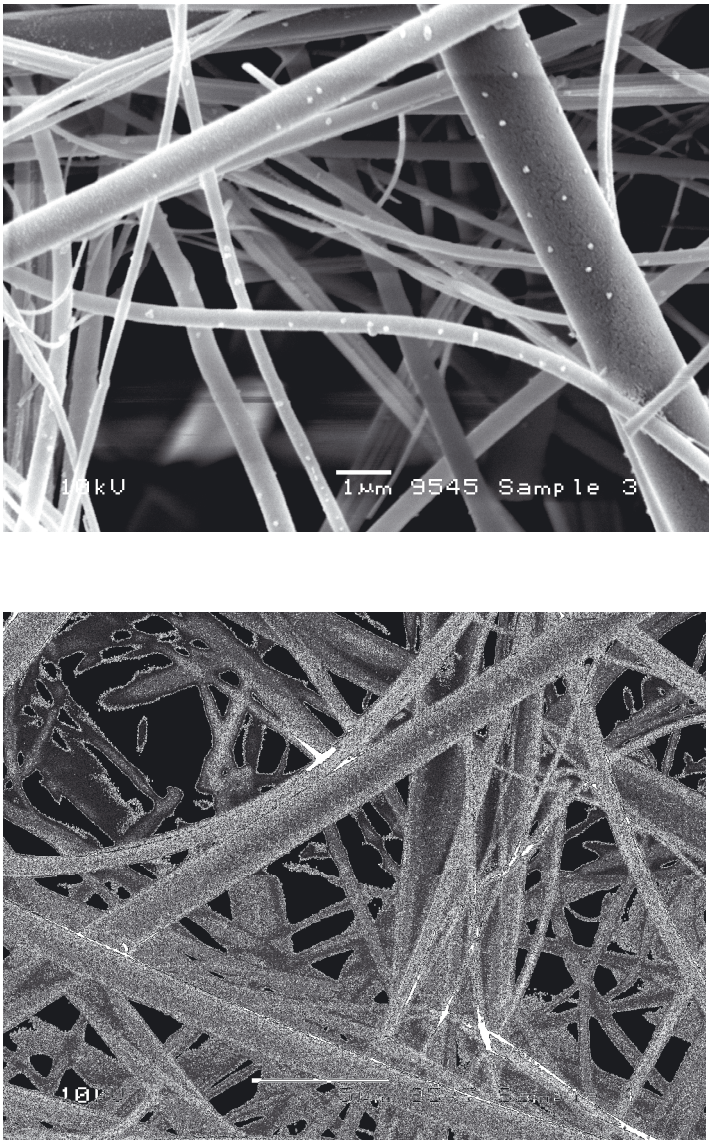

Figure 57: SEM images at two different magnifications (Please see the scale on the image)

2.3. Discussions

In these experiments, the burner was placed in a compartment which operates as a flow reactor with no mechanical mixing. The compartment was supplied with filtered air from its bottom in order to provide a particle free environment. In order to identify the difference in particle emissions from natural gas and methane, experiments were carried out using both fuels individually, in the same procedure, at different flow rates: Particle and gas concentrations were measured at the reactor outlet, before, during and after combustion.

Particle number concentrations before combustion were very low, less than 100 particles/cm^3. These particles which could escape or be released from the particle filter were larger than 80 nm and they did not show any particular size distribution trend, but rather appeared as few peaks. The comparison of the size distribution functions from the test experiments and the preliminary experiments, presented in Figure 30 and in Figure 48 respectively, shows that the particle size distribution function became much more narrow, indicating that the reactor works successfully in terms of excluding any other particle source, else than the cooker.

Once combustion was started (using natural gas), the above mentioned particles remained, but became almost negligible in terms of number concentrations compared to the combustion generated particles, which had a single mode size distribution, with mean diameters between 7 to 8 nm. Due to the settings of the SMPS system, the size ranges below 6nm could not be detected in these measurements. However, TEM studies showed the presence of carbon particles with a few nanometer (2-3nm) diameters.

Since the TEM samples were collected on copper grids coated with carbon film, it was not possible to quantify the carbon in the samples. The EDS spectrum showed the presence of sulfur, copper and iron in the sample. The source of sulfur in the particles is thought to be the odorant, since there was no other source of sulfur in the experiments. Copper signal could be either from the TEM grid itself or the sample. Iron signal is rather thought to be from the sample. The average interlayer distances between the lattices were found to be 0.34 nm, which is known to be the d-spacing of graphite. The SEM images showed the presence of perfectly spherical particles with 105 nm in diameters. This size range was not identified in any of the SMPS measurements. It is thought that these are rather the agglomerates which are formed on the filter surface.

A comparison between the diameters of the particles generated from methane and natural gas was aimed, however the size data collected from methane experiments seem to be incomplete, indicating that the particles generated from methane falls below the lower detection limit of the instrument (2nm).

The observed size range of particles is in agreement with the findings of D'Anna et al (2008) and Minutolo et al (2008), whereas the large particles and/or aggregates (Dp>20nm) reported by Dennekamp et al (2001), Bang et al (2003, 2004), Murr et al (2004) and Murr and Soto (2005) are not observed in the TEM samples. Although the SEM images showed, the presence of perfectly spherical particles with 105 nm in diameter, it is thought that these are agglomerates formed on the filter surface after collection or they are particles in the secondary air which managed to escape the filter, as these particles were not observed in any of the several SMPS and TEM samples.

The particle number concentrations showed a large variation considering the small changes in the fuel flow rates, i.e ~ 4 lpm gas flow rate. This is thought to be due to presence of an uncontrolled factor influencing the whole process. The most likely source is thought to be the primary air intake by the gas jet diffusing from a tiny nozzle. Nonetheless, for low fuel flow rates (< 2 liter/minute), particle number concentrations from methane and natural gas experiments were in the same range (between 3E4 to 4E5 particles/cm^3), while for high fuel flow rates (> 4 liter/minute), natural gas produced more particles (9E4 to 5E5 particles/cm^3) than methane (1E3 to 1E5 particles/cm^3). These concentrations are in good agreement with concentrations reported by Dennekamp et al (2001) (~1.5E5 particles/cm^3).

The effect of secondary air flow rate on the burner performance was studied and it was concluded that burner performance was not affected by the change in the secondary air flow rate, regarding the completeness of combustion.

Last but not least, the burner performance needs to be addressed in order to evaluate the conditions behind the observed particle emissions. In these preliminary experiments, it was observed that CO_2 emissions were higher in the natural gas experiments, compared to methane experiments, carried out with the same fuel flow rate. The difference corresponds to the additional CO_2 emission that would be expected from natural gas due to presence of higher hydrocarbons in the natural gas. In regards to CO emissions, for both fuels, CO emissions were considerably higher in the low flow rate experiments (12 ppmv) than the high flow rate experiments (5 ppmv); which indicates that the burner operates

more efficiently at fuel flow rates larger than 4 liter/minute. In regards to differences between the two fuels, especially at the low flow rate experiments (< 2 liter/minute) CO concentrations seem to be higher in the methane experiments. In regards to nitrogen oxides emissions, for both fuels, the concentrations increased with increasing gas flow rate. In regards to differences between the two fuels, higher NOx concentrations were measured in natural gas experiments compared to methane experiments; i.e: For 4.0 liter/minute fuel flow rate; NOx concentration in methane and natural gas experiments are extrapolated as 7.0ppmv and 9.5ppmv respectively.

2.4. Interpretation summary

The preliminary experiments showed that particles, which have a single mode size distribution, with mean diameters between 7 to 8 nm are emitted from the burner. Due to the settings of the SMPS system, the size ranges below 6nm could not be detected in these measurements. TEM studies showed the presence of carbon particles with a few nanometer (2-3nm) diameters. Both copper and sulphur signals were detected in the EDS study. Since the TEM grid was copper itself, it is not clear whether the copper signal is from the grid material only or also from the particles.

The observed size range of particles is in agreement with the findings of D'Anna et al (2008) and Minutolo et al (2008), whereas the large particles and/or aggregates (Dp>20nm) reported by Dennekamp et al (2001), Bang et al (2003, 2004), Murr et al (2004) and Murr and Soto (2005) are not observed in the TEM samples.

Due to large variations observed in the particle number concentrations with the small changes in the gas flow rates, it is decided to control the primary air addition to the fuel. These experiments are explained in Chapter 3.

2.5. References

Bang JJ, Trillo EA, Murr LE. (2003), Utilization of selected area electron diffraction (SAED) patterns for characterization of air submicron particulate matter collected by a thermal precipitator, Journal of the Air and Waste Management Association, 53, p.227–36.

Bang J.J., Guerrero P.A., Lopez D.A., Murr L.E., Esquivel E.V. (2004), Carbon Nanotubes and Other Fullerene Nanocarystals in Domestic Propane and Natural Gas Combustion Streams, Journal of Nanoscience and Nanotechnology, 4.7, p. 716- 718.

D'Anna, A. (2008), Combustion – Formed Nanoparticles, Manuscript for the invited topical review at the 32nd International Symposium on Combustion, Montreal, Canada.

D'Anna, A; Sirignano, M; Commodo, M; Pagliara, R; Minutolo, P (2008), An Experimental and Modelling Study of Particulate Formation in Premixed Flames Burning Methane, Combustion Science and Technology, 180 (5) , p. 950.

Dennekamp M, Howarth S, Dick C.A.J, Cherriea J.W, Donaldson K, Seaton A (2001), Ultrafine particles and nitrogen oxides generated by gas and electric cooking, Occup. Environ. Med., 58, p.511-516.

Johannessen, J.T., Pratsinis, S.E., Livbjerg,H. (2000), Chemical Engineering Science, 55(1), 177-191.

Minutolo P., D'Anna A., Commodo M., Pagliara R., Toniato G., Accordini C. (2008), Emission of Fine Particles from Natural Gas Domestic Burners, Environmental Engineering Science, in press.

Murr L. E., Bang J.J., Esquivel E.V., Guerrero P.A. and Lopez D.A.(2004), 'Carbon nanotubes, nanocrystal forms, and complex nanoparticle aggregates in common fuel-gas combustion sources and the ambient air', Journal of Nanoparticle Research 6: 241–251.

Murr, L.E., Soto K.F. (2005), A TEM study of soot, carbon nanotubes, and related fullerene nanopolyhedra in common fuel-gas combustion sources, Materials Characterization, 55, p. 50–65.

Chapter 3: Final Experiments

In order to have control on the gas quality, gas flow rates and the amount of primary air addition, modifications were implemented in the experimental set-up which was described in Chapter 2. Rather than using the natural gas from the city pipeline, natural gas was supplied in cylinders by Danish Gas Technology Center (DGC). In order to study the effect of the odorant in the gas, natural gas both with and without odorant were tested. The effect of H_2S and dilution of the natural gas with a corresponding amount of nitrogen is also tested. In addition to the change in gas supply, mass flow controllers were installed in order to deliver the exact gas flow-rate of interest for the fuel and additives, as well as for the primary air which is added in a mixing chamber replacing the primary air supply nozzle.

3.1. Experimental Set-up

3.1.1. Natural Gas Cylinders

In order to keep the gas quality constant, natural gas was supplied in cylinders by DGC. The gas composition was analyzed by DGC using a natural gas analyzer (a gas chromatograph with a Thermal Conductivity Detector, TCD or Flame Ionization Detector, FID), as shown in Figure 58. Based on these compositions, an approximate formula is assigned to each gas to be used in the stochiometric calculations, as presented in Table 10.

3.1.2. Mixing Chamber

In the original kitchen range, the primary air is entrained by a jet of natural gas emerging from a small diameter injector into a mixing tube, as shown in Figure 59. With this configuration, it is difficult to control the amount of primary air added to the gas. Therefore, in order to study the effect of primary air on the particle generation, the primary air supply nozzle is replaced with a mixing chamber (shown Figure 60) where the fuel and particle free primary air are mixed. The mixing chamber is located outside the reactor/compartment, due to elevated temperatures inside the reactor/compartment.

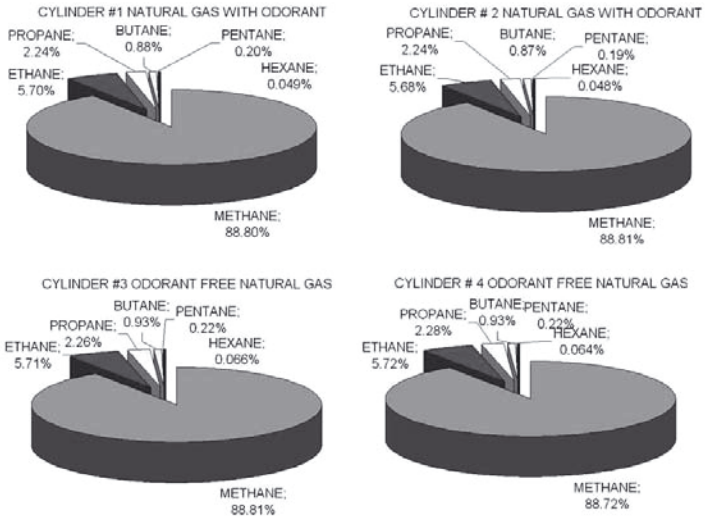

Figure 58: Composition of natural gas in cylinders

Table 10: Approximate formula for gas composition in the cylinders

Cylinder #	Content	Approximate formula	Heating value (J/m^3)	y*
1	NG	$C_{1.117}H_{4.191}$	3.67E+07	1.08
2	NG	$C_{1.116}H_{4.190}$	3.67E+07	1.08
3	OFNG	$C_{1.122}H_{4.204}$	3.68E+07	1.09
4	OFNG	$C_{1.122}H_{4.203}$	3.68E+07	1.09
	CH_4	$C_{1.000}H_{4.000}$	3.39E+07	1.00
* The heat that would be supplied to the system by 1 l/m of gas equals to y times the heat that would be supplied to the system by 1 l/m of methane.				

In the original kitchen range, primary air and gas mixture was travelling a distance of ~20 cm in the close proximity of the burner and it did not create any problem of backwards flame propagation. Therefore, the mixing chamber is placed just below the reactor and connected at the point where the original primary air supply nozzle is located. At this point it is important to note that, the burner installed in its original structure into the reactor/compartment was using warmer primary air than in a real kitchen; however its replacement with the mixing chamber placed outside the reactor/compartment removed this deviation from the real kitchen application. As a common practice in the burner design, the amount of primary air supply corresponds to 40 % - 60 % of the stoichiometric air requirement of the complete combustion of the supplied gas [Turns (2000)]. The

mixing chamber was dimensioned based on this value, the gas flow rates of interest and the dimension of the gas intake fitting (½"). The mixing efficiency in the mixer was tested and it was concluded that mixing of the fuel and primary air is well achieved in the mixer.

In the coming parts of the thesis, an R value is used to report the percent of the stoichiometric air requirement of the fuel added as primary air to the mixer. The corresponding carbon to oxygen (C/O) ratios (mol/mol) and equivalence ratios [$Ø = (C/O)_{experimental} /(C/O)_{stoichiometric}$] are presented in Figure 61.

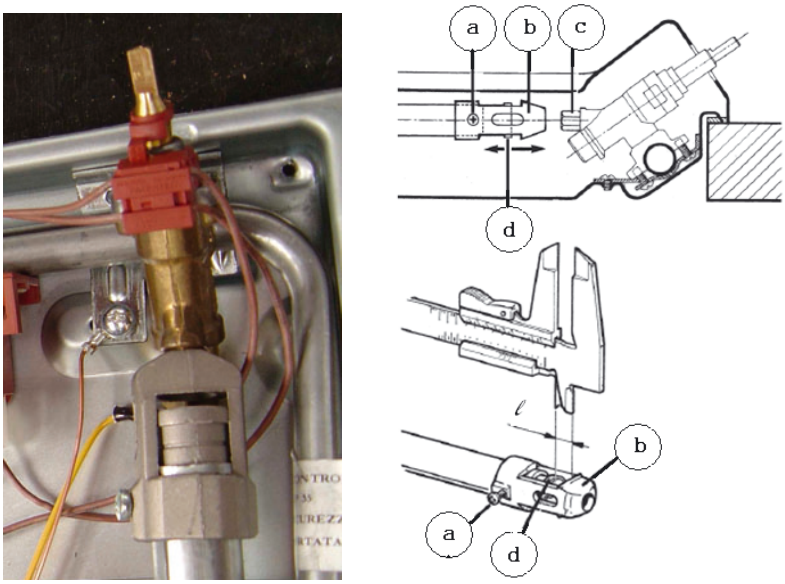

Figure 59: The original primary air supply unit of the kitchen range used in this study (The drawings are reproduced from the instruction manual of the gas cooker used in this study. In order to keep the producer anonymous, reference is not provided)

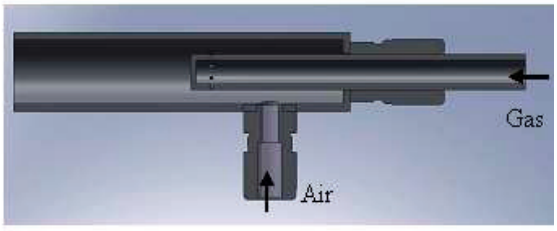

Figure 60: Mixing chamber

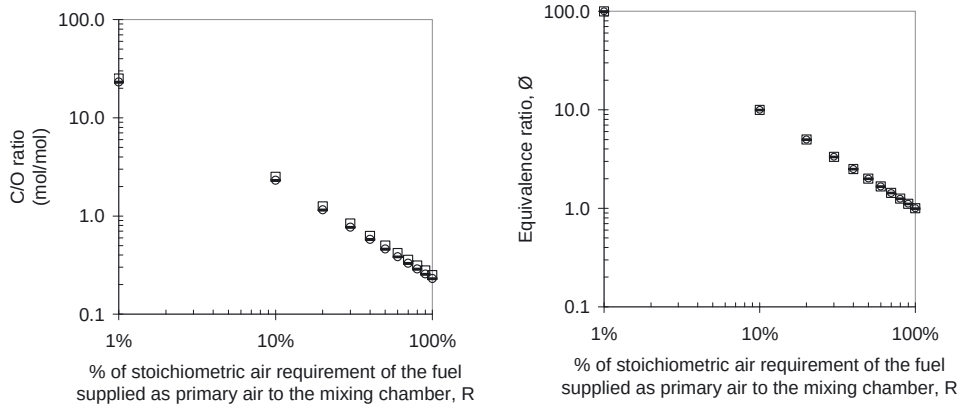

Figure 61: C/O ratios (mol/mol) and equivalence ratios [Ø = $(C/O)_{experimental}$ /$(C/O)_{stoichiometric}$] corresponding to R values for different fuels. Square symbols denote methane, circular symbols denote natural gas and minus sign denotes odorant free natural gas. When no primary air is supplied to the mixing chamber, the corresponding C/O ratio and the equivalence ratio would be infinitive.

3.1.3. Mass flow controllers

In order to have better control of the gas flows, Bronkhorst High Tech. El-flow mass flow controllers (with capacities of 80000, 10000 and 1500 Nml/minute at 20^{o}C, 5 bar) were installed for the flow of fuel, additives (H_2S/N_2) and primary air. The actual flows provided by the MFCs were measured experimentally and used to produce the calibration charts.

3.2. Results

3.2.1. Effect of primary air on emissions from the burner

The effect of primary air on particle generation from domestic gas cookers is studied using methane as the fuel. Experiments were performed with a fuel flow rate of 4 slpm and secondary air flow rate of 400 lpm. Experiments were repeated for 4.26 slpm fuel flow rate, to show the sensitivity of the particle generation to small changes in the fuel flow rate. These results are presented in Figure 62. As it could be seen, the number concentration of particles varies over more than three decades with the amount of primary air supplied. The minimum particle concentrations are observed at primary air flow rates corresponding to 60 – 70 % of the stoichiometric air requirement. As Figure 62 indicates, at primary air ratios higher or lower than this point, particle emissions would go as high as the emissions

from pure diffusion flames, 10^5-10^6 particles /cm^3. Addition of more than 80% of the stoichiometric air requirement as primary air resulted in a flickering and sooting flame, eventually extinguishing the flame partly and thereby decreasing particle number concentrations. Visual observations recorded using a web-cam showed that the flame extinguished at primary air flow rates corresponding to 88% of the stoichiometric air requirement. Images of the flame at different ratios of the stoichimetric air supplied as primary air are presented in Figure 63.

SMPS measurements were performed to determine the size distribution of the particles emitted at different conditions. However it was very difficult and rare to catch a good distribution for all conditions of concern. In Figure 64 and Figure 65, size data collected from a diffusion flame and a partial premixed flame of methane is presented. As it could be seen, the mean diameter of particles emitted from the diffusion flame was around 10 nm, whereas the size data collected from the premixed flame (Figure 65) seems to be incomplete. It is believed that the particles emitted from the partial premixed flame are much smaller and the charging efficiency is too low for the lower range of the detection limits of the SMPS.

Experiments were also performed using natural gas and odorant free natural gas, to evaluate the differences between the three fuels in terms of particle generation. These results are presented in Figure 66. Data is collected only at R values between 30% - 70% due to high CO emissions and extinguishing flame at higher ratios. As seen in Figure 66, the particle number concentrations emitted from the three fuels are quite close to each other, while the ratio of stoichiometric air requirements supplied as primary air which gives the minimum particle emissions seem to be different for each fuel: 65%-70% for methane and 60% - 65% for natural gas. The size distribution data collected from combustion of 4 slpm natural gas with PAF/SAR ratio of 65% and 400 lpm secondary air is presented in Figure 67. Similar to Figure 65, the size distribution data seems strange, pointing an instrument failure.

In Figure 68, a comparison of the particle emissions from 4.26 slpm of methane which results in a heat supply rate of 1.45 Joules/minute is compared to the particle emissions from 4.00 slpm of natural gas, which results in a heat supply rate of 1.47 Joules/minute. As it could be seen, excluding the optimum ratio which results in minimum particle emissions, particle emissions were slightly higher in the case of lower heat supply rate provided by 4.26 lpm methane. This comparison indicates that the particle formation is very sensitive to the type and flow rate of the fuel with which the burner is used.

In conclusion, these final experiments showed that particle generation from domestic gas cookers is extremely sensitive to the primary air addition. Without a precise control of the primary air added to the gas, the particle generation may vary decades. This also explains the wide range of particle number concentrations observed in the preliminary experiments, with the use of 4.2 lpm of methane, presented in Figure 43.

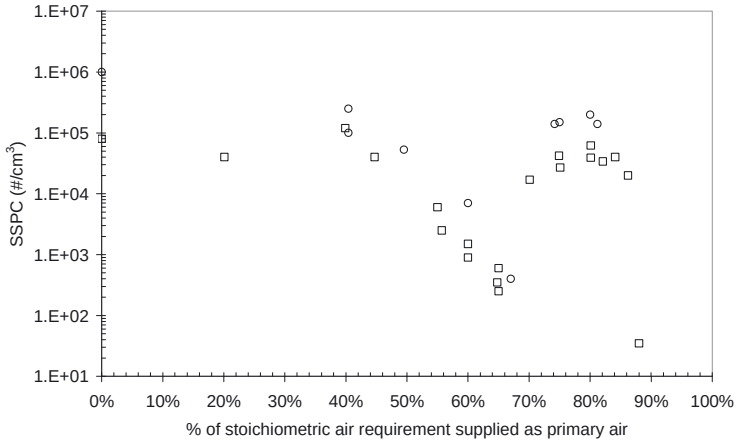

□: 4.00 slpm methane ○: 4.26 slpm methane

Figure 62: Particle number concentrations vs primary air. The square symbols represent the experiments carried out with 4.00 slpm methane and circular symbols represent those with 4.26 slpm methane.

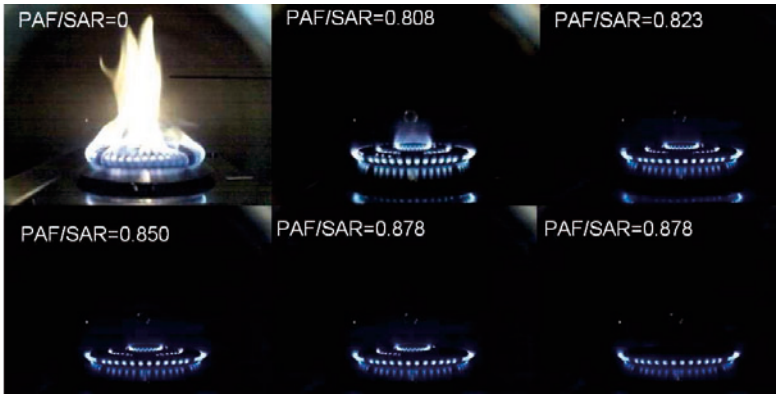

Figure 63 : Images of the flame at different ratios of the stoichimetric air supplied as primary air. Methane flow rate was 4.26 slpm and secondary air flow rate was 400 lpm. PAF denotes for primary air flow rate and SAR denotes for stoichiometric air requirement.

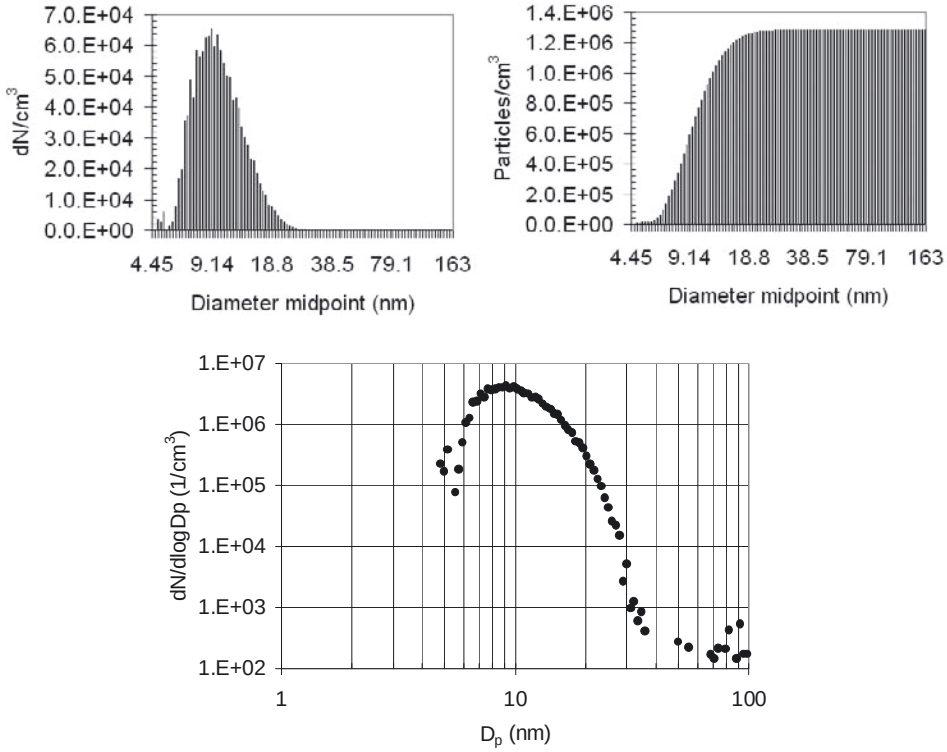

Figure 64: Size distribution data of particles emitted from diffusion flame of 4.26 slpm methane with 400 lpm secondary air flow rate.

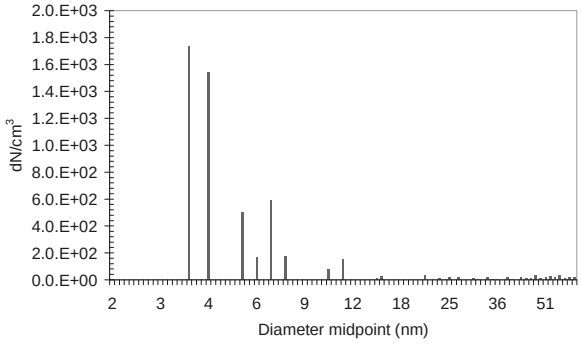

Figure 65: Size distribution data of particles emitted from partial premixed flame of 4.26 slpm methane with primary air flow rate corresponding to 60% of the stoichiometric air requirement and 400 lpm secondary air flow rate.

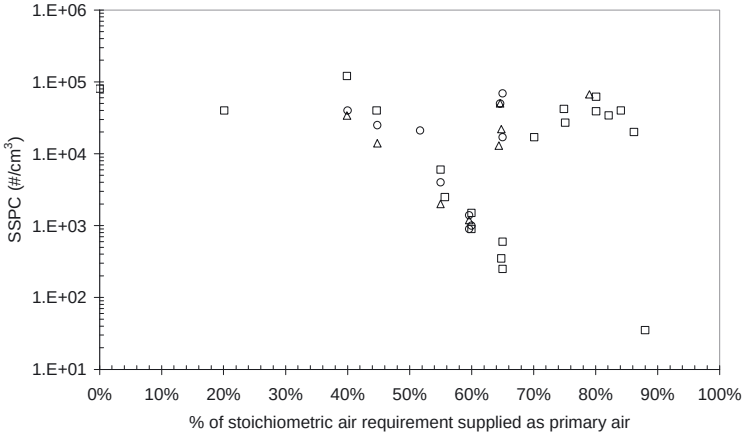

□ : Methane ○: Natural gas Δ: Odorant free natural gas

Figure 66: Particle number concentrations generated at a fuel flowrate of 4 slpm at different primary air flow rates. The square symbols represent the experiments carried out with 4.00 slpm methane, circular symbols represent those with 4.00 slpm natural gas and triangular symbols represent those with 4.00 slpm odorant free natural gas.

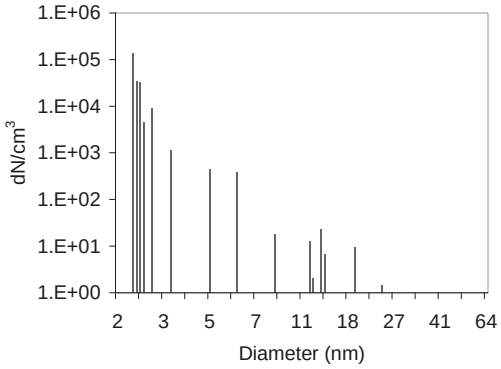

Figure 67: Size distribution data collected from combustion of 4 slpm natural gas with PAF/SAR ratio 65% and 400 lpm secondary air flow rate.

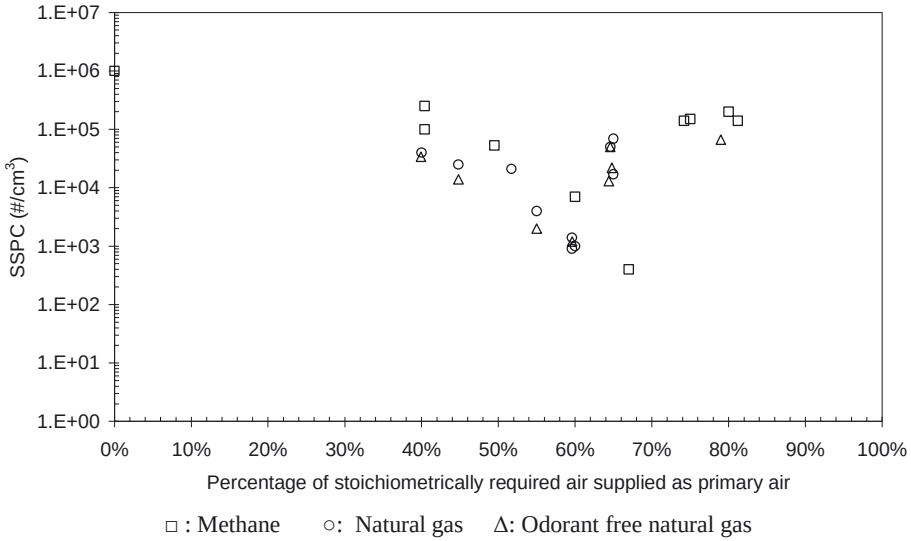

Figure 68: Comparison of particle emissions from experiments where the heat supply rates to the reactor are almost equal. The square symbols represent experiments carried out with 4.26 slpm methane, circular symbols represent those with 4.00 slpm natural gas and triangular symbols represent those for 4.00 slpm odorant free natural gas.

3.2.2. Effect of H_2S and N_2

The effect of presence of sulfur species on particle emissions from the burner can be tested by adding H_2S to methane. Due to the very toxic and corrosive nature of H_2S, it was supplied from a cylinder containing 1140 ppm H_2S in nitrogen. Therefore addition of H_2S resulted in dilution of pure methane to a lower methane content. The studied concentration of H_2S in the fuel was 100 ppm-v, resulting in a nitrogen content of 8.82%; or in other words dilution of the pure methane to 91.18% methane. In order to distinguish between the additive effect and the dilution effect on the particle emissions, experiments were repeated by adding pure nitrogen to methane, thereby preparing a gas mixture with a composition of 91.18% methane and 8.82% nitrogen. The results of these experiments are presented in Figure 69. These results showed that dilution of methane by adding pure nitrogen resulted in lower particle emissions. In the presence of sulfur species in the same grade of methane however, particle emissions laid somewhere between the levels emitted by diluted and undiluted methane experiments. This leads us to the conclusion that presence of sulfur increased the particle emissions.

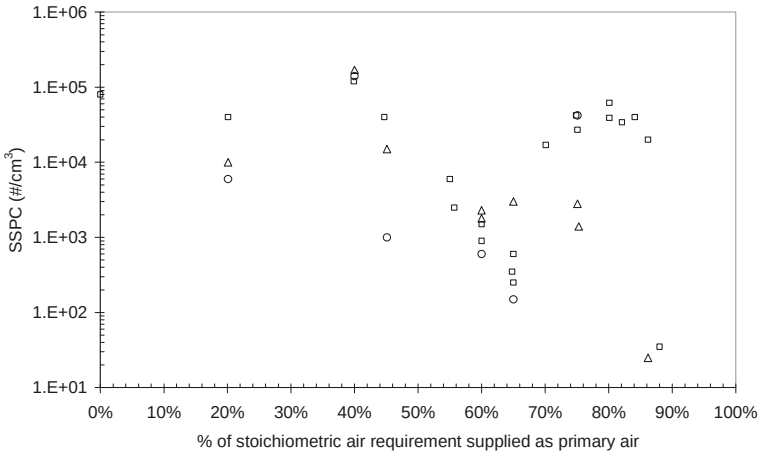

□ : Methane Δ: Methane containing 100ppm H_2S and 8.82% N_2
○: Methane containing 8.83% N_2

Figure 69: Effect of additives, H_2S and N_2 on particle number concentrations. The square symbols represent methane experiments, triangular symbols represent presence of 100ppm H_2S and 8.82% N_2 in the fuel, circular symbols represent presence of 8.83% N_2 in the fuel. The methane flow rate in all experiments is kept as 4 slpm while the secondary air flow rate is kept as 400 lpm.

3.2.3. Effect of secondary air

Effect of secondary air flow rate on the particle emissions was re-examined using methane as the fuel for the two different flow rates of the secondary air: 400 and 600 lpm. The resulting steady state particle concentrations are plotted with respect to fraction of the stoichiometric air requirement supplied as primary air, in Figure 70. As it could be seen, the particle number concentrations measured in case of 600 lpm secondary air flow rates are much less than those measured in case of 400 lpm. If it was only a matter of dilution, the difference would have been only a factor of 1.5; however the difference in most of the cases is almost an order of magnitude. Although the appearance of the flame seemed similar in both cases via visual observations, the difference in particle concentrations point out that the mechanism leading to the formation of particles is affected. As the particles are thought to be formed in the flame, the difference in the particle emissions might indicate that the flame is actually affected by the change in the secondary air flow, in a way that is not visible to the naked eye. One explanation to this could be more rapid cooling of the flame products or the elevated temperatures. On the other hand, particles would be pushed upwards and leave the reactor faster in case of higher secondary air flow rate. This would give a sampling artifact. If the particles remain for a reduced period of time around the sampling probe and /or the forces acting on the

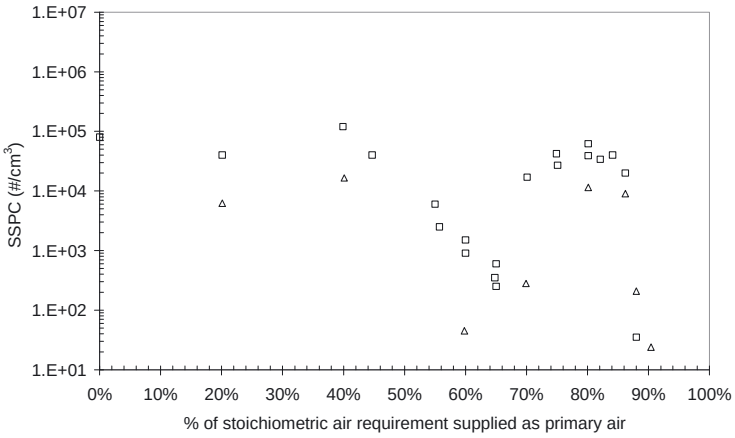

Figure 70: Particle number concentrations generated by 4 slpm methane at different primary air flow rates. The square symbols represent the experiments carried out with 400 slpm secondary air flow rate and triangular symbols represent those with 600 slpm secondary air flow rate.

particles are causing the particles to follow the main streamline and not into the sampling probe, than in case of higher flow rate less particles would be drawn by the sampling probe.

3.2.4. TEM studies

TEM samples were collected on 300 meshed, carbon filmed nickel grids, inserting the KAHLAYPET for a few seconds in the natural gas flame, using 4 slpm natural gas, primary air flow rate corresponding to 60 % of stoichiometric air requirement and secondary air flow rate of 400 lpm. Particles and their EDS spectrum are presented in Figure 71 and Figure 72. The appearance of the particles observed in Figure 71-a, is totally different than any of the previously observed ones. These particles were either not produced in the previous experiments or they were not captured by the sampler. The diameters of the individual looking particles seem to agree with the data collected by SMPS, but if one looks into a larger area of the image, it could be thought that these particles became inter-connected to each other on the grid surface. The particles shown in Figure 71 –b, however, look alike with the previously observed particles, particles of a few nanometer in diameter. This also agrees well with the SMPS measurements in that particles are very small that they rather fall outside the detection limits of the instrument, or the charging efficiency for this range of particles is very low.

As the EDS spectrum shows, particles contained copper, sulfur and oxygen. Be and Cr are known to appear due to the method; and Ni from the grid itself. As the film is covered with a thin layer of carbon, carbon can not be identified in the EDS spectrum.

An EFTEM study was carried out on the same specimen. The mapped species were carbon, copper and sulfur for which the mapping images are presented in Figure 73. The brighter areas indicate a higher concentration of the mapped species. This study showed that copper particles are almost everywhere, not bound to either of the other species, while carbon and sulfur seem to be attached to each other chemically.

An electron energy loss spectroscopy (EELS) study was carried out in order to identify the oxidation level of the copper. An example EELS spectrum is presented in Figure 74. Although the second peak is not perfectly clear, most of EELS spectrums resemble rather to cupric oxide.

a.) 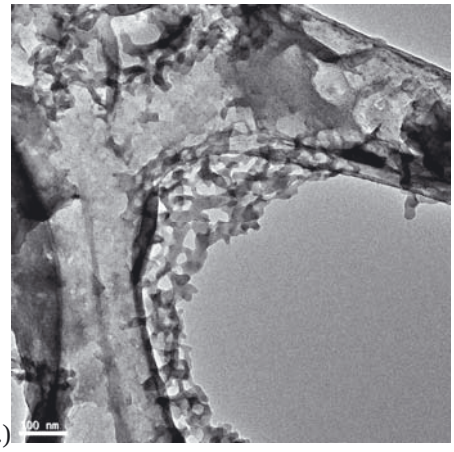

b.) 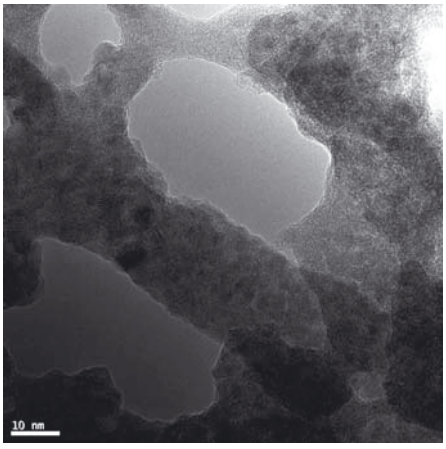

Figure 71: TEM images collected from natural gas combustion.

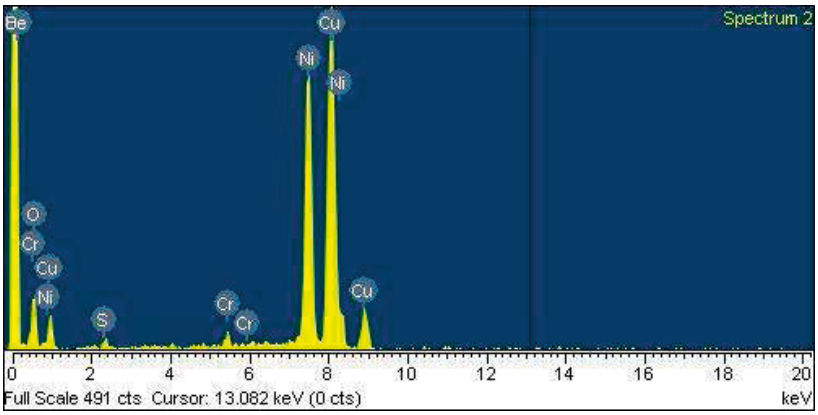

Figure 72: EDS spectrum of the particles collected from natural gas flame.

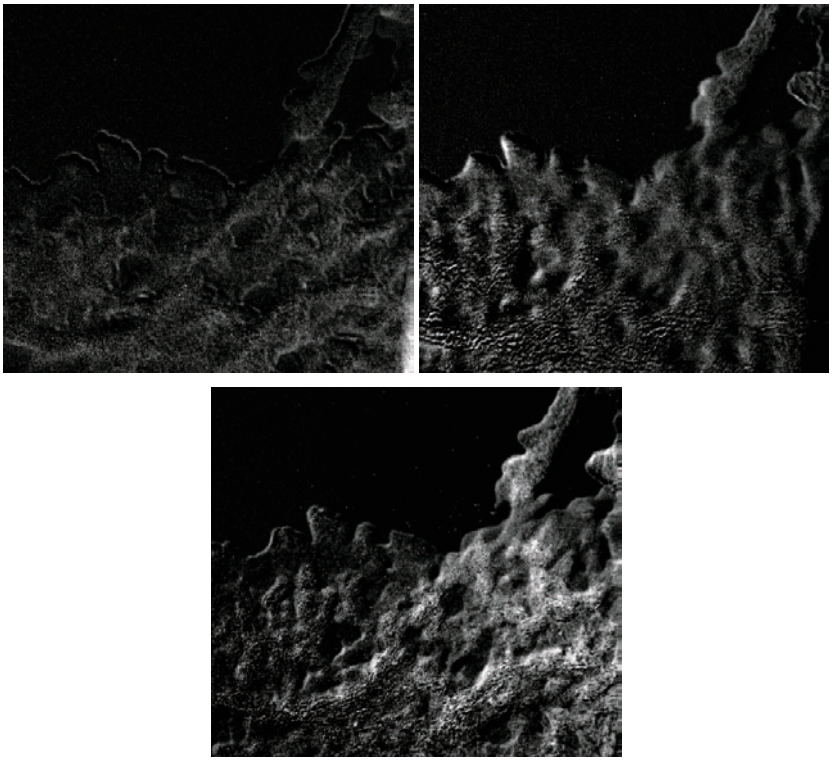

Figure 73: Carbon, copper and sulfur mapping by EELS.

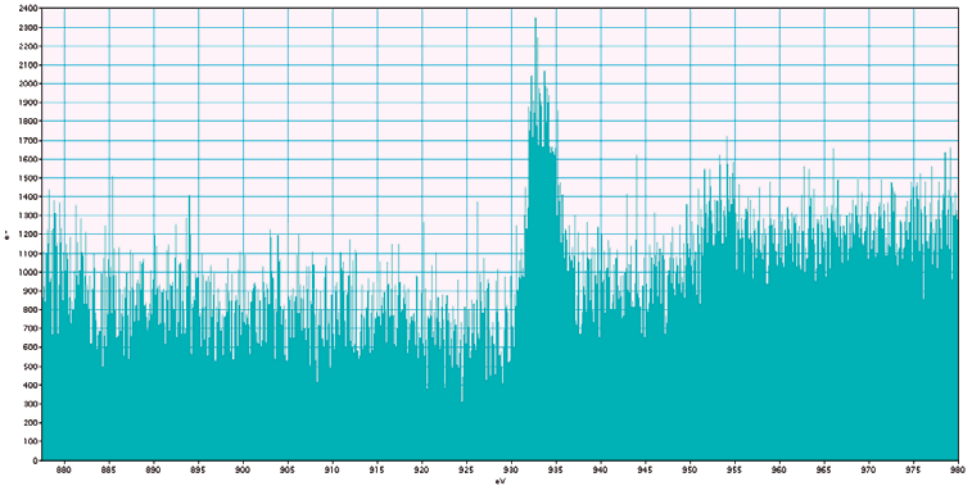

Figure 74:EELS spectrum obtained from the sample

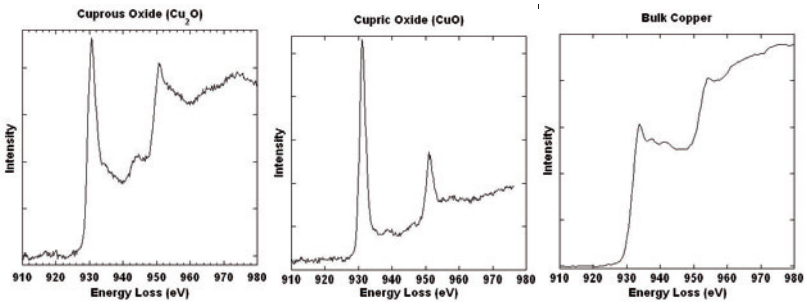

Figure 75: EELS spectrum of cuprous oxide, cupric oxide and bulk copper [Ercius et al].

3.3. Discussion

In these experiments, the fuel flow rate and primary air addition were controlled with mass flow controllers. A comparison was made between the three fuels: Methane, natural gas and odorant free natural gas. For each fuel, the flow rate of the primary air was adjusted such that the ratio of primary air supply to the stoichiometric air requirement of the studied fuel (R) was equal for each experiment carried out with one of the three different fuels.

It was found that particle number concentrations emitted from the three fuels were quite close to each other, with the condition that the equal values of R were used. The particle number concentrations for all fuels were observed to be determined by the amount of primary air supplied. The minimum

particle emissions were observed at different values of R: 65%-70% for methane and 60% - 65% for natural gas, with or without the odorant. At R values higher or lower than this point, particle emissions went as high as the emissions from diffusion flames, 10^5-10^6 particles /cm^3. Addition of more than 80% of the stoichiometric air requirement as primary air resulted in flickering and sooting flame, eventually extinguishing the flame partly and thereby decreasing particle number concentrations. Visual observations recorded using a web-cam showed that the flame extinguished at primary air flow rates corresponding to 88% of the stoichiometric air requirement.

A comparison was aimed between the diameters of the particles generated using different primary air ratios. The mean diameter of the particles from diffusion flame of methane was observed as 10 nm. However, as in the previous attempts to collect size data from methane experiments, the collected size distribution curves from partial premixed flames (using different primary air ratios) seemed to be incomplete. This again indicates that the particles rather fall to the lower detection limit of the instrument (2nm). The latter statement is also valid for natural gas experiments. The presence of particles in this size range is evidenced by the TEM studies. These findings are in agreement with the D'Anna et al's (2008) and Minutolo et al's (2008) findings. Regarding the number concentration of the particles, a direct comparison with D'Anna et al's (2008) work is not reasonable, since their measurements were performed in the flame and the measurements of this study were carried out at the reactor outlet (~ 1 m above the burner). While the precursor particle number concentrations in the methane/oxygen flames produced with R values of 50% and 57% (C/O ratios of 0.50 and 0.44) are calculated in the order of 1E12 particles/cm^3 from D'Anna et al's (2008) work, whereas in this work the particle number concentrations measured at approximately 1 m above the flame is in the range 1E4-1E5 particles/cm^3. It is worth to note here once more that particle emissions are found to be very sensitive to both the primary air addition and the fuel flow rate. Besides the emitted particles from the flame would have gone through oxidation, coagulation, agglomeration and deposition processes, which are not taken into account here. The reported concentration of organic carbon in the domestic cook exhaust by Minutolo et al (2008), 5 **mg/m^3**, is far above the findings of this work, 0.15μg/m^3 (this value is calculated using the size distribution data collected during our experiments and assuming a density of 0.3 g/cm^3); as well as the background annual average $PM_{2.5}$ mass concentrations for continental Europe, which is 4.8 ± 2.4 μg/m^3 [Dingenen et al (2004)] and the WHO guideline values for annual mean concentration of $PM_{2.5}$, which is 10 μg/m^3. Last but not least, considering that the typical 24-hour levels of PM_{10} in biomass-using homes in Africa, Asia or Latin America range from 0.3 to 3 mg/m^3 (WHO (2006), the author believes that the reported value of from Minutolo et al (2008) should rather be 5 **μg/m^3**.

TEM samples, collected on carbon filmed nickel grids, showed that particles contained copper, sulfur and oxygen. This study clarified that the copper signal detected in the preliminary experiments could not be due to the grid itself only. There are three possible sources of copper in the experiments of concern here: The natural gas itself, the burner material and the KAHLAYPET sample holder. According to a study carried out by DGC, natural gas contains 0.003 $\mu g/m^3$ copper, in addition to many other trace metals and elements, as presented in Table 11 . When it comes to the burner material and the KAHLAYPET sample holder, it is of concern that whether the surface temperature on the burner reaches to temperatures high enough to oxidize any copper present in the material. The photographs presented in Figure 76 were taken at the end experiments with natural gas. The black deposits were observed in some experiments and they were identified as soot by thermal gravimetry method; while the yellow to brownish edges in the large image were observed only in a single case and they were not subjected to any analysis due to low amount of the specimen.

Table 11: Metals in natural gas. Source: Målereport 2001, DGC

element	målt værdi [$\mu g/m^3_n$]	detektionsgrænse [$\mu g/m^3_n$]
Sn	0.06	0.06
Zn	0.06	0.06
Pb	0.06	0.06
Cd	0.01	0.01
Ni	0.02	0.02
Co	0.01	0.01
Mn	0.003	0.003
Cr	0.03	0.03
V	0.003	0.003
Cu	0.003	0.003
Sr	0.06	0.06
Na	1.1	0.9
K	0.12	0.12
Ca	6.3	6.3
Hg	27	0.5

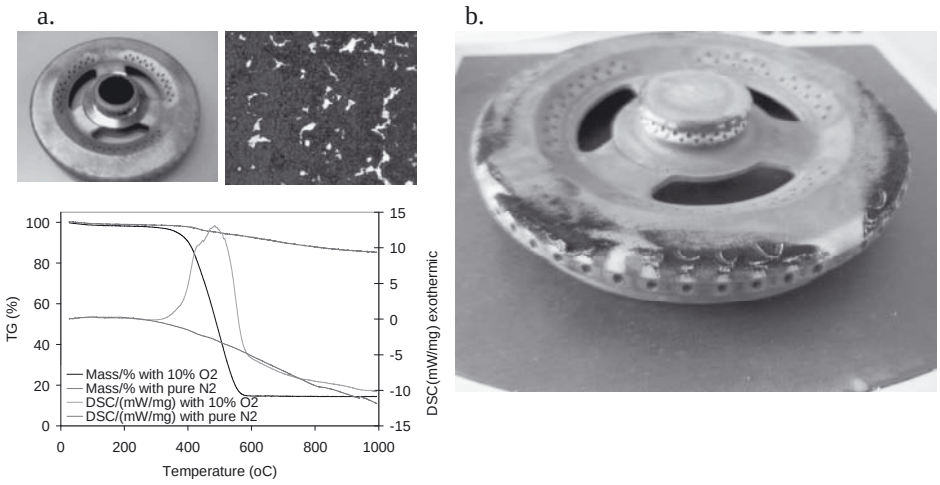

Figure 76: Deposits collected on the burner surface. a. A single experiment carried out during the preliminary experiments: Cooker placed in the reactor without any modification on primary air supply. 4 lpm natural gas was combusted with 100 lpm air supply to enforce soot formation. b. A single experiment carried out during the final experiments: Cooker placed in the reactor , primary air supply nozzle is replaced with a mixing chamber. 4 slpm naturl gas was combusted as diffusion flame with 400 lpm air supply.

The surface temperature of the burner was measured using an IR thermometer in the course of combustion of 4 slpm natural gas with 400 lpm secondary air. The temperature of the burner surface between the three rings of nozzles were measured on average as 137^{o}C on the outermost ring, 157^{o}C on the middle ring and 186^{o}C on the central ring, as presented in Figure 77. In the KAHLAYPET sample holder, temperatures are not expected to be higher than those, since cooling water is circulated behind the copper surface.

At low temperatures (<200 °C), the oxidation of copper is known to start with formation of a Cu_2O layer first. When temperature increases, Cu_2O starts to react with O, and a CuO phase forms gradually (Honkanen et al, 2008). This in fact helps to understand the EELS spectrums better in a way that the obtained spectrums from the sample did not perfectly fit to either of the oxides probably because of the coexistence of both of the species in the same specimen. In regards to the yellow to brownish edges of the collected deposit, which is presented in Figure 76, CuO remains to be a possibility since it appears to be in colors black to brownish, while Cu_2O appears as red.

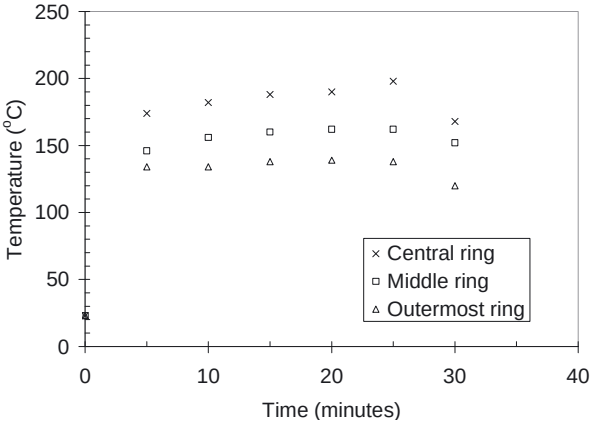

Figure 77: Surface temperatures measured on the burner surface, during combustion of 4 slpm natural gas with R ratio of 60% and 400lpm secondary air. There was no flame at time = 0 and time = 30 minutes.

Figure 78 : A copper tubing photographer before and after insertion into an oven where the temperatures are varied between 100 ^{o}C and 800 ^{o}C.

A simple visual test was applied in order to observe how copper would look after being exposed to high temperatures. A piece of copper tubing was cut into two pieces. One of the pieces was placed in an oven for 40 hours. During this time, the temperature in the oven was increased stepwise from 100^{o}C to 800^{o}C. At the end of this process, the top layer of the copper tubing was observed as presented in Figure 78. This simple test showed that the high temperatures around the burner in the

reactor could cause a change in the structure of the burner material, resulting in release of some material from its surface.

3.4. Interpretation summary

The final experiments showed that primary air has a strong effect on the particle emissions from the burner. Equal flow rates of methane, natural gas and odorant free natural gas when combusted with an equal R value (percentage of the stoichiometric air added as primary air to the fuel) resulted in almost equal particle number concentrations in the reactor outlet. The minimum particle emissions were observed at different values of R: 65%-70% for methane and 60% - 65% for natural gas, with or without the odorant.

The effect of sulfur on particle emissions is made clear by these experiments. Particle number concentrations from combustion of hydrogen sulfur added methane were higher than the same grade of methane at any values of R. Similarly, higher particle number concentrations are observed in the emissions from natural gas compared to the odorant free natural gas.

The EDS spectrum of the TEM samples showed that particles contained copper, sulfur and oxygen. The electron energy loss spectroscopy (EELS) spectrums resembled rather to cupric oxide (CuO). Since nickel grids were used, it became clear that the copper signal detected in the preliminary experiments could not be due to the grid itself only. The possible source of copper is thought to be the natural gas itself, the burner material and the KAHLAYPET sample holder.

The size range of particles is in agreement with the findings of D'Anna et al (2008) and Minutolo et al (2008) whereas the large particles and/or aggregates (Dp>20nm) reported by Dennekamp et al (2001), Bang et al (2003, 2004), Murr et al (2004) and Murr and Soto (2005) are not observed neither in SMPS nor in TEM samples.

3.5. References

Bang JJ, Trillo EA, Murr LE. (2003), Utilization of selected area electron diffraction (SAED) patterns for characterization of air submicron particulate matter collected by a thermal precipitator, Journal of the Air and Waste Management Association, 53, p.227–36.

Bang J.J., Guerrero P.A., Lopez D.A., Murr L.E., Esquivel E.V. (2004), Carbon Nanotubes and Other Fullerene Nanocarystals in Domestic Propane and Natural Gas Combustion Streams, Journal of Nanoscience and Nanotechnology, 4.7, p. 716- 718.

D'Anna, A. (2008), Combustion – Formed Nanoparticles, Manuscript for the invited topical review at the 32nd International Symposium on Combustion, Montreal, Canada.

D'Anna, A; Sirignano, M; Commodo, M; Pagliara, R; Minutolo, P (2008), An Experimental and Modelling Study of Particulate Formation in Premixed Flames Burning Methane, Combustion Science and Technology, 180 (5) , p. 950.

Dennekamp M, Howarth S, Dick C.A.J, Cherriea J.W, Donaldson K, Seaton A (2001), Ultrafine particles and nitrogen oxides generated by gas and electric cooking, Occupational and Environmental Medicine, 58, p.511-516.

Ercius P. and Hyun J. at Cornell University, WEELS - Websource for Electron Energy Loss Spectra, http://people.ccmr.cornell.edu/~davidm/WEELS/index.html.

Johannessen, J.T., Pratsinis, S.E., Livbjerg,H. (2000), Chemical Engineering Science, 55(1), 177-191.

Minutolo P., D'Anna A., Commodo M., Pagliara R., Toniato G., Accordini C. (2008), Emission of Fine Particles from Natural Gas Domestic Burners, Environmental Engineering Science, in press

Murr L. E., Bang J.J., Esquivel E.V., Guerrero P.A. and Lopez D.A.(2004), 'Carbon nanotubes, nanocrystal forms, and complex nanoparticle aggregates in common fuel-gas combustion sources and the ambient air', Journal of Nanoparticle Research 6: 241–251.

Murr, L.E., Soto K.F. (2005), A TEM study of soot, carbon nanotubes, and related fullerene nanopolyhedra in common fuel-gas combustion sources, Materials Characterization, 55, p. 50–65.

Turns S. R (2000), An Introduction to Combustion Concepts and Applications, 2nd Edition, McGraw Hill, New York, ISBN 0-07-235044-x, p.338.

PART C: MODELLING WORK

The experimental work, described in Part B, lead the author to the conclusion that nanoparticles are emitted from domestic gas cookers and the presence of sulfur in the fuel increases the number concentration of these nano-particle emissions. Moreover, the EDX spectrum of the TEM samples indicated the presence of sulfur in the emitted nanoparticles.

The role of H_2SO_4–H_2O binary homogeneous nucleation (BHN) in the formation of nanoparticles (NP) has been addressed by several researchers for many different areas, ranging from aircraft emissions to diesel particulate emissions, as well as in the atmosphere [Brown et al (1997), Clement and Ford (1999), Srivastava et al (2004), Hua and Fangqun (2006)]. Because of the enormous attraction between sulfur trioxide and water, only a very small amount of sulfur trioxide in combustion gas is enough to draw water from the gas and form a fairly concentrated acid [US EPA (1998)]. Since the flow reactor studies of SO_2 oxidation under post-flame conditions [Glarborg et al (1996), Mueller et al (2000)] indicate fractional conversions of SO_2 to SO_3 in the order of a few percent, a question is raised on the likelihood of H_2SO_4–H_2O binary homogeneous nucleation to take place in the emissions from domestic gas cookers.

A reaction mechanism is therefore prepared in order to calculate the SO_3 emissions for different stochiometries (gas, air, H_2S content in the fuel) in the presence of nitrogen oxides and CO in the post flame region of the reactor. Assuming that all SO_3 will be converted to sulfuric acid as temperature falls below 204^oC, sulfuric acid concentrations are calculated. Vehkamaki et al's (2003) parametrisation is then used only in its validity ranges of temperature and relative humidity to calculate the threshold sulfuric acid concentration needed to start nucleation. The sulfuric acid concentrations calculated by CHEMKIN and Vehkamaki's model is then compared to conclude whether there is enough sulfuric acid to start the nucleation process. If CHEMKIN calculations results in a sulfuric acid concentration that is higher than Vehkamaki's parametrisation for nucleation rate (J) of $J= 1/(cm^3s)$, we proceed with calculating the nucleation rate, thereby the particle number concentrations that would be generated. The latter is than compared with the experimental observations. On the other hand, if CHEMKIN calculations result in a sulfuric acid concentration that is much lower than Vehkamaki's parametrisation for $J= 1/(cm^3s)$, we would depart from the thought that the experimentally observed nucleation range particles are partly from the nucleation of sulfuric acid-water system. Vehkamaki's model is also used to calculate the particle concentrations that would

be reached in a kitchen for different emission scenarios using the PM model of the US EPA. In Figure 79, a flow chart summarizing the modelling process is presented.

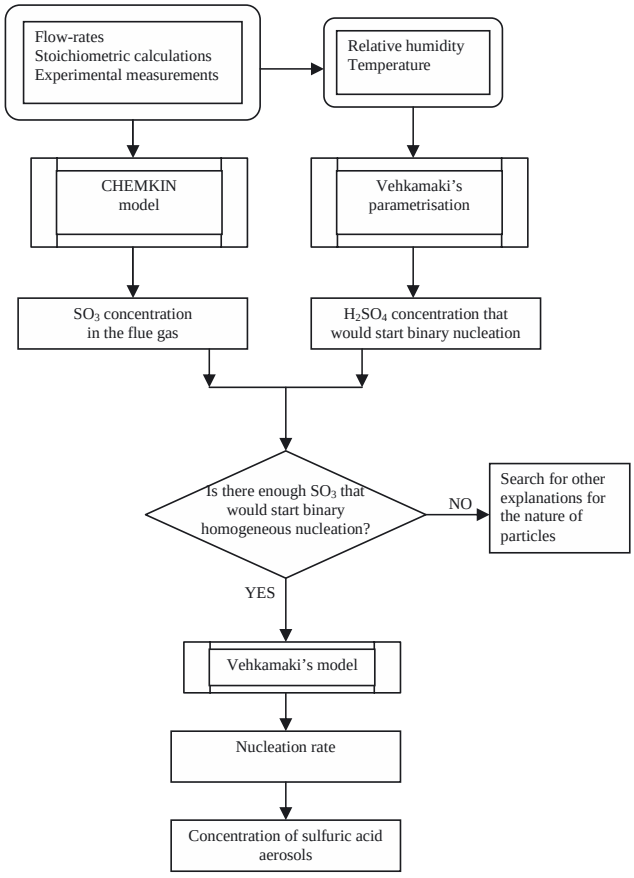

Figure 79: A summary of the model

Chapter 1: Estimation of SO_3 formation

In this chapter, the objective is to estimate the SO_3 formation in case of the experimental conditions of concern in this study. A reaction mechanism is prepared and used in CHEMKIN 4.0.2, plug flow model, for this purpose. The combustion products from stoichiometric combustion of 4 slpm CH_4 containing 100 ppm(v) and 2.5% hydrogen sulfide are entered as input to the reactor. All H_2S in the fuel is assumed to be converted to SO_2. Because of the known interactions of CO, NOx and H_2O under post flame conditions which were studied previously by Glarborg et al (1995); the species NO, NO_2 and CO are also included as components in the input to the reactor.

1.1. The Reaction Kinetics Model

The predominant sulfur-containing product formed by the combustion or slow oxidation of sulfur compounds and elementary sulfur is almost invariably sulfur dioxide. The flow reactor studies of SO_2 oxidation under post-flame conditions [Glarborg et al (1996), Mueller et al (2000)] indicate fractional conversions of SO_2 to SO_3 in the order of a few percent. Using the reaction mechanisms available from Glarborg and his co-workers (1996 - 2007) and Hindiyarti et al (2007), a reaction mechanism is prepared in order to calculate the conversion of SO_2 to SO_3 in the post flame region of the reactor under the experimental conditions of concern in this study. The reaction mechanism is presented in Table 12.

The mechanism includes the major reactions involving species C, H, N, O and S, as well as the interactions between sulfur and nitrogen species. This mechanism is used in CHEMKIN 4.0.2, plug flow model, in order to calculate the SO_3 emissions from the reactor for different stochiometries (gas, air, H_2S content in the fuel) in the presence of nitrogen oxides, carbon monooxide and sulfurdioxide.

Table 12: Reaction Mechanism and Rate Constants, expressed as $k = AT^{\beta} \exp(-E_a/RT)$ (cal, cm^3, mol, s)

Reaction	A	β	Ea			
X=>21O2+79N2	1.70E-1	0	0			
H+O2=O+OH	3.55E+15	-0.41	16600	HES98,LI/DRY04		
H+H+M=H2+M	7.00E+17	-1	0	COH/WES83		
H+H+N2=H2+N2	5.40E+18	-1.3	0	COH/WES83		
H+H+H2=H2+H2	1.00E+17	-0.6	0	COH/WES83		
H+H+H2O=H2+H2O	1.00E+19	-1	0	COH/WES83		
H+O+M=OH+M	6.20E+16	-0.6	0	GLA/MIL98		
H+O2(+M)=HO2(+M)	1.48E+12	0.6	0	GLA/ALZ03	MUE/DRY98,	LI/DRY04
H+O2(+AR)=HO2(+AR)	1.48E+12	0.6	0	GLA/ALZ03	MUE/DRY99	
H+O2(+N2)=HO2(+N2)	1.48E+12	0.6	0	LI/DRY04		
O+O+M=O2+M	1.89E+13	0	-1788	GLA/MIL98	NBS86,MAR96	
O+H2=OH+H	5.06E+04	2.67	6290	GLA/MIL98	MIC92,MAR96	
OH+H+M=H2O+M	8.30E+21	-2	0	GLA/ALZ03	CEC92	
OH+H2=H+H2O	2.14E+08	1.52	3449	GLA/MIL98	MIC92,MAR99	
OH+OH=H2O+O	4.30E+03	2.7	-2486	GLA/MIL98	MIC92	
HO2+H=H2+O2	1.62E+13	0	820	GLA/ALZ03	MUL/DRY99,	LI/DRY04
HO2+H=OH+OH	7.08E+13	0	300	GLA/ALZ03	MUL/DRY99,	LI/DRY04
HO2+H=O+H2O	3.00E+13	0	1720	GLA/MIL98	CEC92	
HO2+O=OH+O2	3.25E+13	0	0	GLA/MIL98	CEC92,LI/DRY04	
HO2+OH=H2O+O2	4.00E+18	-1.8	500	CLR	fit based on exp.	data from KAP/TRO 02
H2O2+H=H2O+OH	2.41E+13	0	3970	NBS86(uncertx5),	HEL/DRY98	,LI/DRY04
H2O2+H=HO2+H2	4.82E+13	0	7950	NBS86(uncertx5),	HEL/DRY98	,LI/DRY05
H2O2+O=HO2+OH	9.55E+06	2	3970	NBS86,MAR99,	LI/DRY04	
H2O2+OH=H2O+HO2	1.00E+12	0	0	HEL/DRY98,	LI/DRY04	
CO+O(+M)=CO2(+M)	1.80E+10	0	2384	GLA/ALZ03	ALL/DRY97,	MUL/DRY 99,MAR99
CO+OH(+M)=HOCO(+M)	1.20E+07	1.83	-236	SEN/GOL03		
CO+OH=CO2+H	1.00E+07	1.475	1300	CLR	fit based on exp.	data from SEN/GOL 03 (atm)
CO+HO2=CO2+OH	3.00E+13	0	23000	GLA/ALZ03	MUL/DRY99	
HOCO(+M)=CO2+H(+M)	1.74E+12	0.31	32928	LAR/STE88		
HOCO+OH=CO2+H2O	4.56E+12	0	-89	YU/FRA05		
HOCO+O2=CO2+HO2	9.91E+11	0	0	NOL/WAG93		
S+H+M=SH+M	6.20E+16	-0.6	0	SEN/HAY02	est	
S+OH=H+SO	3.97E+13	0	0	ALZ/GLA01	DEM/MOL97	
S+O2=SO+O	5.40E+05	2.11	-1450	LU/LIN04		
S+H2=SH+H	1.40E+14	0	19300	ALZ/GLA01	SHI/MAT98	
S2+M=S+S+M	4.80E+13	0	77000	ALZ/GLA01	HIG/MUR80	
S2+H+M=HSS+M	1.20E+25	-2.84	1665	SEN/HAY02		
S2+O=SO+S	1.00E+13	0	0	ALZ/GLA01	SIN/CVE88	
SH+O=H+SO	1.00E+14	0	0	ALZ/GLA01	DEM/MOL97,	TSU/DUP 94
SH+OH=S+H2O	1.00E+13	0	0	ALZ/GLA01	GLA/BOZ96	
SH+HO2=HSO+OH	1.00E+12	0	0	ALZ/GLA01	GLA/BOZ96	
SH+O2=HSO+O	1.90E+13	0	17925	ALZ/GLA01	TSU/MAT97	

SH+SH=S2+H2	1.00E+12	0	0	ALZ/GLA01	est	
SH+S=S2+H	3.00E+13	0	0	ALZ/GLA01	est	
H2S+M=S+H2+M	1.60E+24	-2.613	89100	ALZ/GLA01	SHI/MAT98	
H2S+H=SH+H2	3.50E+07	1.94	904	PEN/MAR99		
H2S+O=SH+OH	7.50E+07	1.75	2900	ALZ/GLA01	GOU/MAR95	
H2S+OH=SH+H2O	2.70E+12	0	0	ALZ/GLA01	TYN/RAV91	
H2S+S=SH+SH	8.30E+13	0	7400	ALZ/GLA01	SHI/MAT96	
HSS+H=SH+SH	9.70E+07	1.62	-1030	SEN/HAY02		
HSS+H=S2+H2	1.20E+08	1.653	-1105	SEN/HAY02		
HSS+H=H2S+S	4.40E+13	0	6326	SEN/HAY02		
HSS+O=S2+OH	7.50E+07	1.75	2900	ALZ/GLA01	est h2s+o	
HSS+OH=S2+H2O	2.70E+12	0	0	ALZ/GLA01	est h2s+oh	
HSS+S=S2+SH	4.20E+06	2.2	-600	SEN/HAY02		
HSS+SH=H2S+S2	6.30E+03	3.05	-1105	SEN/HAY02		
HSS+HSS=HSSH+S2	9.60E+00	3.37	-1672	SEN/HAY02		
HSSH+M=SH+SH+M	6.90E+14	1	57030	SEN/HAY02		
HSSH+H=HSS+H2	5.00E+07	1.933	-1408	SEN/HAY02		
HSSH+H=H2S+SH	2.00E+14	0	0	SEN/HAY02		
HSSH+O=HSS+OH	7.50E+07	1.75	2900	ALZ/GLA01	est h2s+o	
HSSH+OH=HSS+H2O	2.70E+12	0	0	ALZ/GLA01	est h2s+oh	
HSSH+S=HSS+SH	2.90E+06	2.31	1204	SEN/HAY02		
HSSH+SH=HSS+H2S	6.40E+03	2.98	-1480	SEN/HAY02		
SO+M=S+O+M	4.00E+14	0	107000	ALZ/GLA01	PLA/TRO84	
SO+H+M=HSO+M	1.90E+20	-1.31	662	PM	ab initio	
SO+OH=SO2+H	1.10E+17	-1.35	0	ALZ/GLA01	BLI/PIL00	
SO+OH(+M)=HOSO(+M)	1.60E+12	0.5	-400	ALZ/GLA01	GOU/MAR99	
SO+HO2=SO2+OH	3.66E+03	2.42	7660	PM	ab initio	
SO+O2=SO2+O	7.60E+03	2.37	2970	ALZ/GLA01	TSU/MAT97,	
SO+O(+M)=SO2(+M)	3.20E+13	0	0	ALZ/GLA01	PLA/TRO84,	COB/TRO 85
SO(S)+M=SO+M	1.00E+13	0	0	PGL/PM	est	
SO(S)+O2=SO2+O	1.00E+13	0	0	PGL/PM	est	
SO2+OH=SO3+H	4.90E+02	2.7	23840	ALZ/GLA01	DAG/NIC05	see reverse
SO2+OH=HOSO+O	3.90E+08	1.89	76000	ALZ/GLA01	GLA/BOZ96	
SO2+CO=SO+CO2	1.90E+13	0	65900	BAC/MAC05		
SO2+S=SO+SO	6.00E-16	8.21	9600	MUR/MAT03		
SO2+H(+M)=HSO2(+M)	5.30E+08	1.59	2470	BLI/ROB05		
SO2+H(+M)=HOSO(+M)	2.40E+08	1.63	7340	BLI/ROB05		
SO2+O(+M)=SO3(+M)	3.70E+11	0	1689	GLA/MAR04	pm 30 sic (Ar)	
SO2+O(+N2)=SO3(+N2)	3.70E+11	0	1689	YIL/MAR05		
SO2+OH(+M)=HOSO2(+M)	5.70E+12	-0.27	0	BLI/PIL03		
SO2+SO2=SO3+SO	5.00E+07	2	75000	Est		
SO3+SO=SO2+SO2	1.00E+12	0	10000	Est		
SO3+SO=SO2+SO2	7.60E+03	2.37	2980	GLA/MAR04	GLA/MAR04	
SO3+H=SO2+OH	8.40E+09	1.22	3320	PM	ab initio	
SO3+H=HOSO+O	2.50E+05	2.92	50300	ALZ/GLA01	GLA/BOZ96	
SO3+O=SO2+O2	2.80E+04	2.57	29200	Pw		
SO3+O=SO2+O2	4.10E+07	1.71	33000	mar-06		
SO3+O=SO2+O2	7.80E+11	0	6100	YIL/MAR05		
SO3+OH=SO2+HO2	4.80E+04	2.46	27250	Pw		
HSO+H=SO(S)+H2	1.00E+13	0	0	Est	(UL?)	

HSO+OH=SO(S)+H2O	1.00E+13	0	0	Est	(UL?)	
HSO+H=HSOH	2.50E+20	-3.14	920	ALZ/GLA01	GLA/BOZ96	
HSO+H=SH+OH	4.90E+19	-1.86	1560	ALZ/GLA01	GLA/BOZ96	
HSO+H=S+H2O	1.60E+09	1.37	-340	ALZ/GLA01	GLA/BOZ96	
HSO+H=H2SO	1.80E+17	-2.47	50	ALZ/GLA01	GLA/BOZ96	
HSO+H=H2S+O	1.10E+06	1.03	10400	ALZ/GLA01	GLA/BOZ96	
HSO+H=SO+H2	1.00E+13	0	0	*	est (a E12)	
HSO+O+M=HSO2+M	1.10E+19	-1.73	-50	ALZ/GLA01	GLA/BOZ96	
HSO+O=SO2+H	4.50E+14	-0.4	0	ALZ/GLA01	GLA/BOZ96	
HSO+O+M=HOSO+M	6.90E+19	-1.61	1590	ALZ/GLA01	GLA/BOZ96	
HSO+O=O+HOS	4.80E+08	1.02	5340	ALZ/GLA01	GLA/BOZ96	
HSO+O=OH+SO	1.40E+13	0.15	300	ALZ/GLA01	GLA/BOZ96	
HSO+OH=HOSHO	5.20E+28	-5.44	3170	ALZ/GLA01	GLA/BOZ96	
HSO+OH=HOSO+H	5.30E+07	1.57	3750	ALZ/GLA01	GLA/BOZ96	
HSO+OH=SO+H2O	1.70E+09	1.03	470	ALZ/GLA01	GLA/BOZ96	see reverse
HSO+O2=HSO2+O	8.40E-07	5.1	11312	Pm	ab initio	
HSOH=SH+OH	2.80E+39	-8.75	75200	ALZ/GLA01	GLA/BOZ96	
HSOH=S+H2O	5.80E+29	-5.6	54500	ALZ/GLA01	GLA/BOZ96	
HSOH=H2S+O	9.80E+16	-3.4	86500	ALZ/GLA01	GLA/BOZ96	
HOSO(+M)=HSO2(+M)	1.00E+09	1.03	50000	ALZ/GLA01	GOU/MAR99	
HOSO+M=O+HOS+M	2.50E+30	-4.8	119000	ALZ/GLA01	GLA/BOZ96	
HOSO+H=SO2+H2	1.80E+07	1.72	-1286	HU/MAR05		
HOSO+H=SO(S)+H2O	2.40E+14	0	0	HU/MAR05		
HOSO+OH=SO2+H2O	6.00E+12	0	0	Pm	rough est	
HOSO+O2=HO2+SO2	9.60E+01	2.355	-10130	Pm	(T>400K)	
HSO2+H=SO2+H2	5.00E+12	0.46	-262	HU/MAR05		
HSO2+OH=SO2+H2O	1.00E+13	0	0	ALZ/GLA01	est	
HSO2+O2=HO2+SO2	1.10E+03	3.2	-235	pm ab initio		
H2SO=H2S+O	4.90E+28	-6.66	71700	ALZ/GLA01	GLA/BOZ96	
HOSHO=HOSO+H	6.40E+30	-5.89	73800	ALZ/GLA01	GLA/BOZ96	
HOSHO=SO+H2O	1.20E+24	-3.59	59500	ALZ/GLA01	GLA/BOZ96	
HOSHO+H=HOSO+H2	1.00E+12	0	0	ALZ/GLA01	GLA/BOZ96	
HOSHO+O=HOSO+OH	5.00E+12	0	0	ALZ/GLA01	GLA/BOZ96	
HOSHO+OH=HOSO+H2O	1.00E+12	0	0	ALZ/GLA01	GLA/BOZ96	
HOSO2=HOSO+O	5.40E+18	-2.34	106300	ALZ/GLA01	GLA/BOZ96	
HOSO2=SO3+H	1.40E+18	-2.91	54900	ALZ/GLA01	GLA/BOZ96	
HOSO2+H=SO2+H2O	1.00E+12	0	0	ALZ/GLA01	GLA/BOZ96	
HOSO2+O=SO3+OH	5.00E+12	0	0	ALZ/GLA01	GLA/BOZ96	
HOSO2+OH=SO3+H2O	1.00E+12	0	0	ALZ/GLA01	GLA/BOZ96	
HOSO2+O2=HO2+SO3	7.80E+11	0	656	ALZ/GLA01	ATK/TRO92,	DAG/NIC 05 (T<2500K) FLO/HAN 77,HOW/S
N+OH=NO+H	3.80E+13	0	0	SKR/GLA04	GLA/MIL98	MI80 BAU/DRY
N+O2=NO+O	6.40E+09	1	6280	SKR/GLA04	GLA/MIL98	73 LEEDS,M
N+NO=N2+O	3.30E+12	0.3	0	SKR/GLA04	GLA/MIL98	ONAT
H+NO(+M)=HNO(+M)	1.50E+15	-0.41	0	SKR/GLA04	NBS91	SOT/PAG
HNO+H=NO+H2	4.40E+11	0.72	650	SKR/GLA04	GLA/MIL98	92
HNO+O=NO+OH	2.30E+13	0	0	SKR/GLA04	INO/WAS99	

HNO+OH=NO+H2O	3.60E+13	0	0	SKR/GLA04	GLA/MIL98	BAU73
HNO+O2=HO2+NO	2.00E+13	0	16000	SKR/GLA04	GLA/ALZ03	DEA/BOZ 00
HNO+HNO=N2O+H2O	9.00E+08	0	3100	SKR/GLA04	GLA/MIL98	NBS91
NO+HO2=NO2+OH	2.10E+12	0	-480	SKR/GLA04	GLA/MIL98	HOW80
NO+OH(+M)=HONO(+M)	2.00E+12	-0.05	-721	SKR/GLA04	GLA/MIL98	NBS91
NO+O(+M)=NO2(+M)	1.30E+15	-0.75	0	SKR/GLA04	YAR/SUT91,	NBS91
HONO+H=HNO+OH	5.60E+10	0.86	5000	SKR/GLA04	HSU/MEL97	
HONO+H=NO+H2O	8.10E+06	1.89	3850	SKR/GLA04	HSU/MEL97	
HONO+O=NO2+OH	1.20E+13	0	6000	SKR/GLA04	GLA/MIL98	NBS91
HONO+OH=NO2+H2O	4.00E+12	0	0	SKR/GLA04	GLA/MIL98	BUR/RAV 92
HONO+HONO=NO+NO2+H2O	3.50E-01	3.64	12100	SKR/GLA04	MEB/MEL98	
HNO+NO2=HONO+NO	6.00E+11	0	2000	SKR/GLA04	GLA/MIL98	NBS91
NO2+H2=HONO+H	4.50E+12	0	27600	SKR/GLA04	PAR/LIN98	
NO2+H=NO+OH	8.40E+13	0	0	SKR/GLA04	GLA/MIL98	NBS91
NO2+O=NO+O2	3.90E+12	0	-238	SKR/GLA04	GLA/MIL98	NBS91
NO2+HO2=HONO+O2	6.30E+08	1.25	5000	SKR/GLA04	GLA/ALZ03	HOR/WES 98
NO2+NO2=NO+NO+O2	1.60E+12	0	26123	SKR/GLA04	GLA/MIL98	NBS91
NO2+O(+M)=NO3(+M)	1.30E+13	0	0	GLA/MIL98		
NO3+H=NO2+OH	6.00E+13	0	0	GLA/MIL98	BEC/SCH92	
NO3+O=NO2+O2	1.00E+13	0	0	GLA/MIL98	ATK/TRO92	
NO3+OH=NO2+HO2	1.40E+13	0	0	GLA/MIL98	ATK/TRO92	
NO3+HO2=NO2+O2+OH	1.50E+12	0	0	GLA/MIL98	BEC/SCH92	
NO3+NO2=NO+NO2+O2	5.00E+10	0	2940	GLA/MIL98	DEM/RAV90	
N2O(+M)=N2+O(+M)	1.30E+12	0	62570	SKR/GLA04	JOH/GLA92,	ROH/HAN 96
N2O+H=N2+OH	3.30E+10	0	4729	SKR/GLA04	GLA/MIL98	MAR/FON 87
N2O+H=N2+OH	4.40E+14	0	19254			
N2O+O=NO+NO	9.20E+13	0	27679	SKR/GLA04	MEA/AND00	
N2O+O=N2+O2	3.70E+12	0	15936	SKR/GLA04	MEA/AND00	
N2O+OH=N2+HO2	1.30E-02	4.72	36560	SKR/GLA04	GLA/MIL98	MEB/LIN 96
N2O+OH=HNO+NO	1.20E-04	4.33	25080	SKR/GLA04	GLA/MIL98	MEB/LIN 96
N2O+NO=NO2+N2	5.30E+05	2.23	46280	SKR/GLA04	GLA/MIL98	MEB/LIN 96
CO+NO2=CO2+NO	9.00E+13	0	33800	GLA/MIL98	NBS91	
CO+N2O=N2+CO2	2.70E+11	0	20237	SKR/GLA04	GLA/MIL98	NBS91
SH+N=NS+H	1.00E+13	0	0	GLA06	est	(-130)
SH+NO(+M)=HSNO(+M)	1.60E+13	0	0	GLA06	BLA/SLA84	
SH+NO2=HSO+NO	1.80E+13	0	-477	ATK/TRO04		
SH+HNO=H2S+NO	1.00E+13	0	0	GLA06	est	(-)
S+NO(+M)=SNO(+M)	3.40E+13	0.24	0	RAS/MAR06	GOU/MAR04	
S+NO2=SO+NO	3.00E+13	0	-118	CLY/WHI79		
S+HNO=SH+NO	1.00E+13	0	0	GLA06	est	(-156)
SO2+N=NO+SO	6.40E+09	1	6280	GLA06	est	(o2+n)
SO2+NO2=SO3+NO	6.30E+12	0	27000	FRE/PAL77		
SO+N=S+NO	7.00E+12	0	0	WOI/ROT96,	OYA/ASA91,rv	
SO+NO2=SO2+NO	8.40E+12	0	0	ATK/TRO04		
HSO+N=SO+NH	1.00E+13	0	0	GLA06	est	(-96)

HSO+NO2=HSO2+NO	5.80E+12	0	0	ATK/TRO04		
HSNO+H=SNO+H2	3.50E+07	1.94	904	GLA06	est	(h2s+h)
HSNO+H=H2S+NO	1.00E+13	0	0	GLA06	est	(-164)
HSNO+O=SNO+OH	7.50E+07	1.75	2900	GLA06	est	(h2s+o)
HSNO+OH=SNO+H2O	2.70E+12	0	0	GLA06	est	(h2s+oh)
HSNO+O2=SNO+HO2	3.00E+13	0	20000	GLA06	est	
SNO+H=SH+NO	1.00E+13	0	0	GLA06	est	(-164)
SNO+H=NS+OH	1.00E+13	0	0	GLA06	est	(-78)
SNO+O=NO+SO	1.00E+13	0	0	GLA06	est	(-330)
SNO+O=NS+O2	1.00E+13	0	0	GLA06	est	(-148)
SNO+N=NS+NO	1.00E+13	0	0	GLA06	est	
NS+O=N+SO	1.00E+13	0	0	GLA06	Est	
NS+O=S+NO	3.00E+12	0	0	GLA06	WOI/ROT96,rv	
NS+N=N2+S	1.00E+13	0	0	GLA06	Est	
NS+NO2=N2+SO2	8.10E+15	-1.1	0	BLI/HIL02		

As described previously in Part B Chapter 2 of the thesis, secondary air enters the reactor through four ports. Therefore there is a need for a model to describe the mixing of the secondary air with the combustion products emitted from the burner. In the literature, Zwietering model is used to simulate/describe the effect of mixing on reburning [Alzueta et al (1998)] and on the thermal De–NOx process [Glarborg et al (1998)]. In this approach, typically the secondary feed-stream is uniformly distributed along the primary stream over a mixing time [Grcar et al (2005)].Here we present a similar approach.

The input to the reactor consists of the products (H_2O, CO_2 and N_2) from stoichiometric combustion of the fuel and an artificial compound X which dissociates into oxygen and nitrogen, according to the reaction $X \rightarrow 21O_2 + 79N_2$ with a conversion of 99.98 % of X into products. The artificial compound X is introduced in order to simulate the secondary air supplied to the reactor. Thereby the reaction allows us to simulate the mixing of the combustion products from stoichiometric flame and the secondary air in the reactor.

Using the plug flow design equations presented in Figure 80, the first order reaction rate constant for the reaction ($X \rightarrow 21O_2 + 79N_2$) which gives the desired change in the volumetric flow rate is calculated as 0.17 seconds^{-1}, as shown in Table 13.

The temperature profile inside the reactor is measured experimentally and entered as a profile to CHEMKIN 4.0.2 software. A comparison of the actual temperature profile with the CHEMKIN profile, as well as the volumetric flow rate along the reactor is presented in Figure 81. It is assumed that the temperature just above the flame is 1500^{o}K. As it could be seen, there is a good agreement between the temperature measurements and the model. The change in the volumetric flow is also accomplished satisfactorily. In Figure 82, conversion of species X to oxygen along the reactor is presented. 88% conversion of X to products is achieved already at 2 mm above the flame, while complete combustion is achieved at 10 cm. This provides close enough concentrations of oxygen and nitrogen in terms of simulating the reactor used in this work.

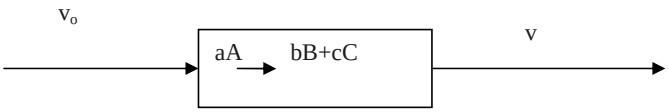

$$S = b + c - a$$

$$\epsilon = y_{X_o} \cdot S$$

$$v = v_o \cdot (1 + \epsilon x)$$

$$k = \frac{v_o \cdot \left[(1+\epsilon) \ln\left(\frac{1}{1-x}\right) - \epsilon x \right]}{V}$$

Figure 80: Plug flow equations used for calculation of the reaction rate constant, where y_{X_o} : initial mole fraction of X , v_o : inlet flowrate (volumetric), v: outlet flowrate (volumetric),

x: conversion of X to products and V: reactor volume.

Table 13 : Calculation of the reaction rate constant for the conversion of X

Fuel: 4 slpm CH_4 Stoichiometric air requirement = 30.1 slpm Flowrate of combustion products = 42.1 slpm Volumetric flowrate of X: v_{Xo}	Inlet flowrate: $v_o = 42.1 + v_{X_o}$ The initial mole fraction of X: $y_{X_o} = \frac{v_{X_o}}{42.1 + v_{X_o}}$ $\in = y_{X_o} \cdot S = \frac{99 v_{X_o}}{42.1 + v_{X_o}}$
Outlet flowrate: v = 400 slpm The desired conversion of X: x = 99.98% Reactor volume: V= 0.33 m^3	$v = v_o \cdot (1 + \in x)$ $400 = (42.1 + v_{X_o}) \cdot (1 + \frac{99 v_{X_o}}{42.1 + v_{X_o}} \cdot 99.98\%)$ $v_{X_o} = 3.6 slpm$ $v_o = 45.7 slpm$ $y_{X_o} = \frac{v_{X_o}}{v_o} = 0.08 mol/mol$ $\in = y_{X_o} \cdot S = 7.8$ $k = \frac{v_o \cdot \left[(1+\in) \ln(\frac{1}{1-x}) - \in x \right]}{V} = 0.17 s^{-1}$

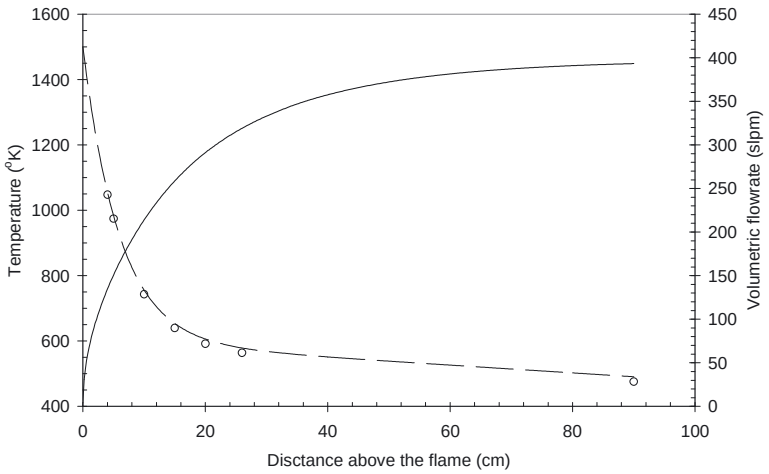

Figure 81: Temperature and volumetric flow rate along the reactor. The circular symbols denote the experimental temperature, while the broken line is the temperature profile model entered to CHEMKIN. The continuous line represents the volumetric flow rate along the reactor, calculated from CHEMKIN.

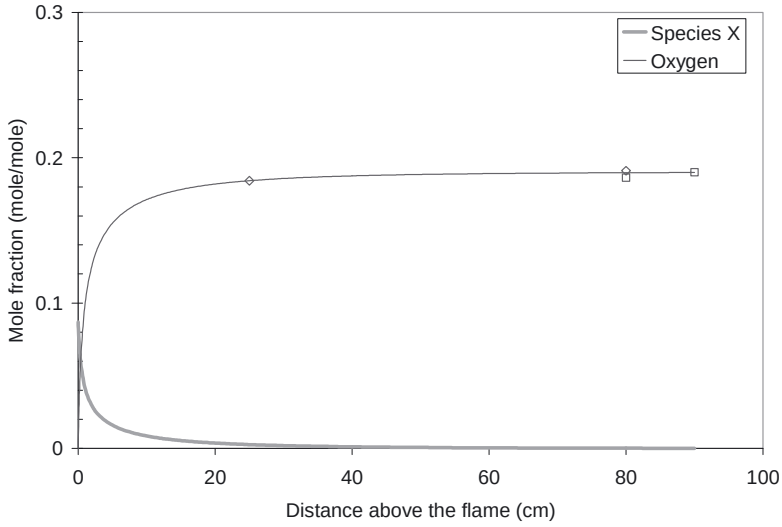

Figure 82: Mole fraction of species X and oxygen along the reactor for the simulation of combustion of 4 slpm CH_4. The diamond and square symbols denote the experimentally measured oxygen concentrations when 4 slpm CH_4 is combsted with 400 slpm air.

1.2. Results

Simulations are carried out to determine the SO_3 emissions resulting from stoichiometric combustion of 4 slpm methane in the presence of 100 ppm(v) and/or ~2.5% H_2S. However, since SO_2 and SO_3 concentrations were not measured in the course of experiments, a comparison of the simulated values to experimentally measured values is not possible.

In the flame region, normally the species NO, NO_2 and CO would be present. The interactions of CO, NOx and H_2O under post flame conditions were studied previously by Glarborg et al (1995). Based on this information, in order evaluate whether these species would create an effect on the resulting SO_3 mole fractions, simulations are carried out for different gas compositions presented in Table 14. The compositions presented here, are those that would result from stoichiometric combustion of 4 slpm of methane with a hydrogen sulfide content of 100 ppm(v) or 2.5% ,in the presence of NO, NO_2 and/or CO. In Table 14, the resulting SO_2 and SO_3 concentrations at the reactor outlet are also presented.

Table 14: Composition of input gas and resulting SO_2 and SO_3 concentrations at the outlet

	Composition of input								Composition of output	
	% mole				ppmv				ppmv	
Case#	CO_2	H_2O	N_2	X	SO_2	NO	NO_2	CO	SO_2	SO_3
1	8.61	17.21	65.58	8.61	10	0	0	0	0.98	0.087
2	8.68	17.35	65.28	8.68	10	0	0	100	0.97	0.085
3	8.67	17.34	65.22	8.67	10	0	0	1000	0.97	0.087
4	8.60	17.21	65.57	8.60	10	0	70	0	1.00	0.061
5	8.60	17.21	65.57	8.60	10	0	70	100	1.01	0.059
6	8.60	17.19	65.51	8.60	10	0	70	1000	1.01	0.058
7	8.60	17.21	65.57	8.60	10	70	0	0	1.01	0.057
8	8.60	17.21	65.57	8.60	10	70	0	100	1.01	0.059
9	8.60	17.19	65.51	8.60	10	70	0	1000	1.01	0.057
10	8.61	17.44	65.12	8.61	2153	0	0	0	224	5.93
11	8.60	17.42	65.06	8.60	2151	0	0	1000	228	6.14
12	8.61	17.44	65.12	8.61	2153	70	0	0	222	7.38
13	8.60	17.42	65.06	8.60	2151	1000	0	0	221	8.17

1.3. Discussion

In our preliminary experiments, NOx concentrations at the reactor outlet in case of 4 slpm fuel flowrate and 400 lpm air flow rate for methane and natural gas experiments were derived as 7.0ppmv and 9.5ppmv respectively. According to our model, this requires presence of 70ppm(v) NO/NOx in the input. Therefore it was decided to run our simulations with 70 ppm(v) NO and/or NO_2 in the input.

The above explained NO/NO_2 concentrations can be compared with standards, regulations and/or emission measurements available, in order to evaluate the burner performance. However, the purpose of the European Gas Appliances Directive is aimed to ensure that gas burning appliances and their associated fittings are safe. The Directive does not include limits on NOx emissions. Australia is one of the few countries that does have emission standards for NO_2 or NOx from domestic appliances. AG101 (1998) requires that the amount of nitrogen dioxide produced by any cooker shall not exceed 15 ng/J when tested at the highest setting. The units specifically refer to emissions of NOx calculated as NO_2. For emissions containing 90% NO and 10% NO_2 by volume, this would correspond to 13.5 ng NO/J and 1.5ng NO_2/J. Using a lower calorific value of 40 MJ/m^3 for the natural gas used in our experiments, for the stoichiometric combustion of 4 slpm natural gas resulting in 70ppmv NO emissions, the amount of nitric oxide produced by the cooker used in this experiment is calculated as 40 ng/J. According to Australian emission standards for domestic appliances, this is too high.

In regards to CO emissions, in our preliminary experiments, CO emissions measured at the reactor outlet were ~ 5 ppm(v) in case of 4 slpm fuel flowrate and 400 lpm air flowrate. According to CHEMKIN simulation results, CO emissions from the reactor would be ~60 ppb(v), even if there would be a release of 1000 ppmv CO from the stoichiometric combustion of 4 slpm of methane. This would indicate that the model overestimates the oxidation of CO to CO_2. On the other hand, according to Li et al (2006), the CO emissions (at 0% O_2) of gas-fired cooker top burners, would go as high as 9750 ppm(v). This would mean that the CO mole fractions entered as input to the model were chosen too low.

Nevertheless, the resulting SO_3 concentrations at the reactor outlet are less than 100 ppb(v) in case of 100 ppm(v) H_2S in the fuel, and less than 10 ppm(v) in case of 2.5 % H_2S in the fuel. In reality, natural gas contains much less sulfur than these two cases. The total sulfur content of natural gas in Denmark is regulated as 10 mg/m^3, which corresponds to ~7 ppm(v). When this is mixed with the stoichiometric air requirement, the total sulfur concentration in the input gas would be around ~1 ppm(v). According to rough model fits presented in Figure 83, the combustion of natural gas which contains 7 ppm(v) of total sulfur; would result in 8-60 ppb(v) of SO_3 at the reactor outlet. The latter range is calculated based on a linear and exponential interpolation of the trend shown by the two known data points.

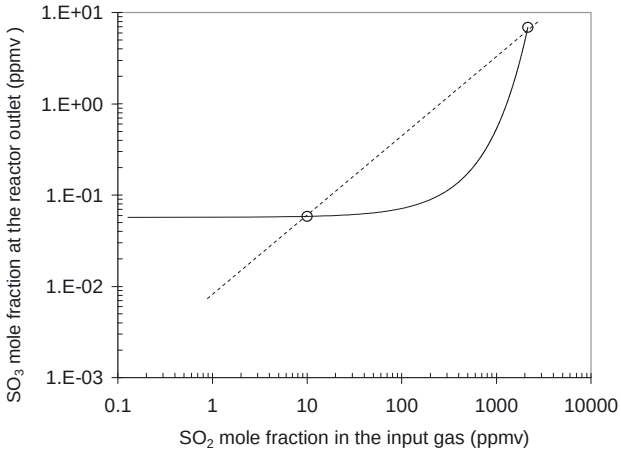

Figure 83: A model fit to estimate the SO_3 mole fraction in the reactor outlet. The circular symbols represent the average of SO_3 mole fractions calculated from the simulations, while the continuous and broken line represent exponential and linear model fits respectively.

1.4. Interpretation Summary

In case of combustion of 4 slpm methane which contains 100 ppm(v) H_2S and 8.8% N_2, with secondary air flow rate of 400 lpm, the emissions from the reactor would contain less than 100 ppb(v) of SO_3. In case of natural gas, SO_3 emissions would be less than 60 ppb(v).

1.5. References

Alzueta, M.U., Bilbao, R., Millera, A., Glarborg, P. Ostberg, M., Dam-Johansen, K. (1998), Modeling Low-Temperature Gas Reburning. NOx Reduction Potential and Effects of Mixing, Energy & Fuels, 12, p.329–338.

Glarborg, P., Kubel, D., Dam-Johansen, K., Chiang, H. Bozzelli, J. W. (1996), Impact of SO_2 and NO on CO oxidation under post-flame conditions, International Journal of Chemical Kinetics, 28 (10) , p. 773-790.

Glarborg, P., Alzueta, M. U. Dam-Johansen, K., Miller, J. (1998), A Kinetic Modeling of Hydrocarbon/Nitric Oxide Interactions in a Flow Reactor, Combustion and Flame, 115 (1-2) , p. 1-27.

Glarborg, P.; Kristensen, P. G.; Dam-Johansen, K.; Alzueta, M. U.; Millera, A.; Bilbao, R.(2000), Nitric Oxide Reduction by Non-hydrocarbon Fuels. Implications for Reburning with Gasification Gases, Energy & Fuels, 14 (4) , p. 828-838.

Glarborg, P., Marshall, P. (2005), Mechanism and modeling of the formation of gaseous alkali sulfates, Combustion and Flame, 141 (1-2) , p. 22-39.

Glarborg P. (2007), Hidden interactions-Trace species governing combustion and emissions, Proceedings of the Combustion Institute, 31 (1) , p. 77-98.

Grcar, J. F., Glarborg, P., Bell, J. B., Day, M.S.; Loren, A.; Jensen, A. D.(2005), Effects of mixing on ammonia oxidation in combustion environments at intermediate temperatures, Proceedings of the Combustion Institute, 30 (1) , p. 1193-1200.

Hindiyarti, L., Glarborg, P., Marshall, P.(2007), Reactions of SO_3 with the O/H Radical Pool under Combustion Conditions, The Journal of Physical Chemistry A, 111 (19) , p. 3984-3991.

US EPA (1998), Emergency Planning and Community Right-To-Know Act - Section 313, Guidance for Reporting Sulfuric Acid (acid aerosols including mists, vapours, gas, fog, and other airborne forms of any particle size).

Vehkamaki H.; Kulmala M.; Lehtinen K.E.J.; Noppel M. (2003), Modelling binary homogeneous nucleation of water-sulfuric acid vapours: Parameterisation for high temperature emissions, Environmental Science and Technology, 37, p3392-3398.

Chapter 2: Threshold acid concentrations for nucleation

In this chapter, the objective is to calculate the threshold sulfuric acid concentrations needed to start nucleation of water and sulfuric acid under the conditions of concern in this study. For this purpose, Vehkamaki et al's (2003) parametrisation is used in its validity ranges of temperature and relative humidity. A comparison between the sulfuric acid concentrations calculated by CHEMKIN and Vehkamaki's model is then performed in order to conclude whether there is enough sulfuric acid to start the nucleation process.

2.1. The Use And Applicability Of Vehkamaki's Model In This Study

According to Vehkamaki et al's (2003) model, the threshold concentrations ($1/cm^3$) of sulfuric acid (total) that produce the nucleation rates J =$1/(cm^3 s)$ and J=$10^6/(cm^3 s)$ depend on temperature and relative humidity according to the following equations:

$$N_a^{J=1}[1/\mathrm{cm}^3] = \exp\left[-2.51369 + 0.105916\,\mathrm{RH} - \frac{2782.56}{T} - \frac{9.37597\,\mathrm{RH}}{T} + 0.142594\,T - 0.000280101\,\mathrm{RH}\,T - 0.0000941073\,T^2 - 10.7831\ln\left(\frac{\mathrm{RH}}{100}\right) + \frac{1530.91\ln\left(\frac{\mathrm{RH}}{100}\right)}{T} + 0.0159638\,T\ln\left(\frac{\mathrm{RH}}{100}\right)\right]$$

$$N_a^{J=10^6}[1/\mathrm{cm}^3] = \exp\left[-32.7828 + 0.0922094\,\mathrm{RH} + \frac{1973.4}{T} - \frac{6.92952\,\mathrm{RH}}{T} + 0.213356\,T - 0.000246469\,\mathrm{RH}\,T - 0.000154046\,T^2 - 10.5619\ln\left(\frac{\mathrm{RH}}{100}\right) + \frac{1579.88\ln\left(\frac{\mathrm{RH}}{100}\right)}{T} + 0.0150701\,T\ln\left(\frac{\mathrm{RH}}{100}\right)\right]$$

where

T : Absolute temperature (^oK)
N_a: Total gas-phase concentration of sulfuric acid ($1/cm^3$)
RH : Relative humidity in percent

Using the above equations, threshold total acid concentrations which would give rise to nucleation rate of 1 and 10^6 particles/cm^3.s are calculated and presented in the units of our interest in Figure 84 and Figure 85. The conversion from molecules/cm^3 to ppm-v is done using the below conversion factor for standard conditions (1mole gas occupies a volume of 22,414 liters at 0^oC temperature and 1 atm pressure):

$$\frac{molecules}{cm^3}\cdot\frac{mol}{6,02214\cdot10^{23}\,molecules}\cdot\frac{22,414 liter}{mol}\cdot\frac{10^3 cm^3}{liter}\cdot10^6\,\frac{ppm-v}{cm^3/cm^3}$$

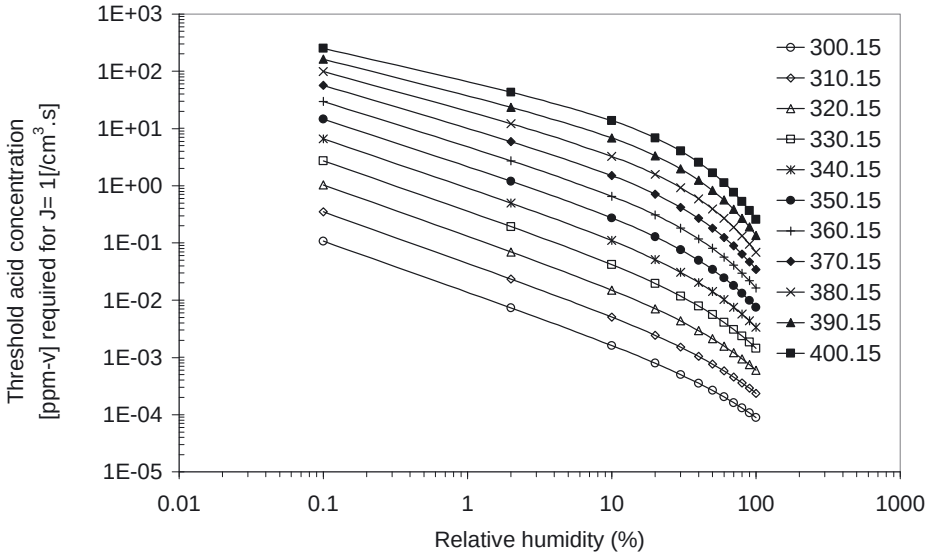

Figure 84: Threshold concentrations (ppm-v) of sulfuric acid (total) that produce nucleation rate of J = 1/(cm^3s) at temperatures between 300.15 – 400.15 ^oK .

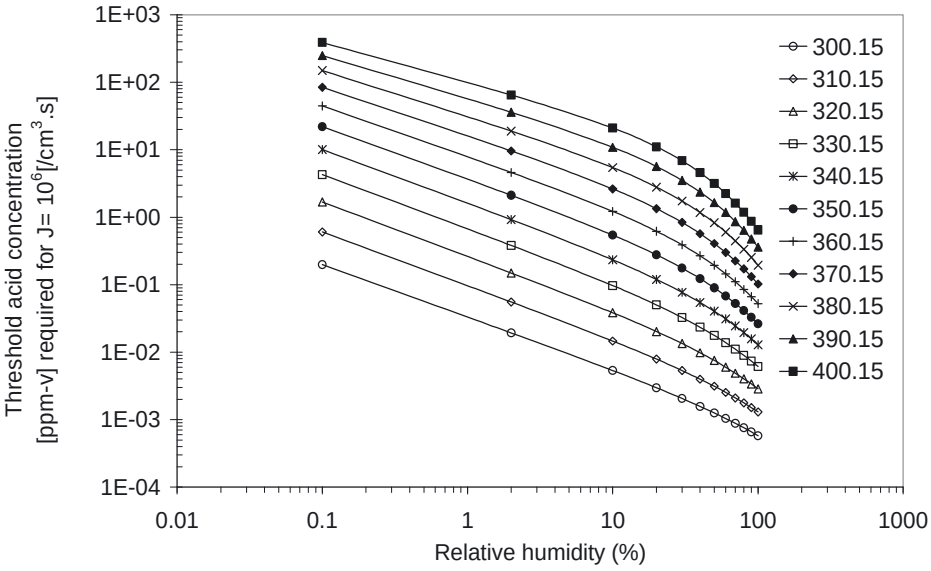

Figure 85: Threshold concentrations (ppm-v) of sulfuric acid (total) that produce the nucleation rate of J = 10^6/(cm^3s) at temperatures between 300.15 – 400.15 ^oK .

As Vehkamaki et al (2003) expressed the validity region of their parametrisations for the range of temperatures, total gas-phase concentrations of sulfuric acid (1/cm^3) and relative humidities, we can identify the conditions for which Vehkamaki's model would be applicable. As it could be seen in Figure 86, from temperature point of view, the model is hardly applicable to the reactor conditions, while the whole range of temperatures in the sampling lines is in the applicability range.

After checking the validity range for the temperature, a similar approach is followed for the relative humidity. The model is found to be applicable for a large range of experimental conditions in case of direct sampling from the reactor outlet, in other words sampling with KAHLAYPET. Assuming that the total pressure equals to atmospheric pressure and the secondary air contains 0.1 % mole fraction of water vapour, relative humidity of the emissions resulting from the complete combustion of the different gas-air flow rates are calculated for the temperature validity range, 300.15 - 400.15 K and presented in Table 15. As Vehkamaki's model is valid for a range of relative humidities between 1 and 100%, those are shaded in the table.

Samples were as well collected using an ejector probe, which provides the necessary dilution and cooling of the sample before the SMPS. The dilution factor introduced in the ejector probe, not only reduces the temperature of the sample but also reduces the concentration of water vapour. The decrease in temperature and concentration of water vapour, results in a change in the relative humidity of the gas. Relative humidities in the ejector probe for the dilution ratio used in the course of the experiments is also presented in Table 15. As the water content of the dilution air was not measured, it is assumed to contain 0.1 % mole fraction of water vapour. The shaded cells represent the conditions where Vehkamaki's model is applicable.

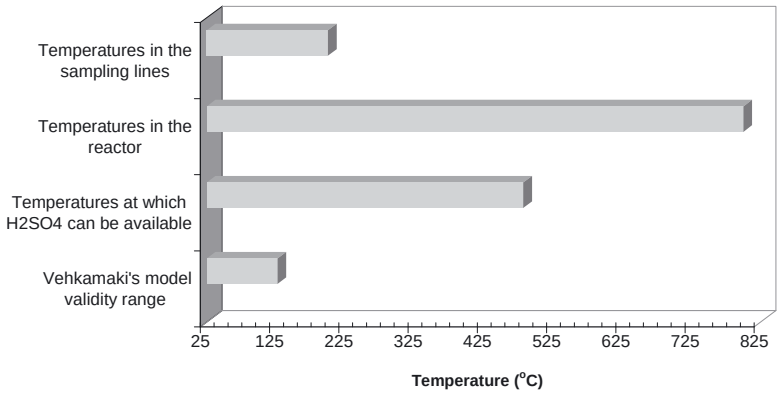

Figure 86: Applicability of Vehkamaki's model form temperature point of view

Table 15: Relative humidities at different temperatures in the sampling lines and the ejector probe

Temperature (K)	Reactor Outlet	Ejector Probe
300.15	56.64%	4.98%
310.15	32.16%	2.83%
320.15	19.02%	1.67%
330.15	11.66%	1.03%
340.15	7.39%	0.65%
350.15	4.81%	0.42%
360.15	3.23%	0.28%
370.15	2.22%	0.20%
380.15	1.56%	0.14%
390.15	1.12%	0.10%
400.15	0.82%	0.07%

2.2. Results

From CHEMKIN simulation results for Case 1 presented in Table 14 previously, it is known that combustion of 4 slpm CH_4 containing 100 ppm(v) H_2S and 8.8% N_2 would result in 87 ppb(v) of SO_3 in the reactor outlet. In case of presence of NO, NO_2 and CO in the amounts presented in Table 14 and assuming that all SO_3 is converted to sulfuric acid as temperature falls below 204^oC, sulfuric acid concentration at the reactor outlet would be approximately between 50 – 90 ppb(v). In case of direct sampling, this concentration would remain the same in the sampling lines, while in case of sampling with the ejector probe it would be reduced to approximately 6 – 9 ppb(v).

In Table 16 and Table 17, threshold sulfuric acid concentrations required to start nucleation in case of direct sampling and sampling with ejector probe are presented. Comparing these threshold concentrations to the calculated sulfuric acid concentrations from CHEMKIN simulations, it is seen that in case of direct sampling, nucleation can take place in the parts of KAHLAYPET and sampling lines where temperature falls below 337 ^oK; while in case of sampling with the ejector probe nucleation would take place in the ejector probe and the smapling lines if temperature falls to 300 ^oK.

In Table 16 and Table 17, in addition to the threshold acid concentrations, the mole fraction of sulfuric acid in the critical cluster (x*) and the nucleation rate (J) for Case 1 (100ppm(v) H_2S and 8.8% (v) N_2 in methane) are presented for a range of temperatures.

In case of direct sampling, the weighted average temperature and the residence time in the sampling lines and the KAHLAYPET is calculated as 60 ^{o}C and 80 seconds. Using this information, the particle number concentration that could be reached is calculated as ~9E7 particles/cm^{3} in case of direct sampling.

In case of sampling with the ejector probe, the average temperature and the residence time in the sampling line is calculated as 300 ^{o}K and 24 seconds. Using this information, particle number concentration that could be reached is calculated as ~3E3 particles/cm^{3} in case of sampling with the ejector probe.

Table 16: Threshold acid concentrations, mole fraction of sulfuric acid in the critical cluster (x*) and nucleation rate (J) for Case 1, in case of direct sampling.

Temperature (K)	RH	Threshold acid ppm-v for J=1/cm^{3}	X*	J (1/cm^{3}.s)
300.15	56.64%	0.0002	0.299	1.23E+14
310.15	32.16%	0.0014	0.315	3.50E+13
320.15	19.02%	0.0075	0.330	3.70E+11
331.40	11.13%	0.0423	0.345	1.16E+05
337.65	8.46%	0.103		

Table 17: Threshold acid concentrations for Case1 in case of sampling with the ejector probe

Temperature (K)	RH	Threshold acid ppm-v for J=1/cm^{3}	X*	J (1/cm^{3}.s)
300.15	4.98%	0.0032	0.37	5.48E+00
310.15	2.83%	0.0170		
320.15	1.67%	0.0822		
330.15	1.03%	0.3489		

2.3. Discussion

Dilution of the sampled gases in an inert, cold gas, when applied to post-combustion gases, necessarily implies gas-to- particle conversion of the inorganic vapours, and that may lead to an unacceptable distortion of the actual particle population and characteristics at the sampling point. In a similar manner, the temperature gradient in the thermophoretic methods, may promote condensation/nucleation of these species, thus altering the sample properties. [Jimenez and Ballester (2005)].

Based on the above mentioned phenomena, a simple test was performed to the ejector probe in the course of our preliminary experiments with natural gas. Once the particle emissions reached to steady concentration levels, the flow rate of the dilution air supplied to the ejector probe was changed. The collected concentration data was than multiplied with the valid dilution ratio for the interval of concern. As there were no major differences observed between the concentrations calculated from different intervals using different dilution ratios, it was decided that the dilution ratio that is used for sampling does not have a role in the generation of particles in these experiments. In our modelling studies, this issue is addressed as a means of second check.

Particles were observed in similar quantities from methane, natural gas and odorant free natural gas experiments, independently from the sampling instrument that is used. Impurities in the methane as reported by our supplier are; O_2 < 30 ppm , H_2< 20 ppm, N_2< 200 ppm and C_nH_m <300 ppm ; but no sulfur species. Therefore the observed particles, at least from methane experiments, can not be purely due to sulfuric acid nucleation. Moreover, particle concentration data collected using the ejector probe and KAHLAYPET for the same experimental conditions, are considerably close to each other. The resulting particle number concentrations from combustion of 4 slpm natural gas with 400 lpm secondary air flow rate, are 9E4 - 5E5 particles/cm^3 for ejector probe usage and 3E4-1E5 particles/cm^3 for KAHLAYPET usage. As the primary to stoichiometric air ratio, R, is not known in case of preliminary experiments, where the samples were collected using the ejector probe, the difference in the concentration ranges is considered to be acceptable.

The threshold sulfuric acid concentration that is required to start binary nucleation of sulfuric acid and water at 330 ^oK and 1% relative humidity (the common, expected conditions inside the ejector probe) is calculated as 0.35 ppmv, using Vehkamaki's parametrisations. Our CHEMKIN simulations showed that in order to have this much of sulfuric acid in the ejector probe, there should have been at least 100ppmv hydrogen sulfide in the fuel (methane).

In our final experiments, experiments were carried out with methane containing 100ppm(v) H_2S and 8.8% N_2, where samples were collected using the ejector probe. In these experiments, the particle concentrations varied between 1E2 to 2E5 particles/cm^3 for varying R ratios. Our modeling results and/or calculations indicate ~9E7 particles/cm^3 in case of direct sampling and ~3E3 particles/cm^3 in case of sampling with the ejector probe. Comparing the experimental results and modeling results in case of sampling with the ejector probe, the particle emissions calculated by the model falls into the range of experimentally measured particle emissions.

In our final experiments, it was observed that particle number concentrations from combustion of hydrogen sulfur added methane were higher than the same grade of methane at any values of R. For instance, for R values 60% and 70%, while the particle number concentration emitted from combustion of methane containing 8.83% nitrogen were 2E2 and 7E2 particles/cm^3 respectively, the latter from methane, containing 8.82% nitrogen and 100ppmv hydrogen sulfur were 2E3 and 3E3 particles/cm^3 respectively. In short, our experimental measurements indicate that the present amount of sulfur is enough to affect the particle generation process. The latter statement is also valid for natural gas experiments, based on the higher particle number concentrations observed in the emissions from natural gas compared to the odorant free natural gas.

As it is known, the sulfur content of the natural gas is only a few ppm. Based on the model which was presented in Chapter 1, it was concluded that, combustion of natural gas which contains 7 ppm(v) of total sulfur; would result in 8-60 ppb(v) of SO_3 at the reactor outlet. In case of direct sampling, this concentration would remain the same in the sampling lines, while in case of sampling with the ejector probe it would be reduced to approximately 1 – 4 ppb(v). Comparing these concentrations to the threshold concentrations presented in Table 16 and Table 17, it is seen that in case of direct sampling, the estimated range of concentrations of sulfuric acid at the reactor outlet is too wide to give a concrete conclusion. In the presence of 8 ppb(v) of sulfuric acid at the reactor outlet, nucleation can only take place in the parts of KAHLAYPET and sampling lines where temperature falls below 320 ^oK. Since the weighted average temperature in the sampling lines and the KAHLAYPET was previously calculated as 60 ^oC (333 ^oK), nucleation would not be expected in this case. On the other hand, if the sulfuric acid concentration at the reactor outlet is larger than 42 ppb(v), than nucleation would take place and this would mean similar levels of particle emissions based on the average temperature in the sampling lines. Similarly, in case of sampling with the ejector probe, the estimated range of concentrations of sulfuric acid at the reactor outlet is too wide to give a concrete conclusion. If the sulfuric acid concentration at the reactor outlet is large than 3 ppb(v), nucleation would take place otherwise not. Experimentally, particle emissions of 1E3- 2E5 particles/cm^3 were observed for

natural gas experiments with varying R values in the course of our final experiments. In these experiments, samples were collected mostly directly. A comparison of the experimentally measured particle concentrations with the modeling results indicate that the actual particle emissions are two order of magnitudes less than those calculated by the model.

2.4. Interpretation Summary

A combined evaluation of the experimental findings with the modeling efforts of this study constitutes the required evidences to conclude that the presence of sulfur favors the particle formation process in the domestic gas cookers, despite the very small amounts of sulfur present in natural gas via the odorant. Since particle emissions from methane experiments were very close to those from natural gas experiments, it is also evident that those particles can not be due to sulfur only. As evidenced by the TEM studies, carbon particles are emitted from domestic gas cookers, and any sulfur present in the gas is incorporated into these particles.

2.5. References

Vehkamaki H.; Kulmala M.; Lehtinen K.E.J.; Noppel M. (2003), Modelling binary homogeneous nucleation of water-sulfuric acid vapours: Parameterisation for high temperature emissions, Environmental Science and Technology, 37, p3392-3398.

Myhre, C. E. L.; Nielsen, C. J.; Saastad, O. W. (1998), Density and Surface Tension of Aqueous H_2SO_4 at Low Temperature, Journal of Chemical & Engineering Data, 43, 617-622.

Chapter 3: Simulations for kitchens

In this chapter, the objective is to determine the inhalation exposure to particles emitted from domestic gas cookers, and provide a comparison between the environmental tobacco smoke and infiltration of ambient $PM_{2.5}$.

3.1. The Model

Since most people spend a large portion of their time indoors, estimation of inhalation exposure to indoor air pollutants is essential. A series of indoor air quality (IAQ) simulation programs are available serving to this purpose, such as RISK (Sparks, 1996), MEDB-IAQ (Zhang, et al., 1999), MCCEM (Koontz and Wilkes, 1999), and CONTAMW (Dols, et al., 2000).

IAQX which stands for Simulation Tool Kit for Indoor Air Quality and Inhalation Exposure, is .a Microsoft Windows-based indoor air quality (IAQ) simulation software package that was developed by the U.S. Environmental Protection Agency for its own use and for specific applications. The first Indoor Air Quality (IAQ) simulation package (IAQX 1), which consists of five stand-alone programs -- was published in October 2000. The latest version (1.0f), modified in July 2005, can be downloaded from the EPA web site. It is designed mainly for advanced users. In addition to performing conventional IAQ simulations, which compute the time/concentration profile and inhalation exposure, IAQX can estimate the adequate ventilation rate when certain air quality criteria are provided by the user.

PM.EXE implements a generic model for indoor particulate matter (PM) developed by W. W. Nazaroff and G. R. Cass (Nazaroff and Cass, 1989). The model takes into consideration: infiltration of ambient PM, interzone air movement, indoor sources, deposition and filtration. The authors describe their model with several equations. Briefly, for a given size group, its mass concentration in zone i is calculated from Equation 20.

Equation 20:

$$V_i \frac{dC_i}{dt} = p\, Q_{0i}\, C_0 + \sum_{j=0}^{n} (1 - f_{ji})\, Q_{ji}\, C_j - \sum_{j=0}^{n} Q_{ij}\, C_i + \sum_{k=1}^{m} R_k - k_D\, V_i\, C_i - C_i \sum_{l=1}^{q} Q_l (1 - f_l)$$

where

Vi = volume of zone i (m^3);

Ci = concentration in zone i (:g/m^3);

t = time (h);

p = penetration factor (unitless);

Q_{oi} = air flow from outside to zone i (m^3/h);

C_0 = concentration in the ambient air ($\mu g/m^3$);

f_{ji} = filter's removal efficiency for air flow from zone j to zone i and j…i (unitless);

Q_{ji} = air flow rate from zone j to zone i and j…i (m^3/h);

Cj = concentration in zone j ($\mu g/m^3$);

Q_{ij} = air flow rate from zone i to zone j and j…i (m^3/h);

R_k = emission rate for indoor source k ($\mu g/h$);

D_k = first-order deposition rate constant (h-1);

Q_l = air flow rate passing through the free-standing air filter l (m^3/h);

f = removal efficiency for the free-standing air filter l (unitless);

n = number of air zones;

m = number of indoor sources in zone i; and

q = number of free-standing air filter/cleaners in zone i.

One fate for particles in indoor air is deposition onto surfaces. Clearly, this process alters the likelihood of human exposure, since a deposited particle cannot be inhaled unless resuspended. The PM deposition rate is size dependent and unlike gas-phase air pollutants, the PM deposition rate has to do with the orientation of the surfaces. For example, the surface types can be: floor, ceiling, and walls. There are a number of theoretical models in the literature for estimating the PM deposition velocity in the indoor environment. The characteristic constant for PM deposition in the indoor environment is reported in the literature as either deposition velocity or deposition rate constant. The first-order deposition rate can be expressed in two ways:

Equation 21: $$R = C\sum_{i=1}^{n}(D_{vi}S_i)$$

Equation 22: $$R \quad D_k VC$$

Equation 23: $$D_k = \frac{\sum_{i=1}^{n} (D_{vi} S_i)}{V}$$

where

R = deposition rate (μg/h);

C = indoor concentration of PM in certain size (μg/m³);

D_{vi} = deposition velocity for surface i (m/h);

Si = area for surface i (m²);

n = number of surface materials;

D_k = first-order deposition rate constant (h-1); and

V = room volume (m³).

Since both D_{vi} and D_k can be found in the literature, this program allows the user to select either equation to compute the deposition rate. When, Equation 1 is chosen, in each zone, more than one surface type can be specified. On the other hand, D_k in Equation 2 is more of a lumped constant and the user does not need to know the surface areas. There are a number of theoretical models in the literature for estimating the PM deposition velocity in the indoor environment. Lai and Nazaroff (2000) presented the deposition velocity as a function of particle diameter and friction velocity, as presented in Figure 87, for a particle with a density of 1.0 g cm^3 at an air pressure of 1 atm, temperature of 293 K for a representative range of friction velocities (0.3, 1.0 and 3.0 cm/s) -which approximately spans the range expected for mechanically ventilated indoor spaces; to different surfaces (a vertical wall, a downward-facing horizontal surface and an upward-facing horizontal surface). As it could be seen, the deposition velocity of a given size of particle does not change dramatically with the inclination of the surface; while it is directly affected with a change in the friction velocity. An order of magnitude change in the friction velocity results in an order of magnitude change in the deposition velocity for any surface considered. Last but not least, the big difference in the deposition velocities of a 1nm particle and a 20nm particle, for the same friction velocity, implies that the size groups to be entered into the software should be kept as small as possible.

Lai and Nazaroff (2000) also calculated a first order deposition rate constant, β (s^{-1}), given by Equation 24.

Equation 24:

$$\beta = \frac{v_{dv}A_v + v_{du}A_u + v_{dd}A_d}{V}$$

Where v_{dv}, v_{du} , and v_{dd} represent the deposition velocities to the vertical, upward-facing, and downward-facing surfaces, respectively; A_v , A_u , and A_d are the total deposition areas of the vertical, upward, and downward surfaces; and V is the room volume. As this formula corresponds to the definition of the rate constant D_k, multiplying β(s^{-1}) with the conversion factor required to convert from seconds to hours, D_k (h^{-1}) can be calculated.

In this program, the PM emission rate from an indoor source can be represented by three emission types: constant, on/off, and time-varying. For the constant type, the emission rate remains constant during the entire simulation period, and the emission rate for each size group is represented by a single value. The on/off type allows the user to define a source that is active only in a user-specified time period. This source type requires the user to provide the source start time, end time, and the emission rates at the start and end times. When the two values are different, the emission rate at any time during the active period is calculated by linear interpolation. The user can provide a data table of the time-varying emission rates by selecting the time-varying source type.

Once the time-concentration data is generated, personal inhalation exposure is calculated by Equation 25.

Equation 25:

$$I_x = R_B \sum_{i=1}^{n-1} \frac{(C_i + C_{i+1})(t_{i+1} - t_i)}{2}$$

where

I_x = inhalation exposure (μg);

RB = breathing rate (m^3/h);

n = number of data points in the time-concentration table;

C_i = concentration at time t_i (μg/m^3); and

C_{i+1} = concentration at time t_{i+1} (μg/m^3).

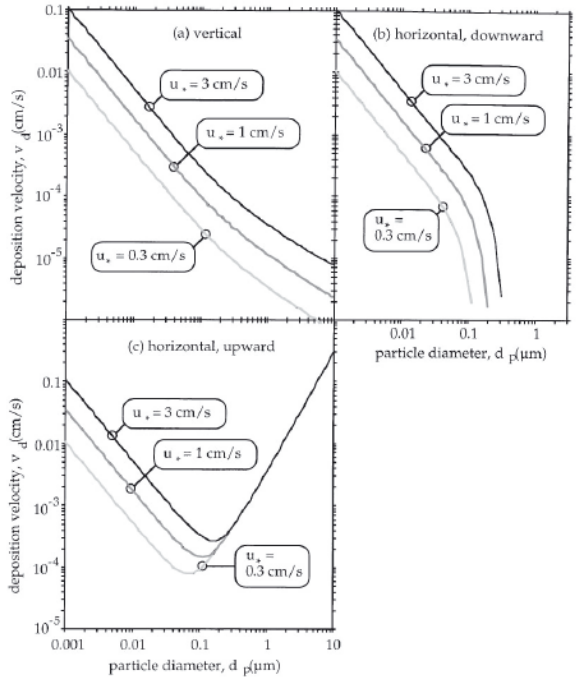

Figure 87 : Deposition velocity as a function of particle diameter and friction velocity, by Lai and Nazaroff (2000): (a) vertical wall, (b) downward-facing horizontal surface and (c) upward-facing horizontal surface. Predictions assume air pressure is 1 atm, temperature is 293 K and particle density is 1.0 g/cm^3.

Adams (1993) measured for a subject population of 160 normally active individuals of both genders, and of varied age (6–77 years) and ethnicity. For ‘‘at rest’’ conditions (lying, sitting, or standing), the mean volumetric breathing rates varied over fairly narrow ranges: 0.44–0.51 m^3 /h for children (6–13 yr), 0.43–0.50 m^3/h for adult females, and 0.54–0.64 m^3/h for adult males. For adult females conducting housework, the mean volumetric breathing rate increased by about a factor of two, to 1.04 m^3 /h.

Ventilation, the process of exchanging indoor air with outdoor air, removes pollutants emitted from indoor sources. Ventilation rates vary among buildings and also with time in a given building. In IAQX either a ventilation flow rate (m^3/h) or an air exchange ratio (the ratio of ventilation flow rate to the volume of the room,) can be defined. Air exchange rates in the residential structures of the United States were found to be well fit by lognormal distributions with geometric mean 0.5 h^{-1} and geometric standard deviation 2.1 by Murray and Burmaster (1995). In regards to penetration of the outdoor PM,

the user is asked to provide the type of outdoor PM concentration data (constant or time varying); infiltration factor; and outdoor PM concentrations. From time to time, the question may be raised in the opposite way: what is the adequate ventilation rate to keep the indoor pollution level below certain criteria? The IAQX program can answer such a question by providing a special simulation mode which calculates the adequate air exchange ratio for three criteria: peak concentration, average concentration and inhalation exposure for a selected pollutant.

3.2. Results

Using a similar method with Lai and Nazaroff (2000) , rate constants for a room with dimensions as presented in Figure 88, are calculated and presented in Figure 89 together with the ones from Lai and Nazaroff's (2000) work. As in the deposition velocities, there is a big difference in the deposition velocities rate constants for a 1nm particle and a 20nm particle, for the same friction velocity implying that the size groups to be entered into the software should be kept as small as possible. The size range of interest (2 -20nm) is divided into ten groups for which an average deposition rate constant is calculated for the three different friction velocities as presented in Table 18.

Using the density of soot precursor particles (0.3 g/cm^3) and the size distribution data collected during stoichiometric combustion of 4slpm methane, which releases 10^5 particles/cm^3, emission rate of the different size groups is calculated as presented in Table 19. Using these emission rates, the concentration – time data is produced for two scenarios, in which the only difference is whether deposition is taken into account or not.

Once concentration – time data is calculated, inhalation exposure simulation is carried out. For the inhalation exposure simulations, a person (adult females, adult males and children) is assumed to have an average breathing rate of 0.50 m^3/h.

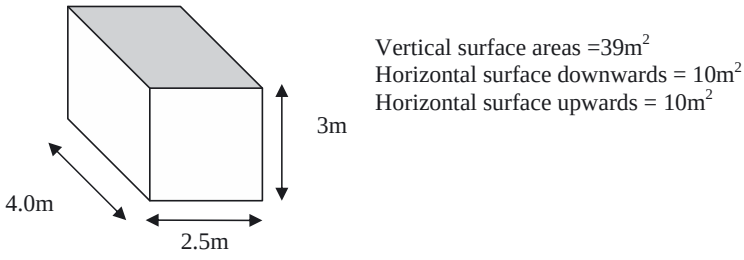

Figure 88: The dimensions of the kitchen used for this study

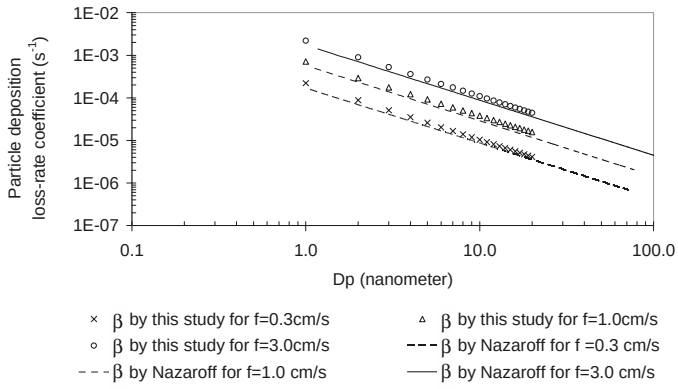

Figure 89: Deposition rate constants

Table 18: Size groups and the corresponding deposition rate constants (h^{-1})

Size groups	Deposition rate constants (h^{-1}) for Friction velocity (cm/s)		
	0.3	1	3
<=2 nm	0.556660	1.803913	5.571224
2<Dp<=3	0.250859	0.844201	2.552500
3<Dp<=4	0.155470	0.534763	1.597092
4<Dp<=5	0.109918	0.384043	1.136882
5<Dp<=6	0.083650	0.295868	0.869820
6<Dp<=8	0.061230	0.219543	0.640479
8<Dp<=10	0.043473	0.158296	0.457795
10<Dp<=12	0.033156	0.122203	0.350990
12<Dp<=15	0.025310	0.094410	0.269332
15<Dp<=20	0.018005	0.068178	0.192844

Table 19: Emission rate (micrograms/hour) for different size groups

Size group (nm)	Emission rate (μg/h)
≤ 2	0.000
2<Dp≤ 3	0.000
3<Dp ≤ 4	0.000
4<Dp ≤ 5	0.039
5<Dp ≤ 6	0.213
6<Dp ≤ 8	1.368
8<Dp ≤ 10	1.586
10<Dp ≤ 12	0.865
12<Dp ≤ 15	0.328
15<Dp ≤ 20	0.013

Simulations are carried out for 4 cases, in which the emission rates presented in Table 19 are emitted from an ON/OFF - linear source in the course of 1 hour, in a room of $30m^3$ volume. The total simulation time is kept as 24 hours in all simulations. The only difference between the four cases is the deposition of the particles. In Case1, deposition is not considered. In Case2, 3 and 4 the deposition rate constant of the particles were calculated assuming a friction velocity of 0.3, 1.0 and 3.0 cm/s respectively. The resulting total concentrations and inhalation exposures from these simulations are presented in Figure 90. As it could be seen, the highest concentration of particles is observed in Case1, where no deposition takes place; whereas the lowest particle concentration is observed in Case 4, where the deposition rate constant is the highest of all cases. Similarly, the highest inhalation exposure is observed in Case1, since the concentration is higher than all the other cases and the lowest inhalation exposure is observed in Case4, since the concentration is lower than all the other cases. It is worth to note that, the latter statement is valid for the total concentrations and total inhalation exposure; as the situation would be different for different size range of particles, whose emission rates are different. In Figure 91, concentration and inhalation exposure of different size groups for all cases are presented individually.

The fraction of particles deposited on the surfaces is calculated simply as the ratio of difference between the highest and lowest concentrations to the highest concentration. As it could be seen in Table 20, at the end of 24 hours, most of the particles would be deposited on the surfaces if the friction velocities are equal to and/or higher than 1.0 cm/s. In IAQX software it is assumed that deposited particles do not resuspend.

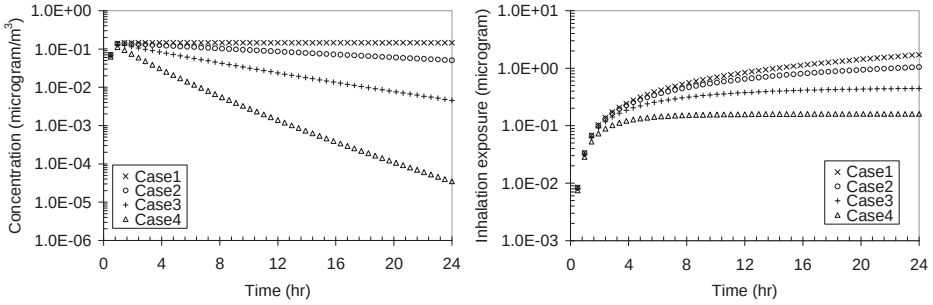

Figure 90: Total concentrations and inhalation exposures ($D_p \leq 20nm$)

Table 20 : Fraction of particles deposited on surfaces

	Fraction of particles deposited on surfaces
Case 1	0.00%
Case 2	27.59%
Case 3	96.46%
Case 4	99.97%

Last but not least, for these scenarios, an adequate vent simulation is carried out in order to determine the required air exchange ratio to reduce the concentrations below a target concentration. As there is no recommended limits for particle concentrations, a value of 0.1 nanogram as inhalation exposure is assigned for particles of size 15nm<Dp<=20nm. The air exchange ratios required to reach this threshold at the end of the 24 hours of simulation time are calculated as 2.19 , 2.17, 2.11 and 2.07 for Case 1, 2, 3 and 4 respectively.

According to experimental observations of Ning et al (2006), the geometric mean diameter (based on number size distribution) of the environmental tobacco smoke (ETS) shortly after smoking a low.tar cigarette for 5-6 minutes in a room of 30m^3 supplied with an air exchange ratio of 3.6 h^{-1}, is 147nm and the corresponding volumetric mean diameter is 416nm. According to Klepeis et al (2003), the average mass median diameter of particle emissions from cigarettes and cigars is 0.2 μm and their emission rate is 0.2–0.7 mg/min for cigars and 0.7–0.9 mg/min for cigarettes. In order to have a comparison in terms of inhalation exposure, simulations are carried out for 30 m^3 room ventilated with an air exchange ratio of 2.14, where a cigarette with a particle emission rate of 0.8mg/min is smoked for 6 minutes. The deposition rate constant of the particles were calculated as 0.0031, 0.0049 and 0.012 cm/s for the friction velocities of 0.3, 1.0 and 3 cm/s, respectively. The results of these simulations are presented in Figure 92.

According to Dingenen et al (2004), background annual average PM_{10} and $PM_{2.5}$ mass concentrations for continental Europe are 7.0 ± 4.1 and 4.8 ± 2.4 μg/m^3, respectively. The study by Hänninen et al (2004) on the infiltration of ambient $PM_{2.5}$ and levels of indoor generated, non-ETS $PM_{2.5}$ in residences of four European cities indicated that the infiltration efficiency of $PM_{2.5}$ particles is similar in all four cities (Helsinki, Basle, Prague, Athens) included in the analysis, ranging from 0.59 to 0.70 and the mean residential indoor concentrations of ambient particles range from 7 (Helsinki) to 21 μg/m^3 (Athens). Simulations are carried out to determine the particle concentrations and inhalation exposures in a room in the absence of any indoor source of particles, while the air exchange ratio is 2.14 and $PM_{2.5}$ concentration in the ambient air is 5.0 μg/m^3 and the infiltration efficiency is 0.65. The

deposition rate constant of the $PM_{2.5}$ is assumed as 0.2 h^{-1}, by interpolation from Nazaroff's (2000) charts. The results of this simulation are presented in Figure 93.

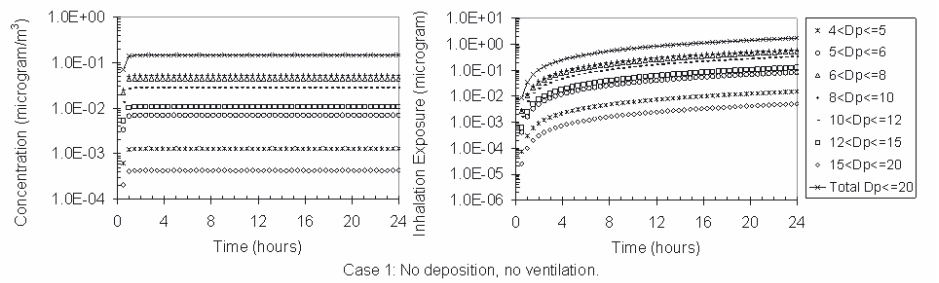

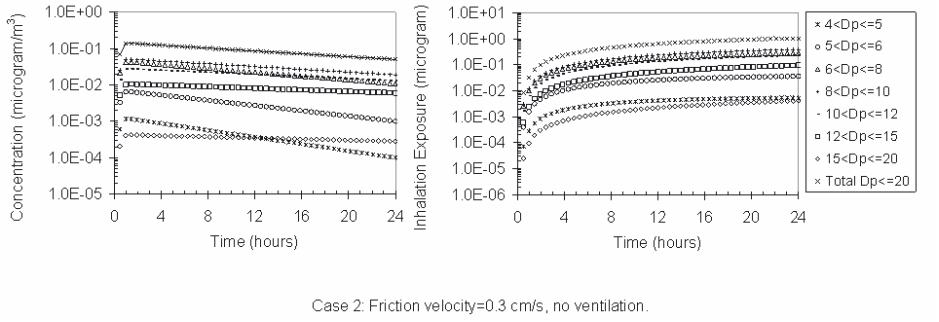

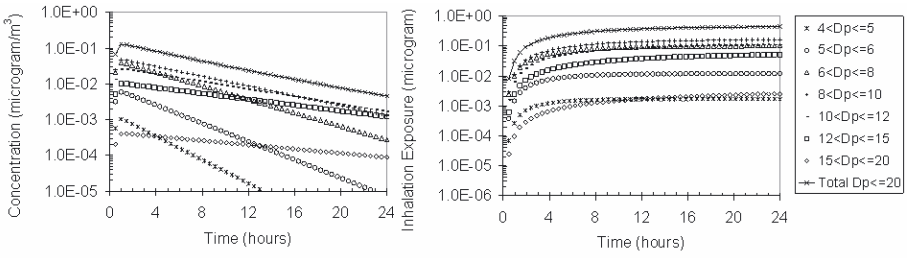

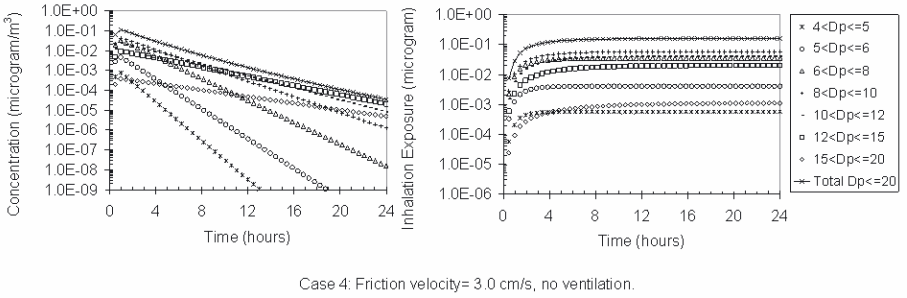

Figure 91: Concentrations and inhalation exposures for different size groups of particles

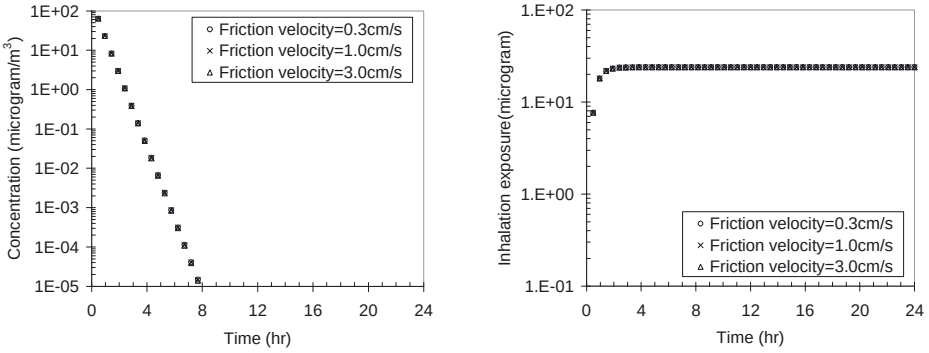

Figure 92: Concentrations and inhalation exposure to environmental tobacco smoke, after smoking a cigarette for 6 minutes, in a 30m^3 room ventilated with an air exchange ratio of 2.14.

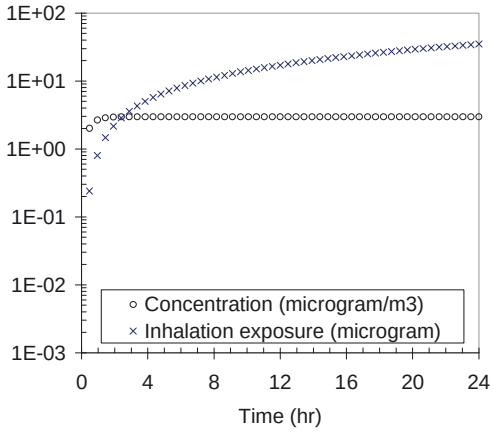

Figure 93: Concentration and inhalation exposure of ambient $PM_{2.5}$ infiltrated into a room of 30 m^3.

3.3. Discussion

Estimation of inhalation exposure to indoor air pollutants is an essential part of multipathway exposure assessment since most people spend a large portion of their time indoors. In recent years, modeling of indoor pollutant sources and sinks has gradually shifted from simple, empirical models to more complex, mass transfer models. While the latter have demonstrated improved accuracy, validity, and scalability, their usefulness has somewhat been overshadowed by their increased complexity. IAQX attempts to resolve this problem by shielding users from mathematical details, allowing them to concentrate on IAQ related issues.

In the calculation of the emission rate factors, the density of the particles is assumed as 0.3 g/cm^3. In their study of in-situ measurements of various properties of traffic-related aerosol particles, Schneider et al (2008) used an effective particle density of 1 g/cm^3 for soot (~100nm) and nucleation mode (~30 nm) and 2 g/cm^3 for the background accumulation mode (> 100nm). The densities of carbon particles with diameters between 5 – 20nm are measured by Schleicher et al (1995) as 1.38 - 0.60 g/cm^3 respectively, as presented in Figure 94. In comparison to these, the density that was used in this study is lower, which means that the reported emissions rates and inhalation exposures to the particles emitted from the gas cookers would be underestimated by a factor of 4 to 6.

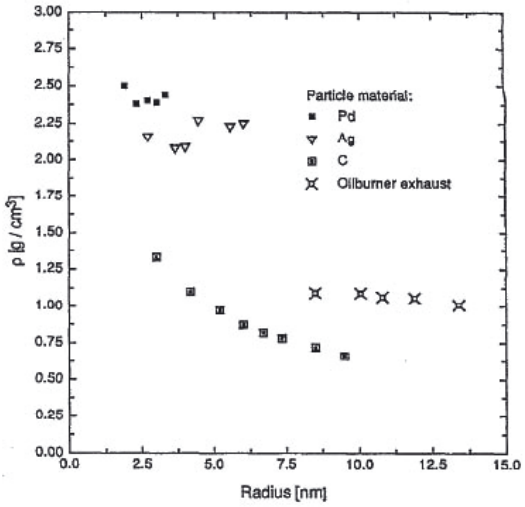

Figure 94: Comparison of the densities of various submicron aerosol species.

The adequate vent simulations are carried out in order to reduce the inhalation exposure to the particles of size 15nm<Dp<=20nm below 0.1 nanogram at the end of 24 hours. As there is no recommended limits for particle concentrations or total exposures that would not give adverse health affects, this limit of 0.1 ng was decided based on the results of the inhalation exposure simulations for the previously described four cases. The lowest inhalation exposure to the particles smaller than 20nm was calculated as 100ng in case of the highest friction velocity. Therefore it was thought that, the reduction of inhalation exposures to 1 ‰ of the latter value would provide a satisfactory improvement.

3.4. Interpretation Summary

Using the density of soot precursor particles (0.3 g/cm^3) and the size distribution data and particle number concentrations observed experimentally during stoichiometric combustion of 4slpm methane, simulations were carried out in order to determine the inhalation exposures that would result in a room with a volume of 30m^3 , at the end of 24 hours, following the operation of a burner for one hour. The highest inhalation exposure is calculated as 2 micrograms, where deposition of the particles onto surfaces was not considered. The lowest inhalation exposure is calculated as 0.1 micrograms, where the friction velocity is highest (3cm/s). The adequate vent simulations showed that by providing an air exchange rate of 2.2, the inhalation exposure to particles of size 15nm<Dp<=20nm can be reduced to 0.1 nanogram.

For comparison reasons, simulations were carried out to calculate the inhalation exposure to environmental tobacco smoke, after smoking a cigarette for 6 minutes, in a 30m^3 room ventilated with an air exchange ratio of 2.14. The inhalation exposure for this case is calculated as 20 micrograms. Last but not least, simulations were carried out to calculate the inhalation exposure to ambient $PM_{2.5}$ infiltrated into a room of 30m^3, where there is no source of particles inside. The inhalation exposure for this case is calculated as 30 micrograms.

Based on the above inhalation exposures, one could conclude that a person would inhale the equal mass of particles at the end of a day, by opening the windows of his 30m^3 room located in an average European city; or at the end of one and a half day by staying in a 30m^3 room which is aired after smoking one cigarette or at the end of approximately hundred days purely by turning on the gas cooker for one hour per day. On the other hand, if these inhalation exposures are converted to particle numbers, assuming that all particles have equal density, the equal mass of particles inhaled from three different cases would correspond to approximately 2E7 particles from gas cooker, 3E3 particles from exposure to environmental tobacco smoke and 1 particle from infiltration of ambient $PM_{2.5}$. Thus the importance of the particle emissions from gas cookers is dependent on whether it is the number or mass of particles inhaled which creates the adverse health effects. Moreover, as these particles are very different in sizes, their penetration into lungs and the health effects would be different.

3.5. References

Adams WC. (1993), Measurement of breathing rate and volume in routinely performed daily activities, Contract No. A033-205. Sacramento, CA: Air Resources Board.

Dingenen, R. V. et al (2004), A European aerosol phenomenology-1: physical characteristics of particulate matter at kerbside, urban, rural and background sites in Europe, Atmospheric Environment, 38 (16), p. 2561-2577.

Guo, Z. (2000), Development of a Windows-based indoor air quality simulation software package, Environmental Modelling and Software with Environment Data News, 15 (4), p. 403-410.

Hänninen O.O.(2004), Infiltration of ambient $PM_{2.5}$ and levels of indoor generated non-ETS $PM_{2.5}$ in residences of four European cities, Atmospheric Environment, 38 (37) , p. 6411-6423.

Klepeis, N. E. (2003), Determining size-specific emission factors for environmental tobacco smoke particles, Aerosol Science and Technology,37 (10) , p. 780-790.

Lai K., Nazaroff A (2000)., Modeling indoor particle deposition from turbulent flow onto smooth surfaces, Journal of Aerosol Science 31 (4) , p. 463-476.

Murray DM, Burmaster DE. (1995),Residential air exchange rates in the United States: Empirical and estimated parametric distributions by season and climate region. Risk Analysis, 15:459–65.

Nazaroff A , Cass G.R. (1989), Mathematical Modeling of Indoor Aerosol Dynamics, Environmental Science and Technology, Vol. 23, No. 2.

Ning Z. (2006), Experimental study of environmental tobacco smoke particles under actual indoor environment, Science of the Total Environment, 367 (2-3) , p. 822-830.

Schleicher B., Kunzel S., Burtscher, H.(1995), In situ measurement of size and density of submicron aerosol particles, Journal of Applied Physics, 78 (7), 4416-4422.

Schneider J., Kirchner U., Borrmann S., Vogt, R., Scheer V.(2008), In situ measurements of particle number concentration, chemically resolved size distributions and black carbon content of traffic-related emissions on German motorways, rural roads and in city traffic, Atmospheric Environment, 42 (18), 4257-4268.

PART D: CONCLUSIONS

In the light of several experiments performed with methane, natural gas and odorant free natural gas, it is concluded that particle emissions from domestic gas cookers is very sensitive to primary air addition. The diameters of the particles emitted from any of these gases are found to be around 10 nm for diffusion flame and 2-5 nm for partially premixed flames. Emission rate of particles with diameters less than 20 nm from domestic gas cookers is calculated to be 3- 4 μg/hr on average.

The particles are identified to be carbonaceous particles containing oxygen and sulfur in case of natural gas as fuel. It is evident that presence of sulfur favors the particle formation process, despite the very small amounts present in natural gas via the odorant. Since particle emissions from methane experiments were very close to those from natural gas experiments, it is also evident that those particles can not be due to sulfur only. However in case sulfur is present in the gas, it is incorporated into the particles. Based on their carbonaceous nature and their diameters in the range of a few nanometers, it is believed that these particles are soot precursor particles just as those particles identified and communicated recently by d'Anna et al (2008). Copper was also identified in the particles, which could be explained by either, its presence in the natural gas or in the materials that were used in this study, i.e: the burner and the sampling probe.

In the light of the simulations carried out with IAQX, it is concluded that air exchange ratios of 2.2 would provide a significant reduction in the inhalation exposures to these particles in the case of average sized kitchens ($30m^3$ volume). The inhalation exposure simulations indicate that a person would inhale the equal mass of particles at the end of a day, by opening the windows of his $30m^3$ room located in an average European city; or at the end of one and a half day by staying in a $30m^3$ room which is aired after smoking one cigarette or at the end of approximately hundred days purely by turning on the gas cooker for one hour per day. On the other hand, if these inhalation exposures are converted to particle numbers, assuming that all particles have equal density, the equal mass of particles inhaled from three different cases would correspond to approximately 2E7 particles from gas cooker, 3E3 particles from exposure to environmental tobacco smoke and 1 particle from infiltration of ambient $PM_{2.5}$. The importance of these emissions from health impact point of view, however, depends on whether it is the mass or numbers of particles inhaled which creates the adverse health effects.

ISBN-10: 87-92481-07-8
ISBN-13: 978-87-92481-07-8
Printed in Denmark by
FRYDENBERG A/S
Baldersgade 12 - 16
DK-2200 Copenhagen N

Department of Chemical
and Biochemical Engineering

DTU Building 229
Søltofts Plads
DK-2800 Kgs. Lyngby
www.kt.dtu.dk